Addressing Challenges in the Treatment of Tuberculosis and Tuberculosis Meningitis: A Pharmacometric Approach

by

Noha Abdelgawad

A Thesis presented for the degree of
DOCTOR OF PHILOSOPHY
in the Division of Clinical Pharmacology
Department of Medicine
UNIVERSITY OF CAPE TOWN

Primary supervisor: Professor Paolo Denti
Co-supervisor: Dr Kamunkhwala Gausi

February 2025

Copyright

Contributions to the field

This thesis includes the following contributions to the field of pharmacometrics and clinical pharmacology.

Full-length original articles:

1. **Abdelgawad, N.**, Chirehwa, M., Schutz, C., Barr, D., Ward, A., Janssen, S., Burton, R., Wilkinson, R. J., Shey, M., Wiesner, L., McIlleron, H., Maartens, G., Meintjes, G., & Denti, P. (2024). Pharmacokinetics of antitubercular drugs in patients hospitalized with HIV-associated tuberculosis: a population modeling analysis *Wellcome Open Research, 7*, 72. https://doi.org/10.12688/wellcomeopenres.17660.3
2. **Abdelgawad, N.**, Tshavhungwe, M., Rohlwink, U., McIlleron, H., Abdelwahab, M. T., Wiesner, L., Castel, S., Steele, C., Enslin, J., Thango, N. S., Denti, P., & Figaji, A. (2023). Population Pharmacokinetic Analysis of Rifampicin in Plasma, Cerebrospinal Fluid, and Brain Extracellular Fluid in South African Children with Tuberculous Meningitis. *Antimicrobial Agents and Chemotherapy, 67(3)*. https://doi.org/10.1093/jac/dkad371
3. **Abdelgawad, N.**, Wasserman, S., Gausi, K., Davis, A., Stek, C., Wiesner, L., Meintjes, G., Wilkinson, R. J., & Denti, P. (2025). Population Pharmacokinetics of Rifampicin in Plasma and Cerebrospinal Fluid in Adults with Tuberculosis Meningitis. T*he Journal of Infectious Diseases*. https://doi.org/10.1093/infdis/jiaf178
4. **Abdelgawad N.**, Wasserman, S., Abdelwahab, M. T., Davis, A., Stek, C., Wiesner, L., Black, J., Meintjes, G., Wilkinson, R. J., & Denti, P. (2023). Linezolid Population

Pharmacokinetic Model in Plasma and Cerebrospinal Fluid Among Patients With Tuberculosis Meningitis. *The Journal of Infectious Diseases*. https://doi.org/10.1093/infdis/jiad413

Scientific conference abstracts:

- Oral presentation: "Population Pharmacokinetic Modeling of Linezolid in Plasma and Cerebrospinal Fluid in Adults with Tuberculous Meningitis for the LASER-TBM Study" – The Union World Conference on Lung Health 2022, Online
- Oral presentation: "Population Pharmacokinetic Modeling for Plasma and Cerebrospinal Fluid Linezolid Concentrations in Adults with Tuberculous Meningitis in the LASER-TBM Study" - Tuberculous Meningitis International Research Consortium 2022, Oxford, UK
- Oral presentation: "Pharmacokinetics of Rifampicin in Plasma, Cerebrospinal Fluid, and Brain Extracellular Fluid in South African Children with Tuberculous Meningitis: Application of Brain Microdialysis" – 12th International Workshop on Clinical Pharmacology of Tuberculosis Drugs 2021, Online
- Poster: "Population pharmacokinetic modeling of rifampicin at standard and high doses in adults with tuberculous meningitis" – 14th International Workshop on Clinical Pharmacology of Tuberculosis Drugs 2023, Online
- Poster: "Population pharmacokinetic modeling of rifampicin at standard and high doses in adults with tuberculous meningitis" – PAGE 2023, A Coruña, Spain

- Poster: “Population Pharmacokinetic Modeling of Linezolid in Plasma and Cerebrospinal Fluid in Adults with Tuberculous Meningitis (LASER-TBM Study)” – PAGE 2022, Ljubljana, Slovenia
- Poster: “Population Pharmacokinetic Analysis of Rifampicin in Plasma, Cerebrospinal Fluid, and Brain Extracellular Fluid in South African Children with Tuberculous Meningitis” – World Conference on Pharmacometrics 2022, Cape Town, South Africa.
- Poster: “Population pharmacokinetics of pyrazinamide in hospitalized TB patients with HIV versus TB outpatients” – PAGE 2021, Online

Declaration of work

I, **Noha Abdelgawad**, hereby declare that the work presented in this dissertation/thesis is my original work, except where acknowledgements indicate otherwise. I confirm that neither the entire work nor any part of it has been, is being, or will be submitted for another degree at this or any other university. Chapters 3 through 7 of the thesis have been published or are under review in international journals. Their contents remain unchanged from the published versions except for formatting adjustments made to maintain consistency within the thesis. All co-authors have provided their written consent to include the publications as part of my PhD.

I empower the university to reproduce for the purpose of research either the whole or any portion of the contents in any manner whatsoever.

Declaration on the Inclusion of Publications in a PhD Thesis

"I confirm that I have been granted permission by the University of Cape Town's Doctoral Degrees Board to include the following publication(s) in my PhD thesis, and where co-authorships are involved, my co-authors have agreed that I may include the publication(s):"

1. **Abdelgawad, N.**, Chirehwa, M., Schutz, C., Barr, D., Ward, A., Janssen, S., Burton, R., Wilkinson, R. J., Shey, M., Wiesner, L., McIlleron, H., Maartens, G., Meintjes, G., & Denti, P. (2024). Pharmacokinetics of antitubercular drugs in patients hospitalized with HIV-associated tuberculosis: a population modeling analysis *Wellcome Open Research, 7*, 72. https://doi.org/10.12688/wellcomeopenres.17660.3
2. **Abdelgawad, N.**, Tshavhungwe, M., Rohlwink, U., McIlleron, H., Abdelwahab, M. T., Wiesner, L., Castel, S., Steele, C., Enslin, J., Thango, N. S., Denti, P., & Figaji, A. (2023). Population Pharmacokinetic Analysis of Rifampicin in Plasma, Cerebrospinal Fluid, and Brain Extracellular Fluid in South African Children with Tuberculous Meningitis. *Antimicrobial Agents and Chemotherapy, 67(3)*. https://doi.org/10.1093/jac/dkad371
5. **Abdelgawad, N.**, Wasserman, S., Gausi, K., Davis, A., Stek, C., Wiesner, L., Meintjes, G., Wilkinson, R. J., & Denti, P. (2025). Population Pharmacokinetics of Rifampicin in Plasma and Cerebrospinal Fluid in Adults with Tuberculosis Meningitis. T*he Journal of Infectious Diseases*. https://doi.org/10.1093/infdis/jiaf178

3. **Abdelgawad N.**, Wasserman, S., Abdelwahab, M. T., Davis, A., Stek, C., Wiesner, L., Black, J., Meintjes, G., Wilkinson, R. J., & Denti, P. (2023). Linezolid Population Pharmacokinetic Model in Plasma and Cerebrospinal Fluid Among Patients With Tuberculosis Meningitis. *The Journal of Infectious Diseases*. https://doi.org/10.1093/infdis/jiad413

Signature: **Date:** 2025/02/14

Signed by candidate

Student Name: Noha Abdelgawad

Student Number: ABDNOH001

Acknowledgements

Completing this PhD has been a journey filled with challenges, growth, and immense learning. I am deeply grateful to those who have supported and guided me along the way.

First and foremost, I extend my deepest gratitude to my supervisor, Prof Paolo Denti, for his invaluable guidance and support throughout this research. Your insightful feedback and encouragement have been instrumental in shaping this work.

I am also profoundly grateful to my co-supervisors, Maxwell Chirehwa, Mahmoud Abdelwahab, and Kamunkhwala Gausi, for their expert advice and valuable insights. Your mentorship has played a crucial role in the development of this thesis.

A special thank you to my colleagues at UCT's pharmacometrics research group for their discussions, and constructive criticism. You made this journey all the more rewarding.

I am truly grateful for the opportunities offered by Pharmacometrics Africa, the Uppsala Pharmacometrics Summer School (UPSS), and my internship at Pharmetheus, both of which provided an enriching learning experience that expanded my knowledge and skills.

I extend my heartfelt gratitude to all the participants in the clinical studies involved in this research and their study team members. This work would not have been possible without your contribution.

I would also like to acknowledge the facilities provided by the University of Cape Town's ICTS High-Performance Computing team: https://ucthpc.uct.ac.za/ where the computations for this research were conducted. The resources provided have been essential in enabling the analyses and simulations required for this thesis.

To my husband, Mahmoud, my parents, Tahani and Mohamed, and my brother, Ahmed, I cannot express enough gratitude for your endless patience, love, and encouragement. Your belief in me, even during the most challenging times, has been my greatest source of strength.

Lastly, I would like to acknowledge the funding agencies and institutions that made this research possible whose support has been invaluable in the completion of this work.

This PhD journey has been both rigorous and fulfilling, and I am profoundly grateful to everyone who has contributed to it in any way. Thank you.

Abstract

Tuberculosis (TB) is the primary cause of death from a single infectious agent worldwide. During the coronavirus disease (COVID-19) pandemic, TB briefly fell to second place, but it has now regained its position as the top infectious killer. It is caused by *Mycobacterium tuberculosis* and mainly targets the lungs, but it can spread to other tissues, which can result in TBM, a more severe and often fatal form that affects the central nervous system (CNS), particularly the meninges. In South Africa, TB and TBM burdens are particularly high due to factors such as high HIV prevalence.

The treatment of TB and TBM presents significant challenges. Firstly, it typically involves numerous antibiotics taken over several months that may cause serious adverse effects, leading to poor adherence, which can result in treatment failure or the development of drug resistance. Secondly, TB management in hospitalised patients becomes more difficult since they often face more advanced stages of the infection, as well as physiological changes that could impact the pharmacokinetics of anti-TB drugs. Lastly, TBM treatment is further complicated by limited antitubercular drug penetration into the CNS due to its protective barriers, disease-related physiological changes to these barriers and neurological complications. A further challenge is the treatment of special populations, such as children, where unique pharmacokinetic and formulation considerations may complicate management. In this thesis, we use pharmacometric modelling and simulation approaches to tackle some of the obstacles encountered in TB and TBM treatment. Firstly, we demonstrate how pharmacometric approaches can

be useful in monitoring adherence to TB drugs. Secondly, we investigated the differences in the pharmacokinetics of rifampicin, isoniazid, and pyrazinamide in hospitalised patients, who are more severely ill, compared to outpatients. Although we found slower rifampicin absorption and higher between-subject variability in pyrazinamide clearance in hospitalised patients compared to outpatients, we did not identify any changes in pharmacokinetics that are expected to be of clinical significance. It is reassuring that hospitalized patients do not seem to have lower antitubercular drug exposures than outpatients. Thirdly, in South African children diagnosed with definite or probable TBM, we estimated the extent of rifampicin's lumbar and ventricular cerebrospinal fluid (CSF) penetration to be ~5% of plasma. We were also able to use the microdialysis technique to obtain brain extracellular fluid samples to present a proof-of-concept that rifampicin enters the brain tissue. These results show that the microdialysis technique is a promising way to study site-of-disease pharmacokinetics in TBM and pave the way for optimisation of TBM regimens. Lastly, in South African adults with TBM/HIV, we described the plasma and CSF pharmacokinetics of standard and high-dose (10 and 35 mg/kg) rifampicin and linezolid. We estimated lumbar CSF penetration of rifampicin to be ~5%, which is in line with the results of our study in children. Linezolid CSF penetration increased with higher CSF total protein levels, peaking at 37%. Neither the duration of rifampicin co-treatment nor the dose level (standard 10 mg/kg vs high 35 mg/kg) was found to affect

linezolid pharmacokinetics. Our findings endorse the continued evaluation of high-dose rifampicin (35 mg/kg) and linezolid for optimizing TBM treatment regimens.

To conclude, thanks to pharmacometric approaches, we could address some of the challenges encountered in TB treatment, namely, using modelling and simulation to monitor drug adherence, understanding the pharmacokinetics of the first-line anti-TB drugs in hospitalised TB patients, and investigating CNS pharmacokinetics of rifampicin and linezolid in TBM patients.

Contents

List of Tables

List of Figures

Abbreviations and Acronyms

1HP	1-month daily regimen of rifapentine and isoniazid
2HRZE/4HR	2-month daily isoniazid, rifampicin, pyrazinamide, and ethambutol, followed by 4 months of daily isoniazid and rifampicin regimen
2HRZE/10HR	2-month daily isoniazid, rifampicin, pyrazinamide, and ethambutol, followed by 10 months of daily isoniazid and rifampicin regimen
3HP	3-month weekly regimen of isoniazid and rifapentine
3HR	3-month daily regimen of isoniazid and rifampicin
4R	4-month daily rifampicin regimen
6H or 9H	6- or 9-month regimen of daily isoniazid
6HRZEto	6-month daily isoniazid, rifampicin, pyrazinamide, and ethionamide regimen
AcINH	N-acetyl isoniazid
ACTG	AIDS Clinical Trials Group
ALT	alanine transaminase
AST	aspartate transaminase
BBB	blood-brain barrier
BCG	Bacillus Calmette–Guérin
BCSFB	blood-cerebrospinal fluid barrier
BPaL	bedaquiline, pretomanid, and linezolid
BPaLM	bedaquiline, pretomanid, and linezolid with moxifloxacin
BRC	conjugated bilirubin
BRT	total bilirubin
BSV	between-subject variability

CC	critical concentration
CommHC	communicating hydrocephalus
COVID-19	coronavirus disease 2019
Cmax	peak plasma concentration
Cmin	minimum concentration
CSF	cerebrospinal fluid
CYP	Cytochrome P450
DiAcHz	diacetyl-hydrazine
DNA	Deoxyribonucleic Acid
DOT	Directly observed therapy
ECF	extracellular fluid
ETV	endoscopic third ventriculostomy
FDC	fixed-dose combination
FFM	fat-free mass
FOCEI	first-order conditional estimation with interaction
InhA	enoyl-acyl carrier protein reductase
IPT	isoniazid preventive therapy
IV	intravenous
KatG	catalase-peroxidase enzyme
LCSF	lumbar cerebrospinal fluid
MD	microdialysis
MDR	multidrug-resistant
MIC	minimum inhibitory concentration

MLE	maximum likelihood estimation
Mtb	*Mycobacteria tuberculosis*
NAT2	N-acetyltransferase 2
NLME	nonlinear-mixed effects
OFV	objective function value
OR	odds ratio
P-gp	P-glycoprotein
PK	pharmacokinetics
PLHIV	people living with HIV
POA	pyrazinoic acid
PopPK	population pharmacokinetics
PTC	peptidyl transferase centre
PXR	pregnane X receptor
RHZE	rifampicin, isoniazid, pyrazinamide, and ethambutol
RNA	ribonucleic acid
RR	rifampicin-resistant
rRNA	ribosomal ribonucleic acid
RUV	residual unexplained variability
SIR	sampling importance resampling
TB	tuberculosis
TBM	tuberculosis meningitis
TI/NR	treatment-intolerant or nonresponsive
Tmax	time to peak plasma concentration

TPT	TB preventative therapy
VCSF	ventricular cerebrospinal fluid
VPC	visual predictive check
WHO	world health organization
XDR	extensively drug-resistant

Chapter 1 : Introduction

Global tuberculosis (TB) burden

Tuberculosis (TB) is an airborne infectious disease caused by the *Mycobacterium tuberculosis* (*Mtb*) bacteria. TB is typically preventable and usually treatable. Despite this, TB is currently the number 1 cause of death from a single infectious agent. COVID-19 caused more deaths during the pandemic years, but as a single infectious agent, TB still holds the top position for global mortality.

Despite prevention, diagnosis, treatment, healthcare access, and research efforts, over 10 million individuals still contract TB annually, and TB-related deaths are nearly double that of HIV/AIDS. TB caused an estimated 1.3 million deaths around the world in 2022. The disruptions caused by COVID-19 are projected to have led to nearly 500,000 additional deaths from TB between 2020 and 2022, in contrast to the expected mortality rates had the trends preceding the pandemic persisted (World Health Organization 2023a). Approximately 2.5 million people suffered from TB in the WHO African Region in 2021, and as many as half a million people died due to the disease in the same year (World Health Organization 2023b) . In South Africa, the estimated incidence of TB cases is 468 per 100,000 of the population. At least 54% of the estimated incidence of TB cases and 57% of the 54,000 deaths attributable to TB in 2022 occurred in people living with HIV (PLWH) (World Health Organization 2023a).

Additionally, about 50% of TB patients and their families must bear a huge economic burden (>20% of annual household income) due to direct medical and

non-medical expenditures, and indirect costs related to reduced work ability and income loss (World Health Organization (WHO) 2023) .

TB is a global health concern with numerous new cases linked to five key risk factors: undernourishment, HIV infection, alcohol use disorders, smoking (specifically among men) and diabetes (World Health Organization 2023a) . PLHIV are ~16 times more likely to fall ill with TB disease than those without HIV, making TB the leading cause of death among people living with HIV. An estimated 39 million people were living with HIV and about 167,000 people died of HIV-associated TB in 2022, two-thirds of whom are in the WHO African Region. In 2022, about 167,000 people died of HIV-associated TB. The WHO African Region has the highest burden of HIV-associated TB. The proportion of TB episodes coinfected with HIV was highest in countries in the WHO African region, exceeding 50% in parts of southern Africa (Joint United Nations Programme on HIV/AIDS (UNAIDS) 2024). The WHO recommends that all PLHIV should get TB preventive treatment (World Health Organization 2024b) .

Global tuberculosis meningitis (TBM) burden

TB typically impacts the lungs (pulmonary TB), although it can also affect other tissues, generally referred to as extrapulmonary TB. Among all the types of TB, tuberculosis meningitis (TBM) is a particularly devastating extrapulmonary manifestation of the disease. It is estimated that over 100,000 cases occur annually, and in patients co-infected with HIV, the mortality and morbidity rate can be as high as 50% (Wilkinson et al. 2017). TBM arises when the *Mtb* invade the meninges, the membranes enveloping the brain and spinal cord. TBM comprises roughly 5 to 10%

of all extrapulmonary TB cases and ~1% of all TB cases (Thakur et al. 2018). Moreover, TBM cases are often underreported because TBM is challenging to diagnose, especially early in infection. The reason is that TBM presents with non-specific clinical symptoms that overlap with other neurological conditions, including infectious meningitis caused by viruses, other bacteria, and fungi. Also, the diagnosis of TBM is often not microbiologically confirmed (Wilkinson et al. 2017; Török 2015).

Children are at a particularly high risk of TBM, with peak incidence in children under 4 years old (Török 2015). Mathematical modelling indicates that over 58% of paediatric TB cases occur in children under 5 years old, with a quarter of them presenting with extrapulmonary TB (Dodd et al. 2017). A 2012 study reported that TB was the leading cause of bacterial paediatric meningitis (~22%) in the Western Cape of South Africa (Wolzak et al. 2012). A systematic review of treatment outcomes involving 1,636 children diagnosed with TBM revealed a mortality of 19.3%, indicating that several thousand infants succumb to TBM annually (Chiang et al. 2014). The neonatal Bacillus Calmette–Guérin (BCG) vaccine is estimated to be 73% effective in preventing TBM, potentially averting around 30,000 cases of the disease among children each year. This estimation aligns with the overall occurrence of approximately 100,000 cases of TBM annually (Wilkinson et al. 2017). Diagnosis of TBM is even more challenging in infants and children. Early symptoms in children are nonspecific and may include cough, fever, vomiting, malaise, and weight loss, usually not accompanied by detectable abnormalities in the CSF. This absence of clinical or CSF evidence of meningitis at the initial presentation can

complicate diagnosis and necessitate further evaluation to confirm or rule out the condition (Török 2015).

Pathogenesis of TB

Mtb is the most common species of bacteria responsible for human TB infections, however, other species of mycobacteria can cause TB-like diseases in humans. TB spreads mainly through airborne droplets, which can stay suspended in the air for several hours when a person with an active TB infection coughs, sneezes or speaks. TB pathogenesis begins when *Mtb* enters the body through inhalation of infectious droplets. After being inhaled, the bacteria travel to the alveoli in the lungs, where alveolar macrophages engulf them. However, *Mtb* has evolved strategies to evade destruction by the immune system and can survive and replicate within these macrophages (Sturgill-Koszycki et al. 1994).

The infection triggers a complex immune response. Infected macrophages release cytokines and chemokines, recruiting other immune cells to the site of infection. Granulomas, organized collections of immune cells, form around the infected macrophages in an attempt to contain the infection. Within granulomas, the bacteria can persist in a dormant state, leading to latent tuberculosis infection. However, in some cases, the bacteria can evade immune clearance and proliferate, leading to the development of active TB disease. This active disease is characterized by tissue damage, necrosis, and the formation of cavities within the lungs, as well as the potential spread of bacteria to other organs. The interplay between *Mtb* and the host immune response determines the outcome of infection (de Martino et al. 2019; Bhatt and Salgame 2007).

Pathogenesis of TBM

The pathogenesis of TBM also begins with the inhalation of *Mtb* bacilli, typically through respiratory droplets expelled by individuals with active pulmonary TB. The bacteria can then disseminate through the bloodstream or lymphatic system to various organs, including the central nervous system (CNS) (Davis et al. 2019). The CNS is an intricate system that comprises many physiological compartments and flows. Physiological compartments are the blood-brain barrier (BBB), the blood-cerebrospinal fluid barrier (BCSFB), brain extracellular fluid (brain ECF), cerebral blood, brain parenchymal cells, and the CSF in the ventricles, the cisterna magna, and the subarachnoid space. CNS fluid flows include the cerebral blood flow (CBF), brain ECF bulk flow, and CSF flow (Yamamoto, Danhof, and de Lange 2017). *Mtb* gains access to the CNS by crossing the protective barriers. The CNS is protected from potential harm by 2 barriers: the BBB and the BCSFB. The BBB is a specialised barrier that is made up of tightly packed endothelial cells lining the blood vessels in the brain. The BCSFB primarily consists of specialised epithelial cells called choroid plexus epithelial cells, which are interconnected by tight junctions forming a physical barrier. The bacilli can breach the barriers via various mechanisms, including transcellular migration or by infecting and disrupting the integrity of endothelial cells (Davis et al. 2019).

Once *Mtb* reaches the CNS, it can infect resident immune cells such as macrophages and microglia, as well as other cell types. Within these cells, *Mtb* can survive and replicate, establishing a focus of infection within the CNS. The presence of *Mtb* triggers a localised inflammatory response within the meninges and

surrounding brain tissue. This response involves the activation of immune cells, the release of pro-inflammatory cytokines, and the mobilisation of more immune cells to the site of infection. The immune response aims to control bacterial growth and clear the infection, but can also contribute to tissue damage and neurological complications. In some cases, the immune response may lead to the formation of granulomas within the CNS, known as tuberculomas. These structures consist of aggregates of immune cells, including macrophages, surrounded by a rim of fibrotic tissue. Within tuberculomas, caseous necrosis may occur, characterised by the central necrotic core surrounded by inflammatory cells (Manyelo et al. 2021; Davis et al. 2019).

TBM can lead to various neurological complications, including hydrocephalus (due to obstruction of cerebrospinal fluid flow), ischemic stroke (caused by vasculitis and thrombosis), cranial nerve palsies, seizures, and cognitive deficits. These complications result from the direct effects of the infection, inflammation, and tissue damage within the CNS (Manyelo et al. 2021; Davis et al. 2019).

Overall, the pathogenesis of TBM involves the invasion of *Mtb* from the primary site of infection, typically the lungs, into the CNS, activation of the host immune response, and subsequent inflammation and tissue damage.

Tuberculosis treatment

TB treatment typically requires multiple antibiotics to effectively eliminate *Mtb* and reduce the risk of the development of drug resistance. The combination of antibiotics and duration of treatment depends on the type and severity of TB

infection and drug susceptibility. First-line antibiotics include rifampicin, isoniazid, pyrazinamide, and ethambutol. These drugs are prescribed according to weight bands, with the recommended daily doses as follows: rifampicin (8–12 mg/kg), isoniazid (4–6 mg/kg), pyrazinamide (20–30 mg/kg), and ethambutol (15–20 mg/kg) (World Health Organization 2022c) .

TB preventive treatment

Since estimates indicate that people living with HIV (PLHIV) are at much higher risk of developing active TB and that TB is the most frequent cause of AIDS-related deaths worldwide, prevention of active TB disease is an important component of efforts to eliminate TB worldwide (World Health Organization 2024b). Isoniazid preventive treatment (IPT) (daily isoniazid for 6 to 9 months) was previously the standard TB preventative therapy (TPT) for all individuals in high and low TB incidence countries. In 2020, the WHO introduced 2 additional regimens: daily rifapentine with isoniazid for 1 month (1HP) and daily rifampicin for 4 months (4R), as alternatives for latent drug-susceptible TB infection (World Health Organization 2024b).

Drug-susceptible TB treatment

Without treatment, mortality rates of active TB disease are as high as 50% (World Health Organization 2023a) . The antitubercular drugs must reach their microbial targets in adequate concentrations and remain for a sufficient period necessary to kill the bacteria. They must be transported from the circulation to the non-vascularized pulmonary lesion, then enter the caseum and necrotic foci, permeate the *Mtb* cell envelope to reach their intracellular targets (Dartois 2014). All patients

with drug-susceptible uncomplicated TB without documented resistance to rifampicin and isoniazid are treated using the 6-month RHZE regimen: rifampicin, isoniazid, pyrazinamide, and ethambutol for 2 months, called the initiation phase, followed by only rifampicin and isoniazid for an additional 4 months, known as the continuation phase. This regimen is typically abbreviated as 2HRZE/4HR (World Health Organization 2022c).

Drug-susceptible TBM treatment

Early correct diagnosis of TBM is very critical for better treatment outcomes. But the diagnosis of TBM remains difficult, particularly in children, which further complicates treatment endeavours (Török 2015). The ideal duration for TBM treatment is not evidence-based, therefore, it differs from one country to another (Litjens, Aarnoutse, and te Brake 2020). Yet, the TBM regimen recommended by the WHO is the same as that for pulmonary TB only with a longer continuation phase of 10 months instead of 4 months (2HRZE/10HR), in addition to the newly recommended short intensive regimen in 2022. The short intensive regimen consists of daily isoniazid, rifampicin, pyrazinamide, and ethionamide for 6 months (6HRZEto), with higher mg/kg doses of isoniazid and rifampicin compared with the 12-month regimen. It was adapted from the regimen used in South Africa (World Health Organization 2022d) . The use of child-friendly, dispersible, and FDC medicines in children is preferred when possible (World Health Organization 2022c) .

In addition to antitubercular antibiotics, adjunctive anti-inflammatory agents such as corticosteroids are usually administered to TBM patients to reduce the

associated vasculitis in different cerebral blood vessels (Cresswell et al. 2019). Moreover, surgical interventions may be required such as in the case of hydrocephalus management in TBM (A. A. Figaji and Fieggen 2010).

Drug-resistant TB treatment

Drug-resistant TB refers to TB infections that evolve and become resistant to the antibiotics typically used for treatment. Multidrug-resistant TB (MDR-TB) is TB that is caused by strains of *Mtb* that are resistant to both rifampicin and isoniazid. Extensively drug-resistant TB (XDR-TB) refers to TB that is resistant to both rifampicin and isoniazid, in addition to resistance to any fluoroquinolone and to at least one of three second-line injectable drugs (capreomycin, kanamycin and amikacin) (World Health Organization 2022a). Patients can develop drug-resistant TB either by being infected with a drug-resistant strain (known as primary resistance) or by developing resistance during treatment (acquired resistance). The latter often occurs due to subtherapeutic drug concentrations or poor adherence to medication regimens (Dheda et al. 2017; Dousa et al. 2020).

Second-line antitubercular drugs for TB treatment include repurposed antibiotics like linezolid, clofazimine, fluoroquinolones (e.g. levofloxacin, moxifloxacin), and aminoglycosides (e.g. streptomycin, amikacin), alongside newer antibiotics such as bedaquiline, pretomanid, and delamanid. The treatment of drug-resistant *Mtb* strains typically involves a combination of second-line drugs, sometimes alongside first-line agents (Dousa et al. 2020).

The WHO has conditionally recommended a new 6–9-month regimen composed of bedaquiline, pretomanid, and linezolid (BPaL) for patients with MDR-

TB and rifampicin-resistant TB (RR-TB), especially those with additional fluoroquinolone resistance and limited or no prior exposure to bedaquiline or linezolid (no more than two weeks) (World Health Organization 2022a). This recommendation was based on the 2020 Nix-TB study, where participants received high-dose linezolid (1200 mg), pretomanid (200 mg), and bedaquiline (400 mg daily for 2 weeks, followed by 200 mg three times weekly for 24 weeks) over a 26-week treatment period (Conradie et al. 2020). In the subsequent TB-PRACTECAL study (Nyang'wa et al. 2022), a variation of the regimen, known as BPaLM, was tested. In this regimen, bedaquiline and pretomanid were administered similarly to the Nix-TB protocol, but the linezolid dose was reduced to 600 mg daily for 16 weeks, followed by 300 mg for 8 weeks. Furthermore, moxifloxacin (400 mg daily) was introduced into the regimen. However, despite its success in pulmonary disease, this regimen has not been implemented for TBM, as its efficacy is contingent on adequate CNS penetration, a factor which preclinical PET imaging data suggest can be substantially lower in brain tissue compared to the lungs (X. Chen et al. 2024).

Pharmacology of antitubercular drugs

The antitubercular drugs investigated in this thesis include rifampicin, isoniazid, pyrazinamide, and linezolid. Their pharmacology is described below.

Rifampicin

Rifampicin, a member of the rifamycins class, is a semisynthetic antibiotic produced from the bacteria *Streptomyces mediterranei*. It has a broad antimicrobial spectrum,

including activity against Mycobacteria. It received approval for use in the treatment of TB in 1967 and has since been a cornerstone in TB treatment regimens (Van Ingen et al. 2011).

Mechanism of action:

Rifampicin exerts its bactericidal effect primarily via inhibiting bacterial RNA polymerase, the enzyme in charge of DNA transcription, effectively blocking the initiation of RNA synthesis and leading to bacterial cell death. The corresponding mammalian enzyme remains unaffected by rifampicin (Tupin et al. 2010; Wehrli 1983). Rifampicin has demonstrated remarkable activity against persisting and dormant populations of *Mtb*, making it a crucial component in shortening the duration of TB treatment and reducing the likelihood of drug resistance emergence. The Minimum Inhibitory Concentrations (MICs) of rifampicin in clinical isolates of drug-susceptible *Mtb* varied between 0.016 and 0.5 mg/L (Chigutsa et al. 2015).

Pharmacokinetics:

Following oral administration, rifampicin's absorption is highly variable (Burman, Gallicano, and Peloquin 2001; Wilkins et al. 2008), reaching peak plasma concentration (C_{max}) of 6–14 mg/L within 1.5–4 hours following a 600 mg oral dose (Donald, Maritz, and Diacon 2011; Sirgel et al. 2005). The variability in rifampicin exposure decreases when taken on an empty stomach (Peloquin et al. 1999). Several studies have shown that food decreases the C_{max} and, to a much lesser extent, the $AUC_{0\text{-}inf}$ of rifampicin, and increases the T_{max} albeit with varying degree (Peloquin et al. 1999; Siegler et al. 1974; Zent and Smith 1995; Polasa, Murthy, and Krishnaswamy 1984). For example, in the study by Peloquin et al., a high-fat meal

reduced the C_{max} by 36%, increased the T_{max} by 103%, and reduced the AUC by 6% (Peloquin et al. 1999). Absorption of rifampicin is affected by gastric pH. Studies have demonstrated that lowering gastric pH leads to serum concentrations twice as high as those seen after alkalinization. On the other hand, antacids did not seem to influence the absorption (G. Acocella 1978).

Rifampicin is about 86% protein bound, mainly to albumin (Boman and Ringberger 1974). Plasma protein binding of rifampicin can become saturated with increasing doses. Yet even with high-dose rifampicin (35 mg/kg), protein binding was found not to be saturated in TB patients with normal albumin levels (Litjens et al. 2019).

Rifampicin is mainly metabolised via acetylation into 25-desacetyl rifampicin, which also exhibits 20% of the antimicrobial activity of the parent compound, in the hepatocytes (Peloquin et al. 1999; G. Acocella et al. 1971). Rifampicin is a known potent inducer of several metabolising enzymes, including cytochrome P450 (CYP) 2C and 3A enzymes, which can implicate it in clinically significant drug interactions (Jamis-Dow et al. 1997). This induction is mediated by the activation of the pregnane X receptor (PXR), which acts as a ligand-activated transcription factor. PXR regulates a panel of drug-metabolising enzymes and transporter proteins. Consequently, when a PXR ligand binds to PXR, it in turn activates the transcription of CYP 3A4 and several other genes (J. Chen and Raymond 2006). This induction also affects rifampicin's own metabolism, a phenomenon called autoinduction. As a result, clearance of rifampicin increases by about 2-fold after two weeks, leading to a decrease in its plasma exposure (M T Chirehwa et al. 2015). It has also been

demonstrated that higher rifampicin doses result in saturable elimination due to the saturation of biliary transport mechanisms (Kenny and Strates 1981; G. Acocella 1978). Both rifampicin and its main metabolite, 25-desacetyl rifampicin, are primarily cleared non-renally and to a lesser extent renally. 25-desacetyl rifampicin is excreted mainly via the bile. Only 10% of rifampicin is excreted unchanged in urine (Peloquin et al. 1999; G. Acocella et al. 1971).

Isoniazid

Discovered in 1952, isoniazid marked a groundbreaking achievement as the first drug to exhibit excellent and specific bactericidal activity in vitro and in vivo against *Mtb*. It is a significant addition to antitubercular drugs because it is highly active and affordable. Notably, its discovery also paved the way for the discovery of another important antitubercular drug, pyrazinamide (Vilchèze and Jacobs 2019; Y. Zhang 2005).

Mechanism of action:

Isoniazid is a prodrug that undergoes activation in the mycobacterial cells by the catalase-peroxidase enzyme (also known as KatG enzyme) that generates isoniazid-derived reactive species, such as nitric oxide, which inhibit the enoyl-acyl carrier protein reductase (InhA) enzyme responsible for the synthesis of mycolic acids, essential components of the mycobacterial cell wall synthesis, leading to impaired cell wall integrity and increased susceptibility to host immune defences (Timmins and Deretic 2006). Isoniazid exhibits bacteriostatic activity against slow-growing *Mtb*, in addition to its bactericidal activity against rapidly growing cells. It is also

effective against both intracellular bacilli in macrophages and extracellular *Mtb* (Mitchison and Selkon 1956).

Pharmacokinetics:

Upon administration, isoniazid is poorly absorbed from the stomach but is well absorbed from the intestine (Mariappan and Singh 2003). Following the standard dose of 300 mg/day oral administration, peak plasma levels reach 5 mg/L within 1 to 2 hours (Peloquin et al. 1997). Isoniazid's bioavailability and absorption may decrease if taken with food, while antacids do not seem to have a significant effect on absorption (Erwin et al. 2019). Isoniazid's level of protein binding is about 14% (Alghamdi, Al-Shaer, and Peloquin 2018).

Isoniazid is metabolised in the liver and intestines via acetylation, mediated by the enzyme N-acetyltransferase (NAT2) into N-acetyl isoniazid (AcINH), a hepatotoxic compound. AcINH is then further acetylated into a harmless compound, diacetyl-hydrazine (DiAcHz), which is easily excreted (Erwin et al. 2019). The acetylation rate differs among individuals due to genetic polymorphisms of the NAT2 gene, resulting in fast, intermediate, and slow acetylator or metabolizer phenotypes. This interindividual variability in acetylation impacts the plasma levels and efficacy of isoniazid. The apparent elimination half-life ranges from 2 to 6 hours (Parkin et al. 1997). Moreover, the NAT-2 polymorphism impacts the patient's susceptibility to isoniazid-induced hepatotoxicity. It has been shown that slow acetylators are at increased risk of toxicity compared to other acetylators (P.-Y. Wang et al. 2012). Approximately 80% of isoniazid's metabolites are excreted in

urine. Less than 10% of oral isoniazid is excreted in faeces and may also be excreted in breast milk (Erwin et al. 2019).

Pyrazinamide

Pyrazinamide is a synthetic nicotinamide analogue first synthesised in the 1930s, but whose antitubercular activity was only discovered in 1952. It is effective in killing slowly or intermittently metabolising semi-dormant bacterial cells that other TB drugs fail to kill (Y. Zhang et al. 2014; Wilkins et al. 2006). Pyrazinamide plays a critical role in shortening TB therapy down to 6 months (Fox, Ellard, and Mitchison 1999).

Mechanism of action:

Pyrazinamide is a prodrug which is converted to its active form, pyrazinoic acid (POA), in the mycobacterial cell by nicotinamidase (PncA). Although the exact mechanism of action of POA is still debated, a recent study showed that POA is a protonphore that demonstrates pH-dependent inhibition of mycobacterial growth (Fontes et al. 2024). Protonphores are molecules that disrupt the normal function of cellular membranes by moving protons (H^+ ions) across them. In simpler terms, they act as "proton shuttles" that mess up the balance of protons inside and outside a cell, particularly across the membrane of structures like mitochondria or bacterial cells (Nicholls and Ferguson 2013). Additionally, POA may disrupt membrane transport and inhibit fatty acid synthesis, further compromising bacterial viability (Y. Zhang et al. 2014). The primary adverse effect is hepatotoxicity, which becomes more severe with higher doses (>3.0 g) and extended use (Y. Zhang et al. 2014).

Pharmacokinetics:

Pyrazinamide is well-absorbed from the gastrointestinal tract following oral administration and reaches maximum concentration within an hour (Lacroix et al. 1989). Food may delay absorption, but it does not affect bioavailability (Peloquin et al. 1998). In the liver, pyrazinamide is metabolised by the microsomal deamidase enzyme to POA and 5-hydroxypyrazinamide via xanthine oxidase, which are further metabolised to 5-hydroxypyrazinoic acid (Lacroix et al. 1989) . The plasma protein binding for pyrazinamide is ~20%. In the liver, pyrazinamide is mainly metabolised to pyrazinoic acid via microsomal deamidase and 5-hydroxypyrazinamide via xanthine oxidase, which are further metabolised to 5-hydroxypyrazinoic acid. These metabolites are mainly cleared renally. The elimination half-life is ~9 hours. (Sarkar, Ganguly, and Sunwoo 2017; Egelund, Alsultan, and Peloquin 2015).

Linezolid

Linezolid is the first member of a more novel class of antibiotics called oxazolidinones to be approved by the FDA in the year 2000 for a variety of infections including pneumonia and skin and soft tissue infections (Hashemian, Farhadi, and Ganjparvar 2018). Linezolid is also effective against Mycobacterium tuberculosis and is an important addition to TB treatment drug regimens, particularly against drug-resistant strains thanks to its mechanism of action that is unique to first-line antibiotics (Wasserman, Meintjes, and Maartens 2016; Leach et al. 2011). Furthermore, linezolid holds promise for TBM treatment (Wasserman et al. 2019). The most used dosage of linezolid for TB is 600 mg daily although some patients require a dose reduction to 300 mg daily (Maartens and Benson 2015).

Mechanism of action:

Linezolid works by inhibiting the process of bacterial protein synthesis. It binds to the bacterial 23S ribosomal RNA (rRNA) peptidyl transferase centre (PTC) of the 50S ribosomal subunit, impeding the formation of the complex crucial for protein synthesis in bacterial cells. By disrupting this process, linezolid suppresses bacterial growth, eventually causing bacterial cell death (Fermeli et al. 2020; Leach et al. 2011).

The use of linezolid in TB treatments is limited by its dose-dependent toxicity (Wasserman et al. 2022). Nearly half of patients treated with linezolid suffer from linezolid-induced adverse events. The most common major adverse effects that result in drug discontinuation or interruption are peripheral neuropathy and anaemia. Other adverse effects include gastrointestinal disturbances, optical neuropathy, thrombocytopenia, and leucopoenia (X. Zhang et al. 2015). The mechanisms of toxicity are not fully known but one proposed mechanism is its binding to human mitochondrial 16S rRNA, which is structurally similar to the *Mtb* target site. Genetic polymorphisms in mitochondrial DNA among other factors such as age and sex are possible predictors of linezolid toxicity (Wasserman et al. 2022; Palenzuela et al. 2005).

Pharmacokinetics:

In healthy volunteers, orally administered linezolid is well absorbed with bioavailability approaching 100%, which means that no dosage adjustment is required when switching between intravenous (IV) and oral administration. Bioavailability is not affected by food (i.e., can be administered with or without food)

(Leach et al. 2011; Paladino 2002). Peak concentrations are reached 0.5 – 2 hours post-dose, which are slightly longer with food. At steady-state, peak plasma concentrations are 25 – 27 mg/L. Linezolid is widely distributed in well-perfused tissues, with a volume of distribution ranging from 40 to 50 L. The plasma protein binding of linezolid is 31% and it is independent of linezolid concentration (Dryden 2011).

Plasma terminal half-life is 3.4 – 7.4 hours (Dryden 2011; Paladino 2002). Approximately 65% of the dose undergoes non-enzymatic oxidative metabolism, producing two pharmacologically inactive metabolites: aminoethoxyacetic acid (metabolite A) and hydroxyethyl glycine (metabolite B), while the rest of the amount is excreted renally unchanged (Dryden 2011; Tan and Yogev 2008). Linezolid is not metabolised by cytochrome P450, nor does it inhibit it (Leach et al. 2011). A small degree of nonlinearity was observed, with a 30% reduction in clearance following a five-fold increase in dosage. However, this nonlinearity is inconsequential within the therapeutic dosage range (Stalker and Jungbluth 2003).

The linezolid MIC ranged from 0.125 to 1 mg/L for *Mtb*. PK/PD goals have been established for linezolid, with a target of $AUC_{0\text{-}24}$ of 119 mg/L/h for efficacy and a C_{min} of 1.38 mg/L for safety (Millard et al. 2018).

Treatment optimisation challenges

Treatment success rates have improved over the past years to 88% for people with drug-susceptible TB (World Health Organization (WHO) 2023). Despite advancements in prevention, diagnosis, and treatment, several challenges persist.

Some of the challenges addressed by the work presented in this thesis are discussed here.

Adherence

Medication adherence refers to the process in which patients follow their prescribed medication regimen as directed (Peh et al. 2021). Adherence to the long course of TB treatment is a complex behaviour influenced by the interaction of various factors, including disease-related, treatment-related, patient-related social and economic factors, and healthcare-related aspects (Peh et al. 2021; Munro et al. 2007). The lengthy treatment period in addition to the high pill burden of the different TB regimens dramatically affects medication adherence. This issue is more pronounced for TB preventive compared to cure treatments because individuals do not suffer from any symptoms, but instead may experience some of the adverse effects of the drugs that necessitate treatment interruption or even discontinuation (Peh et al. 2021; Munro et al. 2007). Adverse effects such as hepatitis, dyspepsia, and arthralgia led to the discontinuation of therapy in up to 23% of TB patients during the intensive phase (Schaberg, Rebhan, and Lode 1996) and up to 50% of TB patients fail to complete their treatment (Munro et al. 2007).

Poor adherence increases the risk of prolonged infectiousness and hence ongoing transmission in the community, disease relapse, treatment failure, and the development or worsening of drug resistance (Alipanah et al. 2018; Volmink and Garner 2008). The development of drug-resistant TB strains is a particularly devastating consequence that further complicates TB treatment. There are about half a million drug-resistant TB cases annually (Monedero-Recuero et al. 2021). It is

the leading cause of death related to antimicrobial resistance worldwide. The first United Nations High-Level Meeting (UNHLM) on TB declared DR-TB a global public health priority in 2018 (Monedero-Recuero et al. 2021).

The WHO recommends that national TB control programmes provide supervision and support for all TB patients to ensure completion of the full course of therapy The WHO advises national TB control programs to oversee and assist all TB patients, ensuring they complete the full course of treatment (World Health Organization 2022b) . The most internationally promoted strategy is the DOT (directly observed treatment) strategy which seeks to improve adherence through health workers, family or community members directly observing patients taking their medication. However, studies conducted in many countries concluded that DOT provides no advantage over self-administered treatment for cure or treatment completion in people receiving treatment for TB (Volmink and Garner 2008).

Treatment in hospitalised and/or critically ill patients

Despite treatment, the mortality rate among TB/HIV patients hospitalised due to a severe case of TB/HIV remains high (11% to 32%). Most of these fatalities happen within 2 weeks, typically occurring 4 or 5 days after hospital admission, with half of the deaths occurring in patients receiving TB therapy (Schutz et al. 2020). Hospitalised TB/HIV patients typically exhibit manifestations akin to bacterial sepsis, including increased venous lactate levels and compromised intestinal barrier. This leads to microbial translocation and increased circulating levels of lipopolysaccharide, triggering an inflammatory reaction (Subbarao et al. 2015; Brenchley et al. 2006).

Hospitalised patients or critically ill patients exhibit several pathophysiological differences from ambulatory patients. These changes could affect the pharmacokinetics of antitubercular drugs, and hence drug exposure levels, which could negatively impact treatment outcomes in these vulnerable patients. Factors such as altered metabolism, changes in organ function, fluid shifts, and drug-drug interactions can all influence how these drugs are absorbed, distributed, metabolised, and excreted in the body. Severely ill patients have been observed to have alterations in gastric pH, delayed gastric emptying, modifications in plasma protein binding, increased volume of distribution, and changes in the intrinsic activity of drug-metabolising enzymes or hepatic blood flow, which may influence drug clearance (Roberts and Hall 2013; Parsons 1977; Blot, Pea, and Lipman 2014). As also noted by Svensson et al., the distribution volume can change over treatment. A 19% lower volume of distribution was observed in TBM patients on day 12 versus day 2 of the study (E. M. Svensson et al. 2020).Other conditions, such as hepatic or renal impairment, may also impact antitubercular drug concentrations. For example, rifampicin concentrations are higher in patients with hepatic impairment since rifampicin is mainly metabolised by the liver (Donald, Maritz, and Diacon 2011). Another example is critically ill patients having higher levels of free linezolid associated with hypalbuminaemia, decreased renal clearance with low body weight and significantly increased inter-patient variability (Millard et al. 2018). Furthermore, because hospitalised patients often receive multiple medications to manage their underlying conditions, potential drug-drug interactions must be carefully evaluated to avoid adverse effects or reduced

effectiveness of antitubercular therapy. Therefore, understanding antitubercular pharmacokinetics and exposure levels in patients hospitalised due to TB is crucial in lowering mortality rates in this cohort. Therefore, TB therapies need to investigate and account for hospitalisation (Kyeyune et al. 2010; Schutz et al. 2020).

Drug penetration into the CNS

The currently prescribed TBM treatment regimen is derived from the treatment established for pulmonary TB, which is not ideal as it probably results in suboptimal levels of antitubercular drugs in the CNS (Wasserman et al. 2019).

Antitubercular drugs for TBM must navigate through the protective barriers, the BBB and the BCSFB. These barriers present a significant therapeutic obstacle by restricting the passage of drugs into the CNS (Pardridge 2012). Drugs can cross these barriers passively, depending on their molecular size and lipophilicity. Moreover, there are active transporters present at the BBB, the BCSFB, and on the membrane of the brain parenchyma that control the passage of drug molecules to the CNS. Various active transport proteins, including efflux pumps, help regulate drug entry into the CNS by expelling drugs back into the blood and CSF. The distribution of these transporters and their expression levels also play a crucial role in determining drug penetration into the brain (Litjens, Aarnoutse, and te Brake 2020; Yamamoto, Danhof, and de Lange 2017). The central nervous system is not a single pharmacokinetic compartment due to the distinct properties of the blood-brain barrier (BBB) and blood-cerebrospinal fluid barrier (BCSFB). There are differences in the expression of drug transporters and permeability across the BBB and the BCSFB, which may lead to heterogeneous drug distribution. Consequently,

drug concentrations can vary markedly between sites, such as between ventricular and lumbar CSF samples. Additionally, TBM patients with hydrocephalus and increased intracranial pressure who require some neurosurgical procedures may even exhibit greater discrepancies in drug distribution.

Furthermore, changes in membrane permeability and protein concentrations associated with TBM can greatly affect the ability of drug molecules to penetrate the CNS tissues (Pardridge 2012). Besides, the quantity and anatomical distribution of the bacilli and their changes over time with treatment are poorly characterised in TBM, which affects their likelihood of being eradicated by antitubercular drugs (Cresswell et al. 2019). These factors add to the complexity of establishing targets and improving TBM treatments.

Another challenge when investigating CNS drug pharmacokinetics and exposures is the infeasibility of obtaining human drug target site concentration in the brain and CNS tissues. To obtain this information, a combination of in vitro, ex vivo, in vivo, and in silico approaches is required (Yamamoto, Danhof, and de Lange 2017). The microdialysis (MD) technique offers a unique opportunity to sample the interstitial fluid of tissues and organs such as the brain. It involves the placement of a semi-permeable dialysis catheter in the tissue (Loxton et al. 2021). MD is a semi-quantitative method that measures only free drug concentrations. However, interpreting drug concentrations in MD samples has a few shortcomings. It is difficult to determine the relative recovery rate in the microdialysate from tissue ECF, i.e., what percentage of the actual concentration in the tissue is retrieved in the MD samples. Additionally, TBM is characterised by perfusion differences due to

variable small and large vessel disease which leads to a highly variable drug distribution in the brain hence the location of the MD probe influences the concentration observed. Other parameters of the MD process such as dialysate flow rate, and size of pore are essential to optimising relative recovery of the drug and need to be tested before sample collection (Rohlwink et al. 2016; Elizabeth C.M. De Lange 2013; Ruiz-Bedoya et al. 2022).

There is limited information on the extent to which antitubercular drugs can cross the protective barriers and reach the CNS, the site of disease. The dosing and duration of nearly all anti-TB drug combinations have not been pharmacokinetically optimized for TBM treatment, and their dose-response relationships remain unclear (Litjens, Aarnoutse, and te Brake 2020; Cresswell et al. 2019). Nonetheless, several clinical trials are underway to optimize TBM treatment regimens (Wasserman et al. 2019).

Drug interactions

A drug interaction arises when a patient's response to a drug is altered by various factors such as food, nutritional supplements, medical conditions, or other drugs. Interactions between drugs (drug-drug interactions) may be beneficial or harmful. Pharmacokinetic drug-drug interactions happen when one drug (the perpetrator) affects the concentration of another drug (the object), leading to clinically significant effects. That could occur by altering the drug's bioavailability, absorption, distribution, metabolism, or excretion (Snyder, Polasek, and Doogue 2012)

Drug-drug interactions (DDIs) pose a considerable challenge in the treatment of patients co-infected with tuberculosis (TB) and HIV. Both diseases

require complex medication regimens, often involving multiple drugs taken concurrently. TB treatment typically consists of several antibiotics, such as rifampicin, while HIV treatment relies on antiretroviral therapy (ART). However, many of these drugs are metabolised by the same cytochrome P450 enzymes in the liver, leading to potential interactions that can alter drug concentrations and efficacy. The interactions between PIs and rifamycins are more extensive and require dose adjustments (Helen McIlleron and Khoo 2011).

For instance, rifampicin, the cornerstone of TB treatment, is notoriously responsible for many drug-drug interactions because it is a potent inducer of many metabolising enzymes, mainly the CYP 450 which can accelerate the metabolism of certain antiretrovirals, compromising HIV control. In addition, it is a substrate of the P-glycoprotein (P-gp), an efflux pump. If rifampicin induces P-glycoprotein activity, it can lead to a decrease in the therapeutic effectiveness of the drug as more of it is pumped out of cells. The discovery of the role of P-gp is relatively recent, suggesting that the potential for P-gp-mediated drug interactions may have been underestimated in the past. Both P-gp and CYP3A4 are implicated in many drug interactions because they share substrate specificity and have similar inhibitors and inducers. For example, a drug that induces CYP3A4 is likely to induce P-gp as well (J. Chen and Raymond 2006). Conversely, some antiretrovirals inhibit these metabolising enzymes, leading to increased levels of TB medications and potential toxicity.

Drug-disease interactions are also a possibility in TB patients living with HIV. For example, some studies have ascribed reductions in rifampicin bioavailability of

32– 50% to HIV infection. Patients with advanced HIV infection may have reduced antitubercular drug exposures as a result of the malabsorption caused by HIV-associated enteropathy and higher susceptibility to enteric infections (Helen McIlleron and Khoo 2011). On the other hand, other studies have not concluded the same, emphasizing the need for consistent and homogeneous studies to be conducted (Daskapan et al. 2019). Therefore, careful consideration and monitoring of drug regimens are essential to optimize treatment outcomes and minimize adverse effects in TB/HIV co-infected patients.

Dose optimization in children

Young children are highly susceptible to severe forms of tuberculosis and its rapid progression to active disease, necessitating treatment regimens as effective as those for adults. But development of first-line antitubercular drugs primarily focused on adult forms of the disease, leading to recommendations and dosages for childhood TB that mimic those for adults, with little consideration given to the impact of HIV infection on drug concentrations in children. Studies have shown that dosing recommendations based on adults often result in lower serum concentrations of antituberculosis agents compared to adults receiving identical mg/kg dosages. On top of that, concerned clinicians may opt for dosages at the lower end of recommended ranges in children to mitigate adverse reactions. This underscores the need for investigating and optimizing TB dosing in children (Donald, Maritz, and Diacon 2011; Helen McIlleron and Khoo 2011).

Thesis justification

TB, including its most debilitating and lethal form TBM, continues to be a major global health concern, with millions of new cases diagnosed annually. Despite medical advancements, TB continues to have formidable health and economic burdens worldwide. In response to these challenges, the World Health Organization (WHO) launched the "End TB" strategy, aiming to eliminate the global TB epidemic by 2030 as part of the United Nations newly established Sustainable Development Goals (World Health Organization (WHO) 2023).

To achieve this goal, there is a need to address the challenges faced in TB and TBM prevention and cure. These challenges include poor adherence, drug interactions, treatment in hospitalised patients and optimising treatment regimens for TBM, especially in children. Preventing TB in PLWHIV can be challenging because of the complex treatment regimens that include many medications both antiretrovirals plus antitubercular drugs. This complex regimen leads to poor adherence, and hence an increased risk of developing active TB. TB treatment regimens also need to be screened for potential drug-drug interactions, particularly when taken with ARTs. Additionally, research into the pharmacokinetics of antitubercular drugs in hospitalised or critically ill patients is needed to offer important insights to inform clinical decisions and enhance treatment strategies in this population, among whom the mortality rates are higher than their outpatient counterparts (Schutz et al. 2020).

Another major challenge is addressing the inadequacy of regimens based on pulmonary TB to achieve optimal exposure to antitubercular drugs at the site of

disease, the CNS. Treatment regimens need to be specifically tailored for the case of TBM, particularly in children and infants. One of the strategies currently pursued in TBM clinical trials is testing higher doses of rifampicin in children and adults which could help shorten treatment periods. Higher doses of rifampicin, up to 35 mg/kg/day have been observed to be safe in previous clinical studies (Aarnoutse et al. 2017). Another approach being investigated is the incorporation of linezolid in TBM treatment regimens. Linezolid is a potent antibiotic with a narrow therapeutic range. There are several endeavours to find the optimal dose and treatment duration that achieve this intricate balance between maximising efficacy and minimising toxicity.

Pharmacometrics has proven to be a very helpful instrument in addressing the research gaps and answering questions on how to optimize TB regimens for different populations. It is extremely efficient in analysing data from pharmacokinetic studies, including ones with sparse sampling, and helping in identifying sources of variability in population parameters and exploring the effects of patient characteristics such as weight, HIV co-infection, etc. Furthermore, by using a model, you can ascribe drug effects to physiological processes, incorporating a semi-physiological approach that can generate new hypotheses. This not only enhances understanding but also allows for simulations and, to some extent, extrapolation. As a result, modelling becomes a powerful tool for predicting outcomes and guiding further research.

Objectives

The general aim of this thesis is to optimise the treatment of TB and TBM employing population pharmacokinetic modelling, also known as, nonlinear mixed-effects modelling (NLME) modelling and using data from studies conducted in adults and children with TB and TBM. The specific objectives are:

- Exploring the utility of pharmacometric modelling and simulation to monitor adherence to TB preventative therapy in PLWHIV.
- Characterise the population PKs of rifampicin, isoniazid, and pyrazinamide in hospitalised TB patients, and investigate if and how they differ from their outpatient counterparts.
- Explore the extent of rifampicin distribution and exposure in lumbar CSF, ventricular CSF, brain ECF, and plasma in children with TBM.
- Explore the extent of rifampicin distribution and exposure in CSF and plasma in adults with TBM.
- Explore the extent of linezolid distribution and exposure in CSF and plasma in adults with TBM.

Chapter 2 : Methodology

Study Designs and Data

This section provides descriptions of the studies, and the data obtained from them used in this thesis. This includes 4 studies carried out in adult or paediatric participants on TB or TBM preventative or treatment regimens . Their details are shown below.

NWCS 440 (a REMEMBER sub-study, ACTG A5274)

The 'Reducing Early Mortality and Early Morbidity by Empiric Tuberculosis Treatment Regimens (REMEMBER)' study was a multi-country randomised clinical study conducted in HIV-positive outpatients initiating antiretroviral therapy with CD4 cell counts of less than 50 cells per μL to compare the survival probabilities of two TPT regimens: isoniazid versus the empirical 4-drug combination treatment. Counterintuitively, the TB incidence rate was higher in the empirical therapy arm than in the monotherapy arm ($p = 0.01$) (Hosseinipour et al. 2016). This prompted the question of whether poor adherence to the medication regimen contributed to the higher TB incidence rate. Therefore, a case-control study was designed to assess medication adherence based on TB medication exposure within the 4-drug combination treatment arm. The assessment was done based on the exposure of rifampicin and pyrazinamide only; isoniazid was excluded due to its short plasma half-life. Participants from the 4-drug combination treatment arm were included in this sub-study (NWCS 440). The participants with confirmed, probable, or clinical diagnosis of pulmonary or extra-pulmonary TB by week 48 (cases) were matched

with participants from the empirical treatment arm without confirmed, probable, or clinical diagnosis of pulmonary or extra-pulmonary TB by week 48 (controls). The case-control matching was done by weight and sex in the ratio of 1:4, i.e. each case was matched with 4 controls. Matching was done according to the method described by Wang (Z. Wang 2012). Only participants who had at least two out of three samples collected at visits on weeks 2, 4, and 8 of the parent study were included. All participants provided written informed consent. Sites obtained ethical approval from local ethics committees.

Pyrazinamide and rifampicin concentrations were quantified in stored plasma samples using a validated liquid chromatography-tandem mass spectrometry (LC-MS) method. The lower limits of quantification were 0.203 µg/mL and 0.075 µg/mL for pyrazinamide and rifampicin, respectively.

KDHTB study

This study aims to investigate the difference in pharmacokinetics and exposures of the antitubercular drugs: rifampicin, isoniazid, and pyrazinamide between hospitalised TB patients and TB outpatients. The study population consisted of two groups: the hospitalised patients and outpatients recruited as controls. The hospitalised study population for this pharmacokinetic (PK) sub-study was a subset of participants enrolled for an observational cohort study investigating the mortality causes in hospitalised TB/HIV patients carried out between November 2014 and November 2016 (Schutz et al. 2020). Patients presenting to Khayelitsha Hospital in Cape Town, South Africa with HIV who needed hospitalisation due to a suspected diagnosis of pulmonary or extrapulmonary TB (i.e., who were too ill to receive initial

treatment as outpatients) and who survived to the third day of TB treatment were enrolled sequentially, as long as they still needed inpatient care and did not require transfer to a tertiary care facility for intensive care or investigations. The study team invited eligible hospitalised patients in the parent study to take part and discussed the study with them. TB outpatients with or without HIV were recruited consecutively from around the same hospital catchment area as controls. Both outpatients with and without HIV were included in the study for logistical reasons. The study team liaised with the clinic staff to ask any new patients when they were started on TB treatment if they would like to discuss taking part in the PK sub-study.

All participants received a once-daily dosing of antitubercular drugs that were given as 4-drug fixed-dose combination (FDC) tablets containing rifampicin, isoniazid, pyrazinamide, and ethambutol at 150/75/400/275 mg, which were either Rifafour e-275 tablets (SANOFI) or Ritib tablets (PHARMACARE)). The number of tablets to be given to each participant is determined based on their weight according to the weight-based dosing of the South African national TB management guidelines outlined in Table 2.1. Clinical data and baseline blood tests were obtained at enrolment. The 12-week mortality outcome was documented for hospitalised patients. None of the study participants were comatose.

Table 2.1: Summary of weight band-based doses in the KDHTB study

Pre-treatment body weight (kg)	**No. of RHZE FDC[a] tablets (150/75/400/275 mg) during intensive treatment phase (daily dose for 2 months)**
30 – 37	2
38 – 54	3

55 -70	4
> 70	5

[a] RHZE FDC: rifampicin, isoniazid, pyrazinamide, and ethambutol fixed-dose combination.

A total of 25 participants (5 outpatients and 20 hospitalised patients) were on ART therapy. While a complete, detailed record of the ART regimen was not available for all participants, we specifically highlighted individual ART drugs with potential DDIs with anti-TB drugs. These included efavirenz (n=9), tenofovir (n=9), lopinavir/ritonavir (n=1), and lamivudine (n=1).

Patient characteristics such as age, sex, weight, height, and details of concomitant medications were collected, and a complete medical history was recorded. Serum chemistry and a complete blood picture were carried out at the Groote Schuur National Health Laboratory Services on each participant on samples taken at enrolment for the PK study. The study was approved by the University of Cape Town Human Research Ethics Committee (UCT HREC reference: 057/2013) on 12 April 2013. All participants signed an informed consent form.

Participants were scheduled for a PK visit during their third day of treatment when blood samples were drawn just before and 1, 2.5, 4, 6, and 8 hours after dose. Participants were required to fast overnight, and they were given a standardized breakfast after the 1-hour sample and a standardized lunch between the 4- and 6-hour sample.

Immediately following their collection, samples were put in an ice bath until being centrifuged in a cooling centrifuge and later stored at -80°C. Plasma rifampicin, isoniazid and pyrazinamide concentrations were determined by validated liquid chromatography with tandem mass spectrometry assays at the

Division of Clinical Pharmacology, University of Cape Town (Smith, van Dyk, and Fredericks 1999). The lower limit of quantification (LLOQ) was 0.117 mg/L for rifampicin, 0.105 mg/L for isoniazid, and 0.203 mg/L for pyrazinamide. The accuracy of the low-, medium-, and high-quality control samples ranged between 99.7% - 100.8% for rifampicin, 98.3% - 100.4% for isoniazid, and 88.1% and 92.3% for pyrazinamide. The precision of the quality control samples ranged from 4.7 – 7.7%, 3.0% - 5.1%, and 2.9% - 3.6% for rifampicin, isoniazid, and pyrazinamide, respectively (Schutz et al. 2020).

Red Cross TBM study

The objective of this study is to characterize the pharmacokinetics of rifampicin in the cerebrospinal fluid and brain extracellular fluid in South African children with TBM. This study enrolled children presenting with definite or probable TBM to the Red Cross War Memorial Children's Hospital in Cape Town, South Africa between January 2017 and September 2019. Clinical management of all participants was done according to standard institutional protocol (A. A. Figaji and Fieggen 2010). All procedures were done for clinical management purposes, and none were carried out solely for research purposes.

The patients were categorized into two groups: (i) patients who underwent neurosurgical procedures to manage TBM hydrocephalus (HCP) and (ii) patients who presented with lowered levels of consciousness, had invasive monitoring with MD, and had placement of external ventricular drain (EVD) that was part of the institutional protocol for urgent decrease of intracranial pressure. Brain

microdialysis was used in critically ill patients to guide therapy based on changes in brain chemistry due to cerebral ischemia (A. A. Figaji and Fieggen 2010).

The study participants were administered the Western Cape regimen that is routinely used in South Africa that comprises rifampicin (20 mg/kg), isoniazid (15-20 mg/kg), pyrazinamide (40 mg/kg), and ethionamide (20 mg/kg) for 2 months followed a 4-months continuation phase of RIF and INH, according to weight-band based dosing. The antitubercular drugs were administered either orally or via a nasogastric tube. Plasma samples were collected on a single day in the first and second week, and whenever possible at 2-, 4-, and 6 hours post-dose. Clinically indicated lumbar and/or ventricular CSF samples were collected at random time points, from procedures in published protocols.

Lumbar and Ventricular CSF: Clinically indicated CSF samples were collected at random time points, from procedures in published protocols (A. A. Figaji and Fieggen 2010), up to 24 hours post-dose into sterile 15-mL tubes and kept on ice. Ventricular CSF samples were taken either at the placement of a ventriculoperitoneal shunt or an external ventricular drain or when clinically indicated from an indwelling external ventricular drain. Lumbar CSF samples were taken either as a diagnostic procedure or for medical therapy of raised intracranial pressure related to hydrocephalus.

Brain ECF using microdialysis technique: A microdialysis catheter with a 100-kDa membrane was placed concurrently with the primary ventricular drain and monitored into the same region (usually right frontal white matter) or sometimes on the side where hypodensity was more prominent on the initial head computed

tomography scan. Microdialysis vials were changed at hourly intervals and analysed at the bedside for clinical purposes. As microdialysis volumes are typically small, remnant hourly samples were pooled over 2–3-hour epochs to ensure sufficient volumes for analysis. Concentrations of substances in the microdialysate are a percentage of the true concentrations in the ECF and not absolute concentrations. This percentage is termed relative recovery.

Total rifampicin was assayed in all samples: plasma, lumbar CSF, ventricular CSF, and brain ECF. Additionally, rifampicin's primary metabolite, 25-desacetyl rifampicin, was assayed in the plasma samples. High-performance liquid chromatography with tandem mass spectrometry detection methods were developed and validated at the Division of Clinical Pharmacology, University of Cape Town for the assays. The method was validated over the ranges 0.117–30.0 µg/mL for rifampicin and 0.0391–10.0 µg/mL for 25-desacetyl-rifampicin in plasma, and 5 to 2500 ng/mL for the rifampicin in CSF and ECF assay.

The study has ethical approval from the University of Cape Town human research ethics committee (UCT HREC 564/2012 and 070/2018). Hospital clearance was obtained from the Western Cape Department of Health. Additionally, the parents or legal guardians of all participants provided informed consent on their behalf.

LASER-TBM study

LASER-TBM is a parallel, randomized, multi-arm, phase 2A clinical trial to evaluate the safety of high-dose rifampicin plus linezolid with or without aspirin for the treatment of TBM in HIV-infected adults. Participants were recruited from four public

hospitals in South Africa and randomized into one of three arms (one control arm and two experimental arms) in the ratio 1.4:1:1. The control arm received the standard RHZE regimen which consists of FDC oral tablets (rifampicin 10 mg/kg, isoniazid 5 mg/kg, pyrazinamide 25 mg/kg, and ethambutol 15 mg/kg) daily according to the WHO weight bands. Participants in the experimental arms received the standard RHZE regimen, plus an additional dose of rifampicin (total oral rifampicin dose 35 mg/kg/day according to weight band dosing (Wasserman et al. 2021)), in addition to linezolid with or without aspirin. They also underwent another randomization to receive either high-dose oral (35 mg/kg) or IV (20 mg/kg) rifampicin for the first 3 days of treatment. After day 3, all participants in the experimental arms continued high-dose rifampicin orally until the end of the study. The high-dose oral rifampicin was administered as standard fixed-dose combination (FDC) tablets topped up with individual rifampicin tablets using bespoke weight bands (Wasserman et al. 2021). Those randomized to IV rifampicin received the full rifampicin dose intravenously (20 mg/kg) as a one-hour infusion. Linezolid was administered at 1200 mg once daily for the first 28 days, then reduced to 600 mg once daily until the end of the study. All participants received adjunctive dexamethasone as per standard practice. The study treatment was provided for 56 days in all arms, after which participants were referred to public sector facilities to complete standard therapy for HIV-associated TBM (Wasserman et al. 2021).

Over the study period, there were six scheduled study visits. Pharmacokinetic sampling was scheduled on two of these visits: on Day 3 (±2 days) and Day 28 (±2 days) of study enrolment. Blood samples were withdrawn pre-dose and at 0.5, 1, 2,

3, 6, 8-10, 24 hours post-dose on Day 3. While on the second visit on day 28, sampling was done pre-dose and at 2-, and 4-hours post-dose. One lumbar CSF sample was withdrawn on each PK visit. The timepoint of the CSF sample was randomized to be in one of the following intervals: 1-3, 3-6, 6-10, and 24 hours after dosing. The study design and sampling schedule are depicted in Figure 2.1 and Figure 2.2. The complete study protocol has been published (Davis et al. 2021). The LASER-TBM study was approved by the University of Cape Town Human Research Ethics Committee (UCT HREC reference: 293/2018), Walter Sisulu University (HREC reference: 012/2019), and the South African Health Products Regulatory Authority (reference number 20180622). The trial is registered on clinicaltrials.gov (NCT03927313) (Wasserman et al. 2021).

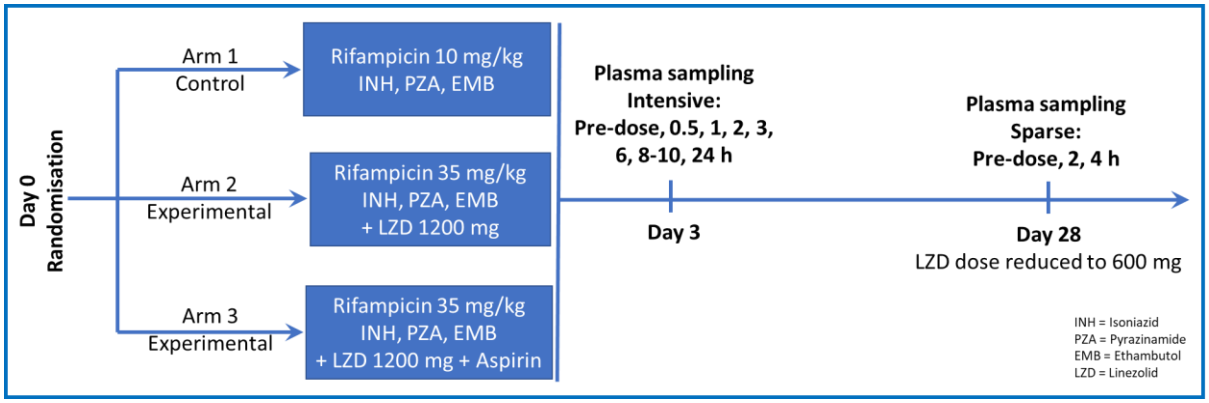

Figure 2.1: LASER-TBM study design

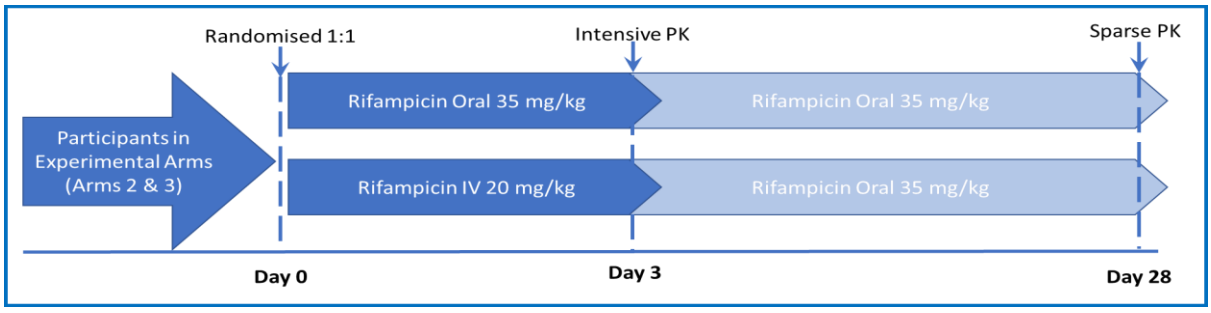

Figure 2.2: LASER-TBM study randomization for rifampicin route of administration

Samples were immediately placed on ice following collection till processing and later stored at -80°C. Total rifampicin, isoniazid, pyrazinamide, and linezolid concentrations were quantified in all collected plasma and CSF samples. Free rifampicin, isoniazid, pyrazinamide, and linezolid concentrations were measured in a subset of the participants' samples. Drug quantification was done using a validated liquid chromatography-tandem mass spectrometry assay developed at the Division of Clinical Pharmacology, University of Cape Town. Additionally, total protein, albumin, and glucose were analysed in CSF samples.

For the protein-unbound drug analysis, absolute recovery and reproducibility were thoroughly evaluated and met international bioanalytical guidelines. The validated method incorporates tight low-temperature handling and neutral pH during the critical ultracentrifugation step, with stability experiments confirming that these conditions successfully preserve the drug–protein binding equilibrium throughout sample work-up. Recovery and reproducibility of the ultracentrifugation step were demonstrated through recovery, matrix, stability, and carryover experiments. QC samples concentrations were set by spiking known amounts of the drug into blank plasma before ultracentrifugation, and their accuracy was continuously verified. Absolute in vivo protein binding cannot be measured directly; laboratory methods (ultracentrifugation, equilibrium dialysis, ultrafiltration) provide an in vitro estimate under defined conditions. Uncertainty is managed in the ultracentrifugation protocol, which is designed to freeze the in-sample equilibrium (low temperature, no pH change, long centrifugal field) and to minimise re-binding by removing only the protein-free layer. Observed unbound

fractions for linezolid after the harshest stress test (six freeze-thaws) still lie within the 68-96 % range expected from the clinical literature, suggesting that the method does not artificially displace drug from proteins. Therefore, while the exact in vivo binding remains uncertain, the validation data show that the assay yields a precise and unbiased estimate of the unbound concentration under controlled conditions, and QC samples continuously check that this performance is maintained.

Pharmacometrics

Pharmacometrics is described as "the science of developing and applying mathematical and statistical models to characterise, understand, and predict a drug's pharmacokinetic, pharmacodynamic, and biomarker-outcomes behaviour". Essentially, pharmacometrics can be dubbed "the science of quantitative pharmacology" (Ette and Williams 2007). In pharmacometrics, models can be categorised into 2 main groups: pharmacokinetic (PK) models and pharmacodynamic (PD) models. PK models describe the relationship between drug concentrations in the body versus time. PD models describe the relationship between drug concentration in the body and the drug effect - whether desired or undesired - that may be evaluated using a biomarker or a clinical endpoint, combined PKPD models, and disease progression models which describe the time course of disease effects (D. R. Mould and Upton 2012). The most used modelling approach in pharmacometrics is NLME, a statistical approach that is also known as population modelling. In this thesis, NLME was employed to characterise the PK of rifampicin, isoniazid, pyrazinamide, and linezolid, however, other statistical approaches were applied to model other data.

Nonlinear mixed-effects modelling approach

The NLME modelling (also referred to as population modelling) approach is a mathematical and statistical framework that allows for analysing data from repeated observations from different subjects in a population. "Nonlinear" refers to the fact that the dependent variable (e.g., concentration) is nonlinearly related to the model parameters and independent variable(s) and the term 'mixed' refers to a model that incorporates both fixed and random effects. Fixed effects define the typical parameters of the observed data on a population level (i.e., population parameters) and random effects are random variables associated with each subject from a population that describe the variability within the data such as the between-subject and within-subject variability (D. R. Mould and Upton 2012) .

Using population modelling offers several advantages compared to traditional non-compartmental analysis: it allows for the analysis of sparse data, the integration of data from various studies, the utilisation of prior knowledge, enhanced statistical power, and it is well-suited for dose individualisation (Bonate 2013).

Model building blocks

An NLME model or a population model is usually comprised of a structural model, a stochastic or statistical model and a covariate model.

1) Structural model

The structural model defines the fixed effects or typical behaviour (typical concentration time course within the population for PK) which is represented by

algebraic or differential equations. For PK models, the structural model allows the quantitative (mathematical) description of the main PK processes, absorption, distribution, metabolism, and excretion, commonly abbreviated as ADME. The building block of the structural PK model is a 'compartment', which denotes a region in the body in which the drug is well mixed and kinetically homogenous. Movements of the drug between the compartments are described by rate constants. Compartments are typically abstract and do not necessarily represent specific body organs but can sometimes refer to real physiologic spaces in the body, such as the liver (D. R. Mould and Upton 2012).

PK compartment modelling can range from highly empirical to deeply mechanistic approaches. At one end of the spectrum, empirical models rely primarily on observed data without extensively considering underlying physiological processes. On the other end of the spectrum are highly mechanistic models that incorporate intricate descriptions of PK processes, often utilising differential equations derived from physiological principles. Between these extremes, hybrid approaches combine elements of empirical and mechanistic modelling to balance biological realism with practical usability. These models incorporate physiological knowledge while also incorporating simplified or empirical components to enhance computational efficiency or accommodate limitations in data availability (Bonate 2013).

Models can be highly versatile, though most are in general based on interconnected compartments with first-order rate constants. In this thesis, we explored alternative modelling approaches to better address specific aspects of the

data to be studied. In this thesis, we employed more tailored solutions for certain challenges, which will be expanded upon in the following sections.

Hepatic Clearance

Clearance is typically described as a first-order rate process from the central compartment. A more mechanistic or physiological approach to modelling pharmacokinetics can be applied, for example, by describing hepatic extraction. Drugs administered orally must pass through the liver before it reaches the systemic circulation. Hepatic extraction or first-pass effect, the pre-systemic elimination which occurs during the first-pass through the liver. In this case the parameter to be estimated is intrinsic clearance (CL_{int}) instead of oral clearance. CL_{int} is defined as the capacity of the liver to clear the blood from drug in the absence of blood flow limitations (Hedaya 2012).

Saturable elimination

Nonlinear pharmacokinetics are observed when the absorption, distribution, or elimination processes can be saturated at high drug concentrations. At high drug concentrations, saturable processes follow zero-order kinetics.

Drugs that are metabolized or excreted by a saturable pathway can have dose-dependent pharmacokinetics after administration of large doses. If nonlinearity in exposure is observed at higher doses, it can be accounted for by incorporating saturation of clearance (i.e. concentration-dependent clearance) into the model. This is described using the Michaelis-Menten equation:

$$Elimination\ rate = \frac{V_{max}.Cp}{K_m + Cp}$$

where V_{max} is the maximal elimination rate, K_m is the drug plasma concentration at which the elimination rate is half the maximal rate, and Cp is the plasma concentration (Hedaya 2012).

Autoinduction of clearance

Conditions such as enzyme induction, product inhibition, and drug-related pathological changes that affect drug excretion can result in nonlinear pharmacokinetics. Autoinduction can be modelled using a more mechanistic approach such as an enzyme turnover model (Smythe et al. 2012) or a more empirical approach using an exponential maturation function (M T Chirehwa et al. 2015).

Parent-metabolite modelling

A parent-metabolite model is a mathematical representation used to understand the relationship between a drug (the parent compound) and its metabolites within the body. The model typically describes the rates at which the parent compound is converted into its metabolites, as well as the elimination rates of both the parent drug and its metabolites. The simultaneous modelling of parent drug and metabolite provide insights into how drugs are processed and transformed in the body and allows the evaluation of the impact of organ impairment or of the effects of drug-drug interactions aiding in dosing optimisation (Ette and Williams 2007).

The rate of conversion of the parent to the metabolite and the distribution volume of the metabolite are structurally not simultaneously identifiable. Unless the metabolite has been administered alone in order to estimate its volume of distribution or the fraction of the parent drug converted to metabolite is known, the

modelling of the parent drug and its metabolite needs to be simplified so that metabolite parameters can be estimated (Ette and Williams 2007).

Since the parent and metabolite molecules have different molecular weights, a correction factor needs to be included in the model to adjust for the difference in molecular weight. Otherwise, all observations can be converted into molar concentrations (Ette and Williams 2007).

Effect compartment modelling

Effect compartment models, also known as link models, are a type of pharmacokinetic/pharmacodynamic (PK/PD) modelling approach used to describe the delay between drug administration and the onset of pharmacological effect. These models have also been used to model the delays between the central (plasma) compartment and another tissue compartment such as the CSF (Sheiner et al. 1979; Savic et al. 2015). Effect compartments are assumed to have a negligible volume compared to the central compartment, with negligible drug transfer between the two compartments. The following differential equation summarizes the kinetics of the effect compartment:

$$\frac{dC_{Eff}}{dt} = k_{plasma-Eff} \cdot \left(PPC \cdot C_{plasma} - C_{Eff}\right)$$

where C_{plasma} and C_{Eff} are the drug concentration at time t in plasma and effect compartment, respectively. The $k_{plasma-Eff}$ is the first-order equilibration rate constant of the drug between the plasma (i.e. central compartment) and the effect compartment, i.e., how fast the change in plasma is reflected in the effect compartment. A higher $k_{plasma-Eff}$ indicates faster equilibration between the plasma and effect compartment. The PPC is the pseudo-partition coefficient. It

represents the ratio of drug exposure between the CSF and plasma, i.e., the extent of drug CSF penetration. A higher PPC indicates more drug distribution into the CSF (Sheiner et al. 1979; Savic et al. 2015). Figure 7.6 in chapter 7 shows the interpretability of the equilibration rate constant and the PPC in the context of the effect compartment modelling approach.

2) Statistical (stochastic) model

Statistical models describe the random effects, i.e., the random unexplained variability in the observed data. This variability is described on different levels: 1) between-subject variability (BSV), 2) within-subject variability (i.e., within a subject on different occasions or visits) and 3) residual unexplained variability (RUV), which describe the magnitude of unexplained differences between the predicted and observed values of the dependent variable (Owen and Fiedler-kelly 2014).

3) Covariate model

Covariate models explain some of the variability in the data using several factors, mainly participant characteristics, such as weight, or renal function (covariates). When specifying an NLME model, parameter-covariate relationships are defined in the covariate model (Owen and Fiedler-kelly 2014; D. Mould and Upton 2013). Covariates are categorised into continuous (e.g. weight, height), or categorical (e.g. sex, genotype). Categorical covariates may have two or more discrete values. The parameter-covariate relationship is usually described relative to a reference covariate level, while the effect of a continuous covariate is often expressed relative to its median value in the relevant patient population.

Body size descriptors such as weight or fat-free mass are important determinants of disposition parameters. Allometric scaling refers to the application of such descriptors to describe variability in clearance and volume of distribution (Holford and Anderson 2017). Such pharmacokinetic parameters tend to scale with body size but not in a linear manner. The most commonly used function to describe this relationship is the power function as shown below.

$$\theta_i = \theta_p . \left(\frac{W_i}{W_p}\right)^{\alpha}$$

Where θ_i is the individual PK parameter of body mass W_i and θ_p is the standardized individual with body mass W_p and α is an empirically derived constant which is set to 0.75 in the case of flow parameters and 1 in the case of volume parameters (B. J. Anderson and Holford 2008).

Parameter Estimation methods

The construction of pharmacometric models involves the estimation of parameters, along with a measure of uncertainty, that characterise drug behaviour within the body. Parameter estimation involves obtaining the best-fitting values for these parameters based on observed data. Parameter estimation of NLME models requires advanced computer applications of numerical analysis techniques (Owen and Fiedler-kelly 2014). In NLME modelling, the most common parameter estimation method is the maximum likelihood estimation (MLE). MLE seeks to find the set of parameter values that maximizes the likelihood of observing the data at hand given the assumed model. For ease of computation, the maximum likelihood

estimation objective function is typically expressed as the negative sum of the log of the likelihoods, yielding a single number– the maximum likelihood estimation objective function value (OFV). The lowest OFV for a specific model and dataset corresponds to the optimal parameter values. Therefore, instead of maximizing a likelihood function, the OFV is minimised (i.e., the lowest OFV corresponds to the maximum likelihood that is the best fit) (Upton and Mould 2014). While the absolute OFV value holds no significance, it serves as a tool for comparing models by ranking them based on their goodness of fit to the same dataset (D. R. Mould and Upton 2012).

Model building process

The raw data was formatted to be NONMEM® compatible before starting the process of model development. The model building process and covariate inclusion was guided by physiological plausibility, model fit diagnostics, and the drop in the objective function (OFV). The likelihood ratio test for the drop in OFV was used to compare between nested models, assumed to be approximately $\chi 2$ distributed with n degrees of freedom, where n is the number of additional estimated parameters. A p-value of 0.05 was generally used for inclusion and 0.01 for retention of model parameters. Model performance was evaluated by means of visual predictive checks (VPC). The precision of final parameters (95% confidence intervals) was obtained by either by nonparametric bootstrapping or sampling importance resampling (SIR) (A.-G. Dosne, Bergstrand, and Karlsson 2017).

Concentrations below the lower limit of quantification (BLQ) were censored according to Beal's M6 method, in which the last censored value in a series during

the absorption phase and the first censored value in a series in the terminal phase were replaced with LLOQ/2 and the other censored values in a series were discarded (S. L. Beal 2001). To account for the larger level of uncertainty in the imputed censored values, their additive error was inflated by LLOQ/2.

Simulations

Simulations play a crucial role in modelling and simulation frameworks by facilitating the exploration of what-if scenarios and alternative parameter estimates. Simulations allow the inquiry about various study design features or conditions without having to perform an experiment, assessing the potential impact of these scenarios on study outcomes and subsequent decision-making processes. Simulation enables the examination of mechanistic explanations within a system and the effects of interventions, thereby expanding our understanding (Owen and Fiedler-kelly 2014; Bonate 2013). Moreover, simulations have several other important uses, including the demonstration and visualization of various model features and assessment of model performance. For example, simulations are used in the goodness of-fit diagnostic such as the visual predictive check (VPC), which shows how well the model fits the observed data (Owen and Fiedler-kelly 2014).

Other modelling approaches

1) Conditional logistic regression

In a matched case-control study, each case and its corresponding controls are referred to as a "matched set." Conditional logistic regression tests, applied in Chapter 3, analyses the relationship between the outcome (e.g., presence of

disease) and predictor variables (e.g., exposure to a risk factor) within these matched sets while accounting for the matching. Cases are matched with controls based on certain criteria, typically to control for potential confounding variables. Matching ensures that cases and controls are comparable with respect to these characteristics. Conditional logistic regression models the relationship between the outcome and predictor variables within each matched set. It estimates the odds ratios (ORs) indicating the strength of association between the predictor variables and the outcome while adjusting for the matching variables. Hypothesis tests and confidence intervals are used to assess the significance of the associations between predictor variables and the outcome. Conditional logistic regression is particularly useful when dealing with matched case-control studies because it properly accounts for the matched nature of the data, providing valid estimates of association while controlling for confounding by the matching variables (Koletsi and Pandis 2017).

2) Deming regression

Deming regression serves as a valuable statistical tool for analysing data that exhibit errors in both the independent and dependent variables. Unlike traditional regression methods that assume measurement errors only in the dependent variable, Deming regression acknowledges the presence of errors in both variables, offering more accurate parameter estimation. In this thesis, we employed Deming regression to investigate the relationship between free (unbound) and total drug concentrations quantified in the same samples and to estimate the degree of

plasma protein binding (Linnet 1998; Deming 1943). This was applied to unbound drug concentrations in Chapters 6 and 7.

Software

The pharmacometric models presented in this thesis were developed using NONMEM® version 7.4 or 7.5. The main estimation method used was first-order conditional estimation with eta-epsilon interaction (FOCEI) (Beal, Sheiner, Boeckmann, & Bauer, 2013). Perl-speaks-NONMEM® (PsN) 4.9.0 was used to aid in the execution and visualization of results from pharmacometric analyses of NONMEM® results such as creating visual predictive checks (VPCs) and running bootstraps or sampling importance resampling (SIR) (Lindbom, Ribbing, and Jonsson 2004). Pirana software version 3.0.0 was used for model management and tracking (Keizer, Karlsson, and Hooker 2013). R software via the R Studio interface, including the packages 'xpose4' and 'xpose' were used for data management, plotting model diagnostics and generating figures. It was additionally used for carrying out conditional logistic regression testing and Deming regression. Berkeley Madonna version 10.2.8, a mathematical modelling software, was used for simulating typical concentration-time profiles. Computationally intensive modelling and simulation were performed using the University of Cape Town's ICTS High-Performance Computing: https://ucthpc.uct.ac.za/.

Chapter 3 : Pharmacokinetic modelling as a tool for assessing patient adherence: application to anti-tuberculosis therapy in the REMEMBER study

Abstract

Purpose

The Reducing Early Mortality and Early Morbidity by Empiric TB Treatment Regimens (REMEMBER) study (AIDS Clinical Trials Group (ACTG) A5274) observed that the 4-drug (empirical) preventive regimen did not reduce tuberculosis (TB) mortality at 24 weeks compared with isoniazid-only treatment. , raising adherence concerns. This analysis assessed adherence in the 4-drug (empirical) arm using drug level measurements and pharmacometrics, comparing those who developed TB (cases) and those who did not (controls)

Methods

A 1:4 matched case-control study analysed stored blood samples collected opportunistically from a subset of participants from the 4-drug treatment arm, at weeks 2, 4, and 8. Rifampicin and pyrazinamide were measured via liquid chromatography with mass spectrometry (LC-MS/MS). Adherence was assessed using 2 thresholds: (i) lower limit of quantification (LLOQ) and (ii) personalised thresholds from model-based simulations based on either the 2.5th or 5th percentile. Population pharmacokinetic models and Monte Carlo simulations were used to predict individualised thresholds according to each drug dose and characteristics

assuming 100% adherence. Conditional logistic regression compared non-adherence between cases and controls.

Results

Among 28 cases and 112 controls, median weights were similar (56.2 kg vs. 55.8 kg). The proportion of samples <LLOQ was 52% (cases) vs. 45% (controls) for rifampicin and 20% (cases) vs. 14% (controls) for pyrazinamide. Non-adherence was significantly higher in cases compared to controls for two pyrazinamide exposure metrics: the week 4 LLOQ ($p = 0.050$) and the week 2 2.5th percentile personalised threshold ($p = 0.023$). In both instances, cases had approximately four times higher odds of non-adherence than controls.

Conclusion

Poor adherence may have contributed to TB incidence in REMEMBER. While not definitive, personalised thresholds from model-based simulations remain useful for adherence assessment.

Introduction

Approximately one-quarter of the world's population is estimated to be infected with the *M. tuberculosis* bacterium, and about 5–10% of those infected will develop active tuberculosis (TB) disease in their lifetime (World Health Organization 2021b). Those at high risk of developing active TB disease are people with weakened immunity, especially people living with HIV (PLWHIV), and even more so, in patients with advanced HIV disease in resource-limited settings (Gupta et al. 2011). Several effective options are recommended for treating latent tuberculosis infection (LTBI).

The historical standard of care has been a 6- or 9-month course of daily isoniazid (6H or 9H). Alternative shorter regimens are now also available, including a 3-month weekly regimen of rifapentine and isoniazid (3HP), a 3-month daily regimen of isoniazid and rifampicin (3HR), a 1-month daily course of rifapentine and isoniazid (1HP), and 4 months of daily rifampicin alone (4R) (World Health Organization 2024a).

The 'Reducing Early Mortality and Early Morbidity by Empiric Tuberculosis Treatment Regimens (REMEMBER) A5274 study was a multi-country randomised clinical study conducted in HIV-positive outpatients initiating antiretroviral therapy with CD4 cell counts of less than 50 cells per μL to assess whether the 4-drug (empirical) treatment would result in lower early mortality compared to isoniazid preventive TB therapy. Counterintuitively, the TB incidence rate was significantly higher in the empirical therapy arm than in the monotherapy arm (Hosseinipour et al. 2016). This prompted the question of whether poor adherence to the 4-drug medication regimen contributed to the higher TB incidence rate.

Poor adherence to medication can be associated with regimens with high pill burden, long duration and can result in reduced treatment effectiveness (Kenneth L. Schaecher FACP, CPC 2013; Hill, Miller, and DeGeest 2011). Poorly tolerated regimens can also be associated with adverse effects, prompting discontinuation (Schaberg, Rebhan, and Lode 1996). A particular challenge with TPT is that the absence of apparent disease or symptoms can diminish motivation for medication adherence (Peh et al. 2021). Several methods can be employed to evaluate patient adherence to medication. These methods vary in their complexity, cost, and

accuracy. They can be classified broadly into indirect and direct. Indirect methods include self-reports, pharmacy dispensing or refill records and pill counts (Farmer 1999), while direct methods include observing the patient taking the medication or measuring drug concentrations in biological samples such as blood or urine. Therapeutic drug monitoring (TDM) combined with modelling and simulation-based approaches can be a valuable tool for assessing patient adherence to medication regimens. Moreover, PK models could be combined with spot checks to ascertain whether drug concentrations are within an expected, personalised range. This approach is predicted to become more and more accessible due to the development of simple, low-cost point-of-care assays.

Among the 4 drugs in standard TB treatment, pyrazinamide and rifampicin are amenable to pharmacometric modelling. Upon oral administration, pyrazinamide is rapidly and completely absorbed from the gastrointestinal tract, with a bioavailability of ~70-90%. It has minimal protein binding and undergoes hepatic metabolism. Its elimination half-life is around 9 hours (Lacroix et al. 1989). Rifampicin is rapidly and well-absorbed from the gastrointestinal tract. Rifampicin is highly protein-bound. It mainly undergoes biliary excretion. It induces several drug-metabolising enzymes and transporters, resulting in autoinduction. Its clearance doubled after ~2 weeks of daily administration. Therefore, steady-state concentrations are reached after ~2 weeks (M T Chirehwa et al. 2015) and for the 300 mg dose, the half-life is about 2.5 hours (Gianni Acocella 1983). Considering that individuals metabolise drugs differently based on their body size, both drugs are dosed based on weight to ensure adequate drug exposure. Weight-based

dosing helps to account for variations in drug distribution, metabolism, and elimination among patients of different weights.

In this paper, we explore the use of pharmacometric modelling and simulation as a tool to assess adherence to antitubercular drugs in participants who developed TB (cases) compared to those who did not (controls) within the 4-drug combination arm in the REMEMBER study.

MATERIALS and METHODS

Study population

We included participants from the 4-drug empirical treatment arm in this sub-study (NWCS 440) to assess their level of drug adherence. Participants were administered 4-drug fixed combination tablets (150 mg rifampicin, 75 mg isoniazid, 400 mg pyrazinamide, and 275 mg ethambutol) with weight-adjusted daily dosing according to the WHO guidelines (Helen McIlleron et al. 2012). The participants with confirmed, probable, or clinical diagnosis of pulmonary or extra-pulmonary TB by week 48 (cases) were matched with participants from the empirical treatment arm without confirmed, probable, or clinical diagnosis of pulmonary or extra-pulmonary TB by week 48 (controls) (Hosseinipour et al. 2016). The case-control matching was done by weight and sex in the ratio of 1:4, with each case matched with 4 controls. Matching was done according to the method described by Wang (Z. Wang 2012). Only participants with at least 2 out of 3 blood samples collected at visits on weeks 2, 4, and 8 of the parent study were included.

Sample collection

Opportunistic plasma samples were used, as the study was not originally designed for pharmacokinetic analysis. Only one blood sample was collected per visit—at weeks 2, 4, and 8—and the exact time of the participant's last dose was neither recorded by the study staff nor reported by the participants. As a result, samples were taken without reference to dosing time. After collection, samples were placed in an ice bath, centrifuged in a cooling centrifuge, and then stored at -80°C.

Drug quantification

Pyrazinamide and rifampicin plasma concentrations were determined in stored plasma samples by liquid chromatography-tandem mass spectrometry (LC-MS) performed in the Division of Clinical Pharmacology, University of Cape Town (Abdelgawad et al. 2024). The LLOQs were 0.203 µg/mL and 0.075 µg/mL for pyrazinamide and rifampicin, respectively. Any concentration value below the LLOQ was censored and reported as <LLOQ. The assessment was done based on the exposure of rifampicin and pyrazinamide only; isoniazid and ethambutol were excluded due to their short plasma half-life.

Methods for identifying medication non-adherence

At weeks 2, 4, and 8, each participant's adherence status was assessed based on their observed drug concentration relative to a predefined threshold. If the observed concentration was below the threshold, the participant was classified as non-adherent. However, a concentration above the threshold does not definitively confirm adherence; rather, it indicates that non-adherence cannot be conclusively ruled out. Additionally, participants were also asked if they missed yesterday's dose

at each visit and this was recorded in the case report form. The concentration-based assessment was applied to both pyrazinamide and rifampicin and at each visit separately. We used 2 different methods to define thresholds for assigning the adherence outcome as shown below.

Method 1: Using the below the lower limit of quantification (<LLOQ) as the threshold.

The first method uses the LLOQ of each drug's assay as the threshold for adherence. If the observed drug concentration is below or equal to the LLOQ, the outcome is considered non-adherent; if it is above the LLOQ, non-adherence is not confirmed.

Method 2: Using personalised thresholds from model-based simulations.

Population pharmacokinetic modelling was used to simulate and propose individualised threshold values for pyrazinamide and rifampicin for each participant. We used previously developed and published models for pyrazinamide (Maxwell T. Chirehwa et al. 2017) and rifampicin (M T Chirehwa et al. 2015) from the TB HAART study, a study in PLWH with smear-positive pulmonary TB investigating factors associated with pharmacokinetic variability in patients with both TB and HIV at different levels of immunosuppression. Both models for pyrazinamide and rifampicin were one-compartment disposition models with a chain of transit compartments to model the absorption. Pyrazinamide exhibited first-order elimination, while rifampicin demonstrated saturation during first-pass metabolism. In both models, the disposition parameters were allometrically scaled for body size using the participant values of fat-free mass. Additionally, the models included

stochastic variability on clearance, bioavailability, absorption rate constant, and absorption mean transit time.

These models were used in a Monte Carlo simulation to generate the individualised ranges (Jonsson and Nyberg 2022; Schoonjans, De Bacquer, and Schmid 2011) within which the observed drug concentrations are expected to be at 24and 48 hours after the last dose if steady-state is assumed (i.e., full induction) and with 100% treatment adherence. Although the drug is meant to be taken every 24 hours, we also simulated drug concentrations at 48 hours. This allows for flexibility in case a participant did not take their dose on time, exactly 24 hours after the last dose. In other words, if there was a delay in taking the most recent dose, the actual time since the last dose may be longer than 24 hours. This 48h thresholds assume that the last dose taken could have been more than 24 hours ago but no longer than 48 hours.

For each patient, visit, and drug (i.e. using the dose they received and their value of fat-free mass), the model simulated n = 500 values. Based on the resulting distribution, two personalised threshold values were selected: the 2.5^{th} and the 5^{th} percentiles for that participant/timepoint. If the observed drug concentration in a participant is below the personalised threshold determined through simulations, the outcome for that visit is classified as 'non-adherent.' Conversely, if the observed concentration is at or above the threshold, there is not enough evidence to support non-adherence.

Statistical analyses

The conditional logistic regression test was used to compare the odds ratio of being non-adherent between the cases and the controls, adjusting for weight and sex. Conditional logistic regression was performed separately for each combination of visit (week 2, 4, and 8) and time point (24h and 48h). A p-value equal to or lower than 0.05 was chosen as significant for the increase in odds.

Software

NONMEM® 7.5.0 was used to run the simulations for Method 2. R 4.0.3 was used for post-processing NONMEM® results and generating figures (Keizer, Karlsson, and Hooker 2013). The R package "Epi" was used to perform conditional logistic regression tests to calculate the odds ratio.

RESULTS

Study data

Twenty-eight participants with confirmed, probable, or clinical TB comprised the "cases" group and were matched with 112 controls by weight and sex, making the total number of participants 140. Table 3.1: Participant characteristics shows the participants characteristics. One case was missing the sample for week 2, two cases were missing the week 4 sample, and two cases were missing their week 8 samples, resulting in a total of 415 observations per drug. For a total of 36 participants, the week 8 visit occurred more than 8 weeks after the study began. Of these, 8 were in the case group and 28 in the control group. A total of 13 participant-visit occurrences (4 cases and 9 controls) reported missing yesterday's dose.

Table 3.1: Participant characteristics

	Median (Min-Max) or n (%)	
	Cases (n = 28)	**Controls (n = 112)**
Males	14 (50%)	56 (50%)
Age (years)	36 (25 - 55)	36 (18 - 58)
Weight (kg)	56 (34 - 81)	56 (30 - 81)
Height (m)	1.63 (1.48 - 1.80)	1.65 (1.49 - 1.89)
Fat-free mass (FFM) (kg)	41.2 (29.9 - 55.6)	41.9 (29.5 - 57.7)

Adherence results

Method 1: Using the below limit of quantification (BLQ) as the threshold.

For pyrazinamide: The number of <LLOQs (non-adherent) was 16 out of 79 (20%) for the cases and 46 out of 336 (14%) for the controls across all 3 visits.

For rifampicin: The number of <LLOQs (non-adherent) was 41 out of 79 (52%) for the cases group and 152 out of 336 (45%) for the control group across all 3 visits.

The results for pyrazinamide and rifampicin split by week are shown in Table 3.2. No differences in odds ratio of non-adherence reached statistical significance for either drug, except for pyrazinamide week 4 (p = 0.05). The odds ratio was 3.72 (95% CI: 1.00 - 13.9). The conditional logistic regression test results for both pyrazinamide and rifampicin at weeks 2, 4, and 8 are shown in Table 3.2. Boxplots of pyrazinamide and rifampicin concentrations and the proportion of observations that are below the LLOQ are depicted in Figure 3.1.

Method 2: Using personalised thresholds from model-based simulations.

At 48h for pyrazinamide and both 24h and 48h for rifampicin, the expected drug levels based on the simulations in all participants were below the LLOQ. This means

that these time points and drugs cannot be used to check whether patients are taking their medication as prescribed. Since the drug levels are expected to be undetectable at these times whether or not a participant took the medication, any measurement below the detection limit would not provide useful information about adherence. In other words, an undetectable drug level at these points does not necessarily mean the participant missed a dose—it is simply due to drug elimination. As shown in Figure 3.2, pyrazinamide is expected to be at LLOQ at 48h. Therefore, the thresholds carried forward to the statistical analysis step were the 2.5th and 5th percentile thresholds for pyrazinamide at 24h. For the 2.5th percentile, 24% of cases were non-adherent compared to 18% of controls. For the 5th percentile, these proportions were 27% for cases and 19% for controls, respectively. The results are presented in Table 3.2. An example of a simulated concentration-time profile, as well as the distribution curve of all 500 simulated concentrations at 24h for one participant on one visit as an example is depicted in Figure 3.2.

The results of the conditional logistic test for the second method are shown in Table 3.3. The odds ratio for the 5th percentile at week 2 was the only statistically significant threshold (p-value = 0.023). The odds ratio was 4.10 (95% CI: 1.21 – 13.9), indicating that the odds of being non-adherent were 4.10 times higher in the case group compared to the control group. For thresholds other than those at week 8, the results suggested a trend towards higher odds of non-adherence among cases compared to controls, as indicated by odds ratios greater than 1. However, at week 8 (2.5th and 5th percentiles), the odds ratios were less than 1, suggesting a potential trend in the opposite direction. But the confidence intervals for these odds ratios

included one, and the p-values were greater than 0.05. Therefore, these differences in odds between the cases and controls were not statistically significant.

Table 3.2: Frequency table of non-adherence based on method 1 (BLQ) and method 2 (personalised thresholds) for pyrazinamide at 24h for visits on weeks 2, 4, & 8

	No. (%) of samples indicating non-adherence			
	Method 1 (BLQ)		**Method 2 (2.5th percentile)**	**Method 2 (5th percentile)**
	Rifampicin	**Pyrazinamide**	**Pyrazinamide**	
Week 2				
Cases	12/27 (44%)	5/27 (19%)	7/27 (26%)	8/27 (30%)
Controls	49/112 (44%)	12/112 (11%)	15/112 (13%)	15/112 (13%)
Week 4				
Cases	15/26 (58%)	7/26 (27%)	7/26 (27%)	7/26 (27%)
Controls	54/112 (48%)	16/112 (14%)	22/112 (20%)	23/112 (21%)
Week 8				
Cases	14/26 (54%)	4/26 (15%)	5/26 (19%)	6/26 (23%)
Controls	49/112 (44%)	18/112 (16%)	23/112 (21%)	27/112 (24%)
Overall				
Cases	41/79 (52%)	16/79 (20%)	19/79 (24%)	21/79 (27%)
Controls	152/336 (45%)	46/336 (14%)	60/336 (18%)	65/336 (19%)

*Overall numbers and percentages were calculated based on the total number of all 3 visits at weeks 2,4, and 8.

Table 3.3: Conditional logistic regression results for method 1 (LLOQ threshold) for pyrazinamide and rifampicin, and method 2 (personalised thresholds) for pyrazinamide at 24h at weeks 2, 4, and 8, adjusting for weight and sex

Method 1	**Pyrazinamide**			**Rifampicin**		
Week	Odds ratio	95% CI	***p*-value**	Odds ratio	95% CI	***p*-value**
2	1.75	0.481 – 6.38	**0.39**	1.23	0.464 – 3.27	**0.68**
4	3.72	1.00 – 13.9	**0.050**[a]	1.53	0.611 – 3.84	**0.36**
8	0.862[a]	0.250 – 2.97	**0.81**	1.00	0.397 – 2.54	**0.99**
Method 2	**Pyrazinamide at 24h**					
	2.5th percentile			**5th percentile**		
Week	Odds ratio	95% CI	***p*-value**	Odds ratio	95% CI	***p*-value**
2	3.34	0.938 – 11.9	**0.063**	4.10	1.21 – 13.9	**0.023**[a]
4	2.01	0.676 – 5.96	**0.21**	1.85	0.634 – 5.42	**0.26**
8	0.791	0.250 – 2.50	**0.69**	0.769	0.257 – 2.31	**0.64**

[a] statistically significant ($\alpha = 0.05$)

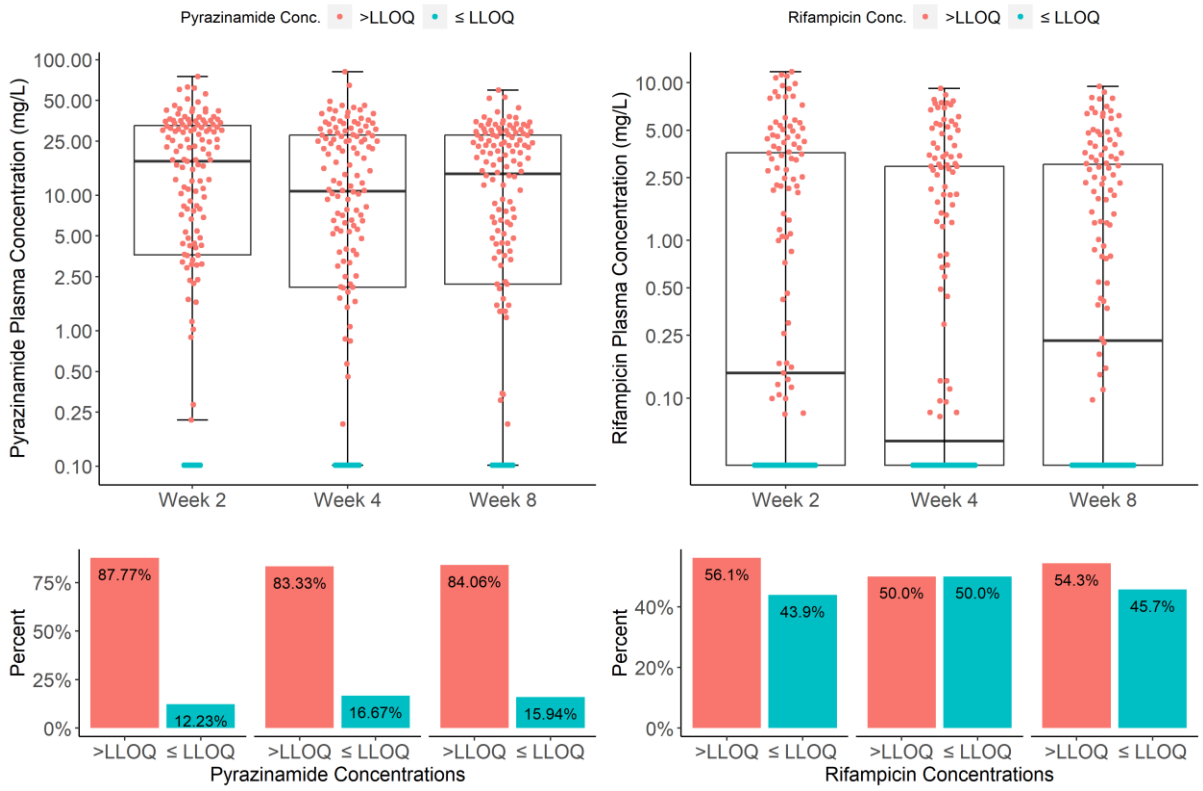

Figure 3.1: Boxplots of pyrazinamide and rifampicin concentrations stratified by visit week. The lower panel shows the proportion of samples that are below or equal the lower limit of quantification (LLOQ)

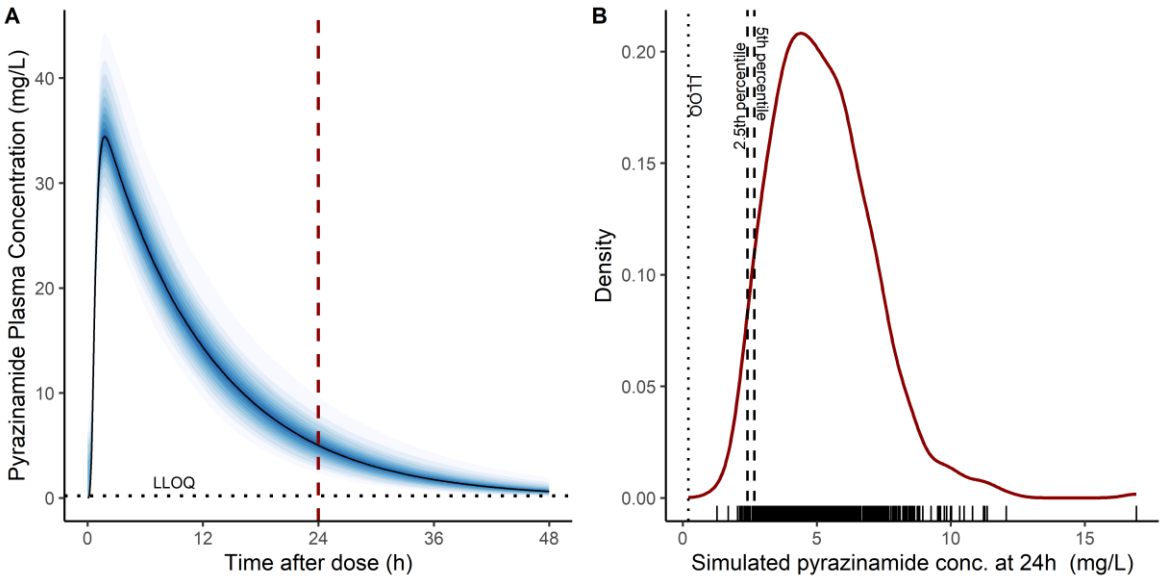

Figure 3.2: A) An example of a simulated (n = 500) plasma concentration vs time after dose profile and B) a cross-section at 24 h showing the distribution curve of all 500 simulated concentrations at 24h for one participant on one visit as an example.

CONCLUSION

In this analysis, we used two methods – one using the LLOQ as a threshold and another using personalised thresholds from model-based simulations – to evaluate drug concentrations and compare adherence to TPT between participants who developed TB and those who did not in the 4-drug combination preventative treatment in the REMEMBER study. Although no significant differences in adherence were observed across all thresholds, statistically significant associations were found for pyrazinamide's LLOQ threshold at week 4 and the 5th percentile personalised threshold at week 2. Cases exhibited ~4 times higher odds of non-adherence compared to controls. The analysis suggests that poor adherence may have played a role in the primary outcome of the REMEMBER study, which is that a

4-drug empiric treatment did not reduce mortality at 24 weeks compared to isoniazid-only preventive therapy in outpatient adults with advanced HIV disease.

To explore whether poor adherence influenced REMEMBER's outcomes, one approach could have been to evaluate adherence separately within each treatment arm: the 4-drug combination and the isoniazid-only. However, our chosen methodology was ultimately decided by the pharmacokinetic properties of the TB drugs. Due to isoniazid's short half-life, adherence could not be reliably assessed in the isoniazid-only arm using drug level measurements, i.e., isoniazid levels are expected to be undetectable after 24 hours regardless of whether the patient is adhering to medication. In the 4-drug combination arm, both pyrazinamide and rifampicin also have relatively short half-lives. We anticipated that pyrazinamide levels would be undetectable after 48 hours, and rifampicin levels even sooner, after 24 hours. Consequently, we utilised pyrazinamide levels measured at 24 hours as an indicator of non-adherence within the 4-drug combination arm. Week 8 results may have been affected by participants who had potentially discontinued pyrazinamide before their week 8 sample was collected. There are two main limitations to this analysis. The first limitation that unrecorded times of the dose administration introduce uncertainty into the analysis and influence the model-predicted drug concentration. However, this is reflective of real-life scenarios where reported times are commonly unavailable or inaccurate. Such analysis could be further improved if the time of the last dose and the blood sampling time were recorded. The second limitation is that adherence was assessed only for the dose taken the day before sampling. This restricts the scope of

adherence evaluation to a single time point, thereby overlooking fluctuations or patterns in adherence behaviour and may provide an incomplete understanding of the participants' overall adherence to the prescribed medication regimen. In conclusion, our analysis of the REMEMBER trial outcomes suggests a trend towards higher nonadherence in the cases group compared to the controls, however, it is not conclusive due to the limitations of the available data. Adherence to medication remains a significant challenge, particularly given the high pill burden of TPT. To address this, a broader range of tools is needed to improve adherence monitoring. Model-based simulations offer promising potential for adherence monitoring. We recommend using this approach to establish personalised thresholds for assessing drug adherence. This method need not be limited to TB drugs but can be applied to a wide range of medications, including antiretrovirals (ARTs). This method is particularly useful for drugs with long half-lives, such as bedaquiline and clofazimine. It is also useful in two key scenarios. First, when a drug exhibits low between-subject variability (e.g. lamivudine), it becomes easier to determine adherence because any deviation from expected levels strongly indicates non-adherence (C. Zhang et al. 2012). In this case, the observed drug concentration can provide a clear signal of adherence. Second, for drugs with high between-subject variability, if this variability can be predicted using observable covariates such as genetics (e.g. CYP2B6 genotype for efavirenz) or renal function. For example, if a drug's pharmacokinetics are largely influenced by renal clearance, individual differences can be accounted for, allowing for a more accurate personalisation of the threshold. Additionally, published pharmacokinetic models of drugs could be

integrated with spot checks to assess whether drug concentrations fall within an expected, model-based personalised range. The development of simple, low-cost point-of-care assays, such as the saliva-based pyrazinamide assay by Chen et al. (R. H. Chen et al. 2025), further facilitates this approach, making adherence monitoring more accessible and practical.

ACKNOWLEDGMENT

I would like to extend my sincere gratitude to my co-authors and collaborators, Maxwell Chirehwa, Kim Scarsi, Mina C. Hosseinipour, Gregory P. Bisson, Sachiko Miyahara, Xin Sun, and Amita Gupta, for their invaluable contributions to this work. I am also deeply grateful to the Adult AIDS Clinical Trials Group A5274 (REMEMBER) Study Team for their essential role in generating the data and supporting this research.

Chapter 4 : Pharmacokinetics of antitubercular drugs in patients hospitalized with HIV-associated tuberculosis: a population modelling analysis

Abstract

Background

Early mortality among hospitalized HIV-associated tuberculosis (TB/HIV) patients is high despite treatment. The pharmacokinetics of rifampicin, isoniazid, and pyrazinamide were investigated in hospitalized TB/HIV patients and a cohort of outpatients with TB (with or without HIV) to determine whether drug exposures differed between groups.

Methods

Standard first-line TB treatment was given daily as per national guidelines, which consisted of oral 4-drug fixed-dose combination tablets containing 150 mg rifampicin, 75 mg isoniazid, 400 mg pyrazinamide, and 275 mg ethambutol. Plasma samples were drawn on the 3rd day of treatment over eight hours post-dose. Rifampicin, isoniazid, and pyrazinamide in plasma were quantified and NONMEM® was used to analyse the data.

Results

Data from 60 hospitalized patients (11 of whom died within 12 weeks of starting treatment) and 48 outpatients were available. Median (range) weight and age were 56 (35 - 88) kg, and 37 (19 - 77) years, respectively. Bioavailability and clearance of the three drugs were similar between TB/HIV hospitalized and TB outpatients.

However, rifampicin's absorption was slower in hospitalized patients than in outpatients; mean absorption time was 49.9% and 154% more in hospitalized survivors and hospitalized deaths, respectively, than in outpatients. Higher levels of conjugated bilirubin correlated with lower rifampicin clearance. Isoniazid's clearance estimates were 25.5 L/h for fast metabolizers and 9.76 L/h for slow metabolizers. Pyrazinamide's clearance was more variable among hospitalized patients. The variability in clearance among patients was 1.70 and 3.56 times more for hospitalized survivors and hospitalized deaths, respectively, than outpatients.

Conclusions

We showed that the pharmacokinetics of first-line TB drugs are not substantially different between hospitalized TB/HIV patients and TB (with or without HIV) outpatients. Hospitalized patients do not seem to be underexposed compared to their outpatient counterparts, as well as hospitalized patients who survived vs who died within 12 weeks of hospitalization.

Introduction

The mortality rate among treated hospitalized HIV-associated tuberculosis (TB/HIV) patients is high, ranging from 11% to 32% (Kyeyune et al. 2010; Schutz et al. 2020). Hospitalized TB/HIV patients usually have some features of bacterial sepsis, with elevated venous lactate levels, and impaired intestinal barrier function, resulting in microbial translocation and high levels of circulating lipopolysaccharide, which mediates an inflammatory response (Subbarao et al. 2015; Brenchley et al. 2006). Delayed gastric emptying and changes in gastric pH have been observed in severely ill patients (Roberts and Hall 2013). The gastrointestinal changes in severely

ill patients could lead to differences in the rate and amount of drug absorption and therefore affect drug exposure (Parsons 1977). Other changes in severely ill patients may include increased volume of distribution, changes in plasma protein binding, and changes in the intrinsic activity of drug metabolizing enzymes or in the hepatic blood flow that may affect drug clearance (Roberts and Hall 2013; Parsons 1977; Blot, Pea, and Lipman 2014). These changes could negatively affect the treatment outcome in vulnerable patients. These changes could affect the levels of drug concentrations. Lower antitubercular drug concentrations have been shown to be associated with delayed sputum culture conversion times as shown by Sekaggya-Wiltshire *et al.* (Sekaggya-Wiltshire et al. 2018) and Mah *et al.* (Mah et al. 2015).

In addition to the extent of disease that could result in variable absorption, rifampicin's extent and rate of absorption is highly variable (Wilkins et al. 2008). Rifampicin is mainly cleared by the liver and undergoes extensive first-pass metabolism (G. Acocella 1978). Saturable elimination has been reported for rifampicin at higher doses due to saturation of the biliary transport mechanisms (G. Acocella 1978; Kenny and Strates 1981). After repeated administration, rifampicin exhibits autoinduction, in which it increases its own metabolism partly by activating the pregnane X receptor (Y. Chen et al. 2004), which in turn induces the B-esterases in liver microsomes, which are responsible for the biotransformation of rifampicin to 25-desacetyl rifampicin (Loos et al. 1985; Jamis-Dow et al. 1997).

Isoniazid also has highly variable pharmacokinetics, mainly due to genetic polymorphism in N-acetyltransferase 2 (NAT-2), the enzyme responsible for metabolizing the drug; the elimination of isoniazid in fast-acetylators is up to six

times faster than the slow acetylators(Ellard and Gammon 1976). Body composition parameters such as weight and fat-free mass (FFM) are usually good predictors of clearance and volume of distribution for many drugs. FFM is generally advised as a better scalar than bodyweight since it accounts for both the difference in body size and composition, unlike weight, which accounts for body size only (Morgan and Bray 1994; McLeay et al. 2012).

The aim of the study was to compare the pharmacokinetics of rifampicin, isoniazid, and pyrazinamide between hospitalized patients and outpatients recruited from the same hospital catchment area. We hypothesize that antitubercular drugs exposures would be lower in hospitalized patients compared to non-hospitalized patients and in hospitalized patients who died versus who survived.

Methods

Study population

The study population is made up of two groups: the hospitalized patients and outpatients recruited as controls. The hospitalized study population for this pharmacokinetic (PK) sub-study was a subset from participants enrolled for an observational cohort study investigating the mortality causes in hospitalized TB/HIV patients carried out between November 2014 and November 2016 (Schutz et al. 2020). Patients presenting to Khayelitsha Hospital in Cape Town, South Africa with TB/HIV who needed hospitalization due to tuberculosis (i.e., who were too ill to receive initial treatment as outpatients) and who survived to the third day of TB treatment were enrolled sequentially, as long as they still needed inpatient care and

did not require transfer to a tertiary care facility for intensive care or investigations. The study team invited eligible hospitalized patients in the parent study to take part and discussed with them the study. TB outpatients with or without HIV were recruited from around the same hospital catchment area as controls. The study team liaised with the clinic staff to ask any new patients when they were started on TB treatment if they would like to discuss taking part in the PK sub-study.

Study design

All participants received a once daily dosing of antitubercular drugs that were given as 4-drug fixed-dose combination (FDC) tablets containing rifampicin-isoniazid-pyrazinamide-ethambutol at 150/75/400/275 mg, which were either Rifafour e-275 tablets (SANOFI) or Ritib tablets (PHARMACARE)). The number of tablets to be given to each participant is determined based on their weights according to the weight-based dosing of the South African national TB management guidelines outlined in Table 2.1 in Chapter 2. Clinical data and baseline blood tests were obtained at enrolment. The 12-week mortality outcome was documented for hospitalized patients.

Ethics and consent

The study was approved by University of Cape Town Human Research Ethics Committee (UCT HREC reference: 057/2013) on 12 April 2013. All participants signed an informed consent form.

Data collection

For each patient, age, sex, weight, height and details of concomitant medications were collected, and a complete medical history was recorded. Serum chemistry and

a complete blood picture were carried out at the Groote Schuur National Health Laboratory Services on each participant on samples taken at enrolment for the PK study.

Participants were scheduled for a PK visit during their 3rd day of treatment, when blood samples were drawn just before and 1, 2.5, 4, 6, and 8 hours after dose. Participants were required to fast overnight, and they were given a standardized breakfast after the 1-hour sample and a standardized lunch between the 4- and 6-hour sample. Immediately following their collection, samples were put in an ice bath until being centrifuged in a cooling centrifuge and later stored at -80°C.

Drug quantification

Plasma rifampicin, isoniazid and pyrazinamide concentrations were determined by validated liquid chromatography with tandem mass spectrometry assays at the Division of Clinical Pharmacology, University of Cape Town (Smith, van Dyk, and Fredericks 1999). The lower limit of quantification (LLOQ) was 0.117 mg/L for rifampicin, 0.105 mg/L for isoniazid, and 0.203 mg/L for pyrazinamide. The accuracy of the low-, medium-, and high-quality control samples ranged between 99.7% - 100.8% for rifampicin, 98.3% - 100.4% for isoniazid, and 88.1% and 92.3% for pyrazinamide. The precision of the quality control samples ranged from 4.7 – 7.7%, 3.0% - 5.1%, and 2.9% - 3.6% for rifampicin, isoniazid, and pyrazinamide, respectively (Schutz et al. 2020).

Pharmacokinetic and statistical analyses

A population pharmacokinetic model was developed for each of the three drugs using nonlinear mixed-effects modelling in NONMEM® version 7.4 and the

algorithm first-order conditional estimation with eta-epsilon interaction (FOCEI) Pirana was used for model management, Perl-speaks-NONMEM (PsN) 4.9.0 was used for post-processing of NONMEM® results and R version 3.6.2 was used for generating the figures (Keizer, Karlsson, and Hooker 2013). Different disposition models with first-order elimination were evaluated. The use of a lag time and transit compartments were tried to capture the delay in the first-order absorption process. Between-subject variability was evaluated for all disposition parameters and between-occasion variability was assessed for bioavailability, and other absorption parameters. Censored below the lower limit of quantification (BLQ) concentration values were handled as per Beal's M6 method, in which the first BLQ values in series were replaced with LLOQ/2 and the subsequent BLQs were discarded (S. L. Beal 2001). Residual unexplained variability was described using a combination of additive and proportional error components. The additive error was bound to be at least 20% of the LLOQ. Allometric scaling of clearance and volume parameters was tested as suggested by Anderson and Holford (B. J. Anderson and Holford 2008) using the fixed power exponents of 0.75 for clearance and 1 for volume. Body weight and FFM, calculated based on the formula in Janmahasatian et al. (Janmahasatian et al. 2005), were both tested for allometric scaling as body size descriptors. Since no NAT-2 genotyping data were available, mixture modelling was used for the isoniazid pharmacokinetic model to distinguish between the clearances of different groups of metabolizers.

Following the development of a basic model, covariate testing was done. Various effects, including hospitalization, patient status (outpatients or hospitalized

who survived or hospitalized who died within 12 weeks), drug formulation, and various biomarkers which indicate general organ dysfunction e.g. aspartate transaminase (AST), alanine transaminase (ALT), serum creatinine, serum urea, albumin, and procalcitonin, were tested on clearance, bioavailability, and absorption parameters for all three drugs. Trefoil factor-3, which is a marker of gut barrier integrity was tested as a covariate on the absorption parameters. The effect of concurrent administration of HIV drugs was tested.

The model development process and covariate inclusion were guided by physiological plausibility, model fit diagnostics including drop in the objective function value (OFV) and inspection of diagnostic plots. Comparison between nested models was done using the likelihood ratio test for the drop in OFV, assumed to be approximately χ^2 distributed with n degrees of freedom, where n is the number of additional estimated parameters. A p-value of 0.05 was generally used for inclusion and 0.01 for retention. Visual predictive checks (VPCs) were used to assess compatibility of the model with the observed data.

Weakly-informative priors on the ratio of the volume of the central compartment (Vc) to the volume of the peripheral compartment (Vp), Vratio (Vc/Vp) with 30% uncertainty were used to stabilize the model for isoniazid PK. The typical values were obtained from a previously published model (Gausi et al. 2021).

The precision of the parameter estimates, expressed as the 95% confidence intervals, was assessed by applying a nonparametric bootstrap with 500 iterations. A non-compartmental pharmacokinetic (PK) analysis of the same participants in this report has previously been published (Schutz et al. 2020).

Variability correlation across the three drugs

Correlations of unexplained variability in the pharmacokinetic parameters: clearance, bioavailability, area under the curve from time 0 to 24 hours ($AUC_{0\text{-}24h}$) and absorption between each of the three drugs were assessed to check if there was any relation between the unexplained variabilities in each pharmacokinetic parameter between the three drugs. There were two occasions per patient. An occasion is defined as any dosing event followed by at least one sample. When checking the correlation between variabilities, only the variability from the primary occasion was included i.e. the occasion associated with the predose was excluded.

Results

Study data

A total of 108 patients completed the study; 60 were hospitalized TB/HIV patients, and 48 were TB outpatients, of whom 29 were HIV-positive. Table 4.1 provides a summary of the participants characteristics. Four hospitalized patients (n=4, 3.7%) had missing height values, which were replaced by the regression-imputed values based on sex. Two hospitalized patients with renal impairment had individual tablets for each drug instead of the FDC to allow adjustment of the ethambutol dose, and one hospitalized patient had the tablets crushed, mixed with water, then inserted via a nasogastric tube. All patients had blood samples collected on the 3rd day of treatment, except for one participant, in whom it was found out during the study that there was an earlier dose, so the collected samples were on the 4th day of treatment. Nine participants were on efavirenz, 9 on tenofovir, 1 on lopinavir/ritonavir, and 1 on lamivudine.

Table 4.1: Participants baseline characteristics

	Median (1st – 3rd Quartile) or no. (%) of participants given			
	Outpatients (n = 48)	**Hospitalized Survivors (n = 49)**	**Hospitalized Deaths (n = 11)**	**Total (n = 108)**
Sex: Females	12 (25%)	25 (51%)	6 (55%)	43 (40%)
Age (years)	36 (32 – 42)	38 (32 - 40)	35 (31 - 50)	37 (32 – 41)
Weight (kg)	58 (52 – 63)	55 (48 - 60)	54 (48 - 60)	56 (49 – 62)
Fat-free mass (kg)	47 (41 – 51)	41 (37 - 47)	38 (35 - 46)	43 (38 – 49)
Total bilirubin (µmol/L)[a]	10.0 (7.00 – 14.0)	9.00 (5.00 – 14.3)	12.0 (9.50 – 15.0)	10.0 (6.00 – 14.0)
Conjugated bilirubin (µmol/L)[b]	6.00 (4.00 – 8.00)	5.00 (2.25 – 8.00)	8.00 (6.00 – 10.0)	6.00 (3.00 – 9.00)
Lactate (mmol/L)[c]	1.60 (1.20 – 1.95)	1.50 (1.10 – 1.95)	2.40 (1.50 – 3.35)	1.60 (1.20 – 2.00)
Aspartate aminotransferase, AST (U/L)[d]	30.0 (21.0 – 50.0)	48.5 (33.8 – 82.3)	64.5 (36.3 – 81.0)	38.0 (27.0 – 69.0)
Alanine aminotransferase, ALT (U/L)[e]	20.0 (13.5 – 30.0)	29.5 (20.0 -49.3)	22.0 (15.0 – 30.5)	24.0 (16.0 – 40.8)
HIV-positive	29 (60%)	49 (100%)	11 (100%)	89 (82%)
Current antiretroviral therapy	5 (17%)	19 (39%)	1 (9%)	25 (23%)
CD4 Count (cells µL^{-1})	142 (35.5 – 241)	69.5 (17.8 – 131)	32.0 (12.5 – 94.0)	71.5 (19.8 - 154)

A total of 108 pharmacokinetic profiles with 632 concentration-time observations for each of the three drugs were available for analysis. The number of observations that were BLQ were 33 (5.2%), 88 (13.9%), and 1 (0.2%) for rifampicin, isoniazid, and pyrazinamide, respectively, most of which were predose samples. The 12-week mortality rate of hospitalized patients was 11/60 (18%). One

participant was lost to follow up after 2 months; the participant's results were included in the survived group. We chose to stratify the analysis of the hospitalized patients into those who survived and those who died within 12 weeks as an indicator of severity of the patients' sickness.

Rifampicin pharmacokinetics

Rifampicin pharmacokinetics was best characterized by a one-compartment disposition model with first-order elimination, and absorption described by a chain of transit compartments. The parameter values of the final model are shown in Table 4.2. The model fit the data well as shown in the VPC in Figure 4.1. Apparent clearance (CL) and apparent volume of distribution (V) were allometrically scaled using FFM as a body size descriptor. Allometric scaling by FFM (difference in OFV, dOFV = -30, df = 2, *p*-value = <0.001) resulted in a more significant drop than scaling by total body weight (dOFV = -7.7, df = 2, *p*-value = 0.02). The typical CL and V values for a participant with the median FFM were 8.82 L/h and 56.8 L, respectively.

Table 4.2: Final population pharmacokinetic parameter estimates for rifampicin, isoniazid and pyrazinamide

Parameter	**Typical value (95% CI)** [a] **[Shrinkage]**		
	Rifampicin	**Isoniazid**	**Pyrazinamide**
Clearance (L/h) [b]	8.82 (8.10 – 9.48)	-	2.61 (2.48 – 2.75)
Clearance of fast metabolizers (L/h)	-	25.5 (22.7 – 28.7)	-
Clearance of slow metabolizers (L/h)	-	9.76 (8.28 – 11.2)	-
Proportion of fast NAT2 metabolizers (%)	-	64.5 (54.4 – 75.8)	-

Volume of distribution (L) [b]	56.8 (53.9 – 61.2)	59.0 (54.7 – 64.2)	36.0 (34.4 – 37.9)
Intercompartmental clearance, Q (L/h)	-	1.43 (0.874 – 2.14)	-
Peripheral volume, Vp (L) [c]	-	30.7 (25.9 – 37.1)	-
Absorption rate constant, ka (h^{-1})	1.38 (1.04 – 1.70)	2.43 (1.80 – 6.50)	1.92 (1.53 – 2.59)
Mean transit time, MTT (h)	0.342 (0.259 – 0.534)	0.442 (0.266 – 0.781)	0.379 (0.220 – 0.566)
No. of absorption transit compartments (.)	12 fixed	8 fixed	4 fixed
Bioavailability, F (%)	100 fixed	100 fixed	100 fixed
% difference in mean absorption time (MAT) for hospitalized survivors [d]	+49.9 (+2.80 – +80.9)	-	-
% difference in MAT for hospitalized deaths [d]	+154 (+63.9 – 351)	-	-
Exponent of power relationship between Clearance and conjugated bilirubin [e]	-0.333 (-0.474 – -0.194)	-	-
Between-subject variability for clearance (BSVCL) (%)	42.4 (37.3 – 49.4) [7%]	25.3 (17.2 – 33.4) [24%]	19.9 (13.2 – 25.0) [9%]
Fold change in BSVCL for hospitalized survivors [f]	-	-	1.70 (1.26 – 2.65)
Fold change in BSVCL for hospitalized deaths [f]	-	-	3.56 (1.64 – 6.53)
Between-occasion variability (BOV) (%) for:			
Bioavailability	21.3 (16.4 – 27.6) [41%]	34.9 (26.6 – 40.3) [31%]	10.5 (4.13 – 15.1) [53%]
Absorption rate constant, ka	119 (100 – 137) [32%]	122 (84.0 - 186) [51%]	75.3 (40.3 – 95.3) [59%]
Mean transit time, MTT	93.8 (67.4 – 111) [49%]	99.7 (45.9 – 172) [57%]	102 (61.9 – 145) [56%]
Proportional error (%)	17.2 (14.9 – 18.5)	13.9 (12.0 – 16.4)	11.4 (7.59– 13.9)
Additive error (mg/L)	0.0234 fixed [g]	0.021 fixed [g]	2.48 (1.47 – 3.44)

[a] Values in parentheses are empirical 95% confidence intervals, obtained with a 500-sample nonparametric bootstrap

[b] The values of CL/F and V/F were allometrically scaled, so the typical values reported here refer to the median body weight of 66 kg and the median FFM of 43 kg of the cohort included in the model.

[c] The peripheral volume, Vp, was calculated from the estimated Vratio (Vc/Vp) and Vc. A prior of 2.02 was included on Vratio with 30% uncertainity.

[d] Patient status effect was modeled on ka and 1/MTT simultaneously using the same effect parameter, theta (θ). ka for hospitalized = TVka × θ; MTT for hospitalized = TVMTT / θ. Mean

absorption time = MTT+1/ka calculated for each group was 1.1 h for outpatients, 1.6 h for hospitalized survivors, and 3.2 h for hospitalized deaths.

[e] *Conjugated bilirubin (BRC) Effect on CL = (BRC/median BRC)* $^{-0.333}$*; CL = TVCL x BRC Effect on CL*

[f] BSVCL for hospitalized = BSVCL × fold change. i.e. BSVCL is 33.8% for hospitalized survivors and 70.8% for hospitalized deaths.

[g] The estimate of the additive component of the error was not significantly different from its lower boundary of 20% of LLOQ, so it was fixed to this value.

No difference in CL or bioavailability was found between hospitalized survivors, hospitalized deaths, and outpatients. Nonetheless hospitalized patients, and even more so those who died in the first 12 weeks, were found to absorb rifampicin slower than outpatients (dOFV = -16.1, df = 2, *p*-value = <0.001). The effect of patient group (outpatients, hospitalized survivors and hospitalized deaths) was modelled on the absorption rate constant (ka) and 1/mean absorption time (MTT) simultaneously using the same effect parameter, theta (θ), as outlined in the formulae below.

$$MTT_{group} = \frac{MTT_{outpatients}}{\theta_{patient\ group\ effect}}$$

$$k_{a_{group}} = \theta_{patient\ group\ effect} \cdot k_{a_{outpatients}}$$

Where $MTT_{outpatients}$ is the typical mean transit time for the outpatients in hours, MTT_{group} is the mean transit time for hospitalized survived or hospitalized deaths group in hours, $k_{a_{group}}$ is the absorption rate constant for hospitalized survivors or hospitalized deaths group in hour^{-1}, and $k_{a_{outpatients}}$ is the typical absorption rate constant for outpatients in hour^{-1}.

On average, hospitalized patients who survived had a mean absorption time (MAT) of 1.6 h (accounting for both MTT and ka), while the value was 2.7 h for

hospitalized patients who died in the first 12 weeks, compared to 1.1 h for outpatients.

Additionally, we found that higher values of conjugated bilirubin (BRC) were correlated with lower values of rifampicin CL (dOFV = -17.3, df = 1, *p*-value = <0.001), according to the power relationship outlined below

$$CL_i = CL_{typical} \cdot \left(\frac{BRC_i}{BRC_{median}}\right)^{\beta_{BRC}}$$

Where CL_i is the clearance for patient *i*, $CL_{typical}$ is the typical clearance, which is 8.82 L/h, BRC_i is the BRC for patient *i*, BRC_{median} is the BRC median in all patients (6 µmol/L) and β_{BRC} is the exponent of power relationship between CL and BRC, estimated to be -0.333. The power function was a better fit for the relationship between BRC and CL compared to linear, piece-wise linear. The relationship is depicted in Figure 4.2. Both total bilirubin (BRT) and BRC were found to correlate significantly with CL; however, the two covariates (i.e. BRT and BRC) are highly positively correlated (r = 0.860), so only one of them was included in the final model. BRC was chosen over BRT because it resulted in a more significant drop in OFV. We tried incorporating saturation of elimination of rifampicin and the first-pass metabolism into the model. However, both models resulted in a marginal improvement of the fit. Therefore, we decided to keep the model more straightforward and not include either saturation or first-pass metabolism in the final model. Also, the inclusion of autoinduction of rifampicin clearance was tested in the model, but did not result in an improved fit for the data.

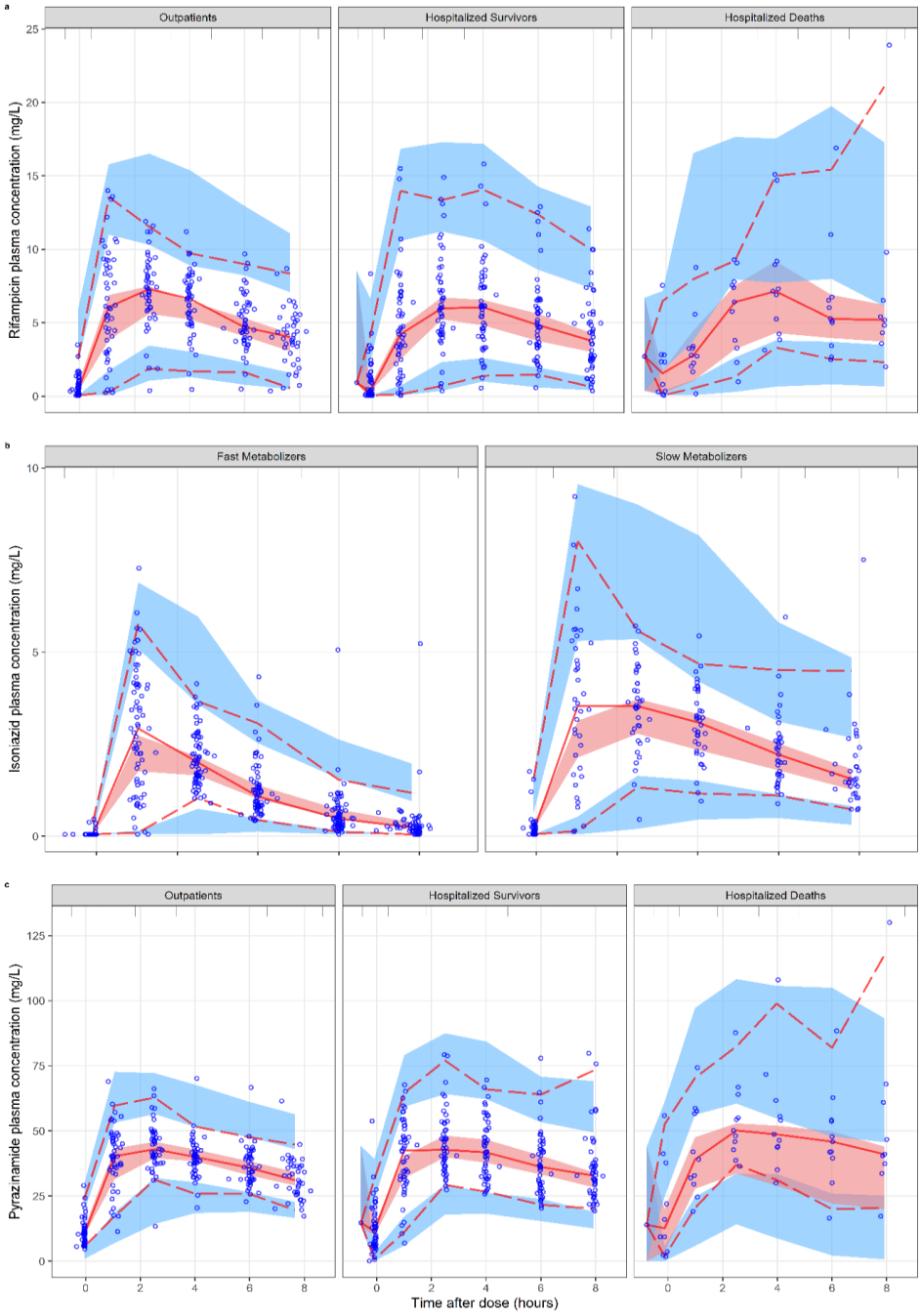

Figure 4.1: Visual predictive check (VPC) (n=1000) showing plasma drug concentration versus time after dose for the final models of each drug

a) for rifampicin stratified by patient group; b) for isoniazid stratified by metabolizer status; c) for pyrazinamide stratified by patient group. The circles are the original observations; the solid line and the dashed lines are the median, 5th and 95th percentiles of the observed data; the shaded areas are the 95% confidence intervals of the same percentiles as simulated by the model. A suitably fitting model will have most of the observed percentiles within the simulated confidence intervals.

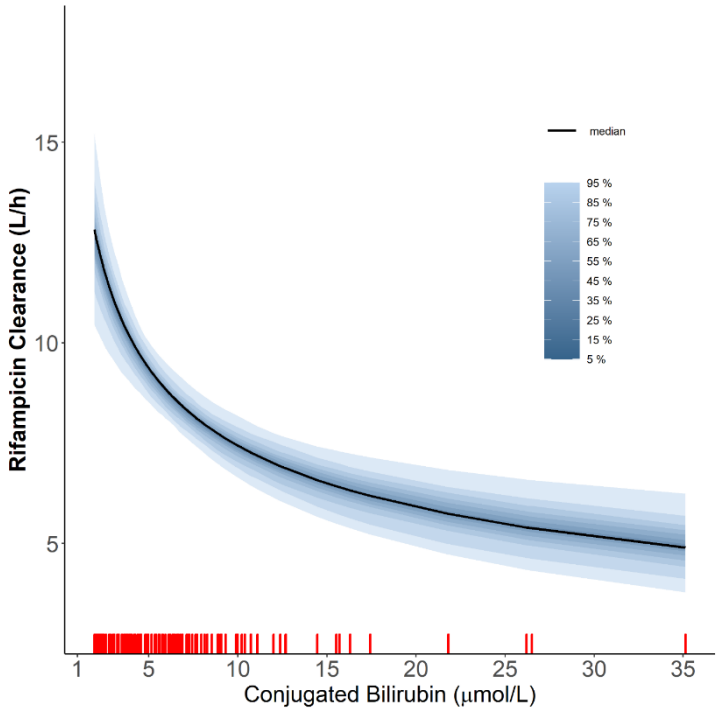

Figure 4.2: The relationship of rifampicin clearance vs the level of conjugated bilirubin using the power function.

The red ticks represent the values of conjugated bilirubin observed in our cohort. The solid line represents the median and the shaded areas represent the uncertainty distribution around the effect due to the precision of parameter estimates.

None of the biomarkers tested were found to correlate significantly to CL, except for the level of venous lactate and AST. However, the correlation between clearance and lactate or AST was less significant than the correlation with BRC, so only the effect of BRC was included in the final model. An effect for the formulation was found to be statistically significant (dOFV = -12.9, df =1, p-value < 0.001), with the individual tablets having 21.8% of the bioavailability of FDC. However, only two participants were on individual tablets (n = 2, 1.85%) instead of the FDC, one of whom vomited during the study.

Isoniazid pharmacokinetics

A two-compartment disposition model with first-order absorption with a chain of transit compartments and first-order elimination proved to fit the data best. The final parameter estimates are shown in Table 4.2. A 2-compartment model was a better fit than the 1-compartment in terms of a significant drop in OFV, which was about 42 points, and by a VPC, but the model was unstable and Vp could not be reliably estimated. To stabilize the estimate of the Vp, a prior was included on the Vratio (Vc/Vp) with a value of 3.728 with 30% uncertainty (Gausi et al. 2021). Allometric scaling of CL and Vc using FFM was used because it caused a more significant drop in the OFV of 24.9 points instead of weight which caused a drop of only 15.5 points. Mixture modelling was used to account for the differences in CL between fast and slow metabolizers in place of NAT2 genotype testing (dOFV = -15.5, df =2, p-value < 0.0005). The proportion of fast metabolizers was estimated to be 64.5%. The typical clearance values were estimated to be 25.5 L/h and 9.76 L/h for fast and slow metabolizers. A three-component mixture distinguishing into fast, intermediate, and slow metabolizers was examined but was not supported by the data. Figure 4.1 includes a VPC for the final isoniazid model stratified by metabolizer type, indicating that the model fit the data well. Isoniazid pharmacokinetics were not different in hospitalized patients compared to outpatients. The final parameter estimates are shown in Table 4.2.

Pyrazinamide pharmacokinetics

A one-compartment disposition model with first-order elimination and first-order absorption with transit absorption compartments best fit the data. Allometry with

FFM was applied to CL and V (dOFV = - 32.6 points for FFM, better than total body weight, dOFV = -28.3). Final parameter values are displayed in Table 4.2. No significant differences were found in the CL, bioavailability, or absorption between hospitalized survivors, hospitalized deaths, and outpatients. The between-subject variability in CL was significantly higher among hospitalized patients, i.e. 20% for outpatients vs 33.8% for hospitalized patients who survived vs 70.8% for hospitalized patients who died within 12 weeks (dOFV = -27, df=2, *p*-value < 0.001). A VPC showing that the model correctly captures the data for pyrazinamide is shown in Figure 4.1.

Neither the HIV status nor the CD4+ cell count influenced the pharmacokinetics of any of the three drugs. The effect of efavirenz co-administration (n = 9) was tested on the CL and bioavailability of all three drugs. No significant effect for the co-administration of efavirenz was found.

The model-derived individual $AUC_{0\text{-}24h}$ and C_{max} for all three drugs are shown in Table 4.3 and are represented graphically in Figure 4.3 in a box and whisker plots.

Table 4.3: C_{max} and $AUC_{0\text{-}24h}$ for rifampicin, isoniazid, and pyrazinamide stratified into outpatients, hospitalized survivors, and hospitalized deaths

	Median (1st - 3rd Quartile)					
	C_{max} (mg/L)			**$AUC_{0\text{-}24h}$ (mg.h/L)**		
	Outpatients	**Hospitalized Survivors**	**Hospitalized Deaths**	**Outpatients**	**Hospitalized Survivors**	**Hospitalized Deaths**
Rifampicin	8.05 (6.77–9.48)	7.41 (5.52 – 9.15)	7.23 (5.83 – 8.00)	65.8 (52.9 – 83.1)	69.1 (38.8 – 86.8)	71.2 (58.7 – 102)
Isoniazid	3.62 (2.55 – 4.31)	4.12 (2.75 – 5.05)	3.45 (2.46 – 4.06)	13.4 (8.90 – 24.6)	15.0 (9.51 – 22.2)	15.1 (7.71 – 39.3)
Pyrazinamide	45.4 (42.7 – 50.0)	48.3 (40.7 – 53.6)	53.8 (43.8 – 62.4)	580 (522 – 637)	610 (459 – 727)	738 (586 – 1080)

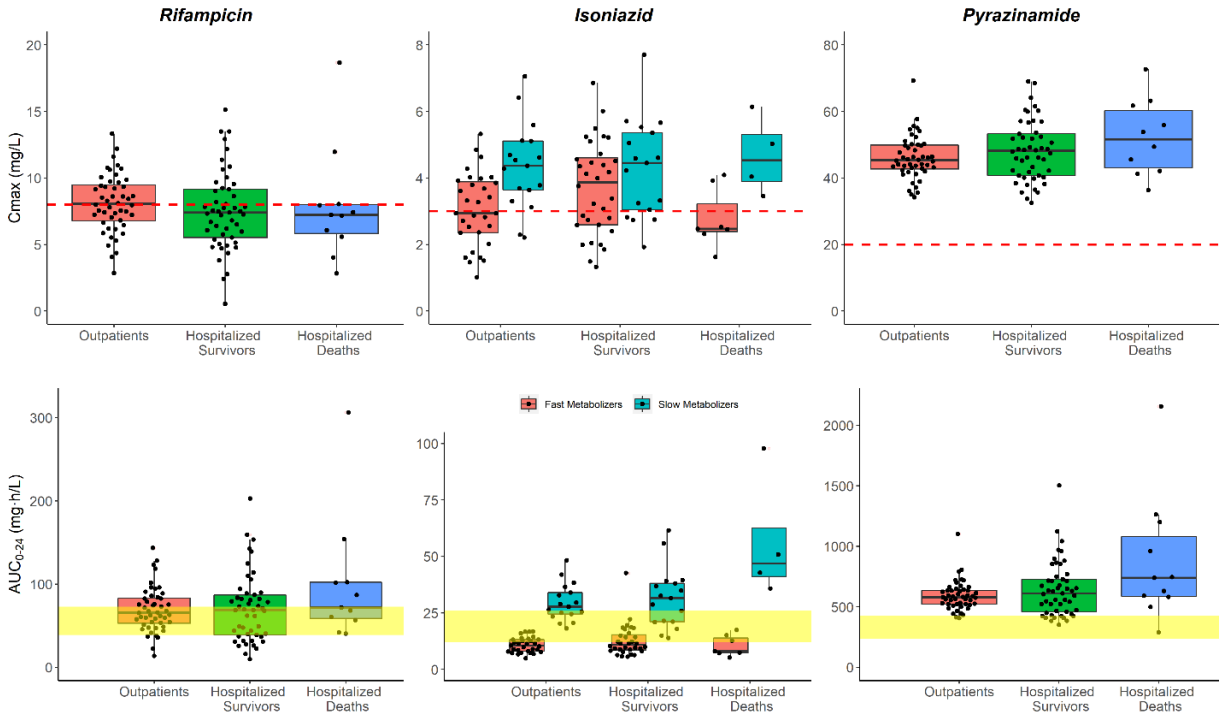

Figure 4.3: Box and whisker plots of the model-derived individual C_{max} and $AUC_{0\text{-}24}$ for the three drugs.

The dots are individual values, and the whiskers represent the 2.5th and 97.5th percentiles. The dashed line represents the currently recommended minimum threshold: 8 mg/L for rifampicin, 3 mg/L for isoniazid, and 20 mg/L for pyrazinamide. The yellow shaded areas represent the exposure targets based on Stott *et al.* for rifampicin (Stott et al. 2018) and Daskapan *et al.* for isoniazid and pyrazinamide (Daskapan et al. 2019). This is only for visualization purposes; no statistical tests can be carried out here since dose amounts are not accounted for.

Variability correlation across the three drugs

The correlations of the remaining unexplained variability in clearance, bioavailability, $AUC_{0\text{-}24h}$ and absorption among the three drugs were assessed and the results are shown in the correlation matrix in Figure 4.4. The equations used to calculate the unexplained variabilities for each parameter are shown below Figure 4.4. Moderate correlations were found for all, except for absorption, which ranged between 68.4% - 84.6%.

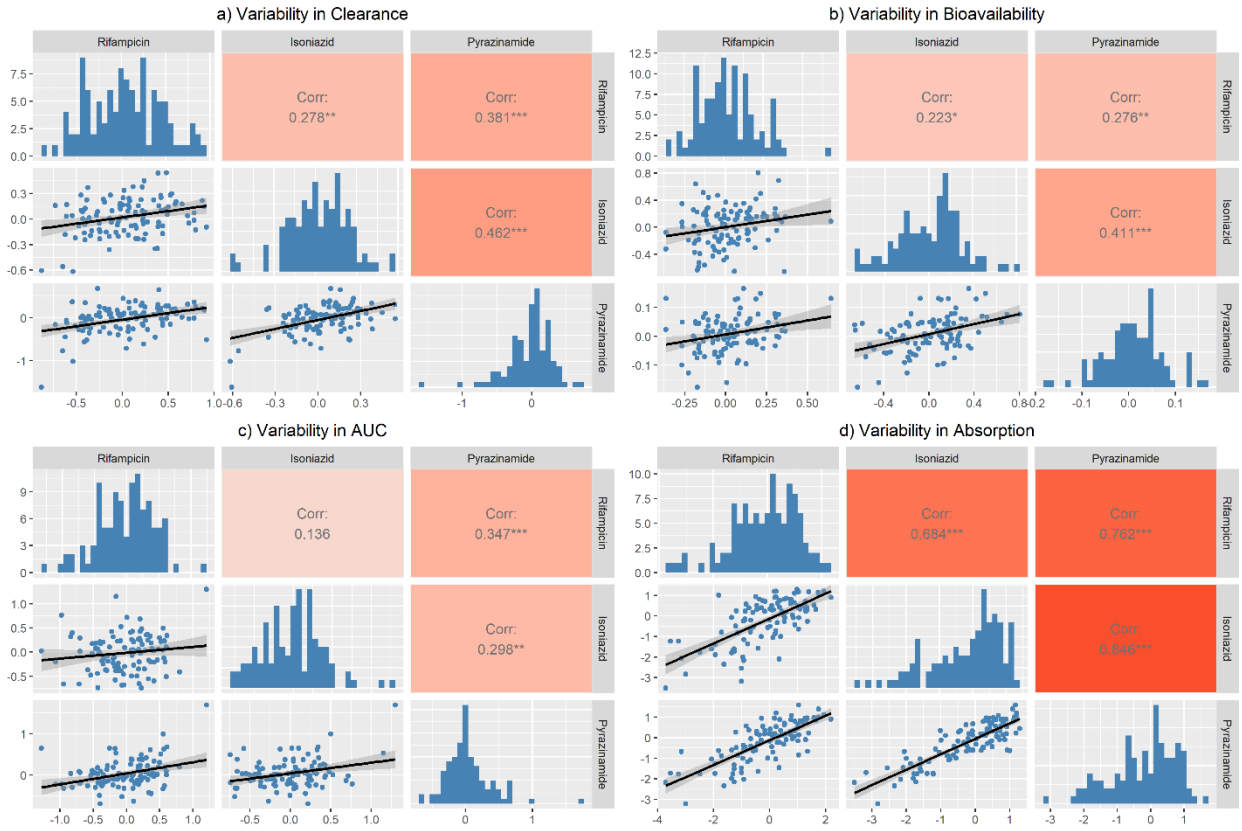

Figure 4.4: Correlation matrix for the unexplained variability.

a) clearance, **b)** bioavailability, **c)** area under the curve ($AUC_{0\text{-}24h}$), and **d)** absorption between the three drugs. The correlation coefficient is shown in the lower panel. Only the variability from the main occasion was included (not the predose). Variability in clearance = BSVCL + BOVCL. Variability in bioavailability = BSVBIO + BOVBIO. Variability in AUC = BSVBIO + BOVBIO - BSVCL. Variability in absorption = BSVKA + BOVKA - BSVMTT - BOVMTT.

Discussion:

The main finding of our analysis is that the overall drug exposures for rifampicin, isoniazid, and pyrazinamide are similar between hospitalized TB/HIV patients who died with 12 weeks, hospitalized TB/HIV patients who survived and TB outpatients. For rifampicin, our model showed that absorption was slower in hospitalized patients, even slower among hospitalized patients who died within 12 weeks, and

that higher levels of bilirubin were associated with lower rifampicin clearance. For pyrazinamide, the between-subject variability in CL was higher among hospitalized patients, and higher among hospitalized patients who died compared to hospitalized patients who survived. While rifampicin absorption is slower in hospitalized patients, the bioavailability is similar between hospitalized who died, hospitalized who survived and outpatients, which indicates that intravenous rifampicin administration may be not be necessary for hospitalized TB patients.

There are limited data comparing the pharmacokinetics of first-line anti-TB drugs between hospitalized patients and outpatients, especially during the first few days of starting treatment. A non-compartmental analysis (NCA) of the data from this pharmacokinetic study was published by Schutz et al. (Schutz et al. 2020). The NCA show that the overall exposures of all three drugs among hospitalized patients and outpatients were similar, which is in line with our findings.

For all three models, we found allometric scaling by FFM to be better than by total body weight in capturing the differences in *CL/F* and *V/F* due to differences in body size. FFM is more physiologically plausible because it takes into account not just body size but also body composition (B. J. Anderson and Holford 2008). Since FFM is a more accurate predictor for *CL/F* and *V/F*, but dosing is done based on weight, patients with lower weights end up being more underexposed. This is supported by Muliaditan et al. (Muliaditan and Pasqua, n.d.), Rockwood et al. (Rockwood et al. 2016), and McIlleron *et al.* (Helen McIlleron et al. 2012) who have shown that patients with lower body weights are underexposed relative to patients with higher body weight. Therefore, we agree with their conclusions that the clinical

recommendation for the use of weight-banded dosing regimens should be reconsidered to take into account the variability in body size and composition.

The pharmacokinetic parameters from our models for rifampicin, isoniazid and pyrazinamide were comparable to those from other similar studies (Wilkins et al. 2008; Denti et al. 2015; Wilkins et al. 2011; Maxwell T. Chirehwa et al. 2017; Wilkins et al. 2006).

Rifampicin PK model

The structural model we developed for rifampicin was similar to previously developed rifampicin models (Wilkins et al. 2008; Muda et al. 2022). However, CL values are lower in this analysis because autoinduction was not included in the model. Regarding the differences in absorption, published articles report that critically ill patients tend to have a more impaired absorption of drugs through a decreased barrier gut function and delayed gastric emptying, which lead to reduced perfusion of the gastrointestinal tract (Roberts and Hall 2013; Parsons 1977; Blot, Pea, and Lipman 2014). We reason that only rifampicin's absorption out of the three drugs was affected by these gastrointestinal changes because of rifampicin's low solubility (Becker et al. 2009), whereas both isoniazid and pyrazinamide have high solubility according to the biopharmaceutics classification system (Becker et al. 2007, 2008). Rifampicin's absorption is mainly from the stomach and proximal intestine (Mariappan and Singh 2003) and is more likely to be easily affected by changes in the gastric pH (G. Acocella 1978). As a result, the C_{max} for hospitalized patients tends to be lower than that of the outpatients, while the $AUC_{0\text{-}24h}$ does not seem to be affected as shown in Figure 4.3. A systemic review

by Muda et al. of rifampicin pharmacokinetic models concludes that the sources of variability in rifampicin's pharmacokinetics are still not fully understood and could be due to factors such as drug-drug interactions, and different formulations (Muda et al. 2022).

Rifampicin and its major metabolite are mostly excreted through the biliary tract, the same tract that excretes bilirubin. Therefore, higher bilirubin levels correlate with lower rifampicin clearances since bilirubin and rifampicin compete for the same elimination pathway (G. Acocella 1978; Lal et al. 1972). While marked differences have been reported in the rate and extent of absorption with different formulations (H McIlleron et al. 2002), only two patients in our study were on individual tablets, and one of them vomited during the study, therefore the effect of formulation was not included in the final model. Saturation of clearance and first-pass metabolism have been reported previously for rifampicin (M T Chirehwa et al. 2015). While there was no significant effect for either HIV status or efavirenz co-administration, previous studies have reached contrasting results regarding both. Some studies found no significant difference in rifampicin concentrations (Helen McIlleron et al. 2012), while others found decreased rifampicin levels in HIV-positive TB patients (Daskapan et al. 2019; Jeremiah et al. 2014; Helen McIlleron et al. 2006). One meta-analysis study found lower plasma exposures for HIV-positive status for all first-line anti-TB drugs, however, the analysis only included children and adolescents (Gafar et al. 2023). Nevertheless, a meta-analysis by Stott et al. concluded that HIV positivity had no effect on rifampicin exposure (Stott et al. 2018).

Isoniazid PK model

The estimated proportion of fast acetylators/metabolizers of 64.5% is in line with the proportion of fast/intermediate acetylators in South Africans from previous publications which ranges between 48% - 60% 39-41 (Mthiyane et al. 2020; Adams et al. 2003; Loktionov et al. 2002). In previously published pharmacokinetic studies in adults, isoniazid's CL ranged between 22 and 26 L/h in fast metabolizers and between 10 and 16 L/h in slow metabolizers, which are similar to this study's results (Denti et al. 2015; Wilkins et al. 2011). We opted for adding a prior on the ratio of the two volumes (Vc/Vp) instead of the Vp because this is expected to be more consistent across studies which may be characterized by different body size and/or differences in bioavailability.

Inadequate exposure of isoniazid has been observed in fast metabolizers across the three patient groups as shown in Figure 4.3; the $AUC_{0\text{-}24h}$ levels on average were below the recommended targets. This effect has been previously reported by Sundell et al. (Sundell et al. 2020).

Pyrazinamide PK model

The values reported for the pyrazinamide model are in line with the values from previously published models. While there were no significant differences in pharmacokinetic parameters between the patient groups, we found a difference in the between-subject variability in CL (BSV-CL). The BSV-CL in outpatients was 19.9, 33.8% among hospitalized patients who survived and 70.8% among hospitalized patients who died. The differences in variability could be explained by the severity

of the illness of the different patient groups. More critically sick patients have factors such as degree of hepatic impairment, sepsis that may lead to more variability.

Variability correlation across the three drugs

There was no strong correlation between the unexplained variability in clearance, $AUC_{0\text{-}24h}$, and bioavailability across the three drugs. The moderate correlation in the unexplained variability in absorption could be explained by the fact that most of the participants were taking an FDC formulation. Therefore, the factors affecting the tablet disintegration and dissolution e.g., manufacturing variables, and drug absorption, e.g., gastrointestinal contents, will be the same across the three drugs in any particular patient.

One limitation of the study is that NAT-2 genotype testing was not carried out for the participants' samples, but this was resolved by using a mixture model to assign each participant to either being a fast or a slow metabolizer. Another limitation is that blood samples were collected on the 3rd day (4th day for one hospitalized participant) of treatment, which did not allow for the inclusion of autoinduction of rifampicin's clearance in the model. However, hospitalized patients are at substantial risk of death within 7 days of admission before autoinduction is established, so the exposures we report here are relevant for these patients. The models cannot be extended to TB patients who are hospitalized for other causes such as renal failure, liver failure, which could significantly alter the antitubercular drugs pharmacokinetics. The study design did not allow us to characterize the possible drug-drug interactions between antitubercular and antiretroviral drugs. However, our study cohort is representative of the general South African population

who gets hospitalized for tuberculosis, and the study was conducted on the 3rd day of treatment since those hospitalized patients are at a substantial risk of death withing 7 days of admission. Another limitation is that ethambutol concentrations were not determined, and we could not investigate if its pharmacokinetics was different in hospitalised patients. However, unlike the other three drugs which are bactericidal, ethambutol is a bacteriostatic drug that is mainly added to tuberculosis treatment regimens to prevent against the development of rifampicin resistance. For this reason, its contribution in the very first days of treatment is expected to be minimal.

In summary, no important differences in any of the exposures of the three drugs: rifampicin, isoniazid, and pyrazinamide between hospitalized TB/HIV patients and TB outpatients were observed. The main findings of the analysis were that rifampicin's absorption is slower in hospitalized patients (and slower in hospitalized patients who died compared to those who survived) and that patients with higher levels of bilirubin had lower rifampicin clearance. Pyrazinamide's clearance was more variable among hospitalized patients (and more variable in hospitalized patients who died compared to those who survived).

Chapter 5 : Population Pharmacokinetic Analysis of Rifampicin in Plasma, Cerebrospinal Fluid, and Brain Extracellular Fluid in South African Children with Tuberculous Meningitis

Abstract

Background

Limited knowledge is available on the pharmacokinetics of rifampicin in children with tuberculous meningitis (TBM) and its penetration into brain tissue, which is the site of infection. In this analysis, we characterize the distribution of rifampicin in cerebrospinal fluid (CSF), lumbar (LCSF) and ventricular (VCSF), and brain extracellular fluid (ECF).

Methods

Children with TBM were included in this pharmacokinetic analysis. Sparse plasma, LCSF, and VCSF samples were collected opportunistically, as clinically indicated. Brain ECF was sampled using microdialysis. Rifampicin was quantified with LC-MS/MS in all samples, and 25-desacetyl rifampicin in the plasma samples. The data was interpreted with nonlinear mixed-effects modelling, with the CSF and brain ECF modelled as “effect compartments”.

Results

Data was available from 61 children, median (min-max) age 2 (0.3-10) years and weight 11.0 (4.8-49.0) kg. A one-compartment model for parent and metabolite

with first-order absorption and elimination via saturable hepatic clearance described the data well. Allometric scaling, maturation, and auto-induction of clearance were included. The pseudo-partition coefficient between plasma and LCSF/VCSF was ~5%, while the value for ECF was only ~0.5%, possibly reflecting low recovery of rifampicin using microdialysis. The equilibration half-life between plasma and LCSF/VCSF was ~4 hours and between plasma and ECF ~2 hours.

Conclusion

Our study confirms previous reports showing that rifampicin concentrations in the LCSF are lower than in plasma and provides novel knowledge about rifampicin in the VCSF and the brain tissue. Despite microdialysis being semi-quantitative because the relative recovery cannot be quantified, our study presents a proof-of-concept that rifampicin reaches the brain tissue and that microdialysis is an attractive technique to study site-of-disease pharmacokinetics in TBM.

Introduction

Tuberculous meningitis (TBM) is the most severe manifestation of tuberculosis (TB) and results in high rates of death and disability. Children are among the most vulnerable populations and TBM remains the most common childhood meningitis in South Africa (Wilkinson et al. 2017). The WHO recommended regimen for TBM is the same as that for pulmonary tuberculosis (TB) but with a longer continuation phase (10 months for TBM vs 4 months for pulmonary TB) (World Health Organization 2014). Due to the poor blood-brain barrier penetration of anti-TB drugs, the TBM regimen probably results in suboptimal concentrations in the central nervous system (CNS) (Wilkinson et al. 2017). Drugs targeted at TBM should

cross several barriers to reach their site of action in the CNS. The systemic circulation is separated from the CNS by the blood-brain barrier (BBB) and the blood-cerebrospinal fluid barrier (BCSFB). These barriers pose a therapeutic challenge by limiting entry of drugs into the CNS. Moreover, disease-specific changes in BBB permeability may have important implications for drug penetration into the brain (Nau, Sörgel, and Eiffert 2010). Recent reports including a report from South Africa investigated a shorter regimen with higher doses that proved successful (van Toorn et al. 2014) which led the WHO to include the short intensive regimen as an alternative in the latest update of their guidelines for TBM treatment in children (released 21 March 2022) (World Health Organization (WHO) 2022).

Most TBM studies investigating CNS concentrations rely on lumbar CSF (LCSF) as a surrogate for anti-TB drug concentrations in the ventricular CSF (VCSF) and in the brain and for which repeated sampling cannot be performed. Microdialysis is a semi-invasive technique that uses a probe implanted in tissue, including the brain (Yamamoto, Danhof, and de Lange 2017). It enables continuous measurement of the unbound concentration of molecules in the interstitial compartment of the brain over time. As such, microdialysis enables sampling of the brain extracellular fluid (ECF) and provides complementary information on the drug distribution in the brain because repeated sampling can be performed (Mindermann, Zimmerli, and Gratzl 1998). However, when used to obtain brain ECF samples, it is only semi-quantitative because the extraction efficiency or relative recovery cannot be calculated (Ungerstedt and Rostami 2004).

Rifampicin is an important drug in the treatment of TBM owing to its potent antimicrobial effect (Gumbo et al. 2007). Following oral administration, rifampicin is readily absorbed, but administration with food makes absorption variable. After absorption, rifampicin enters the hepatoportal system, where it is converted primarily to 25-desacetyl rifampicin and mainly eliminated in the bile (Gianni Acocella 1983). Rifampicin induces its own clearance, with clearance approximately doubling after 2 weeks due to this autoinduction effect. Saturable elimination has been reported for rifampicin at higher doses due to saturation of the biliary transport mechanisms (R. J. Svensson et al. 2018; M T Chirehwa et al. 2015). Rifampicin is widely distributed throughout the body and its plasma protein binding is about 80%, with most of the unbound fraction not ionized and diffusing freely into tissues (G. Acocella 1978). However, due to its lipophilicity and high molecular mass, rifampicin's CSF penetration is suboptimal, particularly when meningeal inflammation is resolving (Kaojarern et al. 1991; Nau, Sörgel, and Prange 1994). Therefore, sampling brain compartments closest to the site of infection would provide useful information. In children, factors such as maturation of enzymes, body size, nutritional status, and disease severity affect children's ability to absorb, metabolize, and eliminate the drug (Brian J. Anderson and Holford 2009).

The objective of this study was to develop a population pharmacokinetic (PK) model for the characterization of rifampicin in plasma, LCSF, VCSF, and brain ECF for children diagnosed with definite or probable TBM. Additionally, simulations were performed to compare rifampicin exposures from the current and former WHO recommended dosing regimens.

Methods

Study participants

Children presenting to the Red Cross War Memorial Children's Hospital with definite or probable TBM were enrolled between January 2017 and September 2019. They were enrolled regardless of how long they have been on rifampicin-based treatment. All patients were managed according to standard institutional protocol (A. A. Figaji and Fieggen 2010) and no procedures were carried out for research. The patients were categorized into two groups: (i) patients who underwent neurosurgical procedures to manage TBM hydrocephalus (HCP) and (ii) patients who presented with lowered levels of consciousness, had invasive monitoring with microdialysis (MD), and had placement of external ventricular drain (EVD) that was part of the institutional protocol for urgent decrease of intracranial pressure. Brain microdialysis was used in critically ill patients to guide therapy based on changes in brain chemistry due cerebral ischemia (A. A. Figaji and Fieggen 2010). Further details about the clinical use of microdialysis are included in the supplementary material. Remnant ECF fluid (after bedside clinical analysis was performed) was frozen at -80 °C and used for rifampicin assays. Ethical approval was obtained from the University of Cape Town human research ethics committee (HREC 564/2012 and 070/2018). Hospital clearance was obtained from the Western Cape Department of Health. In addition, the parents or legal guardians of all participants provided informed consent on their behalf.

Drug administration

All TBM patients were treated according to the Western Cape regimen that is typically used in South Africa which consists of rifampicin (20 mg/kg), isoniazid (15-20 mg/kg), pyrazinamide (40 mg/kg), and ethionamide (20 mg/kg) for 2 months followed by a 4-months continuation phase of rifampicin and isoniazid, according to weight-band based dosing. A hospital nurse administered the anti-TB drugs orally or via nasogastric tube.

Sample collection

Plasma: Three serial blood samples (0.6 mL) were drawn on a single day in the first and second week, and where possible at 2-, 4-, and 6-hours post-dose.

Lumbar and Ventricular CSF: Clinically indicated CSF samples were collected at random time points, from procedures in published protocols (A. A. Figaji and Fieggen 2010), up to 24 hours post-dose into sterile 15-mL tubes and kept on ice. Ventricular CSF samples were taken either at placement of a ventriculoperitoneal shunt or an external ventricular drain, or when clinically indicated from an indwelling external ventricular drain. Lumbar CSF samples were taken either as a diagnostic procedure or for medical therapy of raised intracranial pressure related to hydrocephalus.

Brain ECF using microdialysis technique: A microdialysis catheter with a 100-kDa membrane was placed concurrently with the primary ventricular drain and monitor into the same region (usually right frontal white matter) or sometimes on the side where hypodensity was more prominent on the initial head computed tomography scan. Microdialysis vials were changed at hourly intervals and analysed at the

bedside for clinical purposes. As microdialysis volumes are typically small, remnant hourly samples were pooled over 2–3-hour epochs to ensure sufficient volumes for analysis. Concentrations of substances in the microdialysate are a percentage of the true concentrations in the ECF and not absolute concentrations. This percentage is termed relative recovery. More details on sample collection and bedside protocols can be found in the Supplementary material.

Drug quantification

Total rifampicin was assayed in all samples: plasma, lumbar CSF, ventricular CSF, and brain ECF. Additionally, rifampicin's primary metabolite, 25-desacetyl rifampicin, was assayed in the plasma samples. High performance liquid chromatography with tandem mass spectrometry detection methods were developed and validated at the Division of Clinical Pharmacology, University of Cape Town for the assays. The method was validated over the ranges 0.117–30.0 µg/mL for rifampicin and 0.0391–10.0 µg/mL for 25-desacetyl-rifampicin in plasma, and 5 to 2500 ng/mL for the rifampicin in CSF and ECF assay. A more detailed description of the analytical methods can be found in the Supplementary material.

Population PK analysis

A population pharmacokinetic model was developed to describe rifampicin pharmacokinetics in plasma, CSF, and brain ECF using nonlinear mixed-effects modelling in NONMEM® 7.5.0 and the algorithm first-order conditional estimation with eta-epsilon interaction (FOCE-I). Pirana was used for model management, and Perl-speaks-NONMEM (PsN) 4.9.0 and R 4.0.3 were used for post-processing NONMEM® results and generating figures (Keizer, Karlsson, and Hooker 2013).

Modelling was done sequentially, first developing the joint parent-metabolite model in plasma, including variability and residual error, then developing a full model incorporating the CSF and brain ECF observations, while fixing the population parameter estimates for the plasma joint model.

Rifampicin in plasma joint parent-metabolite model: Previously published rifampicin models in children with pulmonary TB by Denti et al. (Denti et al. 2021) and Zvada et al. (Zvada et al. 2014) were used as a starting point for modelling the rifampicin in plasma data. Thereafter, the parent PK model was extended to include the metabolite. From this data, it is not mathematically possible to estimate both the fraction of parent drug converted to metabolite (FM) and the volume of distribution of metabolite (VM) simultaneously (i.e., the model is structurally unidentifiable). In order to solve this identifiability issue, two methods were tested: the first was to assume that the parent is fully converted to the metabolite, the second was to assume that the volume of distribution of the metabolite is equal to that of the parent.

Therefore, FM was fixed to 1 and the VM and clearance of metabolite (CLM) were estimated. A correction factor was included in the model to adjust for the difference in molecular weight at the conversion of rifampicin (822.94 g/mol) to 25-desacetyl rifampicin (780.90 g/mol). Since rifampicin and its metabolite were quantified simultaneously, a correlation of measurement error factor was included.

Rifampicin in CSF and brain model: The concentrations obtained from the LCSF, VCSF, and brain ECF were modelled using three separate "*effect compartments*" in a manner as described in

$$\frac{dC_{Eff}}{dt} = k_{plasma-Eff} \cdot \left(PPC \cdot C_{plasma} - C_{Eff}\right)$$

where $k_{plasma-Eff}$ is the first-order equilibration rate constant between rifampicin in the central compartment (i.e., plasma) and the effect compartment, and it can also be expressed as equilibration half-life. PPC is the pseudo-partition coefficient which describes the extent of partitioning or penetration of rifampicin between the plasma and each of the effect compartments. C_{plasma} is the predicted rifampicin concentration in plasma at time t. C_{Eff} is the concentration in the effect compartment. Effect compartments are assumed to have a negligible volume compared to the central compartment, with negligible drug transfer between the two compartments.

The effects of CSF and plasma albumin, CSF total protein, CSF glucose, and CSF:plasma albumin ratio were tested as covariates on the PPC, as well as the effects of body weight, age, weight-for-age z-score, duration of rifampicin treatment, and route of administration (oral vs nasogastric tube) on the plasma model parameters. More details regarding the population pharmacokinetic modelling in the supplementary material.

Simulations

Simulations were done in Berkeley Madonna version 10.1.2 using the final model to simulate rifampicin exposures in the different matrices for the typical TBM paediatric patient in the cohort. For all matrices, concentration-time profiles were simulated and areas under the concentration-time curve (AUC_{0-24h}) were calculated. Additionally, Monte-Carlo Simulations were carried out in NONMEM to compare rifampicin exposures following administration according to the newly released

updated WHO dosing guidelines on 21 March 2022 (World Health Organization (WHO) 2022) vs. the previous WHO guidelines, in addition to comparing exposures on the first day of rifampicin treatment vs at steady-state. The AUC_{0-24h} was compared for all weight bands for the updated dosing guidelines using the virtual pediatric population in Wasmann et al. (Wasmann et al. 2021). Simulations were repeated 10,000 times.

Results

Data

A total of 61 children were enrolled in the study. The median age, weight and weight-for-age z-score were 2 (0.3 - 10) years, 11 (4.8 - 49) kg, and -1.23 (-4.97 – 2.44), respectively. Height was missing in 25/61 (41%) of the children. The median duration on rifampicin treatment was 4 (0 – 72) days. A summary of the baseline patient characteristics is shown in Figure 5.1. A total of 307 samples were available, 91 plasma (8 BLQ, 8.4%), 84 lumbar CSF (13 BLQ, 14.8%), 53 ventricular CSF (8 BLQ, 16.0%), and 79 brain ECF (17 BLQ, 21.5%).

Table 5.1**:** Baseline participant characteristics in the Red Cross study

	Median (min - max) or no. (%) of subjects given
	Total (N = 61)
Sex: Females / Males	32 (52.5%) / 29 (47.5%)
Age (years)	2 (0.3 – 10)
Weight (kg)	11 (4.8 – 49)
Weight-for-age z-score [a]	-1.23 (-4.97 – 2.44)
Height [b] **(cm)**	81 (61 – 131)
Height-for-age z-score [a,b]	-0.996 (-7.12 – 1.74)
Days since start of treatment (days)	4 (0 – 72)
Dose per body weight (mg/kg)	18.0 (9.38 – 22.5)

[a] The WHO and CDC tables were used for the calculation of the z-scores

[b] Height and height-for-age z-scores were missing for 25/61 (41.0%) participants

Population PK analysis

The schematic representation of the final structural model is depicted in **Figure 5.1**.

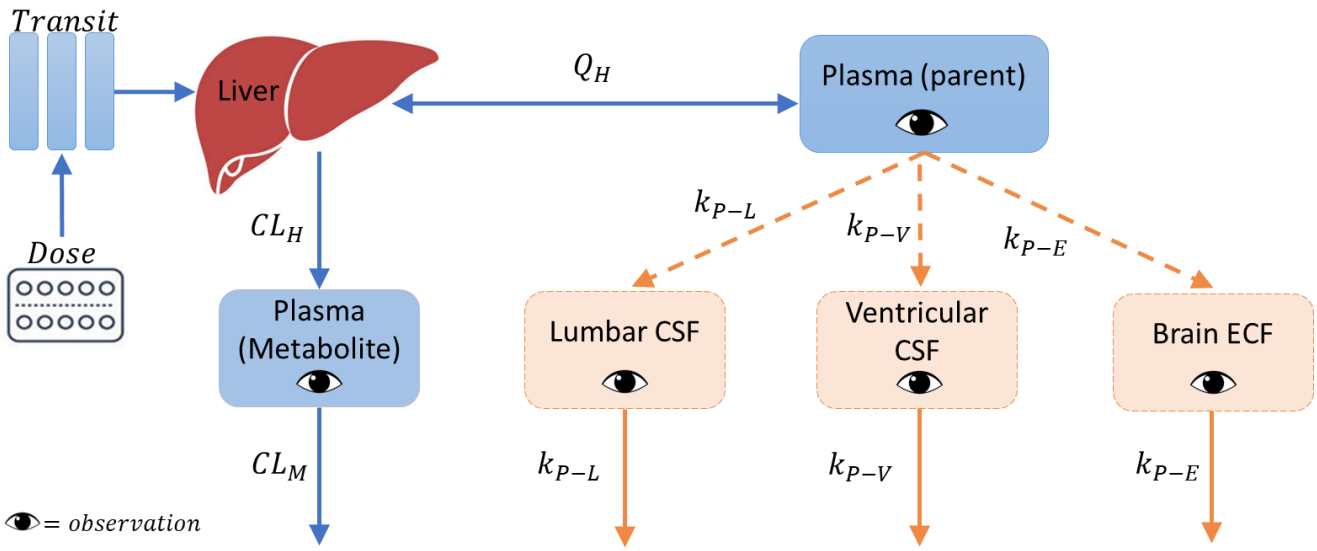

Figure 5.1: Schematic representation of the final model.

CL_H, hepatic clearance; CL_M, metabolite clearance; k_{P-E}, equilibration rate constant plasma-brain extracellular fluid; k_{P-L}, equilibration rate constant plasma-lumbar cerebrospinal fluid (CSF); k_{P-V}, equilibration rate constant plasma-ventricular CSF; Q_H, hepatic flow rate

Rifampicin in plasma joint parent-metabolite model: The final parent-metabolite model is a 1-compartment disposition model with transit compartments absorption with the absorption rate constant, ka, fixed to be equal to the first-order transit rate constant (ktr) to simplify the model. Elimination was characterized with saturable hepatic clearance. The effect of body size on the disposition parameters of both the parent and the metabolite (CL_{int}, V, CLM, and VM) was included in the model using allometric scaling by weight as suggested by Anderson and Holford (B. J. Anderson and Holford 2008). This improved the model fit as shown by the

drop in OFV of 40 points. Allometric scaling using fat-free mass (FFM) was not tested since the height was missing for 41% of the participants. The effect of age on clearance was included by incorporating a maturation factor (MF); a MF as defined by Anderson and Holford (Brian J. Anderson and Holford 2009) was added to the clearance as well since allometry alone cannot account for the differences in clearance between children and adults.

Estimates from Denti et al. (Denti et al. 2021) were used as priors to guide the estimation of $CL_{int,max}$, V, saturation and maturation of clearance and bioavailability parameters, while estimates from Chirehwa et al. (M T Chirehwa et al. 2015) were used as priors for the autoinduction of clearance ($CL^{SS}_{int,max}/CL^{0}_{int,max}$ and $IND50$). The uncertainty for all priors was 10%, except for $CL_{int,max}$ and V, which was 30%. The prior values used are shown in Table 2 footnotes. Uninformative priors, which carry the lowest weight or influence but still allow for good estimation, were used for between-subject variability in clearance. A metabolite compartment was added, where FM was fixed to the reference value of 1 to make the model identifiable. The between-subject variability (BSV) in CLM ($BSVCLM$) was 100% correlated with the BSV in clearance. Thus, subjects were assumed to have the same random effect for both clearance and CLM, then $BSVCLM$ was inflated by a factor that was estimated to be 2.92 as follows: $BSVCLM = BSVCL.factor$. Therefore, allowing for more variability in $BSVCLM$. The effect of nasogastric tube administration was not statistically significant. The final parameter estimates are shown in Table 5.2.

Table 5.2: Final population pharmacokinetic parameter estimates for rifampicin

Parameter	**Typical value (95% CI)** [a]
Plasma (parent) parameters	
Volume of distribution of plasma, $\mathbf{V}$ (L)[b]	18.2 (15.7 – 23.0)
Mean transit time, $\mathbf{MTT}$ (h)[c]	0.251 Fixed
No. of absorption transit compartments, $\mathbf{NN}$ (_)	0.269 (0.037 – 0.556)
Saturation of clearance	
Michaelis-Menten constant, $\mathbf{Km}$ (mg/L)[d]	9.03 (7.45 – 11.2)
Hepatic volume of distribution, $\mathbf{VH}$ (L)[e]	1 Fixed
Hepatic blood flow, $\mathbf{QH}$ (L/h)[e]	90 Fixed
Unbound fraction, $\mathbf{fu}$ (_)	0.2 Fixed
Clearance autoinduction	
Intrinsic clearance at steady-state, $\mathbf{CL^{SS}_{int,max}}$ (L/h)[b]	34.8 (27.3 – 43.1)
$\mathbf{CL^{SS}_{int,max}}$ / Intrinsic clearance at baseline ($\mathbf{CL^{0}_{int,max}}$) (_)[f]	1.60 (1.35 – 1.90)
Induction half-life, $\mathbf{IND50}$ (days)[f]	4.53 (3.69 – 5.52)
Maturation of clearance	
Postmenstrual age when maturation reaches 50%, $\mathbf{TM50}$ (months)[d]	12.2 (10.1 – 14.4)
Shape factor for maturation, $\mathbf{Hill}$ (_)[d]	3.29 (2.73 – 3.97)
Bioavailability, $\mathbf{F}$ (_)	1 Fixed
Maturation of F	
$\mathbf{F}$ at birth (_)[d]	0.642 (0.544 – 0.776)
Age at which $\mathbf{F}$ reaches full maturation, $\mathbf{Age_{Full\ F}}$ (years)[d]	2.80 (2.26 – 3.43)
Between-subject variability in $\mathbf{CL_{int,max}}$ (%)	46.3 (32.6 – 59.5)

Between-occasion variability in **F** (%)	34.9 (26.2 – 44.7)
Between-occasion variability in **MTT** (%)	179 (66 - 245)
Proportional error, parent (%)	33.8 (20.8 – 31.7)
Additive error, parent (mg/L) [g]	0.023 Fixed
Plasma (metabolite) parameters	
Volume of metabolite compartment, **VM** (L)	7.76 (4.14 – 11.7)
Clearance of metabolite, **CLM** (L/h)	13.7 (8.56 – 20.5)
Fraction of parent drug metabolized, **FM** (_)	1 Fixed
Factor for Between-subject variability in **CLM** (-fold)	2.92 (2.48 – 3.65)
Proportional error, metabolite (%)	48.6 (40.1 – 60.3)
Additive error, metabolite (mg/L) [g]	0.008 Fixed
Correlation between errors parent metabolite (%)	85.7 (75.8 – 91.8)

[a] Values in parentheses are the 95% confidence interval, computed with sampling importance resampling (SIR) on the final model. SIR was done sequentially; first for the plasma model then for the effect compartments model, while fixing the plasma model parameter estimates.

[b] The disposition parameters, $CL_{int,max}$, V, CLM, and VM, were allometrically scaled by weight, and the values reported here refer to an 11-kg participant (the median weight in the cohort). Priors from Denti et al. (Denti et al. 2021) with typical values of 8.58 L/h for $CL_{int,max}^{SS}$ and 17.3 L for V were used with 30% uncertainty.

[c] The value of MTT was estimated from the data, but was fixed in the final runs to improve the model stability.

[d] Priors from Denti et al. (Denti et al. 2021) were used with 10% uncertainty. The values of the priors were 12.48 months for TM_{50}, 3.22 for $Hill$, 0.655 for F at birth, and 2.72 years for $\mathrm{Age}_{\mathrm{Full\ F}}$.

[e] These values refer to a 70-kg adult and were scaled allometrically with weight.

[f] Priors from Chirehwa et al. with typical values of 2 for $CL_{int,max}^{SS}$ / Clearance at baseline ($CL_{int,max}^{0}$) and 4.5 days for IND_{50} were used with 10% uncertainty.

[g] The estimate of the additive component of the error was not significantly different from its lower boundary of 20% of LLOQ, so it was fixed to this value.

Rifampicin in CSF and brain model: Rifampicin concentrations in the CSF and brain ECF were linked to the plasma concentrations using pseudo-partition coefficients (PPC) of 4.08% for the lumbar and ventricular CSF and 0.459% for brain ECF, and equilibration rate constants of 0.176 hours^{-1} for CSF and 0.353 hours^{-1} for ECF, which correspond to equilibration half-lives of 3.94 hours for CSF and 1.96 hours for ECF. It was not statistically significant to include in the model separate pseudo-partition coefficients and equilibration rate constants for each of lumbar CSF and ventricular CSF separately. It is important to note that while the typical population PPC value was the same for both lumbar and ventricular CSF, however, on an individual level, each participant had a different PPC for lumbar and ventricular CSF.

The effect of CSF albumin, CSF total protein, and ratio of CSF:plasma albumin on the PPC were not statistically significant. The albumin and total protein values are shown in Table S5.1 in the Supplementary Material. Figure 5.2 shows the VPC of the final model.

Table 5.3: Final population pharmacokinetic parameter estimates for rifampicin for the effect compartments

Effect compartment model	
Pseudo-partition coefficient for lumbar CSF and ventricular CSF, $\boldsymbol{PPC_{P-LV}}$ (%)	4.60 (3.77 – 5.24)
Pseudo-partition coefficient for brain ECF, $\boldsymbol{PPC_{P-E}}$ (%)	0.435 (0.175 – 0.714)
Equilibration rate constant for lumbar CSF and ventricular CSF ($\boldsymbol{h^{-1}}$) [a]	0.163 (0.122 – 0.206)
Equilibration rate constant for brain ECF ($\boldsymbol{h^{-1}}$) [b]	0.330 (0.221 – 0.580)
Between-subject variability in $\boldsymbol{PPC_{P-LV}}$ (%)	21.6 (4.00 – 27.9)

Between-subject variability in $\boldsymbol{PPC_{P-E}}$ (%)	114 (–82.9 - 155)
Proportional error, lumbar CSF (%)	78.6 (72.2 – 98.0)
Additive error, lumbar CSF (mg/L) [c]	0.001 Fixed
Proportional error, ventricular CSF (%)	55.4 (44.4 – 75.5)
Additive error, ventricular CSF (mg/L) [c]	0.001 Fixed
Proportional error, brain ECF (%)	51.1 (40.6 – 69.4)
Additive error, brain ECF (mg/L) [c]	0.001 Fixed

[a] The equilibration rate constant corresponds to an equilibration half-life of 4.23 hours for lumbar CSF and ventricular CSF.

[b] The equilibration rate constant corresponds to an equilibration half-life of 2.09 hours for the brain ECF.

[c] The estimate of the additive component of the error was not significantly different from its lower boundary of 20% of LLOQ, so it was fixed to this value.

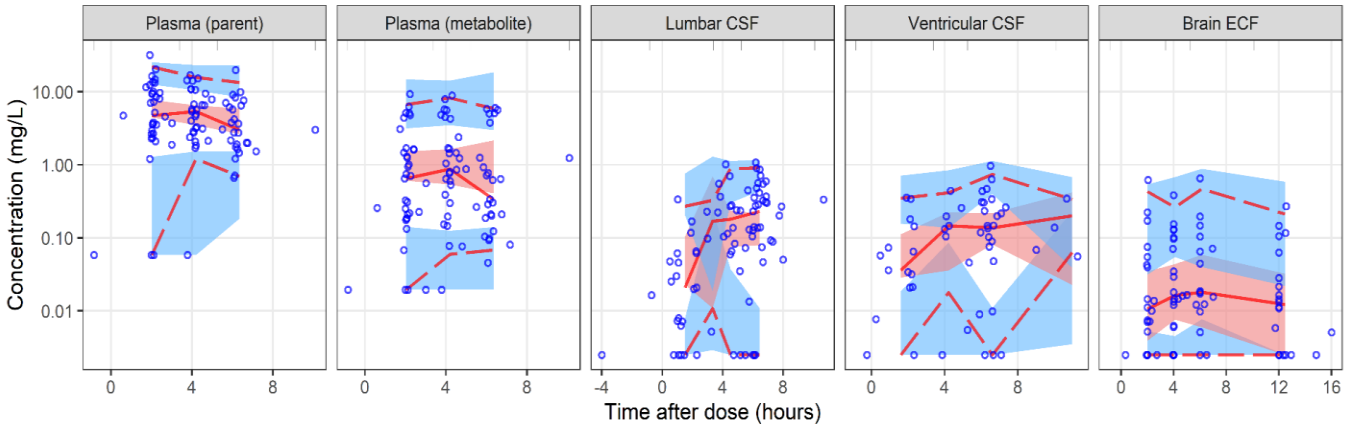

Figure 5.2: Visual predictive check (log scale) for the final model stratified by matrix. The lower, middle, and upper solid lines are the 2.5th, 50th, and 97.5th percentiles of the observed concentrations. The shaded areas are the 95% confidence intervals for the same percentiles. The circles represent the observed concentrations.

Simulations

The typical child with TBM in this cohort was 2 years old and weighed 11 kg. According to the short intensive regimen in the 2022 WHO guidelines (World Health Organization (WHO) 2022), this child would receive 4 HR 50/75 dispersible

tablets (i.e., total dose of rifampicin is 300 mg, 27.3 mg/kg) vs. 3 tablets of RHZ 60/30/150 (i.e., total dose of rifampicin is 180 mg, 16.4 mg/kg) according to the 2014 WHO guidelines. The simulated typical concentration-time profiles in plasma, lumbar and ventricular CSF, and brain ECF are presented in Figure 5.4, in which we can see that with the newer regimen, the exposures in both plasma and CSF are higher, which is particularly important in TBM since it is important to attain high exposure early in treatment. Figure 5.4 shows the simulated exposure in terms of AUC_{0-24h} for the same compartments. Figure 4.3in the supplementary shows the simulated AUC_{0-24h} for plasma, CSF, and ECF across all weight bands.

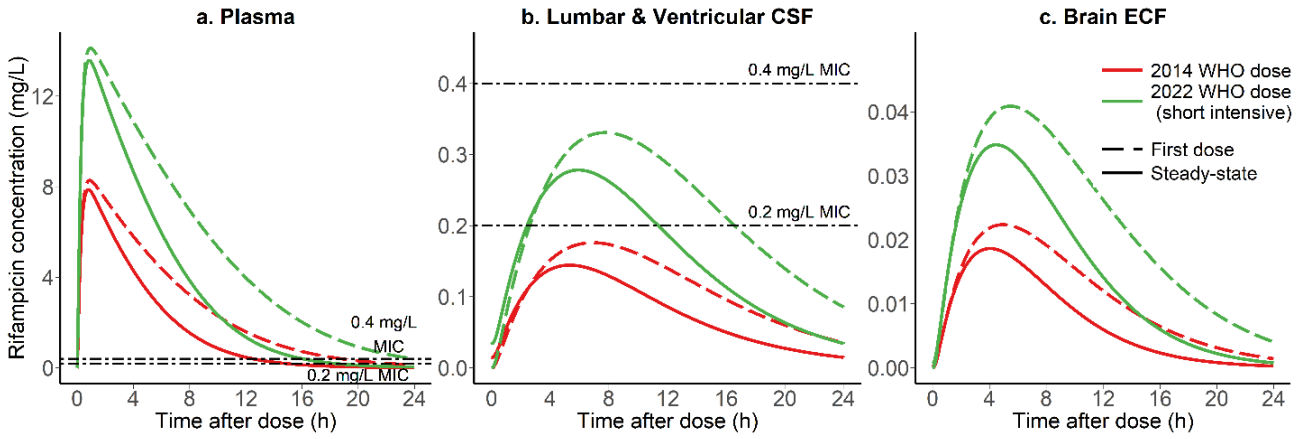

Figure 5.3**:** Simulated typical concentration-time profiles for the typical participant (11 kg and 2 years of age).

a) plasma, b) lumbar and ventricular cerebrospinal fluid, and c) brain extracellular fluid *Please note that true rifampicin concentrations in the brain tissue are unknown as relative recovery cannot be calculated)* shown for the 2014 WHO regimen and the 2022 WHO short intensive TB meningitis regimen, as well as for the first-dose vs the steady-state. The dashed lines represent the MIC levels of 0.2 and 0.4 mg/L (Rastogi, Labrousse, and Goh 1996).

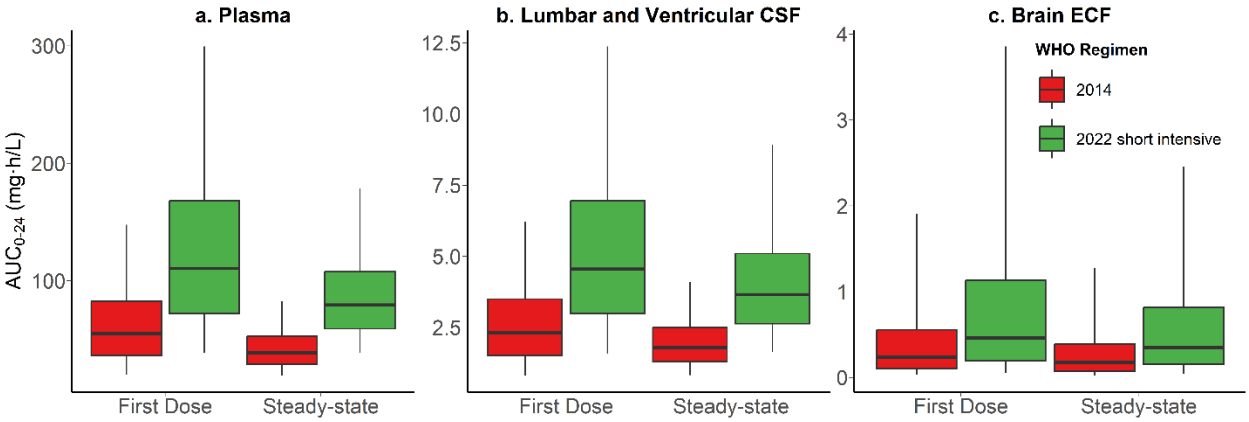

Figure 5.4: Expected exposures in terms of area under the curve ($\mathrm{AUC_{0-24h}}$) for the typical participant (11 kg and 2 years of age).

a) plasma, b) lumbar and ventricular CSF, and c) brain ECF (*Please note that true rifampicin concentrations in the brain tissue are unknown as relative recovery cannot be calculated)* for the 2014 WHO regimen and the 2022 WHO short intensive TB meningitis dosing recommendations, as well as, for the first-dose vs the steady-state. The box represents the median and interquartile range, and the whiskers correspond to the 5th and 95th percentiles.

Discussion

In this study, we characterised the pharmacokinetics of rifampicin in in plasma, lumbar and ventricular CSF, and brain ECF children with TBM. The population equilibration delay was 4 hours between plasma and lumbar as well as ventricular CSF and was 2 hours between plasma and brain ECF. As described by the PPC, the extent of rifampicin's penetration was 5% for the lumbar and ventricular CSF and 0.4% for the brain ECF. Importantly, our study is the first to report ventricular and ECF, which significantly adds to the limited knowledge available on rifampicin's distribution into the central nervous system. These sites are more likely to reflect drug concentrations at the site of TBM infection than the plasma and lumbar (spinal)

CSF, of previously published pharmacokinetic models, and therefore extend our understanding of rifampicin exposure in the brain. Increasing evidence from protein, inflammatory mediator, and transcriptomic data suggests that spinal CSF and ventricular (brain) CSF are different (Rohlwink et al. 2019, 2017), in part perhaps because of the frequency of spinal disease in TBM patients that may affect CSF dynamics (Rohlwink et al. 2016) but also potentially because of barrier permeability differences between brain and spinal cord capillaries.

Recognizing the limits of spinal CSF to study brain penetration of drugs, the use of microdialysis to interpret drug concentrations in the brain is reported as a gold standard technique for quantitative and time-resolved analysis of brain PK studies (Elizabeth C.M. De Lange 2013). However, the interpretation of drug concentrations using microdialysis has some limitations. First, it is difficult to determine the relative recovery rate in the microdialysate from tissue ECF, i.e., what percentage of the actual concentration in the tissue is retrieved in the MD samples. Second, TBM is characterized by perfusion differences due to variable small and large vessel disease; therefore, distribution of drug in the brain may be highly variable (Rohlwink et al. 2016; Ruiz-Bedoya et al. 2022). Nevertheless, our recovery of rifampicin in the brain ECF provides proof-of-concept that rifampicin does penetrate the brain tissue – its targeted site of action in paediatric TBM patients. Furthermore, under static conditions, the method provides the first demonstration of repeated measures of rifampicin in the brain, i.e., the relative values provide multiple measures in a single patient over several timepoints post-dose. The simulations show that the short-intensified regimen recently included in the 2022

WHO operational handbook provides drug exposures that are higher and more equal across the different weight bands.

The difference in the plasma-brain ECF and plasma-CSF equilibration rate could be attributed to changes in CSF volume which may affect pressure equilibrium and the concentration gradient between brain and CSF (E.C.M. de Lange 1997). Furthermore, previous simulations showed that a change in CSF dynamics changed the CSF pharmacokinetic profiles but not necessarily the brain ECF profiles regardless of the drug's physiochemical properties (Saleh et al. 2021). Pathologically, CSF dynamics will be affected by hydrocephalus, where CSF volume in the ventricles is larger (which will affect dilution of drug entering through the choroid plexus or brain interstitium) and spinal subarachnoid disease (which will affect circulation between brain and spinal CSF) (Saleh et al. 2021). Finally, differences in the blood-spinal cord barrier (compared to the blood brain barrier) (Chopra et al. 2021) and the influence of reduced CSF flow on permeability must also be taken into account (Hansotto Reiber 2003). Collectively, these findings reiterate that caution must be applied when interpreting lumbar CSF as a proxy for brain ECF concentrations in CNS diseases (Saleh et al. 2021).

Due to the sparseness of the plasma data collected, priors from previous models(M T Chirehwa et al. 2015; Denti et al. 2021) were used to stabilize the estimation of the plasma model's parameter estimates. $CL_{int,max}$ is somewhat lower than the values from Denti et al. (Denti et al. 2021), Garcia-Prats et al. (Opti-Rif trial) (Garcia-Prats et al. 2021), and Zvada et al. (Zvada et al. 2014) in South African children with pulmonary tuberculosis. This could be attributed to the fact that

children with TBM are typically sicker than those with pulmonary TB, and particularly the children in this study cohort who were mostly in ICU and had hydrocephalus requiring intervention. In addition to surgical interventions, critically ill patients have pathophysiological changes that may affect drug pharmacokinetics (Blot, Pea, and Lipman 2014). The plasma and CSF concentrations obtained in our cohort are similar to those from studies in children with TBM receiving doses between 15-20 mg/kg (Donald 2010; Panjasawatwong et al. 2020). In the study by Panjasawatwong et al. (Panjasawatwong et al. 2020) in children with TBM, the pseudo-partition coefficient estimated was 17% vs 4% in our model. In their model, the lumbar CSF observations were modelled as a CSF compartment linked to the plasma compartment, with a (E. M. Svensson et al. 2020) Their model relies on an empirical formula to calculate the CSF compartment volume. We get around the need to estimate a CSF volume by modelling the CSF as an effect compartment. Svensson et al. (34) and Savic et al. (35) have published models in adults with TBM, where the pseudo-partition coefficients and equilibration half-lives were 5% and 2 hours and 8% and 6 hours, respectively. In addition, in previously published animal models, the brain tissue:plasma rifampicin concentrations ratios were reported to be between 0.02 - 0.05 (Ruiz-Bedoya et al. 2022; Tucker et al. 2018). Both studies found the rifampicin CSF concentrations to be lower than those in the brain tissue/lesion. However, comparing ECF concentrations to either the plasma or the CSF in our study should be cautiously interpreted since the absolute concentrations in the brain ECF samples obtained with MD cannot be calculated. Levels of CSF protein or albumin are expected to correlate with the pseudo-partition coefficient, since

these are often considered markers of the degree of inflammation of the blood-brain barrier and hence its permeability to drugs. Svensson et al. (E. M. Svensson et al. 2020) found a linear relationship between the CSF protein level and rifampicin penetration into the lumbar CSF; with each 10-fold change in protein levels, the penetration coefficient increases by 63%. In Panjasawatwong et al. (Panjasawatwong et al. 2020), there is an exponential relationship between CSF protein concentration and the PC where an increase of 1 g/L in CSF protein concentration resulted in a 1.28-fold increase in PC. In our analysis, we did not find a significant effect for either the levels of albumin or total protein, which could be due to fewer samples and narrower range of CSF protein values in our cohort. However, we previously demonstrated differences in biomarkers, inflammatory mediators and differential gene expression in time-linked samples in patients with TBM. Combined with the recognition that reduced spinal CSF may increase protein concentrations in spinal CSF compared to ventricular CSF (Hansotto Reiber 2003), these factors may contribute to the explanation of lack of effect.

Both strengths and limitations in our study are related to the use of microdialysis sampling technique. MD provides the unique opportunity to obtain rifampicin samples from the brain tissue, which is the site of infection/drug action, in addition to, the opportunity for serial/continuous sampling. On the other hand, the MD conditions e.g., flow rate, semipermeable membrane pore size may affect the drug's recovery in addition to the limitations mentioned above. The exact location of MD catheter placement in the brain tissue may also affect the concentrations measured, however, there is currently no method that accomplishes

both spatial and temporal resolution in studying the brain. It has also been suggested that the CSF collection method may influence drug concentrations; however, the CSF drains were in the lateral ventricle which is likely the best location for CSF sampling as it is the most proximal location based on current knowledge on where the bulk of CSF is produced and on CSF flow dynamics (Battal et al. 2011; Di Paolo et al. 2013). Comparison of ventricular CSF and lumbar CSF is limited by the opportunistic nature of sampling and not all patients had time-linked samples for comparison; there may be bias in why some participants had ventricular or lumbar sampling and not both. Lastly, these data – like the existing literature on rifampicin pharmacokinetics in TBM – report only total rifampicin concentrations, while only the unbound fraction that is active. Our use of the 100kDa membrane reflects total drug concentration rather than unbound drug. Unfortunately, there are no data available for rifampicin protein binding in the CSF. CSF protein binding dynamics is expected to be different than that of the plasma since the CSF protein levels are different and are more variable between patients.

To overcome some of the methodological limitations of MD, suggested future research include in-vitro experiments to optimize the microdialysis method. In terms of study design, since oral absorption may be variable, particularly in critically ill patients, the use of intravenous administration of rifampicin would be an attractive alternative to eliminate the variability in rifampicin absorption following oral administration and improve our description of plasma PK, as well as to mitigate the challenges of administering drugs to children e.g., crushing tablets and administration by an oral syringe. If more CSF and brain ECF samples could be

obtained, a more complex mechanistic model that accounts for drug transfer between the LCSF, VCSF, and brain ECF could be tested. Still, there is a substantial amount of the underlying physiology in humans that require better definition and some uncertainties that still exist, largely because of lack of human data and methodological limitations in the existing animal data. For example, the flux between the ECF and ventricular CSF has been predicted but not yet fully understood or quantified (Elizabeth C.M. De Lange 2013; Saleh et al. 2021). The flux with the spinal CSF, also needs better definition because of the influence of relative blocks of CSF flow in pathology (Hansotto Reiber 2003) and the increased permeability of the tight junctions of capillaries supplying the spinal cord (Bartanusz et al. 2011).

In conclusion, we show that rifampicin's extent of penetration into both the lumbar and ventricular CSF is ~5% and provide proof-of-concept that rifampicin reaches the brain tissue. Still, further studies need to be conducted to better define antitubercular drug exposure in CSF and brain in children with TBM, including unbound drug, and treatment strategies to increase this exposure.

Supplementary materials

Sample collection details

Plasma: Three serial blood samples (0.6 mL each) were sampled on a single day in the first and second week, and, where possible at 2-, 4-, and 6-hours post-dose. Whole blood was drawn through an indwelling peripheral venous catheter in patients who did not have a routine arterial line. The venous line was inserted to

coincide with clinically indicated routine sampling to ensure that the patient does not endure additional veno-punctures. Whole blood samples were collected in a vacutainer EDTA blood collection tube and kept on ice. These were immediately processed and biobanked at -80 °C within 30 minutes, pending bioanalysis.

Lumbar and Ventricular CSF: Clinically indicated CSF samples were collected at random time points up to 24 hours post-dose into sterile 15 mL tubes and kept on ice. The samples were immediately spun at 1400 rpm for 10 minutes to separate CSF from any tissue pellets or blood and stored at -80°C within 30 minutes of sampling until analysis. Briefly, LCSF was collected for standard diagnostic and/or therapeutic procedures. Repeat lumbar punctures were performed to treat raised intracranial pressure (ICP) in patients with communicating HCP (CommHC) (A. A. Figaji and Fieggen 2010). The frequency of lumbar punctures depends on the persistence or resolution of raised ICP. In addition, VCSF was obtained from 1) ventriculoperitoneal shunt (VPS) placement as a definitive treatment for non-communicating HCP (NCHC) or failed medical treatment of communicating hydrocephalus (CommHC), 2) external ventricular drain (EVD) insertion, routine testing for bacteriology, and during air encephalograms and/or column tests to distinguish between CommHC and NCHC, or 3) endoscopic third ventriculostomy (ETV) in a selection of patients with NCHC. Our standard protocol for treating HCP in TBM is previously published (a a Figaji, Fieggen, and Peter 2003).

Brain ECF using microdialysis (MD) technique: The MD catheter was placed concurrently with the EVD and monitor into the same region (usually right frontal white matter) or sometimes on the side where hypodensity was more prominent on

the initial head computed tomography scan. The MD probe in a standard manner: it was perfused with a physiological solution (CNS Perfusion fluid, MDialysis) at a constant flow rate of 0.3 μL/min using an infusion pump (CMA 107, MDialysis, Stockholm, Sweden). Molecules in the interstitium of the brain diffuse through a 100 KDa pore size (MDialysis, Stockholm, Sweden) semipermeable membrane at the tip of the catheter, along their concentration gradient in the brain and were collected into a vial. MD vials were changed at hourly intervals for bedside monitoring of brain extracellular fluid and analyzed at the bedside (ISCUSFlex, MDialysis) for clinical purposes to observe changes in glucose, lactate, pyruvate, glycerol and glutamate using an automated system. Briefly, glucose and the lactate/pyruvate ratio are used to monitor the energy status of the brain with respect primarily to the adequacy of substrate delivery for aerobic metabolism. Patients with TBM are at high risk of stroke due to perfusion-limiting vasculitis. Evidence of brain ischemia can be addressed by more aggressive treatment of intracranial pressure, increasing blood pressure, and increasing systemic oxygenation. Glycerol is a measure of ongoing cellular breakdown. Glutamate is a measure of excitotoxicity. Remnant fluid after bedside analysis was kept on ice and biobanked at -80°C within 6 hours of collection. As MD volumes are typically small, hourly samples were pooled over 2–3-hour epochs to ensure sufficient volumes for liquid chromatography tandem mass spectrometry analysis (>20 μL). Concentrations of substances in the microdialysate are a percentage of the true concentrations in the ECF and not absolute concentrations. This percentage is termed relative recovery.

Analytical method details

Rifampicin was analysed in all samples: plasma, lumbar CSF, ventricular CSF, and brain ECF. Additionally, rifampicin's primary metabolite, 25-desacetyl rifampicin, was analysed in the plasma samples. Liquid chromatography tandem mass spectrometry assays were developed and validated at the Division of Clinical Pharmacology, University of Cape Town. Plasma samples were processed with a protein precipitation extraction method using rifampicin-d3 and 25-desacetyl-rifampicin-d3 as internal standards, followed by high performance liquid chromatography with tandem mass spectrometry detection using an AB SCIEX API 3000 instrument. Isocratic chromatography was performed on a Discovery C18 (5 µm, 50 mm x 4.6 mm) analytical column. The analyte, metabolite and internal standards were monitored at mass transitions of the protonated precursor ions 823.4, 781.5, 826.5, and 784.5 to the product ions 791.4, 749.4, 794.4, and 752.4 for rifampicin, 25-desacetyl-rifampicin, rifampicin-d3 and 25-desacetyl-rifampicin-d3, respectively. The calibration curves both fit a quadratic (weighted by $1/x^2$) regression over the ranges 0.117–30.0 µg/mL for rifampicin and 0.0391–10.0 µg/mL for 25-desacetyl-rifampicin. The combined accuracy and precision statistics of the limit of quantification, low, medium, and high-quality controls (three validation batches [n=18]) were between 101% and 107% and between 2.7% and 3.7% for rifampicin and 25-desacetyl-rifampicin, respectively.

CSF samples were processed with a protein precipitation extraction method using acidified acetonitrile and ascorbic acid, followed by high performance liquid chromatography with tandem mass spectrometry detection using an AB SCIEX API

5500Q instrument. Liquid chromatography was performed on a Poroshell 120 EC-C18 (2.7 µm, 4.6 mm x 50 mm) analytical column. Rifampicin and rifampicin-d3 were monitored at mass transitions of the protonated precursor ions 823.4 and 826.5 to the product ions 791.4 and 794.4, respectively. The calibration curve fit a quadratic (weighted by $1/x^2$) regression over the range 5 to 2500 ng/mL. The combined accuracy and precision statistics of the limit of quantification, low, medium, and high-quality controls (three validation batches [n=18]) were between 88.9% and 102.9% and between 3.8% and 8.3% for rifampicin.

Population pharmacokinetic analysis

Residual unexplained variability was described using a combined proportional and additive error model, with the additive error for all samples set to be at least 20% of the LLOQ. Concentrations below the lower limit of quantification (BLQ) were censored according to Beal's M6 method, in which the last censored value in a series during the absorption phase and the first censored value in a series in the terminal phase were replaced with LLOQ/2 and the other censored values in a series were discarded (S. L. Beal 2001). To account for the larger level of uncertainty in the imputed censored values, their additive error was inflated by LLOQ/2.

Model development and covariate inclusion were guided by physiological plausibility, model fit diagnostics including the drop in the objective function value (OFV) and inspection of diagnostic plots, including visual predictive checks (VPCs). Comparison between nested models was done using the likelihood ratio test for the drop in OFV, assumed to be approximately χ^2 distributed with *n* degrees of freedom, where *n* is the number of additional estimated parameters. Covariates

were added in a stepwise manner in order of importance determined by the largest significant drop in the OFV. A *p*-value of 0.05 was generally used for inclusion and 0.01 for retention.

Table S5.1: Summary of albumin and total protein values in plasma, lumbar and ventricular cerebrospinal fluid (CSF), and brain extracellular fluid (ECF)

	Median (min - max) of all samples			
	Albumin (g/L)		**Total protein (g/L)**	
	N	Median (IQR)	N	Median (IQR)
Lumbar CSF	191	1.97 (2.83)	47	2.73 (3.46)
Ventricular CSF	193	0.489 (0.448)	31	0.890 (0.835)
Plasma	147	32.0 (7.00)	-	-
LCSF : plasma	68	0.052 (0.098)	-	-
VCSF : plasma	82	0.017 (0.011)	-	-

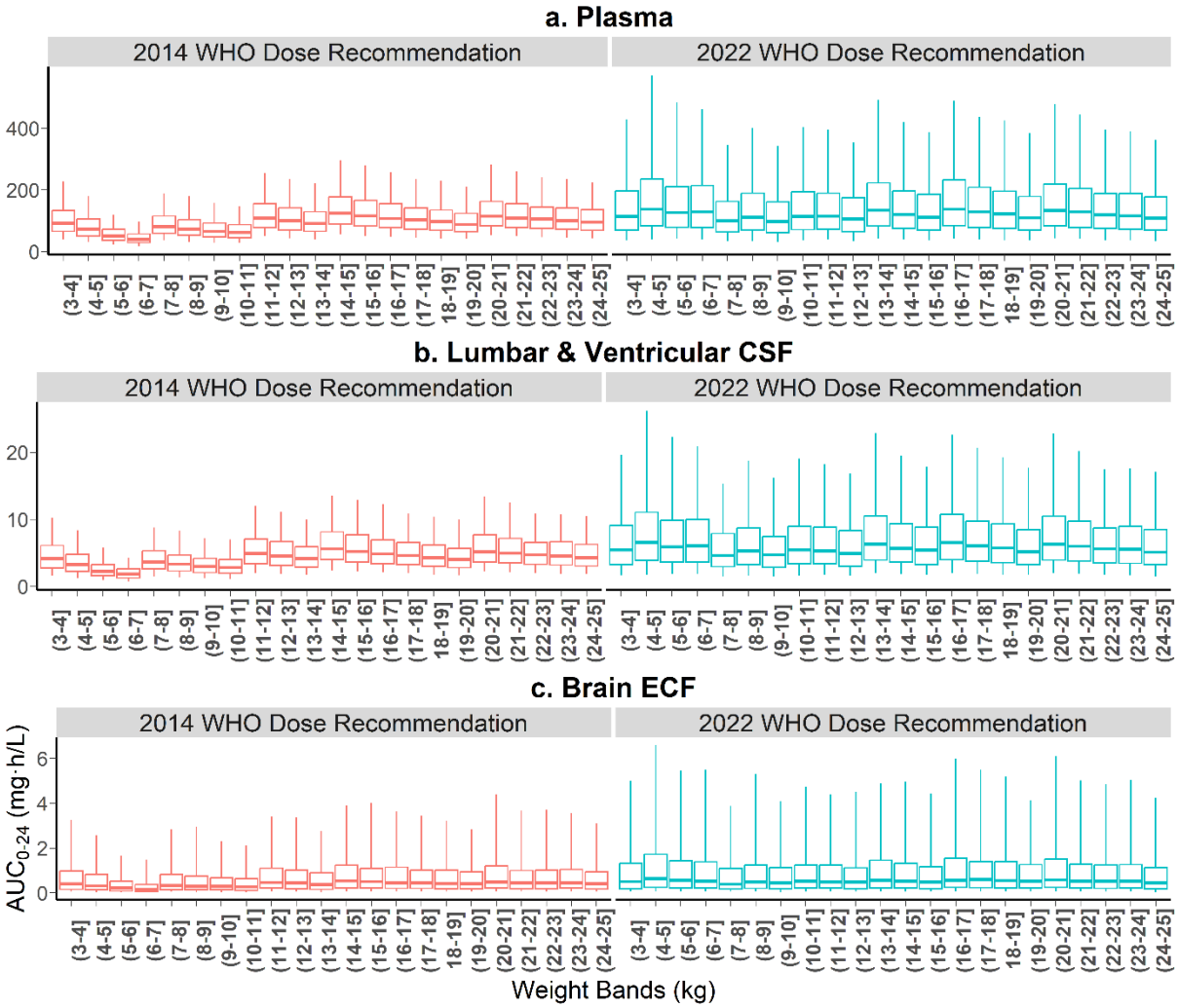

Figure S5.5 Exposures at steady-state as area under the curve 24h (AUC_{0-24h}) across all dosing weight bands.

in a) plasma, b) cerebrospinal fluid (CSF) (lumbar and ventricular), and c) brain extracellular fluid (ECF) shown for both the 2014 WHO dose regimen recommendation and the 2022 WHO short intensive regimen

Chapter 6 : Population pharmacokinetics of rifampicin in plasma and cerebrospinal fluid in adults with tuberculosis meningitis

Abstract

Background

Several ongoing clinical trials are evaluating high-dose rifampicin (up to 35 mg/kg) for tuberculous meningitis (TBM). However, rifampicin pharmacokinetics at higher doses are not fully characterised, particularly in cerebrospinal fluid (CSF), the site of TBM disease.

Methods

In a randomised controlled trial, adults with HIV-associated TBM were assigned to experimental arms of high-dose rifampicin (oral 35 mg/kg or intravenous 20 mg/kg) plus linezolid, with or without aspirin, or a control arm that received the standard-of-care with 10 mg/kg oral rifampicin. Rifampicin concentrations, including the unbound fraction, were measured on plasma samples and CSF collected on days 3 and 28 of study enrolment. Data were analysed using non-linear mixed effects modelling.

Results

400 plasma and 44 CSF rifampicin concentrations from 48 participants were used for model development. Median (min-max) age and weight were 39 (25-78) years, and 60 (30-107) kg, respectively. Rifampicin pharmacokinetics was best described

by a 2-compartment disposition model with first-order transit oral absorption and elimination via saturable hepatic extraction. Typical clearance values for the standard dose for day 3 and day 28 were 33.1 L/h and 41.4 L/h, respectively; high dose values were 46.1 L/h and 70.2 L/h. The CSF-plasma ratio was estimated to be ~6% and the equilibration half-life was 3.2 hours. Simulated standard-dose rifampicin did not reach CSF concentrations above the critical concentration for *M. tuberculosis*.

Conclusion

CSF penetration with standard dose rifampicin is low. Our findings support continued evaluation of high-dose rifampicin for TBM treatment.

Introduction

Tuberculosis meningitis (TBM) is a severe form of extrapulmonary tuberculosis (TB) involving the central nervous system (CNS). Despite treatment, case-fatality is ~25% in HIV negative individuals and up to 50% in those living with HIV, with permanent disability in around 20% of survivors (Dodd et al. 2021; Wasserman et al. 2019). Most deaths from TBM occur early in the illness, therefore, more rapid and effective treatment may improve outcomes (Jaipuriar et al. 2019).

One way to achieve this is to optimise dosing to ensure attainment of therapeutic drug concentrations in the CNS, the site of the disease (Wasserman et al. 2019). Drugs targeted at TBM need to cross several barriers, including the blood-brain barrier (BBB) and the blood-cerebrospinal fluid barrier (BCSFB) that separate the systemic circulation from the CNS. This should occur rapidly and at adequate

concentrations for effective antitubercular activity. Disease-related changes in BBB permeability and dynamic changes in protein concentrations may importantly influence for drug penetration into the CNS (van Toorn et al. 2014).

Rifampicin remains the cornerstone of TBM management but is still dosed at 10 mg/kg, the same as for pulmonary TB whose disease site is in the lungs. Clinical studies of pulmonary TB show a correlation between rifampicin dose and sputum culture conversion (Sekaggya-Wiltshire et al. 2018), suggesting that higher doses may be beneficial to achieve higher site-of-disease exposures and potentially better clinical outcomes. There is evidence that rifampicin doses (≥30 mg/kg) are required to achieve adequate intralesional concentrations in TBM (Tucker et al. 2018) and that CSF concentrations increase with higher doses (Cresswell et al. 2021). This has led to several trials investigating higher dose rifampicin for TBM: clinical outcomes of this approach have been variable and there remains uncertainty around the dose selection that optimises CSF exposure.

Orally administered rifampicin is well absorbed with >86% absolute bioavailability (Mariappan et al. 2005). It exhibits non-linear elimination with a saturable first-pass effect at higher doses (Boeree et al. 2015; R. J. Svensson et al. 2018) and it induces many enzymes and transporters via activation of the Pregnane X receptor, including those involved in its clearance. For this reason, rifampicin clearance is expected to double after about two weeks of administration (M T Chirehwa et al. 2015). It is highly protein-bound (~80%), with poor penetration in CNS tissues (G. Acocella 1978). Rifampicin plasma pharmacokinetics has been extensively described among pulmonary TB populations, but limited data is

available on its CSF pharmacokinetics, especially among patients with TBM where disease effects may influence penetration and equilibration into this compartment. We therefore characterised rifampicin pharmacokinetics in both plasma and CSF in adults with HIV-associated TBM following the administration of high-dose rifampicin either orally (35 mg/kg) or intravenously (20 mg/kg) and standard-dose rifampicin orally (10 mg/kg).

Methods

Parent study and interventions

This was a pharmacokinetic substudy of LASER-TBM, a phase 2A trial investigating the safety and tolerability of intensified antibiotic therapy in adults with HIV-associated TBM. Participants were enrolled within 5 days of antituberculosis treatment initiation from four hospitals in South Africa, and randomly assigned to either a control group that received the standard-of-care TBM regimen (rifampicin 10 mg/kg, isoniazid 5 mg/kg, pyrazinamide 25 mg/kg, and ethambutol 15 mg/kg, administered as fixed-dose combination (FDC) tablets) according to World Health Organization (WHO) weight bands, or one of two experimental regimens. Individuals allocated to experimental arms received additional rifampicin plus oral linezolid 1200 mg daily with or without aspirin. They underwent a second randomisation to receive either high-dose oral (35 mg/kg) or intravenous (IV) (20 mg/kg) rifampicin for the first 3 days of treatment; after day 3, all participants in the experimental arms continued oral high-dose rifampicin 35 mg/kg daily until the end of the study. The high-dose oral rifampicin was administered as FDC tablets

topped up with individual rifampicin tablets using bespoke weight bands designed to balance exposures across weight groups (Wasserman et al. 2021). Those in the IV rifampicin group received the full rifampicin 20 mg/kg dose as a one-hour infusion. All participants received adjunctive corticosteroids. More details about LASER-TBM can be found in the publication by Davis et al. (Davis et al. 2023).

The study was approved by the University of Cape Town Human Research Ethics Committee (UCT HREC reference: 293/2018), Walter Sisulu University (HREC reference: 012/2019), and the South African Health Products Regulatory Authority (reference number 20180622). The trial was registered on clinicaltrials.gov (NCT03927313). Informed consent was obtained from all participants or their proxies.

Pharmacokinetic sampling

All trial participants underwent pharmacokinetic sampling on days 3 (visit 1) and 28 (visit 2) (±2 days) after study enrolment. Plasma samples were collected at pre-, 0.5, 1, 2, 3-, 6-, 8-10- and 24-hours post-dose on day 3 and at pre-, 2-, and 4-hours post-dose on day 28. One lumbar CSF sample was collected at each sampling visit, with sampling time randomised to intervals of 1-3, 3-6, 6-10-, and 24 hours post-dose. Immediately following collection samples were processed on site and stored at -80°C.

Total (protein-bound and -unbound) rifampicin concentrations were quantified in all collected plasma and CSF samples, and free (unbound) plasma rifampicin concentrations were measured in a subset of participants. Drug quantification was performed by a validated liquid chromatography-tandem mass

spectrometry assay developed at the Division of Clinical Pharmacology, University of Cape Town. Additional details regarding the assay method are presented in the supplementary material.

The unbound fraction (fu) of plasma rifampicin was estimated using Deming regression to regress measured free concentrations against total concentrations with an intercept of zero (Deming 1943; Linnet 1998). Participant characteristics, clinical information, and blood chemistry were obtained on each visit. Total protein, albumin, and glucose were measured in CSF samples.

Pharmacokinetic modelling

Population pharmacokinetic modelling was used to describe total rifampicin plasma and CSF concentrations. The model was developed stepwise: first, we used the IV dosing plasma concentrations to test different disposition models; second, we included the oral dosing plasma concentrations; and finally, we added the CSF concentrations. For the CSF "effect" compartment we estimated a pseudo-partition coefficient (PPC) i.e., CSF to plasma drug ratio, and an equilibration half-live ($T_{1/2eq}$), i.e., the delay in equilibration between the plasma and CSF as described in the supplementary material. All plasma and CSF parameters were estimated simultaneously. A previously published model by Chirehwa et al. (M T Chirehwa et al. 2015) was used as a starting point to develop the plasma pharmacokinetic model. We compared saturable hepatic elimination (and first-pass effect) versus linear clearance. We also tested different approaches to describe clearance autoinduction. These included an exponential model with clearance increasing as a function of days on rifampicin treatment (M T Chirehwa et al. 2015), an enzyme

turnover model (R. J. Svensson et al. 2018), and estimating separate typical intrinsic clearance and the fraction unbound ($CL_{int,max}.f_u$) values for each visit. Allometric scaling was applied for all disposition parameters using the fixed power exponents of 0.75 for clearance parameters and 1 for volume parameters (B. J. Anderson and Holford 2008). Either total body weight or fat-free mass (FFM) (calculated based on the formula in Janmahasatian et al. (Janmahasatian et al. 2005)) were tested as body size descriptors. Lag time and transit compartments were tested to capture the delay in absorption. We tested the inclusion of between-subject and between-visit variabilities for the disposition parameters and bioavailability, and between-occasion variability for the absorption parameters. An occasion was defined as any dosing event with at least one observation post-dose, and a visit refers to a pre-dose sample, dosing, and post-dose observations on a visit to the clinical site.

The influence of potential covariates on plasma pharmacokinetic parameters was tested following the development of the structural model. Covariates included the effect of rifampicin dose, duration since start of treatment and study arm. We also tested whether FDC tablets and top-up individual tablets had significantly different bioavailability since this has previously been reported (Kengo et al. 2023; Court et al. 2018). The effect of various laboratory and clinical covariates were tested on PPC, including CSF protein, CSF albumin, CSF glucose, polymorphonuclear cells, lymphocytes, and the Glasgow Coma Scale. Additional details for the modelling methods and imputation of missing covariates are provided in the supplementary material. Covariate selection was based on the drop in objective function values (OFV) and physiological plausibility.

Simulations

The final model was used to predict the area under the concentration-time curve from time 0 to 24 hours post-dose ($AUC_{0\text{-}24h}$) and the concentration at 24 hours post-dose (C_{24h}) for the available concentration-time profiles. We also predicted concentration-time profiles in plasma and CSF following both standard-dose (10 mg/kg) and high-dose (35 mg/kg) rifampicin for a typical participant in this cohort. The critical concentration (CC) referenced in the WHO Technical Report on critical concentrations for drug susceptibility testing of isoniazid and the rifamycins (rifampicin, rifabutin and rifapentine) (World Health Organization 2021a) was used as a reference value. Minimum inhibitory concentration (MIC) tests were not performed on M. tuberculosis isolates from the patients of this study.

Results

Study data

49 participants underwent pharmacokinetic sampling on day 3 and 34 participants were sampled on day 28, providing a total of 411 plasma (56 BLQ) and 46 CSF (13 BLQ) samples for model development. We excluded rifampicin concentrations from one participant (who had observations only for the first visit) due to dislocation of the IV catheter and tissue extravasation of the drug.

Baseline clinical characteristics are summarised in Table 6.1. The median (min-max) age, weight, and FFM were 39 (25-78) years, 60 (30-107) kg, and 45 (30-59) kg, respectively. The median duration since the start of rifampicin-based TB

treatment was 5 days (range 1 – 8) on the first visit and 30 days (range 26 – 38) on the second.

Table 6.1: Participant characteristics

	Median (Min. – Max.) or no. (%)	
	Visit Day 3 (n = 49)	**Visit Day 28 (n = 34)**
Males	27 (55.1%)	20 (58.8%)
Age (years)	39 (25-78)	39 (25-57)
Weight (kg)	59.5 (30-107.2)	61.7 (37.4-105.1)
Height (m) [a]	1.60 (1.48-1.80)	1.60 (1.49-1.80)
Fat-free mass (kg) [b]	45.2 (30.3-59.4)	45.5 (32.4-60)
Days on rifampicin until PK visit date [c]	4 (0-7)	30 (26-38)
CSF total protein (g/L) [d]	1.16 (0.2 - 55)	1.21 (0.2 - 55)
CSF albumin (mg/L) [e]	387 (46 – 7601)	373 (46.0 - 1269)
CSF glucose (mmol/L) [d]	3.05 (0.05 - 5.9)	2.8 (0.3 - 5.9)
Antiretroviral therapy (ART):		
Previous ART	14 (28.6%)	10 (29.4%)
ART Naïve	20 (40.8%)	14 (41.2%)
On ART	15 (30.6%)	10 (29.4%)

[a] Heights were missing for 29 and 19 participants on day 3 and day 28, respectively. The missing heights were imputed based on sex and weight according to the details provided in the supplementary file. The median (min – max) values reported here are for the non-missing values (i.e., it does not include the imputed values).

[b] Fat-free mass was calculated based on sex, weight, and height according to the formula in Janmahasatian *et al.* (Janmahasatian et al. 2005)

The median (min – max) values reported here are for the non-missing values (i.e., it does not include the imputed values).

[c] This refers to the total number of days since the start of treatment which was ~1-3 days before the investigational product start date until the PK visit date; All participants were assumed to be on standard-dose (10 mg/kg) rifampicin when starting treatment and before study enrolment.

[d] CSF total protein and CSF glucose values were missing for 17 and 8 participants on day 3 and day 28, respectively.

[e] CSF albumin values were missing for 23 and 13 participants on day 3 and day 28, respectively.

Pharmacokinetic modelling

Plasma pharmacokinetics of rifampicin concentrations was best described by a two-compartment disposition model (dOFV = -10.9, *p*-value = 0.004 compared to one-compartment disposition), with first-order absorption preceded by a chain of transit compartments and elimination with saturable hepatic extraction. A depiction of the structural model is shown in Figure 6.1. Robust estimation of the Km was challenging therefore we used a prior from the model by Chirehwa et al. to guide its estimation (M T Chirehwa et al. 2015). The model fit improved significantly upon including clearance saturation versus linear clearance (dOFV = 10.6, *p*-value < 0.005).

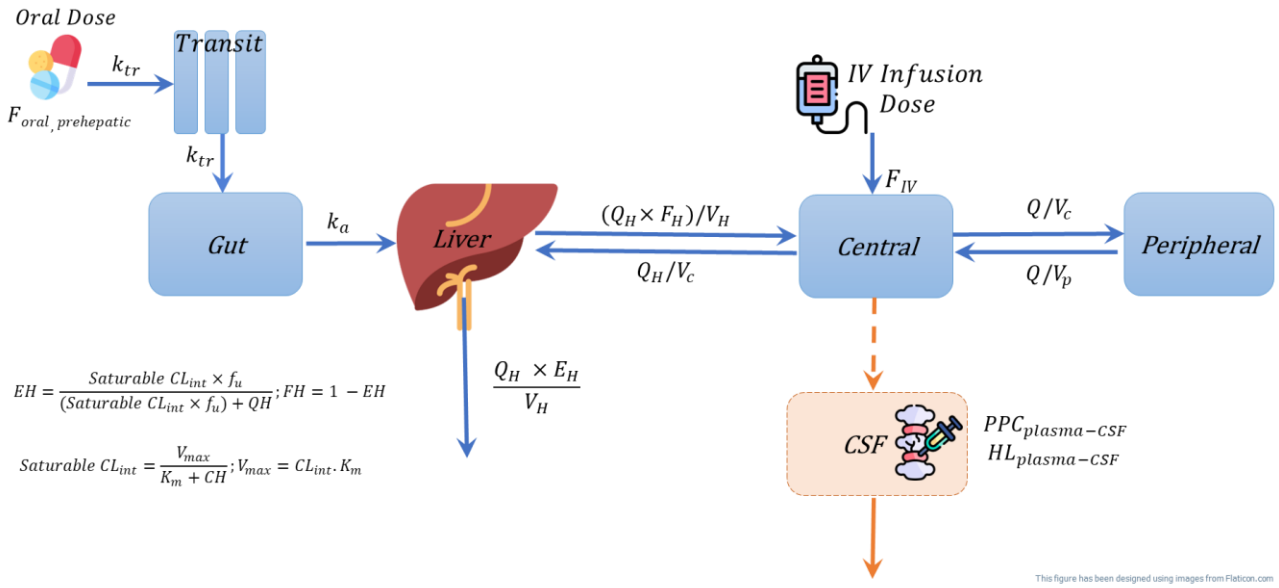

Figure 6.1: Illustration of the final structural model.

Foral,prehepatic is the prehepatic oral bioavailability, FIV is the absolute intravenous bioavailability, ktr is the first-order rate constant for drug passage through transit compartments, ka is the first-order absorption rate constant, QH is the hepatic blood flow, FH is the hepatic bioavailability, EH is the hepatic extraction, VH is the hepatic volume of distribution, Vc is the central volume of distribution, Vp

is the peripheral volume of distribution, Q is the intercompartmental clearance, Km is the Michaelis-Menten constant, Vmax is the maximum rate of elimination, CH is the hepatic drug concentration, and CLint is the intrinsic clearance. PPCplasma-CSF is the pseudo-partition coefficient which represents the ratio of drug in CSF to plasma and HLplasma-CSF is the equilibration half-life between plasma and cerebrospinal fluid, which describe how soon the change in plasma is reflected in the CSF.

Assuming the bioavailability of the IV dose was 100%, oral prehepatic bioavailability (before first-pass hepatic extraction) was estimated at 93.4%. Clearance was higher in participants receiving larger doses of rifampicin and at visit 2 compared to visit 1: attempts to describe this using the exponential change over time suggested by Chirehwa et al. (M T Chirehwa et al. 2015) or an enzyme turnover model similar to Svensson et al (R. J. Svensson et al. 2018) (also using priors to help guide parameter estimation) did not result in robust parameter estimation as the models did not converge properly. Therefore, clearance was estimated by separate $CL_{int,max}.f_u$ values for each visit. The typical values of $CL_{int,max}.f_u$ for the standard dose were 33.1 L/h for visit 1 and 41.4 L/h for visit 2, while the high dose values were 46.1 L/h for visit 1 and 70.2 L/h for visit 2. Allometry with FFM resulted in a better model fit compared with body weight (drop in OFV 33.1 points (p-value < 0.0001) for FFM versus 13.7 points (p-value < 0.001) for body weight). We did not find a statistically significant difference in bioavailability for the FDC and the individual top-up tablets, or for biomarkers such as creatinine, AST, or ALT.

CSF equilibration half-life and the PPC were estimated to be 3.1 hours and 5.3%, respectively. None of the covariates tested resulted in a statistically significant effect on the PPC or the equilibration half-life. All parameter estimates are

presented in Table 6.2 and the visual predictive check for both the plasma and CSF observations are displayed in Figure 6.4, showing good agreement between observed concentrations and model predictions.

Plasma protein binding was calculated as 82.8% and there was no evidence of nonlinearities in binding at higher rifampicin concentrations (Figure 6.5**)**.

Table 6.2 Final population pharmacokinetic parameter estimates for rifampicin in plasma and cerebrospinal fluid

Parameter [b]	**Estimate (95% confidence interval)** [a]
$CL_{int,max}.f_u$ for standard-dose on visit 1 (L/h) [c]	33.1 (25.2 – 42.9)
$CL_{int,max}.f_u$ for standard-dose on visit 2 (L/h) [c]	41.4 (28.0 – 58.3)
$CL_{int,max}.f_u$ for high-dose on visit 1 (L/h) [c]	46.1 (34.2 – 62.3)
$CL_{int,max}.f_u$ for high-dose on visit 2 (L/h) [c]	70.2 (51.0 – 95.5)
Michaelis-Menten constant, Km (mg/L) [d]	2.97 (2.01 – 4.56)
Central volume of distribution, V (L) [c]	27.3 (22.8 – 34.0)
Prehepatic oral bioavailability, (.) [e]	0.934 (0.852 – 0.991)
Intravenous bioavailability, F (.)	1 fixed
Peripheral volume of distribution, Vp (L)	31.5 (25.3 – 37.1)
Intercompartmental flow, Q (L/h)	11.0 (7.45 – 14.4)
Absorption rate constant, ka (h^{-1})	0.486 (0.365 – 0.638)
Mean transit time, MTT (h)	0.634 (0.467 – 0.791)
No. of absorption transit compartments, NN (.) [f]	19 fixed

Equilibration half-life to CSF, $HL_{plasma\text{-}CSF}$ (h)	3.20 (2.06 – 4.93)
Pseudo-partition coefficient to CSF, $PPC_{plasma\text{-}CSF}$ (.)	0.0593 (0.0544 – 0.0672)
Between-subject variability (BSV) in $CL_{int,max}.f_u$ (%)	25.3 (24.1 – 26.6)
BSV in central volume (%)	17.2 (14.8 – 18.5)
BSV in infusion duration (%) [g]	17.0 (14.9 – 18.6)
Between-occasion variability (BOV) in $F_{oral,prehepatic}$ (%)	18.2 (16.7 –20.1)
BOV in ka (%)	78.1 (55.8 – 95.6)
BOV in MTT (%)	111 (87.7 - 137)
Proportional error plasma (%)	25.2 (22.3 – 29.7)
Additive error plasma (mg/L) [h]	0.0234
Proportional error CSF (%)	98.4 (91.8 – 99.9)
Additive error CSF (µg/mL) [i]	2.31 (1.77 – 2.93)

[a] Values in parentheses are the 95% confidence interval, computed with sampling importance resampling (SIR).

[b] Hepatic volume of distribution (V_H), hepatic intercompartmental clearance (Q_H), and fraction unbound (fu) were fixed to 1 L, 90 L/h and 0.2, respectively.

[c] All disposition parameters were allometrically scaled by fat-free mass (FFM). The typical values reported here refer to the typical participant with a median FFM of 45 kg.

[d] Km was estimated using a prior from Chirehwa et al. (M T Chirehwa et al. 2015) of 3.35 mg/L with 30% uncertainty.

[e] This refers to the oral bioavailability from the gastrointestinal tract before hepatic extraction.

[f] Number of transit compartments was estimated in earlier runs and fixed in later runs for model stability

[g] The infusion duration is 1 hour according to the protocol. Between-subject variability (BSV) was included to account for error in infusion rate duration or time.

[h] The estimate of the additive component of the error was not significantly different from its lower boundary of 20% of lower limit of quantification (LLOQ) (0.117 mg/L), so it was fixed to this value.

[i] The lower boundary of the additive error was fixed to 50% of the LLOQ (0.005 mg/L).

Simulations

The simulated standard dose CSF profile did not reach concentrations above the rifampicin CC of 0.5 mg/L (World Health Organization 2021a), whereas the high-dose achieved concentrations above this CC level (Figure 6.2**)**. Model-derived individual steady-state $AUC_{0\text{-}24h}$ and trough concentrations are summarised in Table 6.3 and depicted in Figure 6.3

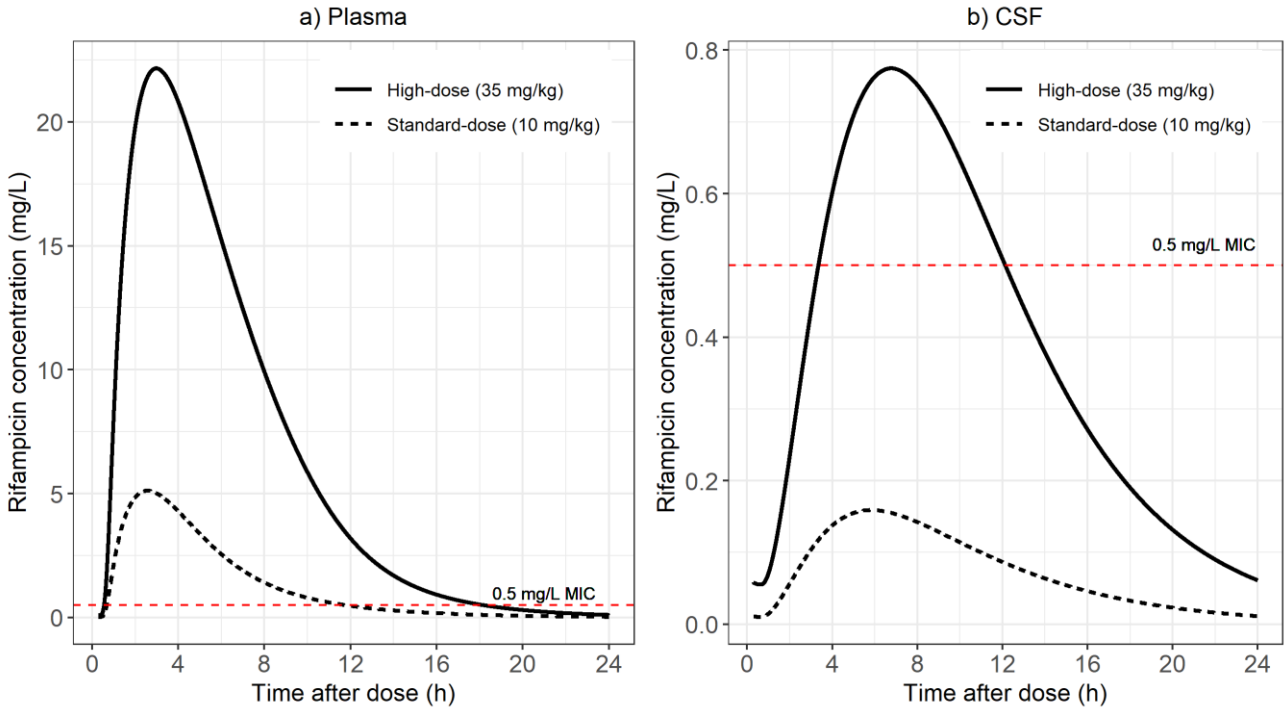

Figure 6.2**:** Simulated typical concentration-time profiles for plasma and cerebrospinal fluid (CSF) for high-dose (35 mg/kg) and standard-dose (10 mg/kg) oral daily at steady-state.

The solid and dashed lines represent the high- and standard-dose, respectively. The horizontal dotted line shows the critical concentration (CC) value of rifampicin for *M. tuberculosis* (0.5 mg/L)

Table 6.3 Model-derived rifampicin area under the curve for 24 hours (AUC_{0-24}) and concentrations at 24 hours post-dose (C_{24})

		Median (Min. – Max.) [N]			
		High-dose (35 mg/kg)		Standard-dose (10 mg/kg)	
		Day 3	Day 28	Day 3	Day 28
AUC_{0-24} (mg.h/L)	Plasma	239 (120 – 668) [28]	160 (58.4 – 477) [20]	40.5 (16.4 – 122) [19]	35.1 (13.4 – 59.8) [13]
	CSF	15.4 (7.13 – 38.1) [17]	8.50 (3.61 – 14.8) [11]	2.33 (1.05 – 4.93) [9]	2.32 (0.754 – 3.41) [8]
C_{24} (mg/L)	Plasma	0.551 (0.0628 – 12.0) [29]	0.120 (0.0303 – 2.85) [21]	0.0473 (0.0182 – 0.574) [19]	0.0374 (0.00758 – 0.181) [13]
	CSF	0.173 (0.0327 – 0.658) [17]	0.0556 (0.0199 – 0.173) [12]	0.0144 (0.00929 – 0.0421) [9]	0.0175 (0.00870 – 0.0399) [8]

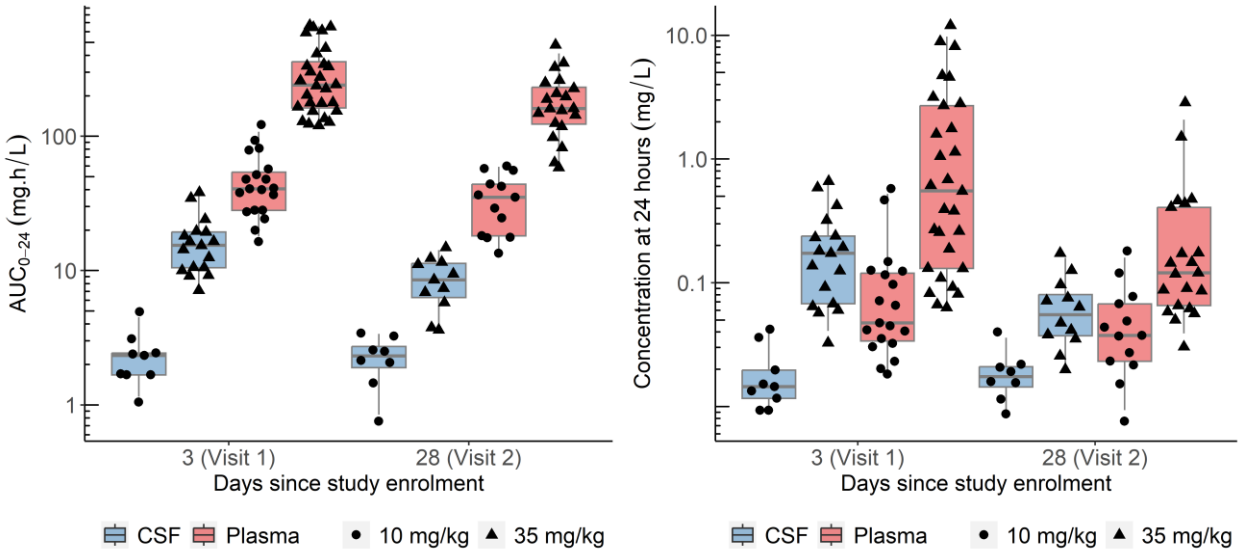

Figure 6.3: Box and whisker plots of the secondary model-derived exposure parameters.

Area under concentration curve for 24 hours (AUC0-24) (left) and concentration at 24 hours post-dose (C24) (right) stratified by dose group. The dots represent individual values, and the whiskers are the 2.5th and 97.5th percentiles.

Discussion

We characterised the pharmacokinetics of rifampicin in plasma and CSF among South African adults with HIV-associated TBM. Our population pharmacokinetic model was based on data following both high (35 mg/kg) and standard (10 mg/kg) dosing, as well as oral versus intravenous administration. The CSF partition coefficient of rifampicin, a measure of drug penetration, was estimated to be ~6%, and the equilibration half-life, indicative of the delay between the plasma and CSF concentrations, was ~3 hours. Rifampicin plasma clearance increased over time and was relatively lower for the standard dose than the high dose.

Previous rifampicin CSF models for TBM have been developed based on studies in children and adults receiving doses between 15-20 mg/kg (Savic et al. 2015; E. M. Svensson et al. 2020; Panjasawatwong et al. 2020; Abdelgawad et al. 2023). Their estimates for PPC ranged from 4.60 to 8.07% and for equilibration half-life between 2.07 and 5.78 hours, in line with our findings. An exception is a study by Panjasawatwong et al. (Panjasawatwong et al. 2020), which reported a PPC of 17% in children with TBM administered rifampicin at 10 mg/kg. While the plasma and CSF observed concentrations were similar to the standard-dose arm in our study, a different modelling approach was used to estimate CSF penetration. The CSF was modelled as a "real" distribution compartment (with volume fixed for each participant based on an empirical formula according to their age) and the presence of mass transfer to and from the central compartment. In our analysis, we circumvented the need to estimate a CSF volume by modelling the CSF as an effect

compartment, assuming no volume of distribution for the CSF compartment with no or negligible transfer to and from the plasma.

Similarly to Savic et al. (Savic et al. 2015) and Abdelgawad et al. (Abdelgawad et al. 2023), we did not find a significant effect from CSF albumin or total protein concentrations, a marker of meningeal inflammation, on rifampicin partitioning into CSF. This is in contrast to other studies which have demonstrated a positive correlation between rifampicin CSF penetration and increasing CSF protein levels (E. M. Svensson et al. 2020; Panjasawatwong et al. 2020), which could be explained by increased permeability of the protective barriers in TBM, leading to higher concentrations of both protein and total drug in the CSF. Another reason could be that increased CSF protein production from local inflammation leads to changes in CSF drug binding kinetics and higher total drug levels. Measuring free (unbound) drug concentrations in the CSF could provide a clearer understanding of the relationship between CSF proteins and drug concentrations. Lack of an association between CSF protein and drug exposure seen in our study could be due to the small sample size and the narrow range of CSF protein values in our cohort.

Other findings aligned with previous reports. With data obtained from IV administration, we estimated prehepatic oral bioavailability at 93.4%, which aligns with the previously reported absolute bioavailability of >86% (Mariappan et al. 2005), though our estimate refers to the fraction of drug available before hepatic extraction. Use of IV data enabled characterisation of a 2-compartment disposition model, previously described for rifampicin when IV data was available (Cresswell et al. 2021). The degree of plasma protein binding observed in our study, 82.8%,

agrees with the literature for TB patients (Boman and Ringberger 1974). We did not observe an increase in f_u with higher plasma concentrations, which would have indicated saturation of plasma protein binding. We observed relatively constant protein binding over the observed concentration range suggesting plasma protein binding does not become saturated with higher rifampicin exposures. Lack of saturation up to rifampicin doses up to 35 mg/kg was also observed in another study involving patients with pulmonary TB receiving of rifampicin (Litjens et al. 2019). Since only the unbound non-ionized fraction can cross membrane barriers and diffuse freely into tissues, this indicates that about 34% of free rifampicin crosses into the CSF.

Simulations based on our model predict that the standard 10 mg/kg dose of rifampicin achieves CSF concentrations far below the critical concentration for *M. tuberculosis* for most TBM patients. This is overcome with the 35 mg/kg dose, supporting ongoing clinical evaluation of high dose rifampicin for TBM. However, no CSF target concentrations have been established for rifampicin efficacy in TBM and the CC may be an inappropriate pharmacodynamic measure because it is determined under *in vitro* conditions that differ substantially from those in the CSF (Donald 2010).

Our analysis had some limitations. In our model, we were unable to characterise clearance autoinduction semi-mechanistically using an enzyme turnover model or an exponential maturation model. This is because the study participants had started rifampicin treatment approximately a week before the first plasma samples were collected and observations from the uninduced state (first day

of treatment) were unavailable. Additionally, there is uncertainty regarding the actual dose and duration of treatment before study enrolment. Also, plasma sampling on the second visit was done only up to 4 hours thus affecting the estimation of $CL_{int,max}.f_u$ for the second visit. Secondly, only one CSF sample could be obtained per visit due to the invasive nature of lumbar CSF sampling with high variability in the CSF observations. This makes it difficult to distinguish between-subject variability from random variability (e.g. error due to sample assays), requiring large proportional error for CSF observations.

In summary, we successfully developed a population pharmacokinetic model for rifampicin in both plasma and CSF for adults with HIV-associated TBM. This model provides a tool to identify rifampicin dosing strategies to optimise TBM treatment once exposure targets have been defined. Our major finding was that rifampicin has poor CSF penetration, providing rationale for ongoing evaluation of high dose rifampicin and, potentially, novel rifamycin-free regimens, to improve treatment outcomes in TBM.

Supplementary materials

Drug quantification

Rifampicin concentrations were measured with validated assays in the Division of Clinical Pharmacology laboratory at the University of Cape Town. The assays met FDA validation criteria. The total plasma assay involved a protein precipitation extraction, followed by isocratic liquid chromatographic separation, and mass spectrometry detection. The calibration range was 0.117 to 30 µg/mL. Plasma was

separated using ultracentrifugation, and the plasma protein-free fraction was analysed using solid-phase extraction and liquid chromatography with mass spectrometry detection. The calibration range was 0.0600 to 5.00 µg/mL. The CSF assay required protein precipitation and gradient liquid chromatography with mass spectrometry detection. The calibration range was 0.005 to 2.5 µg/mL.

Imputation of missing covariates

Missing heights were imputed using multiple linear regression as suggested by Johansson and Karlsson (Johansson and Karlsson 2013) since it was missing in 60% of the participants. In the first step, participant characteristics, namely sex, weight, and height from a study in a similar population (Brust et al. 2021) were used to develop a multiple linear regression model for height versus weight by sex and accounting for residual variability in heights. Secondly, this multiple linear regression model was used to estimate the missing heights in NONMEM using a random effect model as shown in the equation below:

$$Ht_i = \beta + \alpha . Wt_i . e^{\eta_i}$$

Where Ht_i is the individual height in meters and Wt_i is the individual weight in kilograms. β and α are the model mean intercept and slope respectively. η_i is the random effect accounting for the individual difference from the mean values. The η_i values are assumed to be normally distributed with mean zero and variance ω^2.The values of β and α are 1.51 and 0.00133 for females and 1.53 and 0.00281 for males respectively. the values of ω_2 were 0.00215 and 0.00170 for females and male respectively. NONMEM implementation can be found in the NONMEM code provided.

Pharmacokinetic Modelling

a) Nonlinear clearance

For the plasma model, the nonlinearity in clearance observed at higher doses was accounted for by a concentration-dependent CL described by the following equation:

$$V_{max} = CL_{max} \cdot K_m$$

where V_{max} is the maximal elimination rate in mg/h, CL_{max} is the maximal clearance in L/h apparent with rifampicin plasma concentration (C_{plasma}) approximating 0, while K_m is the C_{plasma} in mg/L at which the elimination is half of V_{max}.

b) Effect compartment modelling for CSF

The CSF concentrations were modelled as dependent on plasma concentrations using an effect compartment, as previously proposed and implemented by Sheiner et al. (Sheiner et al. 1979) and Savic et al (Savic et al. 2015). Effect compartments are assumed to have a negligible volume compared to the central compartment, with negligible drug transfer between the two compartments. The following differential equation summarises the kinetics of the effect compartment:

$$\frac{dC_{CSF}}{dt} = k_{plasma-CSF} \cdot \left(PPC \cdot C_{plasma} - C_{CSF}\right),$$

where $k_{plasma-CSF}$ is the first-order equilibration rate constant of the drug between the central compartment (i.e., plasma) and the effect compartment (i.e., CSF), PPC is the pseudo-partition coefficient, C_{plasma} and C_{CSF} are the drug concentration at the time t in plasma or CSF, respectively.

Between-subject, between-visit, and between-occasion variabilities were tested for the different plasma and CSF parameters. Each PK sampling day (day 3 and day

28) was considered a separate visit. Each dose and its following samples were considered a separate occasion, therefore the dose before the sampling visit along with the predose concentration were treated as a separate occasion from the dose administered during the PK visit and the following concentrations.

Residual unexplained variability was described using a combined proportional and additive error model, with the additive error for all samples set to be at least 20% of the LLOQ. Concentrations below the lower limit of quantification (BLQ) were censored according to Beal's M6 method, in which the last censored value in a series during the absorption phase and the first censored value in a series in the terminal phase was replaced with LLOQ/2 and the other censored values in a series were discarded (S. L. Beal 2001). To account for the larger level of uncertainty in the imputed censored values, their additive error was inflated by LLOQ/2. Also, the M3 method was tested as there was a large fraction of BLQ values in the CSF but it did not result in a meaningful difference in the parameter estimates. On the other hand, it caused longer run times and, most importantly, less stable final parameter estimates. For this reason, we proceeded with the M6 method (S. L. Beal 2001).

The process of model development and covariate inclusion was guided by physiological plausibility, model fit diagnostics, and the drop in the objective function value (OFV). The likelihood ratio test for the drop in OFV was used to compare nested models, assumed to be approximately $\chi 2$ distributed with n degrees of freedom, where n is the number of additional estimated parameters. A p-value of 0.05 was generally used for inclusion and 0.01 for retention. Model

performance was evaluated through visual predictive checks (VPC). The VPC for the final model stratified into plasma and CSF concentrations is shown in Figure 6.4. Final parameters precision (95% confidence intervals) was obtained by sampling importance resampling (SIR) (A. G. Dosne et al. 2016).

The model was developed using NONMEM® 7.5 with first-order conditional estimation with eta-epsilon interaction (FOCE-I). Pirana 3.0.0 software was used for model management; Perl-speaks-NONMEM® (PsN) 5.2.6 and R 4.0.4 via RStudio were used for post-processing NONMEM® results and generating figures (Keizer, Karlsson, and Hooker 2013).

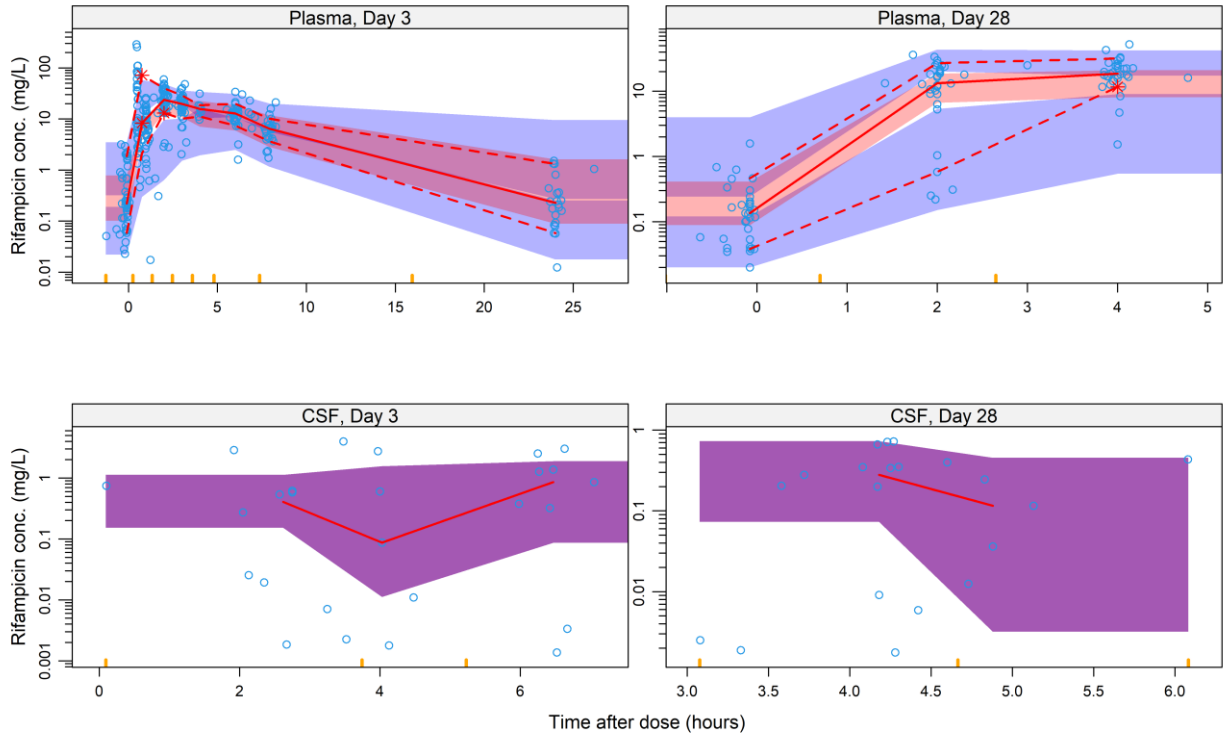

Figure 6.4: Prediction-corrected visual predictive check (VPC) (n=500).
The VPC shows drug concentration versus time after dose for the final models stratified by matrix (plasma or CSF) and visit (day 3 or 28), dose. The dots are the original observations; the solid line is the median and the dashed lines are the 10th and 90th percentiles of the observed data; the shaded areas are the 90%

confidence intervals of the same percentiles as simulated by the model. A suitably fitting model will have most of the observed percentiles within the simulated confidence intervals.

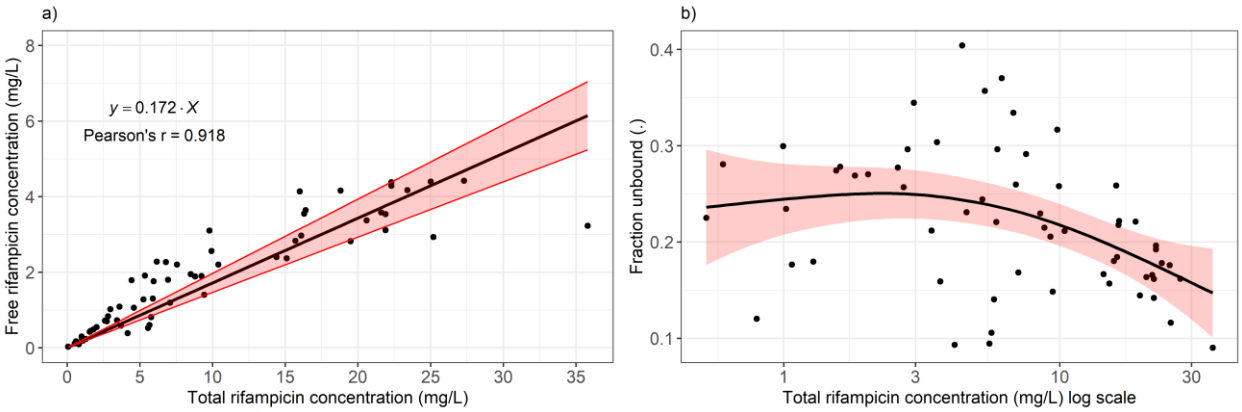

Figure 6.5: Binding plots for plasma protein binding of rifampicin

a) Free versus total concentration (mg/L) in the same sample. The slope of the regression equation represents the unbound fraction and was estimated using generalised Deming regression with constant error assumption (Deming 1943; Linnet 1998). b) LOESS regression of fraction unbound versus total rifampicin concentrations (mg/L). There was no apparent trend between the two variables.

Chapter 7 : Linezolid population pharmacokinetic model in plasma and cerebrospinal fluid among patients with tuberculosis meningitis

Abstract

Background

Linezolid is evaluated in novel treatment regimens for tuberculous meningitis (TBM). Linezolid pharmacokinetics have not been characterized in this population, particularly in CSF where exposures may be affected by changes in protein concentration. Linezolid co-administration with high-dose rifampicin, has also not been studied. We aimed to characterize linezolid plasma and CSF pharmacokinetics in adults with TBM.

Methods

In LASER-TBM pharmacokinetic substudy, the intervention groups received high-dose rifampicin (35mg/kg) plus linezolid 1200mg/day for 28days, then reduced to 600mg/day. Plasma sampling was done on day 3 (intensive) and on day 28 (sparse). A lumbar CSF sample was obtained on both visits.

Results

30-participants, median(min-max) age and weight of 40(27–56) years and 58(30–96)kg, contributed 247 plasma and 28 CSF observations. Plasma pharmacokinetics was described by one-compartment model with first-order absorption and saturable elimination. Maximal clearance was 7.25L/h, and Km was 27.2mg/L.

Rifampicin co-treatment duration did not affect linezolid pharmacokinetics. CSF-Plasma partitioning correlated with CSF total-protein up to 1.2g/L where the partition-coefficient reached maximal value of 37%. Plasma-CSF equilibration half-life was ~3.5hours.

Conclusion

Linezolid was readily detected in CSF despite high-dose rifampicin co-administration. These findings support continued clinical evaluation of linezolid plus high-dose rifampicin for the treatment of TBM in adults.

Introduction

TBM is the most fatal and debilitating form of tuberculosis with a particularly high burden among people living with HIV (Dodd et al. 2017). One reason for severe outcomes is that the current treatment regimen for TBM is based on treatment for pulmonary TB, and may result in suboptimal central nervous system (CNS) concentrations (Wasserman et al. 2019). Drugs targeted at TBM should cross several barriers to reach the site of disease, including the BBB and the BCSFB that separate the systemic circulation from their site of action in the CNS. These barriers pose a therapeutic challenge by limiting entry of drugs into the CNS. Moreover, disease-related changes in BBB permeability and dynamic changes in protein concentrations may have important implications for drug penetration into the brain (Pardridge 2012).

Linezolid, an oxazolidinone antibiotic, is highly effective for the treatment of drug-resistant pulmonary TB. Linezolid is also used to treat Gram-positive bacterial

infections in the CNS (Pintado et al. 2020; Beer, Pfausler, and Schmutzhard 2009; Hoefnagel et al. 2008), where good drug penetration has been documented, making it an attractive candidate for TBM treatment (Nau, Sörgel, and Eiffert 2010; Rupprecht and Pfister 2005; Villani et al. 2002). Small observational studies have shown improved clinical parameters with linezolid use in children and adults with TBM (Sun et al. 2014; Li et al. 2016). Based on these encouraging observations, linezolid is being investigated as part of intensified antibiotic therapy in several clinical trials for TBM (Davis et al. 2023) .

Specific features of TBM may influence the pharmacokinetics (PK) of linezolid, with potential implications for safety and efficacy, given its narrow therapeutic window. These include host factors (such as body size) and disease factors, including CSF protein concentrations and BBB permeability. Also, clinical trials provide linezolid along with high-dose rifampicin in TBM treatment regimens. As a potent inducer of the cytochrome P450 system and upregulator of drug transporters (Finch et al. 2002), rifampicin could potentially affect the PK of linezolid. Studies in healthy volunteers and pulmonary TB have shown a moderate reduction in linezolid exposure when co-administered with standard dose rifampicin (Gandelman et al. 2011; Gebhart, Barker, and Markewitz 2007). The impact on site of disease (CSF) concentrations and clinical implications of this pharmacokinetic interaction is unknown but could theoretically lead to suboptimal treatment or the development of antimicrobial resistance.

The objectives of this analysis were to describe the PK of linezolid in plasma and CSF of adults with TBM, to explore the effect of high-dose rifampicin on

linezolid PK, evaluate covariate effects on plasma and CSF drug levels, and simulate exposures for optimized dosing strategies.

Methods

Study data

This was a sub-study of LASER-TBM (Davis et al. 2021), a phase IIb, open-label trial that evaluated safety and PK of intensified antibiotic therapy in adults with HIV and TBM (Davis et al. 2023). Participants were enrolled from 4 public hospitals in Cape Town and Gqeberha, South Africa, and randomized to study interventions within 5 days of starting antituberculosis treatment. The standard of care (control) group received fixed-dose combination oral tablets (rifampicin 10 mg/kg, isoniazid 5 mg/kg, pyrazinamide 25 mg/kg, and ethambutol 15 mg/kg) according to World Health Organization (WHO) weight bands. Participants allocated to experimental groups were administered the standard regimen with a higher dose of rifampicin (35 mg/kg in total, using bespoke weight bands (Wasserman et al. 2021)) and linezolid for 56 days (1200 mg once daily for the first 28 days, then reduced to 600 mg once daily) with or without aspirin. All participants received adjunctive dexamethasone.

Pharmacokinetic sampling visits were scheduled on Day 3 (±2 days) and Day 28 (±2 days) after study entry. At the Day 3 visit, plasma was collected at pre-dose, 0.5, 1, 2, 3, 6, 8-10, and 24 hours post-dose (intensive) and on Day 28 at pre-dose, 2-, and 4-hours post-dose (sparse). Sparse sampling was performed on Day 3 for participants who declined intensive sampling or for whom intensive sampling could

not be done. One lumbar CSF sample was collected at each pharmacokinetic sampling visit, with sample timing randomized to intervals of 1-3, 3-6, 6-10, and 24 hours after dosing. Clinical information was collected, and full blood count and serum chemistry were obtained at each visit. Total protein, albumin, and glucose were measured in CSF samples.

Linezolid plasma and CSF concentrations were measured in the Division of Clinical Pharmacology at the University of Cape Town. The plasma assay summary has been described previously (Garcia-Prats et al. 2019). Cholesterol and 4-beta hydroxy cholesterol (4β-OHC) were also measured in pre-dose plasma samples collected on both PK visits. 4β-OHC is a metabolite of cholesterol formed by CYP3A4 and the ratio between its concentration and that of cholesterol is used as a marker of CYP3A4/5 endogenous activity (Diczfalusy et al. 2011). Additionally, the unbound concentration of linezolid in plasma was quantified in a subset of samples to estimate the degree of plasma protein binding. Details of analytical assays are outlined in the supplementary file.

Informed consent was obtained from all participants or their proxies. The study was approved by the University of Cape Town Human Research Ethics Committee (UCT HREC reference: 293/2018), Walter Sisulu University (HREC reference: 012/2019), and the South African Health Products Regulatory Authority (reference number 20180622). The trial is registered on clinicaltrials.gov (NCT03927313).

Pharmacokinetic modelling

Nonlinear mixed-effects modelling was used to create a population PK model describing linezolid PK in both plasma and lumbar CSF. The model was developed sequentially; first describing plasma linezolid and then including CSF concentrations.

For the plasma PK, we tested one- and two-compartment disposition models with linear or saturable elimination and first-pass effect. The CSF concentrations were described using a hypothetical effect compartment linked to the central (plasma) compartment, which estimates the first-order equilibration rate constant of linezolid between the central and the effect compartments ($k_{plasma-CSF}$) and the pseudo-partition coefficient (PPC). Further details on modelling approach are available in the supplementary file.

Following the development of the structural model, we tested the effect of potential covariates including creatinine clearance (calculated with the Cockcroft-Gault equation (Cockcroft and Gault 1976)), age, study visit, duration of concomitant rifampicin treatment, study site, and treatment arm. For the CSF PK parameters PPC and $k_{plasma-CSF}$, we also tested the effect of CSF total protein, albumin, and glucose concentrations. The precision of the parameter estimates of the final model, expressed as 95% confidence intervals and %RSE, was assessed using SIR (A.-G. Dosne, Bergstrand, and Karlsson 2017).

In the plasma samples with matched free and total linezolid concentrations available, the free concentrations were regressed against the total concentration

with intercept of zero using Deming regression (Deming 1943; Linnet 1998). The fraction unbound (fu) was estimated from the slope of the regression line.

Simulations

The model-derived area under the concentration-time curve from time 0 to 24 hours post-dose ($AUC_{0\text{-}24h}$) and the concentration at 24 hours post-dose (C_{24h}) were calculated for the available profiles. Monte Carlo simulations (n=10,000) were performed using final model parameters to simulate concentration-time profiles in plasma and CSF following daily linezolid doses of 600 mg or 1200 mg at steady-state for a typical participant with median FFM of 45 kg and CSF protein of 0.995 mg/mL.

Results

Study data

Thirty participants underwent PK sampling on the first PK visit on day 3 of the study and 18 participants had PK sampling at the second PK visit on day 28, one of whom was excluded from this analysis because all 3 samples were BLQ (later confirmed to have missed dosing). Reasons for missing the second PK visit included death, interrupting linezolid dose due to adverse events, or withdrawing consent. There were 247 plasma concentrations (6 were BLQ, 2.43%) and 28 CSF concentrations (7 were BLQ, 25%) available for PK modelling. All participants were receiving linezolid 1200 mg daily at the first PK visit; on day 28, 13 received 1200 mg and 4 received 600 mg. Baseline clinical characteristics are summarized in Figure 7.1. Median CD4 count was 137 cells/mm^3 (range 2 to 890). Median duration on rifampicin therapy

was 5 days (range 0 – 7) at the Day 3 PK visit and 30 days (range 27 – 38) at the Day 28 visit. Median CSF total protein concentrations decreased from 1.46 g/L (range 0.31 – 54.7) at Day 3 to 0.75 g/L (range 0.22 – 2.19) at Day 28.

Table 7.1: Clinical characteristics

	Median (Min. – Max.) or No. (%)	
	Visit Day 3 (n = 30)	**Visit Day 28 (n = 17)**
Males	18 (60%)	11 (65%)
Age (years)	40 (27 – 56)	37 (27 – 51)
Weight (kg)	58 (30 – 96)	61 (37 – 81)
Height (m) [a,c]	1.61 (1.48 – 1.80)	1.61 (1.57 – 1.80)
Fat-free mass (kg) [b,c]	45 (30 – 59)	48 (32 – 60)
Serum creatinine (mmol/L)	61 (27 – 87)	50 (34 – 86)
4-beta hydroxy-cholesterol/cholesterol (molar ratio x10^{-5})[d]	1.48 (0.313 – 6.79)	1.90 (0.384 – 5.50)
Daily linezolid oral dose: **1200 mg** **600 mg**	 30 0	 10 7
Duration of rifampicin treatment (days) [e]	5 (0 – 7)	30 (27 – 38)
CSF total protein (g/L)	1.46 (0.310 – 54.7)	0.750 (0.220 – 2.19)
CSF albumin (g/L)	3.32 (0.93 – 23.34)	4.47 (0.46 – 11.41)
CSF glucose (mmol/L)	2.9 (1.0 – 5.3)	3.2 (2.2 – 3.6)
Antiretroviral therapy (ART): **Previous ART** **ART Naïve** **On ART**	 11 (37%) 10 (33%) 9 (30%)	 6 (35%) 5 (29%) 6 (35%)
No. of participants concomitantly on: **Tenofovir/Emtricitabine/Efavirenz** **Abacavir/Lamivudine/Lopinavir**	 7 2	 5 1

[a] Heights were missing for 18/30 (60%) participants and imputed based on sex and weight as outlined in the supplementary file.

[b] Fat-free mass was calculated based on sex, weight, and height according to the formula in Janmahasatian *et al.* [21]

[c] The median (min – max) values reported here are for the non-missing values (i.e., it does not include the imputed values).

[d] The ratio of 4β-OHC to cholesterol was missing in 4 and 3 participants on day 3 and day 28, respectively.

[e] This refers to the total number of days since the start of tuberculosis treatment, which was ~1-3 days before the recruitment into the study and start of the investigational treatment. Participants were on standard-dose (10 mg/kg) rifampicin when starting treatment and then switched to high-dose (35 mg/kg) rifampicin at the start of the study.

Pharmacokinetic modelling

The plasma PK of linezolid was best characterised by a one-compartment disposition model, saturable elimination with Michaelis–Menten, and first-order absorption preceded by a chain of transit compartments. Saturable elimination resulted in a better model fit than linear elimination (dOFV = -9.03, *p*-value = 0.00205, df = 1). A schematic diagram of the model is shown in Figure 7.1. Two-compartment disposition was tested but did not result in a significant improvement of fit. Maximal clearance ($CLmax$) and volume of distribution (V) were allometrically scaled using FFM (drop in objective function value (dOFV) = -30, compared to dOFV = -7.7 when using total body weight). In a typical participant (median FFM 45 kg) the value of maximal clearance ($CLmax$) was 7.25 L/h, the Michaelis-Menten constant (Km), which is a parameter that governs saturable hepatic elimination and represents the linezolid concentration at which half the $CLmax$ is reached, was 27.2 mg/L, and the volume of distribution (V) was 40.8 L. The inclusion of between-visit variability in $CLmax$ improved the model fit, but no systematic increase or decrease with time on treatment was observed. Longitudinal changes in clearance were explored by testing auto-inhibition and duration of rifampicin co-treatment, but no significant effect was found for either. We also could not find any effect when testing the ratio of 4β-OHC to cholesterol, creatinine clearance, or age on $CLmax$ and bioavailability (F). The final parameter estimates are presented in Table 7.2. A visual predictive check showing adequate model fit is depicted in Figure 7.5 in the supplementary file.

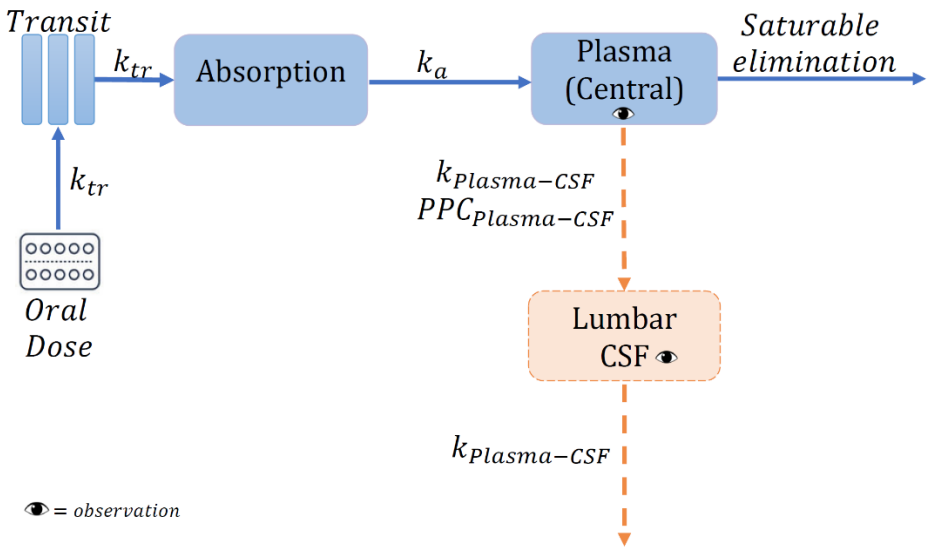

Figure 7.1: Schematic representation of the final model.

k_{tr} is the rate constant for the drug passage through the transit compartments, $k_{Plasma-CSF}$, equilibration rate constant plasma-cerebrospinal fluid CSF) which describes how soon the change in plasma is reflected in the CSF; $PPC_{Plasma-CSF}$, the pseudo-partition coefficient which represents the ratio of drug in CSF to the plasma.

Table 7.2: Final population pharmacokinetic parameter estimates for linezolid in plasma and lumbar cerebrospinal fluid

Parameter	**Estimate (95% confidence interval)** [a] **[%RSE]** [a]
Maximal clearance, $CLmax$ (L/h) [b]	7.25 (6.09 – 8.86) [9.93]
Michaelis-Menten constant, km (mg/L)	27.2 (16.0 – 46.4) [29.1]
Volume of distribution, V (L) [b]	40.8 (37.9 – 43.6) [3.65]
Bioavailability, F (.)	1 Fixed
Mean transit time, MTT (h)	0.211 (0.112 – 0.342) [28.6]

No. of absorption transit compartments, NN (.)	5.68 (2.36 – 11.8) [43.5]
Absorption rate constant, ka (h^{-1})	1.21 (0.831 – 1.76) [19.6]
Proportional error plasma (%)	21.5 (18.8 – 24.7) [7.06]
Additive error plasma (mg/L) [d]	0.173 (0.0379 – 0.355) [47.1]
Between-subject variability (BSV) in $CLmax$ (%)	9.60 (3.44 – 13.9) [51.9]
Between-visit variability (BVV) in $CLmax$ (%)	20.3 (15.3 – 26.9) [30.7]
Between-occasion variability (BOV) in ka (%)	87.9 (66.4 – 110) [25.9]
BOV in MTT (%)	110 (75.8 - 144) [32.8]
Equilibration rate constant to CSF, $k_{plasma-CSF}$ (h^{-1}) [e]	0.198 (0.0849 – 0.340) [33.7]
Maximal pseudo-partition coefficient to CSF, PPC_{max} (.)	0.365 (0.238 – 0.566) [23.2]
CSF protein at which PPC_{max} is reached, $CSF\ protein_{max}$ (mg/mL) [f]	1.18 (0.730 – 1.90) [24.4]
Proportional error CSF (%)	91.5 (63.3 – 151) [23.4]
Additive error CSF (mg/L) [d]	0.02 Fixed

[a] Values in parentheses are the 95% confidence intervals and those in square brackets are the % relative standard errors, both computed with sampling importance resampling (SIR) on the final model.

[b] The values of $CLmax$ and V were allometrically scaled, so the typical values reported here refer to the typical participant, i.e. a median FFM of 45 kg.

[d] The estimate of the additive component of the error was not significantly different from its lower boundary of 20% of LLOQ, so it was fixed to this value.

[e] Corresponds to an equilibration half-life of 3.5 (2.04 – 8.16) h

[f] For CSF protein < $CSF\ protein_{max}$ $(i.e., the\ breakpoint)$: $PPC_i = PPC_{max}.(slope.(CSF\ protein - breakpoint))$, where the $breakpoint$ was estimated to be 1.18 mg/mL, and the $slope$ was calculated to be 0.847 from the following equation: $slope = (amplitude - intercept)/(breakpoint - 0)$, where

the $intercept$ and $amplitude$ were fixed to 0 and 1, respectively. For CSF protein ≥ $CSF\ protein_{max}$: $PPC_i = PPC_{max}$. The PPC-CSF protein relationship is depicted in **Figure 2**, and more details are provided in the supplementary file.

The CSF concentrations were linked to the plasma concentrations with an equilibration half-life of 3.5 hours (95% confidence interval, 2.04 - 8.16) and the steady-state equilibrium ratio (PPC), indicating the relative amount of linezolid exposure in CSF, which was dependent on CSF protein levels. The PPC-CSF protein relationship was described using a piece-wise linear (broken-stick) function, where the PPC increased with higher CSF protein levels until a maximal CSF protein value where the PPC plateaued (i.e., a maximal PPC value). The breakpoint was estimated, while the slope (i.e., the change in PPC per change in CSF protein) was calculated from the breakpoint and the intercept (minimum PPC) which was fixed to be 0 to prevent the estimation of negative values of PPC which are physiologically unplausible. For each 0.1 mg/mL increase in CSF protein, we found an increase of 3% in PPC up to 1.18 mg/mL of CSF protein, after which the PPC reached a maximal value of 0.365 (95% CI, 0.238 – 0.566) (Figure 7.2). Both CSF protein and CSF albumin were found to correlate significantly with PPC; however, the two are highly positively correlated. Only CSF protein was included in the final model because it resulted in a more significant drop in OFV and because albumin is a component of the proteins measured.

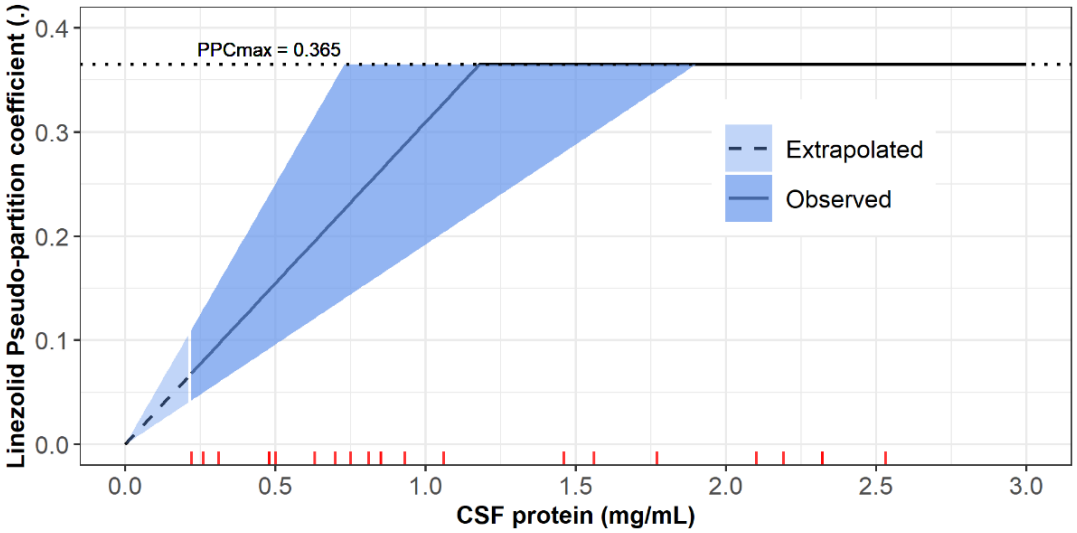

Figure 7.2: The relationship of PPC vs the CSF protein level using the piece-wise (broken-stick) function.

The solid line represents the median and the shaded areas represent the uncertainty around the estimates of the breakpoint (the maximal CSF protein value at which $PPCmax$ is reached) and the calculated slope. The dashed line depicts the extrapolated part of the PPC-CSF protein relationship for CSF protein values outside the range observed in the study cohort (The lowest observed value was 0.22 mg/mL). The vertical ticks represent the values of CSF protein observed in our cohort (CSF protein values above 3 mg/mL were truncated for better figure visibility. Some of the ticks are overlapping because there are some duplicated CSF protein values).

The regression plots of linezolid free concentrations versus total concentration (mg/L) and of linezolid fu versus total linezolid concentrations (mg/L) are shown in Figure 7.7and Figure 7.8 in the supplementary file. There was no apparent trend of changing fu across the observed total linezolid concentration range.

Simulations

The simulated plasma and CSF concentration time profiles for the typical participant in our cohort following a once daily dose of either 600 mg or 1200 mg linezolid are depicted in Figure 7.3 and model-derived individual values for the steady-state $AUC_{0\text{-}24h}$ and trough concentrations are summarized in Table 7.3.

Table 7.3: Linezolid model-derived area under the curve for 24 hours and concentrations at 24 hours post-dose

	Median (Min. – Max.)			
	Plasma		**Cerebrospinal fluid**	
Daily oral dose	**1200 mg (n = 40)**	**600 mg (n = 7)**	**1200 mg (n = 40)**	**600 mg (n = 7)**
$AUC_{0-24h}\ (mg \cdot h/L)$	278 (87.3 - 762)	93.7 (66.7 - 167)	81.6 (19.7 - 234)	24.0 (6.55 - 56.8)
$C_{24}\ (mg/L)$	1.69 (0.154 - 13.5)	0.406 (0.0614 - 1.67)	1.32 (0.327 - 6.48)	0.369 (0.0495 - 1.02)

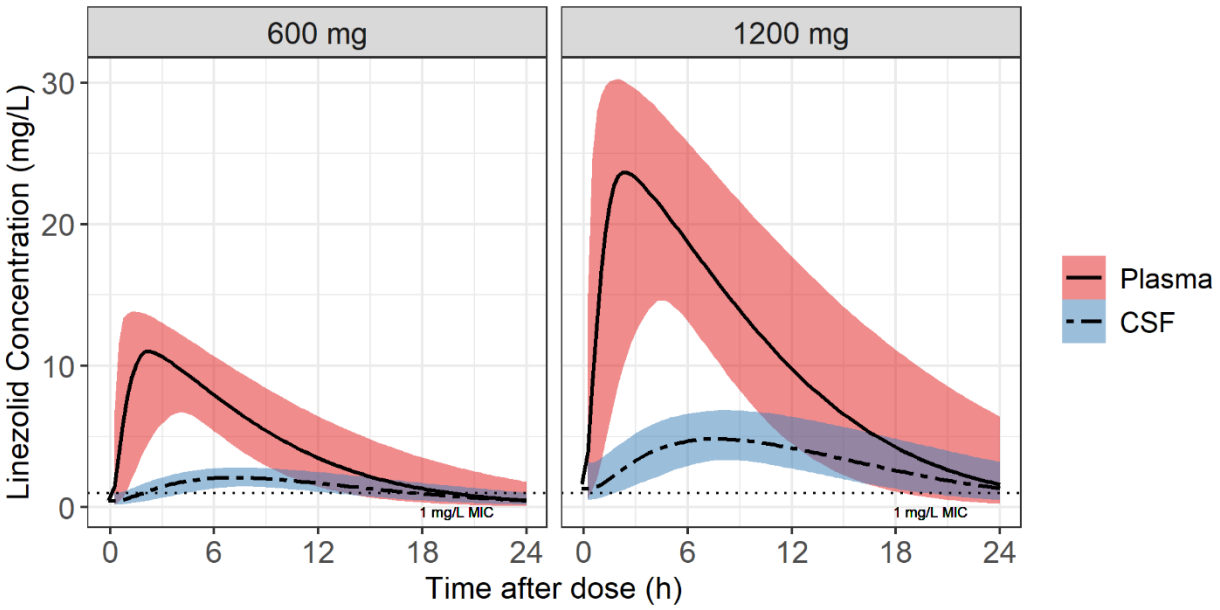

Figure 7.3: Simulated typical concentration-time profiles for plasma and cerebrospinal fluid (CSF) for the 1200 mg and 600 mg oral daily dose of linezolid. The solid and dashed lines represent the median for the plasma and CSF, respectively and the shaded areas represent the 90% confidence intervals. The horizontal dotted line indicates the wild-type minimum inhibitory concentration (MIC) value of linezolid for *Mtb*.

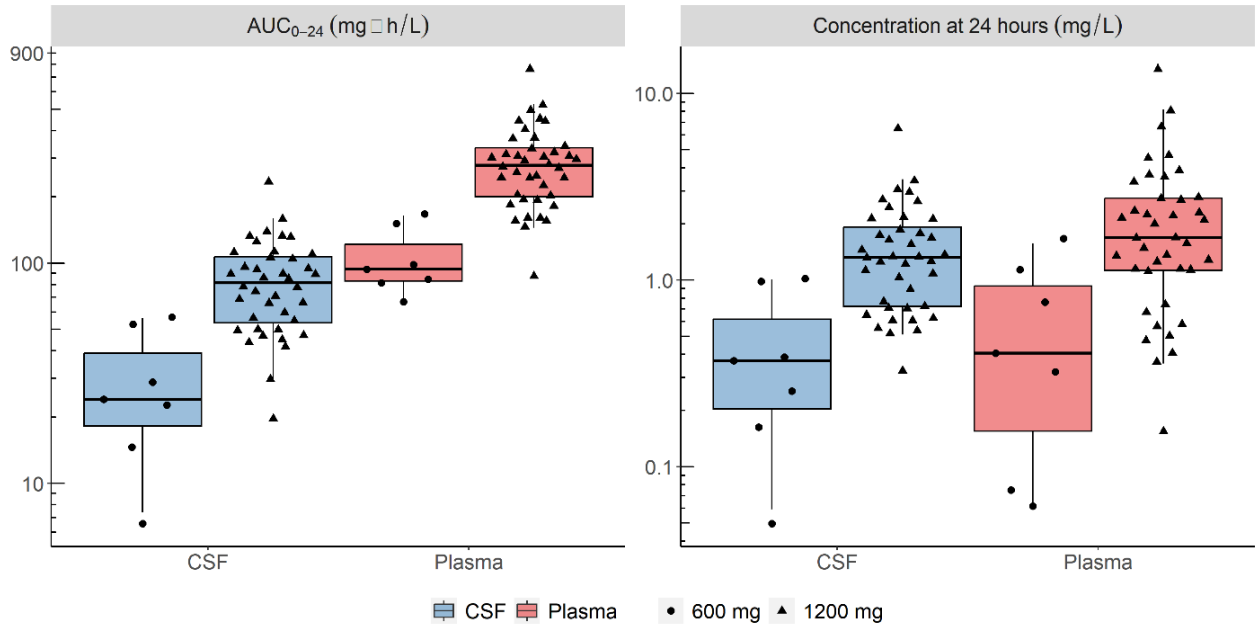

Figure 7.4: Box and whisker plots showing the secondary model-derived exposure parameters, AUC_{0-24h} and concentration at 24 hours post-dose (C_{24h}) stratified by dose.

The boxes represent inter-quartile range, while whiskers are the 2.5th and 97.5th percentiles. The dots represent individual values (n = 7 for 600 mg and 40 for 1200 mg of which 30 on day 3 and 10 on day 28).

Discussion

Linezolid is being evaluated in several clinical trials as part of enhanced antimicrobial therapy for TBM. This is based on limited clinical evidence from small observational studies in TBM (Sun et al. 2014; Li et al. 2016) and reports of successful use in gram-positive CNS infection. However, there is scarce information on linezolid exposure in the CSF, especially among patients with TBM, a presumed requirement for clinical efficacy in this condition. We characterized the PK of linezolid in plasma and CSF from a cohort of South African patients with HIV-associated TBM. The extent of linezolid penetration into the CSF was ~30% on

average of plasma exposure and correlated with CSF protein concentrations – CSF penetration was higher in participants with higher CSF protein, reaching a maximal value of ~37%. Co-administration with high-dose rifampicin (35 mg/kg/day), when comparing the duration on rifampicin treatment on day 3 versus day 28 did not have a significant effect on the PK of linezolid.

Several prior studies may help to contextualize our findings. A recent observational study reported CSF linezolid concentrations from 17 TBM patients (only one with HIV) who received linezolid 600 mg daily (Kempker et al. 2022). The median CSF concentrations were 0.90 mg/L and 3.14 mg/L and the CSF/serum ratios were 0.25 and 0.59 at 2- and 6-hours post-dose, respectively. CSF linezolid concentrations have also been reported from two small cohorts of neurosurgical patients receiving 600 mg linezolid intravenously every 12 hours. In the smaller study (n = 7) the mean observed CSF-to-plasma AUC ratio was 0.565 (n = 7), the mean (±standard deviation) $AUC_{0-\infty}$ after the first dose was 37.7 (±23.9) mg·h/L and AUC_{0-12h} after the fifth dose was 53.7 (±50.3) mg·h/L. In the slightly larger study (n = 14) mean observed CSF-to-plasma AUC ratio was 0.66 and mean (±standard deviation) AUC in CSF was 101 ±59.6 mg.h/L (Viaggi et al. 2011; Myrianthefs et al. 2006). Direct comparison is limited because of differences in population (HIV status, disease type and severity), dosing and administration, and drug assays. CSF/plasma concentration and AUC ratios should be cautiously interpreted in these prior studies (Kempker et al. 2022; Viaggi et al. 2011; Myrianthefs et al. 2006) since observed CSF and plasma concentrations were compared at the same timepoints, not accounting for delay in distribution between the plasma and CSF. Despite having

access to only a single CSF sample per visit (due to the invasive nature of lumbar puncture), using a model-based approach allowed us to describe the time course for linezolid entry into CSF. The limitation of sparse CSF sampling in our study was further mitigated by randomizing participants to different sampling times so that CSF samples could be obtained over the full dosing interval. Another limitation is the relatively high proportion of BLQ CSF samples, which gives a high variability in the observed CSF concentrations that is reflected in the proportional error estimate for the CSF observations. To test the effect of these samples on our analysis, we conducted a sensitivity analysis after excluding the BLQ samples. Excluding the BLQ samples mainly affected the estimate of the proportional error – which decreased but did not affect the estimates of the pseudo-partition coefficient and the equilibration half-life. Additionally, we performed a parametric bootstrap (stochastic simulation and estimation, SSE) which yielded uncertainty values in line with the values obtained from SIR, thus corroborating our confidence in the results (Lindbom, Ribbing, and Jonsson 2004).

Other studies have also reported a relationship between the levels of CSF total protein (or albumin) and antituberculosis drugs in TBM (E. M. Svensson et al. 2020; Panjasawatwong et al. 2020). In a paediatric population there was a linear relationship between log-transformed CSF protein concentration and the CSF penetration of rifampicin, with a 63% increase in the penetration coefficient for every 10-fold change in protein levels (E. M. Svensson et al. 2020). In another paediatric TBM cohort, an exponential function was used to describe the relationship between CSF protein concentrations and the partition coefficient of

rifampicin where an increase of 1 g/L in CSF protein concentration resulted in a 1.28-fold increase in the partition coefficient (Panjasawatwong et al. 2020).

There are two plausible, potentially overlapping, explanations for our finding of a correlation between CSF protein levels and extent of CSF linezolid partitioning. In a healthy state, the BCSFB is intact and only a small fraction of plasma proteins can enter into the CNS, leaving only unbound drug fraction available for penetration into this compartment (Nau, Sörgel, and Eiffert 2010). Inflammation associated with TB meningitis may increase BCSFB permeability causing both plasma protein and total drug concentrations to be higher in the CSF. Another possible explanation for this relationship is higher endogenous CSF protein production from local inflammation leading to alterations in CSF drug binding kinetics and higher concentrations of total drug in TBM. Quantification of free drug CSF concentrations may help to further delineate CSF protein-drug relationships.

Linezolid is provided with high dose rifampicin (35 mg/kg/day) in ongoing efficacy trials for TBM. Because of prior reports of a drug-drug interaction between rifampicin and linezolid, plus the likelihood of a rifampicin dose effect on metabolizing enzyme activity (Williamson et al. 2013) which could affect the linezolid plasma exposure and hence the CSF exposure, we investigated a potential effect of rifampicin on linezolid PK. In our study, there was no control group of participants who received only linezolid without rifampicin to clearly identify a drug-drug interaction. However, estimated linezolid clearance in our cohort was comparable to that reported from patients receiving linezolid for drug-resistant pulmonary TB without concomitant rifampicin. In addition, since the maximal

cytochrome (CYP) P450 induction effect of rifampicin occurs after at least a week (J. Chen and Raymond 2006), we investigated the effect of the duration of rifampicin therapy (rather than rifampicin co-administration as categorical covariate) on linezolid PK, and could not detect any significant trends. Furthermore, we found no relationship between 4β-OHC:cholesterol or 4β-OHC alone (as predictive biomarker of enzyme induction by rifampicin) and linezolid clearance or bioavailability. Our data indicate that even if rifampicin had an effect on linezolid exposures, it is unlikely to be clinically relevant.

In contrast to our findings, other smaller studies among healthy volunteers and non-TB patients have demonstrated a reduction in linezolid exposure when co-administered with rifampicin (Okazaki et al. 2019; Hashimoto et al. 2018; Gandelman et al. 2011; Egle et al. 2005). This interaction has been variously attributed to either a large increase in the expression of the CYP3A4 isoenzyme that typically has a small contribution to linezolid clearance (Gandelman et al. 2011) or to increased upregulation of linezolid intestinal secretion by rifampicin induction of P-glycoprotein (P-gp) (Egle et al. 2005). There is no definitive evidence that linezolid is a substrate of P-gp, plus it is mainly (~68%) metabolized in the liver via morpholine ring oxidation, which is independent of the CYP450 system, with the remainder excreted unchanged via the kidneys (Gandelman et al. 2011).

As reported for pulmonary TB patients, saturable elimination was observed at higher linezolid plasma concentrations, resulting in non-linear PK (Imperial et al. 2022). Despite subtle differences in Michaelis-Menten elimination kinetics (Km) our estimates for $CLmax$ and V are in line with previously published linezolid models

(Imperial et al. 2022; Tietjen et al. 2021; Alghamdi et al. 2020; Kamp et al. 2017; McGee et al. 2009; Meagher et al. 2003). Prior models based on data from non-TB (Plock et al. 2007) and pulmonary TB patients (Mockeliunas et al. 2022), included an empirical inhibition compartment to describe concentration- and time-dependent autoinhibition of elimination. We also tested this approach, but it did not result in a better model fit for our data, and clearance values estimated by these models are similar to ours.

An overview of these models and a comparison with the current work is summarized in Table S7.1in the supplementary file.

Our analysis had several limitations. First, the sparse plasma sampling (3 samples) performed during the 2nd PK visit does not allow for robust estimation of the non-linearity in clearance, especially since only 7 participants were on the reduced dose (600 mg). However, the model fit improved significantly (p-value < 0.001) when including saturation of clearance with higher concentrations, supporting this conclusion. Secondly, a limitation of the PPC-CSF protein relationship in our model is that the minimum PPC was fixed to 0 – meaning no linezolid enters the CSF - to prevent the estimation of negative values of PPC which are physiologically implausible. However, a CSF protein value of 0 is also not observed in people where it varies between 0.2% and 0.5% of the total protein concentration of blood (H. Reiber 2001). It is considered that 80% of CSF proteins originate in blood and that CSF proteins are diluted in a molecule-size-dependent concentration gradient (Hansotto Reiber 2003). Finally, we did not undertake simulations to estimate probability of target attainment because a PK efficacy target

is not established for TBM. While our simulations do suggest that 1200 mg daily dosing will achieve linezolid concentrations above the critical concentration MIC for *M. tuberculosis*, it is important to note that this putative efficacy target is established in-vitro under conditions that are completely different from CSF Additionally, drug protein binding (and relative free fraction of active drug) in the CSF is unknown.

In conclusion, we successfully developed a population PK model for linezolid among adults with HIV-associated TBM, demonstrating that linezolid penetrates into the CSF, a surrogate compartment for site of disease in TBM, at potentially therapeutic concentrations, even with concomitant use of high-dose rifampicin. More investigations on the CSF protein binding dynamics of linezolid are required to better understand its CSF partition. These findings support continued clinical evaluation of linezolid together with rifamycins for the treatment of TBM in adults. Our model provides a platform that can be used for exploring alternative linezolid dosing strategies in TBM once effective and safe treatment targets are established for this condition.

Supplementary materials

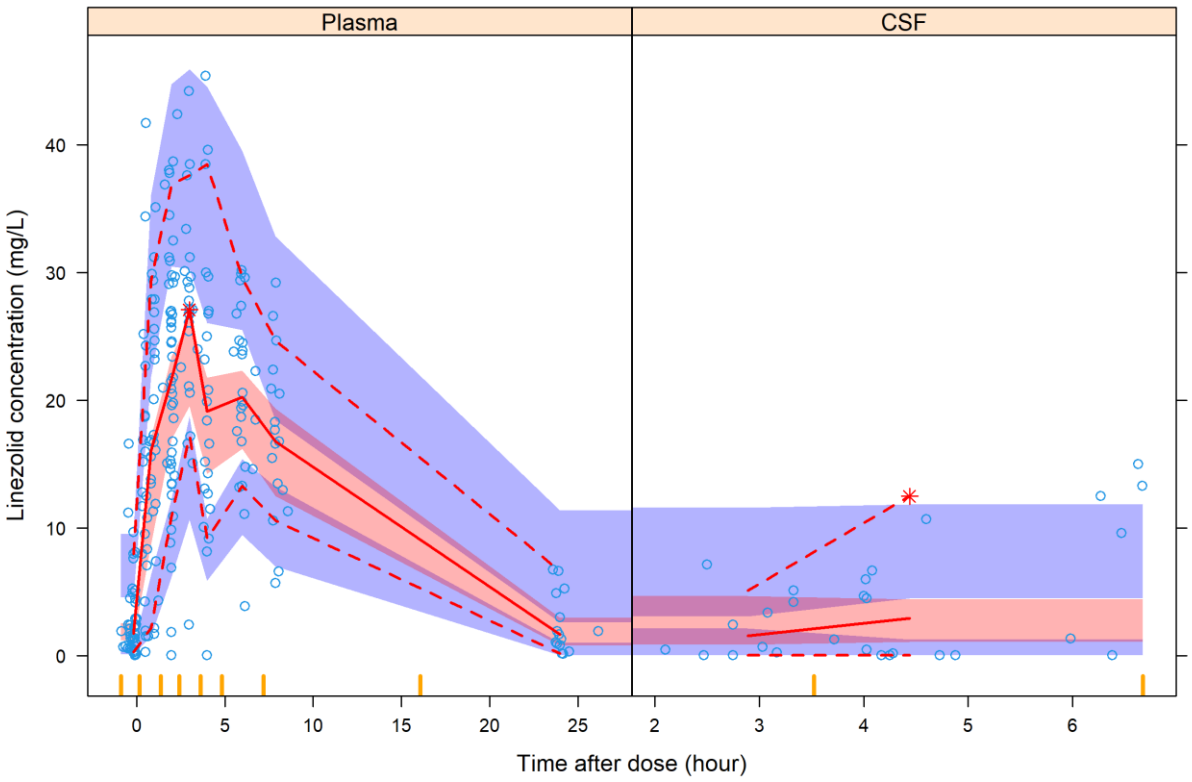

Figure 7.5: Visual predictive check (VPC) (n=1000) showing plasma drug concentration versus time after dose for the final models stratified into plasma and cerebrospinal fluid.

The dots are the original observations; the solid line is the median and the dashed lines are the 10th and 90th percentiles of the observed data; the shaded areas are the 95% confidence intervals of the same percentiles as simulated by the model. A suitably fitting model will have most of the observed percentiles within the simulated confidence intervals.

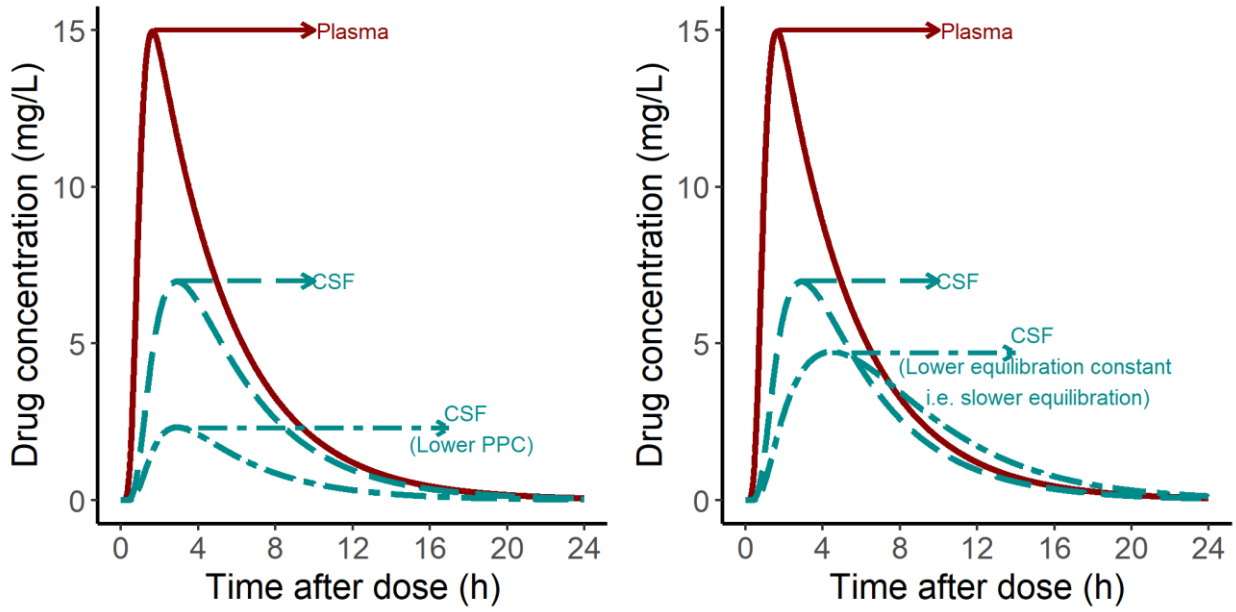

Figure 7.6 Demonstration on the interpretability of the equilibration rate constant and the PPC in the context of effect compartment modelling approach.

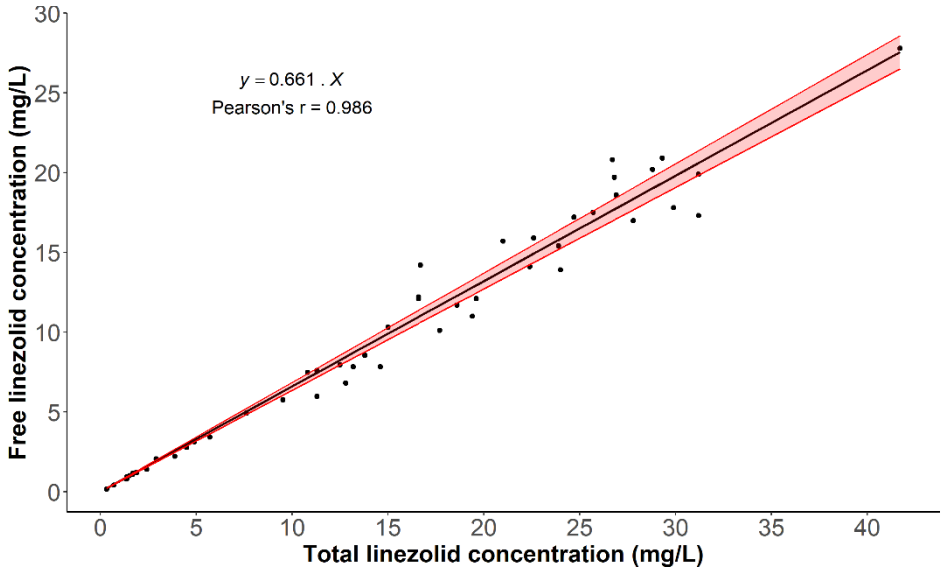

Figure 7.7 Free linezolid concentration (mg/L) versus the total linezolid concentration in the same sample.

The slope of the regression equation represents the fraction of unbound linezolid The slope was estimated using generalized Deming regression with constant error assumption (Deming 1943; Linnet 1998).

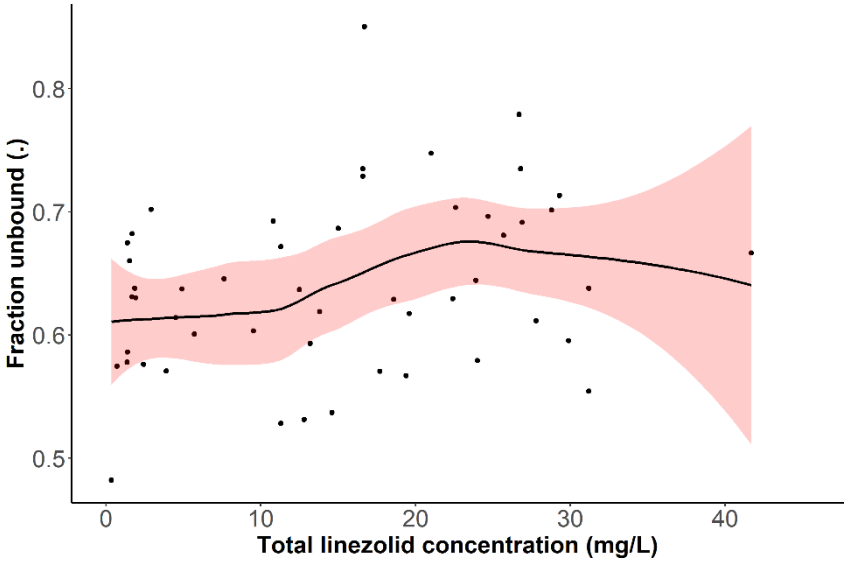

Figure 7.8 LOESS regression between linezolid fraction unbound and total linezolid concentrations(mg/L).

There was no apparent trend between the two variables

Laboratory assays

Linezolid

The CSF samples were processed with a protein precipitation extraction method using linezolid-d3 as the internal standard, followed by high-performance liquid chromatography with tandem mass spectrometry detection on a SCIEX API 3200 instrument. The analyte and internal standard were monitored at mass transitions of the protonated precursor ions 338.2 and 341.1 to the product ions 296.3 and 297.3 for linezolid and linezolid-d3, respectively. The calibration curve fitted a quadratic regression (weighted by 1/x) over the range of 0.1 to 20 mg/L. The accuracy of the quality control samples during sample analysis was between 103.5 and 105.5%, with precision of less than 2.1%.

Free linezolid

The free linezolid assay consisted of ultracentrifugation and dilution, followed by on-line solid phase extraction (SPE) and high-performance liquid chromatography with tandem mass spectrometry detection (LC-MS/MS). On-line SPE was achieved using a Restek Viva BiPh 5 µm, 50 mm x 1.0 mm column, and LC separation was achieved using an Agilent Poroshell 120 EC- C18 2.7 µm, 50 mm x 2.1 mm column, with a total run time of 6.5 minutes. A Sciex API 3200 mass spectrometer at unit resolution in the multiple reaction monitoring mode was used to monitor the transitions of the protonated precursor ions at 338.2 and 341.2 to the product ions at 296.2 and 297.2 for linezolid and linezolid-d3, respectively. Electrospray ionisation was used for ion production. The calibration curve was fitted with a quadratic regression (weighted by 1/x) based on peak area ratios over the range of 0.100 – 30.0 µg/mL. The accuracy of the quality control samples was between 101.1 and 104.4%, with a coefficient of variation of less than 8%.

4-beta hydroxy cholesterol (4β-OHC)

4β-OHC was measured with a high-performance liquid chromatography with tandem mass spectrometry assay in the Division of Clinical Pharmacology at the University of Cape Town. The extraction process involved a liquid-liquid extraction, which uses alkaline hydrolysis using potassium hydroxide and chemical derivatization using picolinic acid. Stable isotope labelled 4β-hydroxy cholesterol-d7 (4β-OHC-d7) was used to prepare calibration standards and quality control samples in human plasma. Endogenous 4β-OHC was measured using the surrogate analyte, 4β-OHC-d7. 4β-OHC -d4 was used as the internal standard.

Chromatographic separation was done with gradient elution on a Gemini C6 Phenyl analytical column. A Sciex 5500 mass spectrometer at unit resolution in the multiple reaction monitoring acquisition mode was used to monitor the transition of protonated ions to their respective product ions. Electrospray ionization in the positive mode was used for ion production. The calibration curve fitted a quadratic regression (weighted by $1/x^2$) over the range of 2.00 to 500 ng/mL.

Pharmacokinetic modelling

Nonlinear mixed-effects modelling in NONMEM® 7.5 with first-order conditional estimation with eta-epsilon interaction (FOCE-I) was used to develop a population pharmacokinetic model that describes linezolid pharmacokinetics (PK) in both plasma and lumbar cerebrospinal fluid (CSF). Pirana 3.0.0 software was used for model management; Perl-speaks-NONMEM® (PsN) 4.9.0 and R 4.0.4 via RStudio were used for post-processing NONMEM® results and generating figures (Keizer, Karlsson, and Hooker 2013). For the plasma model, the nonlinearity in clearance observed at higher doses was accounted for by a concentration-dependent CL described by the following equation:

$$Vmax = CLmax \cdot Km$$

where $Vmax$ is the maximal elimination rate in mg/h, $CLmax$ is the maximal clearance in L/h apparent with linezolid plasma concentration (Cp) approximating 0, while Km is the Cp in mg/L at which the elimination is half of $Vmax$. Lag time and transit compartments were tested to capture the delay in the absorption process. Allometric scaling of clearance and volume parameters was tested as per Anderson and Holford (B. J. Anderson and Holford 2008) using the fixed power exponents of

0.75 for clearance and 1 for volume and either total body weight or fat-free mass (FFM) (calculated based on the formula in Janmahasatian et al.(Janmahasatian et al. 2005)) as body size descriptors.

Between-subject, between-visit, and between-occasion variabilities were tested for the different plasma and CSF parameters. Each PK sampling day (day 3 and day 28) was considered as a separate visit. Each dose and its following samples were considered a separate occasion, therefore, the dose before the sampling visit along with the predose concentration were treated as a separate occasion from the dose administered during the PK visit and the following concentrations. Residual unexplained variability was described using a combined proportional and additive error model, with the additive error for all samples set to be at least 20% of the LLOQ. Concentrations below the lower limit of quantification (BLQ) were censored according to Beal's M6 method, in which the last censored value in a series during the absorption phase and the first censored value in a series in the terminal phase was replaced with LLOQ/2 and the other censored values in a series were discarded (S. L. Beal 2001). To account for the larger level of uncertainty in the imputed censored values, their additive error was inflated by LLOQ/2. Also, the M3 method was tested as there was a large fraction of BLQ values in the CSF but it did not result in a meaningful difference in the parameter estimates. On the other hand, it caused longer run times and, most importantly, less stable final parameter estimates. For this reason, we proceeded with the M6 method (S. L. Beal 2001).

The process of model development and covariate inclusion was guided by physiological plausibility, model fit diagnostics, and the drop in the objective

function value (OFV). The likelihood ratio test for the drop in OFV was used to compare between nested models, assumed to be approximately χ2 distributed with n degrees of freedom, where n is the number of additional estimated parameters. A p-value of 0.05 was generally used for inclusion and 0.01 for retention. Model performance was evaluated by means of visual predictive checks (VPC). The VPC for the final model stratified into plasma and CSF concentrations is shown in Figure S1. Final parameters precision (95% confidence intervals) was obtained by sampling importance resampling (SIR) (A. G. Dosne et al. 2016).

Imputation of missing covariates

Missing covariates such as CSF protein, CSF albumin, and CSF glucose levels were imputed by the median. A different approach was used for the missing heights (necessary for fat-free mass calculation) since it was missing in 60% of the participants. Missing heights were imputed using multiple linear regression as suggested by Johansson and Karlsson (Johansson and Karlsson 2013). In the first step, participant characteristics, namely sex, weight, and height from a study in a similar population (Brust et al. 2021) were used to develop a multiple linear regression model for height versus weight by sex and accounting for residual variability in heights. Secondly, this multiple linear regression model was used to estimate the missing heights in NONMEM using a random effect model as shown in the equation below:

$$Ht_i = \beta + \alpha . Wt_i . e^{\eta_i}$$

Where Ht_i is the individual height in meters and Wt_i is the individual weight in kilograms. β and α are the model mean intercept and slope respectively. η_i is the

random effect accounting for the individual difference from the mean values. The η_i values are assumed to be normally distributed with mean zero and variance ω^2.The values of β and α are 1.51 and 0.00133 for females and 1.53 and 0.00281 for males respectively. the values of ω_2 were 0.00215 and 0.00170 for females and male respectively. NONMEM implementation can be found in the NONMEM code provided.

Effect compartment modelling for CSF concentrations

The CSF concentrations were modelled as dependent on plasma concentrations using an effect compartment, as previously proposed and implemented by Sheiner et al. (Sheiner et al. 1979) and Savic et al (Savic et al. 2015). Effect compartments are assumed to have a negligible volume compared to the central compartment, with negligible drug transfer between the two compartments. The following differential equation summarizes the kinetics of the effect compartment:

$$\frac{dC_{CSF}}{dt} = k_{plasma-CSF} \cdot \left(PPC \cdot C_{plasma} - C_{CSF}\right),$$

where $k_{plasma-Eff}$ is the first-order equilibration rate constant of the drug between the central compartment (i.e., plasma) and the effect compartment (i.e., CSF), PPC is the pseudo-partition coefficient, C_{plasma} and C_{CSF} are the drug concentration at time t in plasma or CSF, respectively. Figure 7.6 shows the interpretability of the equilibration rate constant and the PPC in the context of effect compartment modelling approach.

Table S7.1 Overview of Linezolid previously published popPK models and current work[a].

	Study population	**Dose**	**CL (L/h)**	**V (L)**	**Q (L/h)**	**Vp (L)**	**Km (mg/L)**
(Abdelwahab et al. 2021)	DR-TB	300 & 600 mg	3.57	40.2	-	-	-
(Tietjen et al. 2021)	MDR-TB	300, 350, 450, or 600 mg bid	7.69	45.2	-	-	-
(Alghamdi, Al-Shaer, and Peloquin 2018)	DS-TB & MDR-TB	300 – 600 qd 600 mg qd or bid	6.32	40.6	-	-	-
(Plock et al. 2007)	Healthy volunteers and septic patients	600 mg bid	11.1	20.2	75.0	28.9	-
(Meagher et al. 2003)[b]	Multidrug-resistant gram-positive infections	600 mg bid	6.85	39.3	9.09	23.6	1.46
(Imperial et al. 2022)[c]	XDR or TI/NR MDR-TB patients	linezolid dosages of 600 or 1200 mg total daily (twice- or once-	7.9	49	0.8	14	16

		daily) for 6 months					
Current work[c]	TBM patients with HIV	1200 mg for 4 weeks followed by 600 mg	7.25	40.8	-	-	27.2

[a] None of the patients were co-administered with Rifampicin except for the current population.

[b] LZD popPK was described by parallel first-order and Michaelis-Menten elimination models. The CL value represents the average total clearance over the first week.

[c] LZD PK was described by a non-linear clearance (Michaelis-Menten).

XDR = extensively drug-resistant

TI/NR MDR-TB = treatment-intolerant or nonresponsive TB patients

Chapter 8 : Conclusion

Summary and discussion

In this thesis, I leveraged pharmacometric modelling approaches to tackle some of the knowledge gaps encountered in TB prevention and treatment with particular emphasis on TBM. Through rigorous modelling and simulation approaches, I provided insights into adherence evaluation, and treatment regimen optimisation for hospitalised patients and TBM paediatric and adult patients to improve clinical outcomes.

In **Chapter 3**, I demonstrate how modelling and simulation can be leveraged to evaluate adherence. In this study, pyrazinamide concentrations at 24 h were used as an adherence measure. Nonadherence thresholds were set based on the LLOQ (method 1) and a personalised thresholds from model-based simulations (method 2). The analysis suggests that poor adherence may have influenced the primary outcome of the REMEMBER study, but there is insufficient evidence to definitively attribute this outcome to non-adherence. Despite the limited utility of model-based simulations combined with drug concentration measurements in this case, they hold promise for other drugs, for example, drugs with long half-lives as discussed in the "Future Perspectives" section. Additionally, the adherence threshold obtained through model simulations proved more sensitive than using a simple LLOQ-based approach.

In **Chapter 4**, I examined whether the higher mortality rates observed among hospitalised TB patients compared to those treated as outpatients could be attributed to differences in the pharmacokinetics of the antitubercular drugs

rifampicin, isoniazid, and pyrazinamide, leading to lower drug exposures. As discussed for the treatment challenges in Chapter 1, several physiological changes in sick patients can alter drug pharmacokinetics, potentially leading to underexposure. However, contrary to expectations, our analysis revealed no clinically significant differences in drug exposure between hospitalised patients and outpatients, as well as between hospitalised patients who died within 12 weeks and those who survived. There does not seem to be a pharmacokinetic basis for the observed mortality. However, the question remains whether hospitalised patients could benefit from higher rifampicin doses or IV rifampicin. It's crucial also to recognise that the higher mortality observed in hospitalised TB patients may not stem from antibiotic underexposure or inefficacy, as shown in our study. The underlying severity of inflammation or sepsis could instead be the primary driver of mortality, indicating a need for interventions beyond increased antibiotic dosage.

A negative correlation was found between bilirubin levels and rifampicin clearance. Rifampicin and its major metabolite are mostly excreted through the biliary tract; therefore, rifampicin and bilirubin have been reported to compete for the same pathway (G. Acocella 1978; Lal et al. 1972). It is unclear whether elevated bilirubin levels are the cause for reduced rifampicin clearance or if it is reduced activity of the excretion pathway shared between rifampicin and bilirubin that leads to higher levels of both. Another possible alternative explanation, as suggested by some studies (L. H. te Brake et al. 2021; L. H. M. Te Brake et al. 2016; Asaumi et al. 2019), is a more complex, non-competitive inhibitory action of rifampicin on key transport proteins responsible for clearing bilirubin (e.g. Multidrug Resistance-

Associated Protein 2). Therefore, dose adjustment recommendations cannot be made at this time, and further research is needed. Moreover, I noted more variable rifampicin absorption and higher between-subject variability in pyrazinamide clearance among hospitalised patients compared to outpatients, and among hospitalised patients who died within 12 weeks versus those who survived. However, overall exposures are not likely to be clinically significant. The modelling approach utilised collected data more effectively than traditional pharmacokinetic study designs, especially when dealing with several confounders. It also factors in different doses, dosing times, and other individual participant characteristics (e.g. weight) to quantify drug exposures. This allows for identifying population subgroups that might otherwise not be found (Bonate 2013).

A potential source of bias in this study could be the exclusion of patients who did not survive beyond day 3, when the PK visit is carried out. The study may exclude the most critically ill patients who die shortly after hospitalisation, potentially leading to a survival bias. However, reports indicate that the majority of the inpatient TB/HIV deaths occur within 2 weeks and often at a median of 4-5 days after admission. Crucially, our study design captured patients within this critical window. If a significant survival bias were present, a trend would have been observed between hospitalised and outpatients; however, no such trend was observed. The patients in the study were followed for 12 weeks, and hospitalised patients who died vs those who survived would be an indication of the severity of the disease. Other biomarkers (e.g. lactate levels) were also tested in the PK model as indicators of disease/sepsis severity.

Chapters 5 – 7 present findings from two clinical studies conducted in TBM patients. A major limitation in TBM clinical studies is the limited number of participants and observations per participant, particularly CNS samples, because of the invasive nature of the lumbar puncture procedure used to obtain these samples. Typically, only 1 to 2 lumbar punctures can be performed during the study period. Population modelling methods are invaluable in this context because they enable more effective analysis when the available data is sparse and not collected according to a set sampling schedule. It can also integrate different types of observations (e.g. plasma and CSF) and unlike in a traditional NCA, modelling can take into consideration the delay between drug kinetics in plasma and CSF.

By analysing rifampicin observations collected opportunistically from lumbar CSF, ventricular CSF, brain ECF, and plasma from children with TBM, I presented novel findings about rifampicin pharmacokinetics in the CNS in **Chapter 5**. The extent of distribution of rifampicin is ~5% in lumbar CSF and ~0.5% in ventricular CSF and brain ECF. Despite the shortcomings discussed in the chapter on MD that make it difficult to interpret ECF results, it provides a novel proof-of-concept that rifampicin gets into the brain tissue. Due to the sparse plasma sampling, modelling allowed for incorporating prior knowledge to better characterise the plasma model upon which the CNS model was based.

Likewise, I employed PK modelling to explore CSF distribution and activity of rifampicin and linezolid in adult patients with TBM co-infected with HIV in **chapters 6 and 7**, respectively. I estimated the CSF partition coefficients at ~5% for rifampicin, which is in agreement with our results in children with TBM (see Chapter

5). CSF penetration of linezolid increases with increasing total protein levels, peaking at 37%. Although rifampicin is a potent inducer of the cytochrome P450 system and an upregulator of drug transporters (Finch et al. 2002), its co-treatment duration did not appear to affect linezolid pharmacokinetics.

Beyond characterising data, once a model is developed, the model can be used to answer "what if" questions – a process known as simulation. The developed models can simulate different dosing scenarios to optimise treatment regimens (Bonate 2013). The models developed for TBM in this thesis could be employed for further investigations of other dosing regimens. I have used simulations in this thesis to simulate typical concentration time profiles for different scenarios. For example, comparing the exposures across vs weights for the 2014 WHO dose regimen recommendation and the 2022 WHO short intensive regimen for TBM treatment in children in **Chapter 5**. In summary, while NCA is straightforward and useful for initial drug evaluations, modelling offers a more detailed, flexible, and predictive approach, making it increasingly valuable for pharmacokinetic studies.

There does not seem to be pharmacokinetic basis for the observed mortality. However, the question remains whether hospitalised patients could benefit from higher rifampicin doses or IV rifampicin. Growing evidence suggests that higher doses of rifampicin are both beneficial and well-tolerated. While pharmacokinetic differences do not justify higher doses, hospitalized patients may still benefit from intensified treatment. Further research is needed to explore this approach.

Future Perspectives

Towards better adherence assessment

Based on the discussion presented in **Chapter 3**, I recommend using a pharmacometric modelling and simulation approach to establish personalised thresholds for assessing drug adherence. This method is not limited to TB drugs but can be applied to a wide range of medications, including antiretrovirals (ARTs). This method is particularly useful for drugs with long half-lives such as bedaquiline and clofazimine. It is also useful in two key scenarios. First, when a drug exhibits low between-subject variability (e.g. lamivudine), it becomes easier to determine adherence because any deviation from expected levels strongly indicates non-adherence (C. Zhang et al. 2012). In this case, the observed drug concentration can provide a clear signal of adherence. Second, for drugs with high between-subject variability, if this variability can be predicted using observable covariates such as genetics (e.g. CYP2B6 genotype for efavirenz) or renal function. For example, if a drug's pharmacokinetics are largely influenced by renal clearance, individual differences can be accounted for, allowing for a more accurate personalization of the threshold. This ability to model and adjust for predictable sources of variability enhances the utility of the pharmacometrics approach, making it a valuable tool in assessing adherence.

Towards better TB treatments in hospitalised patients

As shown in Chapter 4 indicate that hospitalised patients do not seem to have lower drug exposures than outpatients. Therefore, there is no pharmacokinetic basis for the observed mortality. However, the question remains whether hospitalised

patients could benefit from higher rifampicin doses. Growing evidence suggests that higher doses of rifampicin are both beneficial and well-tolerated, so hospitalized patients may still benefit from intensified treatment. Further research is needed to explore this approach.

Previous reports have shown that rifampicin absorption is highly variable (Wilkins et al. 2008) and that FDC and individual tablets usually have different bioavailabilities. Variability in absorption is further compounded when drugs are administered to young children; the dose is typically administered with an oral syringe and often involves incremental dosing rather than a single administration. Future research could also consider administering rifampicin intravenously. Moreover, this variability complicates the accurate correlation of plasma and CSF observations and the identification of other sources of variability in studies in TBM patients. To address these issues and ensure more reliable data, I suggest considering administering IV rifampicin in future clinical trials.

Towards better TBM treatments in adults and children:

In moving towards an effective TBM treatment, the objective is to ultimately achieve concentrations of antitubercular drugs within the human brain and central nervous system (i.e., the site of infection) sufficient for microbial eradication. This entails: 1) a better understanding of antitubercular pharmacokinetics and exposure in the various CNS tissues and CSF and 2) the establishment of antitubercular drug exposure targets and exposure-response relationships.

The value of microdialysis

Microdialysis holds significant promise in advancing CNS pharmacokinetic studies by offering real-time monitoring of drug concentrations in the extracellular fluid of the brain and the spinal cord. Currently, it is the only method that accomplishes spatial and temporal resolution in studying brain drug concentrations, nonetheless, there are some research gaps related to its use in TBM clinical studies. I suggest that future studies optimise the use of MD in clinical studies for drugs used in TBM treatment. In MD, conditions such as flow rate, and semipermeable membrane pore size among other factors affect the recovery of the drug in the catheter, in addition, the exact location of MD catheter placement in the brain tissue may affect the concentrations measured (Kho et al. 2017).

MD is an invasive procedure that is not feasible for routine use in TBM patients in clinical trials. However, in cases where it is required for clinical management, data can be collected opportunistically. Even with a small sample size, the data obtained would be highly valuable for investigating drug concentrations in brain tissue. Despite its limitations, the strength and precision of these measurements make MD a promising tool for further research in this area. Ultimately, optimising MD conditions for diverse drug molecules will enhance the utility of this technique in CNS pharmacokinetic studies, facilitating more precise drug delivery strategies and improving therapeutic outcomes for neurological conditions such as TBM.

The value of preclinical tools

Secondly, pharmacokinetic observations at the site(s) of infection such as meninges and brain cannot be obtained in humans, instead, single time point spinal CSF observations are usually used as a surrogate. However, these samples do not accurately represent total exposure at the site(s) of infection (Litjens, Aarnoutse, and te Brake 2020). This highlights the need for improved preclinical tools to measure drug distribution and activity at the site of disease (Lanni et al. 2023). Preclinical animal models that recapitulate neurological and immunopathological features of human disease in combination with human plasma and CSF data would be extremely valuable for predicting the site of disease drug exposures. An example of that is the model developed by Lanni et al. (Lanni et al. 2023) that was used to show that rifabutin at human-equivalent doses achieved potentially therapeutic exposure in relevant CNS tissues, supporting further evaluation in clinical trials (Wasserman et al. 2024).

Moreover, quantitative systems pharmacology (QSP) models can also be employed to extend beyond mechanistic models. When combined with preclinical animal models, QSP models could provide valuable insights into drug exposure at the site of disease. This integration enhances the ability to predict therapeutic outcomes and optimize drug development strategies (Androulakis 2016).

Understanding changes in protein binding

One of the clinical characteristics of TBM is inflammation of the protective barriers (Wilkinson et al. 2017). Therefore, understanding how pathophysiological changes in the protective barriers, such as the degree of inflammation in the BBB and BCSFB,

and the extent of leakage, impact the levels of total CSF protein and CSF albumin is essential. These changes can influence the degree of drug binding within the CSF, affecting the amount of free drug capable of penetrating the CNS tissues and exerting a pharmacological effect. For future clinical studies involving the collection of CSF samples, I advise quantifying unbound drug concentrations and CSF total protein and/or albumin. By assessing unbound drug concentrations alongside changes in barrier integrity and CSF composition, researchers can better elucidate the pharmacokinetic behaviour of drugs in the CNS including the levels of active drugs available to exert pharmacological effect within the CNS, optimise dosing regimens, and enhance therapeutic outcomes.

Establishing CNS exposure targets

Finally, understanding the CNS pharmacokinetics of antitubercular drugs is only one aspect of the challenge. To achieve a comprehensive understanding, it is crucial to establish CNS exposure targets that ensure both efficacy and safety for all antitubercular drugs used to treat TBM. It is important to note that the MICs used as putative efficacy targets are established in vitro under conditions that differ significantly from those in the CSF and CNS. These laboratory conditions do not fully replicate the complex environment of the CSF, where factors such as local immune responses can influence the drug's effectiveness. Consequently, the relevance of MICs determined in vitro to actual therapeutic outcomes in the CNS remains uncertain, necessitating further research to validate these targets in a clinical context.

Towards better investigation of drug-drug interactions:

Combining linezolid with rifampicin, particularly at doses > 10 mg/kg in TBM treatment regimens is a new promising direction under investigation in TBM clinical trials. However, rifampicin is notorious for its drug-drug interactions due to its induction of many metabolising enzymes and transporters via activation of the Pregnane X receptor, which can potentially affect the exposure of concomitant drugs (Jamis-Dow et al. 1997). As I have alluded to in Chapter 5, the high-dose (35 mg/kg) rifampicin and linezolid combination seems promising in getting more effective TBM treatment regimens, since I were not able to detect any interaction between linezolid and high-dose rifampicin. Nonetheless, a limiting factor in our study was the absence of a study arm who did not receive any rifampicin. Hence, future clinical trials should focus on understanding the interactions between rifampicin and linezolid to ensure the safety and effectiveness of this treatment combination. A drug-drug interaction may have clinically significant consequences since rifampicin is a potent inducer of the cytochrome P450 system and, while the exact elimination pathway of linezolid remains unclear, research suggests it could involve an unidentified cytochrome P450 enzyme (Finch et al. 2002; Plock et al. 2007). Similarly, future studies need to address the question of possible drug-drug interactions of rifampicin with different ARTs.

Furthermore, for studies involving rifampicin, a more powerful study design to characterize the level of autoinduction is to collect samples on the first day of starting treatment and again after steady-state is reached, ~3-4 weeks later. This approach allows for a more detailed characterisation of the autoinduction of

clearance. Rifampicin is a strong inducer of cytochrome P450 enzymes, especially CYP3A4. Through autoinduction, it accelerates its own metabolism as well as that of other drugs metabolized by these enzymes. This can result in lower plasma concentrations and reduced therapeutic effectiveness of co-administered drugs, potentially requiring dose adjustments. Some studies have also used 4β-hydroxycholesterol or the 4β-hydroxycholesterol : Cholesterol ratio as endogenous markers for the degree of CYP3A4 induction (Diczfalusy et al. 2011; Hole et al. 2018; Kim et al. 2018).

Additionally, sampling should allow for the full characterization of the concentration-time profile. For example, sampling should be up to ~3.3 half-lives to capture the terminal elimination phase (Hallare and Gerriets 2023). This can be done in a subset of patients rather than all, as PopPK modelling allows for effective analysis of intensive sampling in a few individuals combined with sparse sampling across a larger group. As previously outlined in **Chapter 6**, the first samples in the LASER-TBM PK study were taken ~5-7 days after starting rifampicin treatment initiation, which limited the ability to describe clearance semi-mechanistically.

Physiologically-based pharmacokinetic (PBPK) simulations are also becoming an increasingly reliable platform for predicting DDIs. It predicts drug pharmacokinetics in humans by combining data from multiple in vitro and clinical studies, assessing how drug-related factors (e.g., physicochemical properties) and physiological system characteristics influence drug exposure (Hong et al. 2022). The predictive power of PBPK simulations in modelling CYP enzyme-mediated DDIs is well established (Hong et al. 2022; Wagner et al. 2016).

Conclusion

Developing optimal TB prevention and treatment regimens that are effective and safe is imperative to successfully combat this global epidemic. This need is even more pressing for TBM, where treatment is particularly challenging due to the difficulty of drug penetration into the CNS, the primary site of infection.

While optimizing drug regimens by identifying the most effective drugs, dosages and duration is essential, patient adherence is equally critical—after all, even the best treatments are ineffective if they are not taken as prescribed. Beyond answering scientific questions about the best regimen, it is vital to bridge the gap between research and real-world implementation. Pharmacometrics can play key roles in both aspects, helping to design effective therapies while also supporting strategies to improve adherence and public health outcomes.

Given the high cost of clinical trials, pharmacometrics is a powerful tool for addressing many unanswered questions in the field. Modelling and simulation approaches can significantly reduce the cost of TB clinical trials, particularly in resource-limited settings, by optimizing sampling strategies, addressing study objectives with fewer patients, utilizing sparse samples, and predicting pharmacological success and target attainment. Additionally, these approaches enable the pooling of datasets across different studies, maximizing the use of existing data. In certain populations, such as critically ill patients, children, or those with TBM, modelling and simulation allow for opportunistic analyses, providing valuable insights that might otherwise be difficult to obtain through traditional clinical trials.

The research presented in this thesis contributes to the current body of knowledge by providing recommendations on the utility of modelling and simulation to measure adherence. That is in addition to characterising the pharmacokinetics of rifampicin, isoniazid, and pyrazinamide in patients hospitalised due to TB, plus characterising the CSF pharmacokinetics of rifampicin in children and adults with TBM, and of linezolid in adults with TBM and HIV. The presented models serve as a platform to enhance study design, facilitate result interpretation, and optimize TB treatment strategies, as well as improve treatment adherence.

Appendix 1: NONMEM code

Final NONMEM code for results presented in Chapter 3

For simulation of pyrazinamide concentrations

```
; 1. Based on:
; Model desc: max.accum.dose=1 C24-C48 Sim
$SIZES       PD=-1000 LVR=-150 LTH=-200 MAXFCN=10000000 LNP4=-
150000 DIMTMP=1000 ; Settings for the memory of NONMEM
$PROBLEM    REMEMBER ADHERENCE SIM CONC AT 24H & 48H PZA
$INPUT       ID PID ARMTYPE=DROP CASE GRP WHAT=DROP VISIT TIME
OCC EVID AMT DV BLQPZA MDVPZA AGE SEXF HT WT FFM FAT TABNUM PROB
$ABBREVIATED PROTECT
$ABBREVIATED  DECLARE  INTEGER  NDOSE  INTEGER  MAX_ACCUM_DOSES
;needed to define variables for dose accumulation
$DATA      simpza_31.01.21.csv IGNORE=@ ;IGNORE(ID.EQ.26)
$SUBROUTINE ADVAN13 TRANS1 TOL=8 ATOL=8 ;SSTOL=3 SSATOL=3
$MODEL      NCOMPS=2 COMP=(ABS DEFDOSE) ;Gut_PZA
            COMP=(CENTRAL DEFOBSERVATION) ;Central compartment
$PK
;TO PRINT ONLY SIMULATED CONC ROWS
; EXCL=0
; IF(EVID.EQ.1) EXCL=1

MXSTEP=5000    ; Maximal number of numerical integration steps
Advan 9 and 13
```

```
;-----Allometric  Scaling----------------------------------------
TVFFM = 42.10
TVWT  = 56.88
TVFAT = 14.21
ALLMCLWT=(WT/TVWT)**0.75
ALLMVWT=WT/TVWT
ALLMCLFFM=(FFM/TVFFM)**0.75
ALLMVFFM=FFM/TVFFM
;-----Typical  Parameters-----------------------------------------
DAY = 28
CLBS=THETA(3)          ; CL DAY0
CL28=THETA(4)          ; CL DAY28
NATVCL=CLBS + (CL28-CLBS)*(DAY/28)  ; Ensures that we estimate
clearance on day 28
PROPERR   = THETA(1)     ;Proportional error sigma
ADDERR          = THETA(2)          ;Additive error sigma
TVCL            = NATVCL * ALLMCLFFM          ;Clearance [L/h]
TVV       = THETA(5) * ALLMVFFM         ;Volume, central [L]
TVBIO           = THETA(6)          ;Bioavailability
TVKA            = THETA(7)          ;Absorption  rate  constant
[1/h]
TVMTT           = THETA(8)          ;Mean transit time [h]
TVNN            = THETA(9)          ;Number     of     transit
compartments
```

```
;-----Between-Subject  Variability------------------------------
BSVCL     = ETA(1)
BSVV      = ETA(2)
BSVBIO         = ETA(3)
BSVKA          = ETA(4)
BSVMTT         = ETA(5)
; ;-----Between-Visit Variability-------------------------------
BVVCL = 0
IF(VISIT.EQ.2)      BVVCL = ETA(6)
IF(VISIT.EQ.4)  BVVCL = ETA(7)
IF(VISIT.EQ.8)  BVVCL = ETA(8)
BVVV = 0
IF(VISIT.EQ.2)      BVVV = ETA(9)
IF(VISIT.EQ.4)  BVVV = ETA(10)
IF(VISIT.EQ.8)  BVVV = ETA(11)
BVVBIO = 0
IF(VISIT.EQ.2)      BVVBIO = ETA(12)
IF(VISIT.EQ.4)  BVVBIO = ETA(13)
IF(VISIT.EQ.8)  BVVBIO = ETA(14)
BVVKA = 0
IF(VISIT.EQ.2)      BVVKA = ETA(15)
IF(VISIT.EQ.4)  BVVKA = ETA(16)
IF(VISIT.EQ.8)  BVVKA = ETA(17)
BVVMTT = 0
IF(VISIT.EQ.2)      BVVMTT = ETA(18)
```

```
IF(VISIT.EQ.4)  BVVMTT = ETA(19)
IF(VISIT.EQ.8)  BVVMTT = ETA(20)
;-----Individual  Parmeters-------------------------------------
CL   = TVCL * EXP(BSVCL + BVVCL)
V    = TVV*EXP(BSVV + BVVV)
BIO  = TVBIO*EXP(BSVBIO + BVVBIO)
KA   = TVKA*EXP(BSVKA + BVVKA)
MTT  = TVMTT*EXP(BSVMTT + BVVMTT)
NN   = TVNN

;-----Initialization of Compartments---------------------------
A_0(1) = 0.0000001  ;gut
A_0(2) = 0.0000001  ;central
K20  = CL/V

;-----Transit Compartments with Dose Accumulation--------------
-------; IMPORTANT!!! This code will NOT work if ALAG1 (or ALAGx)
is defined in the code above.
; DO NOT USE ALAGx, use the parameter TLAG or re-assign it below
; If you want to use a delay before the transit starts the
absorption, re-assign the variable here.
; NOTE that you MUST uncomment also CALLFL=-2
;TLAG    = TVTLAG + BVVTLAGTR ;Additive model
; TLAG = Reassign here a variable added above! Do NOT use
ALAGx!!!
```

```
TLAG = 0
; CALLFL = -2
; Setting CALLFL = -2 makes sure the PK subroutine gets called
with every event record,
; with ADDL and lagged doses, and at modeled event times that
are not explicitily a line in the dataset.
; It is here so that the TLAG and ADDL work
; It does not apply to the ERROR or ADVAN9 or ADVAN15 routines.

; Set SS = 0 if SS is not used in the dataset
SS = 0
; IMPORTANT!!! This sets the maximum number of doses that will
be remembered by NONMEM the super-imposition
; With MAX_ACCUM_DOSES=2, the code "accumulates" the latest 2
dose.
; If you want to increase this, you must also uncomment below
the code for the doses beyond the 2nd
MAX_ACCUM_DOSES = 1
; This is the time after which the transit should be turned off
(absorption completed)
; It is meant to save computational time when accumulating if
you are SURE that there is no absprtion
; at times after dose longer than FORGET.
; A reasonable value would be several times MTT, i.e. FORGET >
10*MAX(MTT)
```

```
FORGET = 1000
F1 = 0 ; I need to set bioavailability in compartment 1 to 0 for
this implementation of the transit compartment absorption
KTR = (NN+1)/MTT ; **The number of actual transit compartments
is NN+1, so this number can never be 0**

IF (NEWIND/=2.OR.EVID>=3) THEN ; For each new individual or
RESET or RESET+DOSE event
NDOSE = 0 ; Reset the dose number
     DOSETIMESS = 0
     PIZZASS = 0
     KTRVECSS = -1
     NNVECSS = -1
     SWITCHSS = 0

     DOSETIME0 = 0
     PIZZA0 = 0
     KTRVEC0 = -1
     NNVEC0 = -1
     ENDIF
; This works for ANY dose, also for ADDL non-event doses (thanks
to CALLFL=-2)
IF(AMT >0 .AND. MOD(NDOSE,MAX_ACCUM_DOSES) == 0) THEN
     DOSETIME0 = TIME + TLAG
     PIZZA0 = LOG(BIO*AMT*KTR + 1E-12) - GAMLN(NN+1)
```

```
     KTRVEC0 = KTR
     NNVEC0 = NN
ENDIF
; I am using SWITCHSSNXT so that, as soon as another record is
seen, the SS switch goes off.
; I am using a switch as opposed to SS per se because the
original SS value carries on with ADDL series,
; that should not be treated as SS
SWITCHSS = 0
; (USING ADDL with SS) In such a series of ADDL doses, SS would
remain the same as the originating dose event record
; but DOSREC(i)>0. Hence, DOSREC(i)==0 makses sure that the SS
code gets executed only the first time
; This takes care of the SS part of the dose, if SS is used
; DOSREC()==0 makes sure this is NOT a trailing ADDL dose.

IF(AMT >0 .AND. SS>0 .AND. DOSREC(AMT)==0) THEN
     SWITCHSS = 1
     DOSETIMESS = TLAG
     PIZZASS = LOG(BIO*AMT*KTR + 1E-12) - GAMLN(NN+1)
     KTRVECSS = KTR
     NNVECSS = NN
ENDIF
; Increase dose counter
IF(AMT >0) NDOSE = NDOSE + 1
```

```
;============================================================
$DES
; This overlaps the effect of the last 5 doses accumulating them
in TRANSIT
TRANSIT = 0
KTT = 0

TEMPO = T-DOSETIME0
IF   (SWITCHSS==0   .AND.   TEMPO>0   .AND.   TEMPO<FORGET   .AND.
KTRVEC0>0) THEN
     KTT = KTRVEC0*(TEMPO)
     TRANSIT = TRANSIT + EXP(PIZZA0 + NNVEC0*LOG(KTT) - KTT)
ENDIF

; It the SWITCHSS is on, this is executed within the routine to
find the SS values.
; DOSETIMESS is centred around 0 (+TLAG) for this calculation.
The values of PIZZA, KTR and NN are those from the latest dose
record (NDOSE)
IF (SWITCHSS >0 .AND. T >DOSETIMESS) THEN ;
     KTT = KTRVECSS*(T-DOSETIMESS)
     TRANSIT = EXP(PIZZASS + NNVECSS*LOG(KTT) - KTT)
ENDIF
DADT(1) = TRANSIT -KA*A(1)
DADT(2) = KA*A(1) -K20*A(2)
```

```
$ERROR
IPRED=A(2)/V

; DEFINE LLOQ VALUE
; LLOQ could be study-specific, e.g if you have data from
different labs in your analysis
; In that case, you can use IFs, or you can define the values
as covariates in the dataset
LLOQ = 0.203 ; DEFINE YOUR OWN LLOQ HERE

; DEFINE censoring threshold (CENS_THR, generally LOD)
; Generally the same as LLOQ, but not if the LLOQ data was
released by the lab.
; If censoring threshold is not explicitly indicated, we can
generally assume it to be the limit of detection (LOD).
; The signal-to-noise ratio is generally assumed to be 10 at the
LLOQ, and 3 at the LOD
; https://en.wikipedia.org/wiki/Detection_limit;
; Keizer RJ, Jansen RS, Rosing H, Thijssen B, Beijnen JH,
Schellens JHM, Huitema ADR.
; Incorporation of concentration data below the limit of
quantification in population pharmacokinetic analyses.
; Pharmacol Res Perspect [Internet]. 2015 Mar;3(2):e00131.
Available from: http://doi.wiley.com/10.1002/prp2.131
```

```
CENS_THR = LLOQ ; inferred LOD = 30% of LLOQ
IMPUTED_BLQ = LLOQ/2
PROP = IPRED*PROPERR
; ADD is defined as 20% of LLOQ + THETA(.)
; The lower bound of THETA(.) can be zero, if it goes there, we
can fix it to zero and ADD will be 20% of LLOQ
; REMEMBER that when you report the value of ADD and its
uncertainty, you need to work out numbers, as NONMEM gives
uncertainty on THETA, not ADD
; An alternative approach is to set the lower bound of the THETA
for the additive error to 20% of the LLOQ.
; In that case, one does not have to worry about adjusting the
precision.
; On the other hand, this cannot be done if you have different
LLOQs within your analysis (e.g. different labs)
ADD = ADDERR+(LLOQ*0.2)
;ADD = THETA(6)+(LLOQ*0.5)
; For BLQ==1 (i.e. first CENSORED value in a series, which was
imputed to CENS_THR/2), we add extra additive error on the
concentrations,
; since the value in DV has been imputed and therefore more
uncertain.
IF (ICALL/=4.AND.BLQPZA==1) THEN
     ADD = ADD+(LLOQ/2)
     ;ADD = ADD+(CENS_THR/2)
```

```
ENDIF
NO_FIT = 0
; For BLQ==2 (i.e. the trailing CENSORED values in a series that
were imputed to CENS_THR/2), we don't want these to influence
the fit,
; we only want them for simulation-based diagnostics such as the
VPC.
; So we define a separate error structure for these points. It
has no proportional component
; (PROP = 0, as we would not want these points to affect our
estimate of proportional error)
; and a FIXED and HUGE additive component (ADD = 1000000000,
large with respect to the readings of concentration),
; so that the values do not affect the fit. It's also a good
idea to repeat the diagnostic plots without the BLQ=2 points

IF (ICALL/=4.AND.BLQPZA==2) THEN
     PROP = 0
     ADD = 10000000000
     NO_FIT = 1
ENDIF

W = SQRT(ADD**2+PROP**2)
; Protective code
IF (W.LE.0.000001) W=0.000001
```

```
IRES=DV-IPRED
IWRES=IRES/W
Y = IPRED + W*ERR(1)
; To prevent simulation (ICALL==4) of negative values. It set a
positive lower bound for Y, so that VPCs in the log-scale can
be plotted
IF (ICALL==4.AND.Y<=CENS_THR) Y = CENS_THR/2
; To calculate time after dose.
IF(AMT>0) THEN
     TIMEDOSE = TIME
     AMOUNTDOSE = AMT
ENDIF
TAD = TIME-TIMEDOSE
; REPLICATE INDICATOR
REPI=IREP

;-----Retrieve Amount in Each Compartment-----
AA1 = A(1)
AA2 = A(2)
$THETA  (0,0.0436681,2) FIX ; 1. PROPERR
$THETA  (0,0.36876,10) FIX ; 2. ADDERR [mg/L]
$THETA  (0,3.34508,10) FIX ; 3. CLBS[L/h]
$THETA  (0,3.83049,10) FIX ; 4. CL28[L/h]
$THETA  (0,43.1646,100) FIX ; 5. TVV [L]
$THETA  1 FIX ; 6. BIO
```

```
$THETA  (0,3.53583,10) FIX ; 7. KA
$THETA  (0,0.542055,5) FIX ; 8. MTT [h]
$THETA  (0,3.34456,4) FIX ; 9. NN
;$THETA  48 FIX                          ; 10.TLAG
;$THETA  0 FIX ; 10.TLAG
;-----------------------------------------------------------
$OMEGA  0.0267137  FIX  ;   1. BSVCL
$OMEGA  0  FIX  ;    2. BSVV
$OMEGA  0.0114623  FIX  ;  3. BSVBIO
$OMEGA  0  FIX  ;   4. BSVKA
$OMEGA  0  FIX  ;  5. BSVMTT
$OMEGA  BLOCK(1) FIX
 0.0177203  ;      BVVCL
$OMEGA  BLOCK(1) SAME
$OMEGA  BLOCK(1) SAME
$OMEGA  BLOCK(1) FIX
 0  ;       BVVV
$OMEGA  BLOCK(1) SAME
$OMEGA  BLOCK(1) SAME
$OMEGA  BLOCK(1) FIX
 0.014188  ;     BVVBIO
$OMEGA  BLOCK(1) SAME
$OMEGA  BLOCK(1) SAME
$OMEGA  BLOCK(1) FIX
 0.704627  ;      BVVKA
```

```
$OMEGA  BLOCK(1) SAME
$OMEGA  BLOCK(1) SAME
$OMEGA  BLOCK(1) FIX
 0.28027  ;     BVVMTT
$OMEGA  BLOCK(1) SAME
$OMEGA  BLOCK(1) SAME
; $OMEGA  BLOCK(1) FIX
; 1  ;    BVVTLAG
; $OMEGA  BLOCK(1) SAME
; $OMEGA  BLOCK(1) SAME
$SIGMA  1  FIX  ; 25. RESIDUAL
;$ETAS    FILE=run001.phi TBLN=2
$SIMULATION (1234) ONLYSIM SUBPROBLEM=500

$TABLE       FILE=simpza001.csv REPI ID PID CASE GRP VISIT OCC
EVID AMT TIME TAD Y DV PRED IPRED CL V BIO KA MTT BSVCL BSVV
BSVBIO BSVKA BSVMTT BVVCL BVVBIO BVVKA BVVMTT NOPRINT NOAPPEND
NOHEADER FORMAT=,
```

For simulation of rifampicin concentrations

```
; Model desc: max.accum.dose=1 C24-C48 Sim
$SIZES      PD=-1000 LVR=-150 LTH=-200 MAXFCN=10000000 LNP4=-150000
            DIMTMP=1000 ; Settings for the memory of NONMEM

$PROBLEM    REMEMBER ADHERENCE SIM CONC AT 24H & 48H RIF
```

```
$INPUT      ID PID ARMTYPE=DROP CASE GRP WHAT=DROP VISIT TIME OCC EVID
AMT DV BLQRIF MDVRIF AGE SEXF HT WT FFM FAT TABNUM PROB

$ABBREVIATED PROTECT

$ABBREVIATED DECLARE INTEGER NDOSE INTEGER MAX_ACCUM_DOSES ;needed to
define variables for dose accumulation

$DATA       simrif_31.01.21.csv IGNORE=@

$SUBROUTINE ADVAN13 TRANS1 TOL=8 ATOL=8 ;SSTOL=3 SSATOL=3

$MODEL      NCOMPS=3
                 COMP=(ABS DEFDOSE) ;RIF_Gut
                 COMP=(LIVER) ;RIF Liver compartment
              COMP=(CENTRAL DEFOBSERVATION) ;RIF_Central compartment

$PK
;TO PRINT ONLY SIMULATED CONC ROWS
; EXCL=0
; IF(EVID.EQ.1) EXCL=1

MXSTEP=5000      ; Maximal number of numerical integration steps Advan
9 and 13

;-----Allometric Scaling ------------------------------------;;
```

```
WT & FFM from the HAART study; very close to this study's population
(medWT=55.75, medFFM=41.98)
TVFFM = 42.10
TVWT  = 56.88
TVFAT = 14.21

ALLMCLWT=(WT/TVWT)**0.75
ALLMVWT=WT/TVWT

ALLMCLFFM=(FFM/TVFFM)**0.75
ALLMVFFM=FFM/TVFFM

ALLMCLFAT=(FAT/TVFAT)**0.75
ALLMVFAT=FAT/TVFAT

;-----Typical Parameters-----------------------------
PROPERR    = THETA(1)      ;Proportional error sigma
ADDERR          = THETA(2)            ;Additive error sigma

DAY = 1
IF(VISIT.EQ.2) DAY = 14
IF(VISIT.EQ.4) DAY = 28
IF(VISIT.EQ.8) DAY = 56
;-------------------------AUTOINDUCTION--------------
CLBS=THETA(3)          ; CL STRAT1=0
CLSS=THETA(4)          ; CL STEADY STATE
IND50=THETA(5)         ; INDUCTION HALF LIFE
```

```
TVCL=(CLBS+(CLSS-CLBS)*(1-EXP(-LOG(2)*DAY/IND50)))*ALLMCLFFM
;-----------------------------------------------------
       TVV  =THETA(6)*ALLMVFFM ; Pop V
       TVKA =THETA(7)          ; Pop KA
       TVBIO = 1                 ; Pop F
       TVMTT = THETA(8)          ; Pop MTT
       TVNN = THETA(9)           ; Pop NN

;--------------------------HEPATIC CL-----------------------;
TVVH=THETA(10)*ALLMVFFM    ; VOLUME OF LIVER WITH ALLOMETRIC SCALLING
TVQH=THETA(11)*ALLMCLFFM   ; PLASMA FLOW RATE
TVFU=THETA(12)             ; UNBOUND PLASMA FRACTION OF RIF

;--------------------------BSV----------------------------;
BSVCL = ETA(1)
BSVV = ETA(2)
BSVKA = ETA(3)
BSVBIO = ETA(4)
BSVMTT = ETA(5)

;-----Between-Visit Variability-------------------------
BVVCL = 0
IF(VISIT.EQ.2)   BVVCL = ETA(6)
IF(VISIT.EQ.4)  BVVCL = ETA(7)
IF(VISIT.EQ.8)  BVVCL = ETA(8)
```

```
BVVV = 0
IF(VISIT.EQ.2)   BVVV = ETA(9)
IF(VISIT.EQ.4)  BVVV = ETA(10)
IF(VISIT.EQ.8)  BVVV = ETA(11)

BVVBIO = 0
IF(VISIT.EQ.2)   BVVBIO = ETA(12)
IF(VISIT.EQ.4)  BVVBIO = ETA(13)
IF(VISIT.EQ.8)  BVVBIO = ETA(14)

BVVKA = 0
IF(VISIT.EQ.2)   BVVKA = ETA(15)
IF(VISIT.EQ.4)  BVVKA = ETA(16)
IF(VISIT.EQ.8)  BVVKA = ETA(17)

BVVMTT = 0
IF(VISIT.EQ.2)   BVVMTT = ETA(18)
IF(VISIT.EQ.4)  BVVMTT = ETA(19)
IF(VISIT.EQ.8)  BVVMTT = ETA(20)

;------------------INDIVIDUAL PARAMETERS----------------------;
CL=TVCL*EXP(BSVCL+BVVCL)
V =TVV*EXP(BSVV+BVVV)
KA=TVKA*EXP(BSVKA+BVVKA)
BIO=TVBIO*EXP(BSVBIO+BVVBIO)
MTT=TVMTT*EXP(BSVMTT+BVVMTT)
NN=TVNN
```

```
VH=TVVH

QH=TVQH

FU=TVFU

;-------------------------SATURABLE------------------------------

CLINT=CL

LOGKM = THETA(13) ; LOG KM - calculated from data set - median of max
conc in the liver

VMAX  = CLINT*EXP(LOGKM) ; max enzymatic rate ;from eq. CLint = Vmax/KM


;-----Initialization of Compartments-----------------------------

A_0(1) = 0.0000001    ;gut

A_0(2) = 0.0000001    ;liver

A_0(3) = 0.0000001    ;central


;-----Transit Compartments with Dose Accumulation-----------------

; IMPORTANT!!! This code will NOT work if ALAG1 (or ALAGx) is defined
in the code above.

; DO NOT USE ALAGx, use the parameter TLAG or re-assign it below

; If you want to use a delay before the transit starts the absorption,
re-assign the variable here.

; NOTE that you MUST uncomment also CALLFL=-2

;TLAG    = TVTLAG + BVVTLAGTR ;Additive model

; TLAG = Reassign here a variable added above! Do NOT use ALAGx!!!

TLAG = 0

; CALLFL = -2
```

```
; Setting CALLFL = -2 makes sure the PK subroutine gets called with
every event record,
; with ADDL and lagged doses, and at modeled event times that are not
explicitily a line in the dataset.
; It is here so that the TLAG and ADDL work
; It does not apply to the ERROR or ADVAN9 or ADVAN15 routines.

; Set SS = 0 if SS is not used in the dataset
SS = 0

; IMPORTANT!!! This sets the maximum number of doses that will be
remembered by NONMEM the super-imposition
; With MAX_ACCUM_DOSES=2, the code "accumulates" the latest 2 dose.
; If you want to increase this, you must also uncomment below the code
for the doses beyond the 2nd
MAX_ACCUM_DOSES = 1

; This is the time after which the transit should be turned off
(absorption completed)
; It is meant to save computational time when accumulating if you are
SURE that there is no absprtion
; at times after dose longer than FORGET.
; A reasonable value would be several times MTT, i.e. FORGET >
10*MAX(MTT)
FORGET = 1000
```

```
F1 = 0 ; I need to set bioavailability in compartment 1 to 0 for this
implementation of the transit compartment absorption

KTR = (NN+1)/MTT ; **The number of actual transit compartments is
NN+1, so this number can never be 0**

IF (NEWIND/=2.OR.EVID>=3) THEN ; For each new individual or RESET or
RESET+DOSE event

      NDOSE = 0 ; Reset the dose number

      DOSETIMESS = 0
      PIZZASS = 0
      KTRVECSS = -1
      NNVECSS = -1
      SWITCHSS = 0


      DOSETIME0 = 0
      PIZZA0 = 0
      KTRVEC0 = -1
      NNVEC0 = -1
ENDIF

; This works for ANY dose, also for ADDL non-event doses (thanks to
CALLFL=-2)
```

```
IF(AMT >0 .AND. MOD(NDOSE,MAX_ACCUM_DOSES) == 0) THEN
      DOSETIME0 = TIME + TLAG
      PIZZA0 = LOG(BIO*AMT*KTR + 1E-12) - GAMLN(NN+1)
      KTRVEC0 = KTR
      NNVEC0 = NN
ENDIF

; I am using SWITCHSSNXT so that, as soon as another record is seen,
the SS switch goes off.
; I am using a switch as opposed to SS per se because the original SS
value carries on with ADDL series,
; that should not be treated as SS
SWITCHSS = 0
; (USING ADDL with SS) In such a series of ADDL doses, SS would remain
the same as the originating dose event record
; but DOSREC(i)>0. Hence, DOSREC(i)==0 makses sure that the SS code
gets executed only the first time
; This takes care of the SS part of the dose, if SS is used
; DOSREC()==0 makes sure this is NOT a trailing ADDL dose.

IF(AMT >0 .AND. SS>0 .AND. DOSREC(AMT)==0) THEN
      SWITCHSS = 1
      DOSETIMESS = TLAG
      PIZZASS = LOG(BIO*AMT*KTR + 1E-12) - GAMLN(NN+1)
      KTRVECSS = KTR
      NNVECSS = NN
ENDIF
```

```
; Increase dose counter
IF(AMT >0) NDOSE = NDOSE + 1

$DES
; This overlaps the effect of the last 5 doses accumulating them in
TRANSIT
TRANSIT = 0
KTT = 0

TEMPO = T-DOSETIME0
IF (SWITCHSS==0 .AND. TEMPO>0 .AND. TEMPO<FORGET .AND. KTRVEC0>0) THEN
      KTT = KTRVEC0*(TEMPO)
      TRANSIT = TRANSIT + EXP(PIZZA0 + NNVEC0*LOG(KTT) - KTT)
ENDIF

; It the SWITCHSS is on, this is executed within the routine to find
the SS values.
; DOSETIMESS is centred around 0 (+TLAG) for this calculation. The
values of PIZZA, KTR and NN are those from the latest dose record
(NDOSE)
IF (SWITCHSS >0 .AND. T >DOSETIMESS) THEN ;
      KTT = KTRVECSS*(T-DOSETIMESS)
      TRANSIT = EXP(PIZZASS + NNVECSS*LOG(KTT) - KTT)
ENDIF

;Transfer rates:RIF==================================
```

```
 CH = A(2) / VH ; drug conc in liver
  ; set saturable elimindation to zero for pts with negative
concentrations in liver
  ; product of a logarith cannot be negative - this would not work
  ; normal Michalis-Mentel equation gives you a rate =k*A = CL*C
  ; but we want to get CL, so you divide the rate by concentration -
and get saturable clearance
  ; equation is placed in $DES because saturable clearance changes
over time
  SAT_CL=0
  IF (CH>0) SAT_CL=VMAX/(1+EXP(-(LOG(CH)-LOGKM))) / (CH)
  ;transformation based on better Emax model, wider search in log
parametrisation

  EH  = (SAT_CL*FU)/((SAT_CL*FU)+QH) ; fraction undergoing first pass
extraction
  FH  = 1 - EH ;fraction available after 1st pass to go to systemic
circulation
  ;CLH = EH * QH ; hepatic clearance

K20=(QH*EH/VH)
K23= (QH*FH/VH)
K32=(QH/V)

;DIFFERENTIAL EQNS:RIF
DADT(1) = TRANSIT -KA*A(1)
DADT(2)= KA*A(1)-K23*A(2)+K32*A(3)-K20*A(2)
```

```
DADT(3) =  K23*A(2)-K32*A(3)

$ERROR
IPRED=A(3)/V

; DEFINE LLOQ VALUE
; LLOQ could be study-specific, e.g if you have data from different labs in your analysis
; In that case, you can use IFs, or you can define the values as covariates in the dataset
LLOQ = 0.075 ; DEFINE YOUR OWN LLOQ HERE

; DEFINE censoring threshold (CENS_THR, generally LOD)
; Generally the same as LLOQ, but not if the LLOQ data was released by the lab.
; If censoring threshold is not explicitly indicated, we can generally assume it to be the limit of detection (LOD).
; The signal-to-noise ratio is generally assumed to be 10 at the LLOQ, and 3 at the LOD
; https://en.wikipedia.org/wiki/Detection_limit;
; Keizer RJ, Jansen RS, Rosing H, Thijssen B, Beijnen JH, Schellens JHM, Huitema ADR.
; Incorporation of concentration data below the limit of quantification in population pharmacokinetic analyses.
; Pharmacol Res Perspect [Internet]. 2015 Mar;3(2):e00131. Available from: http://doi.wiley.com/10.1002/prp2.131
```

```
CENS_THR = LLOQ ; inferred LOD = 30% of LLOQ

IMPUTED_BLQ = LLOQ/2

PROP = IPRED*PROPERR
; ADD is defined as 20% of LLOQ + THETA(.)
; The lower bound of THETA(.) can be zero, if it goes there, we can
fix it to zero and ADD will be 20% of LLOQ
; REMEMBER that when you report the value of ADD and its uncertainty,
you need to work out numbers, as NONMEM gives uncertainty on THETA,
not ADD
; An alternative approach is to set the lower bound of the THETA for
the additive error to 20% of the LLOQ.
;  In  that  case,  one  does  not  have  to  worry  about  adjusting  the
precision.
; On the other hand, this cannot be done if you have different LLOQs
within your analysis (e.g. different labs)

ADD = ADDERR+(LLOQ*0.2)

; For BLQ==1 (i.e. first CENSORED value in a series, which was imputed
to CENS_THR/2), we add extra additive error on the concentrations,
; since the value in DV has been imputed and therefore more uncertain.
IF (ICALL/=4.AND.BLQRIF==1) THEN
      ADD = ADD+(LLOQ/2)
      ;ADD = ADD+(CENS_THR/2)
ENDIF
```

```
NO_FIT = 0
; For BLQ==2 (i.e. the trailing CENSORED values in a series that were
imputed to CENS_THR/2), we don't want these to influence the fit,
; we only want them for simulation-based diagnostics such as the VPC.
; So we define a separate error structure for these points. It has no
proportional component
; (PROP = 0, as we would not want these points to affect our estimate
of proportional error)
; and a FIXED and HUGE additive component (ADD = 1000000000, large
with respect to the readings of concentration),
; so that the values do not affect the fit. It's also a good idea to
repeat the diagnostic plots without the BLQ=2 points

IF (ICALL/=4.AND.BLQRIF==2) THEN
      PROP = 0
      ADD = 10000000000
      NO_FIT = 1
ENDIF
W = SQRT(ADD**2+PROP**2)
; Protective code
IF (W.LE.0.000001) W=0.000001

IRES=DV-IPRED
IWRES=IRES/W

Y = IPRED + W*ERR(1)
```

```
; To prevent simulation (ICALL==4) of negative values. It set a
positive lower bound for Y, so that VPCs in the log-scale can be
plotted
IF (ICALL==4.AND.Y<=CENS_THR) Y = CENS_THR/2

; To calculate time after dose.
IF(AMT>0) THEN
      TIMEDOSE = TIME
      AMOUNTDOSE = AMT
ENDIF

TAD = TIME-TIMEDOSE

; REPLICATE INDICATOR
REPI=IREP

;-----Retrieve Amount in Each Compartment----------------------------
AA1 = A(1)
AA2 = A(2)

$THETA  (0,0.108105,1) ; 1. PROPERR
$THETA  (0.04,0.0644782,10) ; 2. ADDERR [mg/L]
$THETA  (0,93.1624) ; 3. CLBS [L/h]
$THETA  (0,175.993) ; 4. CLSS[L/h]
$THETA  (0,4.52475,10) ; 5. IND50[L/h]
$THETA  (0,50.0752,100) ; 6. V  [L]
```

```
$THETA  (0,1.96344,10) ; 7. KA [1/h]
$THETA  (0,0.712014,5) ; 8. MTT[h]
$THETA  (0,19.3342,50) ; 9. NN
$THETA  1 FIX ; 10. VH
$THETA  50 FIX ; 11. QH PLASMA FLOW
$THETA  0.2 FIX ; 12. FU FRACTION_UNBOUND
$THETA  (0,1.20794,3) ; 13. log(KM) [log(mg/L)] - natural log with
base e

$OMEGA  0.0507363  ;  1. BSVCL
$OMEGA  0.0200823  ;  2. BSVVRIF
$OMEGA  0  FIX  ;  3. BSVKARIF
$OMEGA  0  FIX  ; 4. BSVBIORIF
$OMEGA  0  FIX  ; 5. BSVMTTRIF
$OMEGA  BLOCK(1) FIX
 0.0477937   ;     6-8 BVVCL
$OMEGA  BLOCK(1) SAME
$OMEGA  BLOCK(1) SAME
$OMEGA  BLOCK(1) FIX
 0  ;       9-11 BVVVRIF
$OMEGA  BLOCK(1) SAME
$OMEGA  BLOCK(1) SAME
$OMEGA  BLOCK(1) FIX
 0.0121545  ;    12-14 BVVBIO
$OMEGA  BLOCK(1) SAME
$OMEGA  BLOCK(1) SAME
$OMEGA  BLOCK(1) FIX
```

```
 0.658575  ;     15-17  BVVKA
$OMEGA  BLOCK(1) SAME
$OMEGA  BLOCK(1) SAME
$OMEGA  BLOCK(1) FIX
 0.39269  ;    18-20  BVVMTT
$OMEGA  BLOCK(1) SAME
$OMEGA  BLOCK(1) SAME

$SIGMA  1  FIX  ; 1. RESIDUAL

$SIMULATION (1234) ONLYSIM SUBPROBLEM=500 PARAFILE=ON

$TABLE       FILE=simrif001.csv REPI ID PID CASE GRP VISIT OCC EVID
AMT TIME TAD Y DV PRED IPRED PROPERR ADDERR
CLBS CLSS CL IND50 V KA MTT NN VH QH FU
BSVCL BSVV BSVKA BSVBIO BSVMTT
BVVCL BVVV BVVBIO BVVKA BVVMTT
NOPRINT NOAPPEND NOHEADER FORMAT=,
```

Final NONMEM code for results presented in Chapter 4

Rifampicin

```
;; 1. Based on:
; Model desc: Rifampicin.Model.KDHTB
; Settings for the memory of NONMEM
$SIZES      PD=-1000 LVR=-150 LTH=-200 MAXFCN=10000000 LNP4=-150000
```

```
$PROBLEM    |ADVAN2_TRANS1_RIF_DATA|
$INPUT      ID DAT2=DROP TIME OCC WHAT=DROP
            EVID AMT DV RIF_BLQ MDV
                EVID_INH AMT_INH INHCONC INH_BLQ MDV_INH
            EVID_PZA AMT_PZA PZACONC PZA_BLQ MDV_PZA
            AMT_EMB
            VPC_TIME
            PATIENT HOSPITALIZED DIED
                AGE SEXF WT HT FFM FAT BRC

; DEFINE ETAS FOR OCCASSION
$ABBREVIATED REPLACE ETA(OCC_BIO)=ETA(,6 to 7 by 1)
$ABBREVIATED REPLACE ETA(OCC_KA)=ETA(,8 to 9 by 1)
$ABBREVIATED REPLACE ETA(OCC_MTT)=ETA(,10 to 11 by 1)

; IGNORE=@ will skip any line starting with any non-numerical
character
$DATA      alldat_final_simulated.csv IGNORE=@

$SUBROUTINE ADVAN5 TRANS1 ;TOL=8 ATOL=8 ; TOL is the precision to
solve differential equations

$MODEL      NCOMPS=13 ; NUMBER OF COMPARTMENTS (ABSORPTION COMPATMENT
(DEFINED AS FIRST ONE) AND CENTRAL COMPARTMENT DEFIEND AS 2ND
COMPARTMENT
            COMP=(TRANSIT1,DEFDOSE) ;1 GUT TRANIST 1 (F1 is associated
with first compartment)
```

```
              COMP=(TRANSIT2) ;2 GUT TRANIST 2
              COMP=(TRANSIT3) ;3 GUT TRANIST 3
              COMP=(TRANSIT4) ;4 GUT TRANIST 4
              COMP=(TRANSIT5) ;5 GUT TRANIST 5
              COMP=(TRANSIT6) ;6 GUT TRANIST 6
              COMP=(TRANSIT7) ;7 GUT TRANIST 7
              COMP=(TRANSIT8) ;8 GUT TRANIST 8
              COMP=(TRANSIT9) ;9 GUT TRANIST 9
              COMP=(TRANSIT10) ;10 GUT TRANIST 10
              COMP=(TRANSIT11) ;11 GUT TRANIST 11
              COMP=(ABS) ;12 GUT ABS
              COMP=("CENTRAL",DEFOBS) ;13 CENTRAL CMT


$PK
; Allometric scaling
TVFFM = 43.5
TVWT = 56
TVFAT = 11.3

ALLMCLWT=(WT/TVWT)**0.75
ALLMVWT=WT/TVWT

ALLMCLFFM=(FFM/TVFFM)**0.75
ALLMVFFM=FFM/TVFFM

ALLMCLFAT=(FAT/TVFAT)**0.75
```

```
ALLMVFAT=FAT/TVFAT

; LACTATE_IMP = LACTATE
; IF (LACTATE.EQ.-99) LACTATE_IMP = 1.6

; TIMETOBREAKFAST_IMP = TIMETOBREAKFAST
; IF (TIMETOBREAKFAST.EQ.-99) TIMETOBREAKFAST_IMP = -4.82

; CRP_IMP = CRP
; IF (CRP.EQ.-99) CRP_IMP = 127

; AST_IMP = AST
; IF (AST.EQ.-99) AST_IMP = 37.5

; ALT_IMP = ALT
; IF (ALT.EQ.-99) ALT_IMP = 24

; TPROT_IMP = TPROT
; IF (TPROT.EQ.-99) TPROT_IMP = 80

; ALBUMIN_IMP = ALBUMIN
; IF (ALBUMIN.EQ.-99) ALBUMIN_IMP = 30

; UREA_IMP = UREA
; IF (UREA.EQ.-99) UREA_IMP = 5

; CREAT_IMP = CREAT
```

```
; IF (CREAT.EQ.-99) CREAT_IMP = 68


; HOSP_EFF = 1
; IF (HOSPITALIZED.EQ.1) HOSP_EFF = THETA(9)


; INDBIO = 1
; IF (FDC.EQ.0) INDBIO = THETA(10)
;--------------PATIENT EFFECT ON ABSORPTION(KA & MTT)---------------
PATKAMTT = 1 ; FOR OUTPATIENTS
IF (PATIENT.EQ.1)     PATKAMTT=THETA(9) ; SURVIVED INPATIENTS
IF (PATIENT.EQ.2)     PATKAMTT=THETA(10) ; DIED INPATIENTS


;----------------------Log BRC EFFECT ON CLEARANCE------------------
BRCMED = 6
BRCCL = 1


IF (BRC.NE.-99) THEN
      BRCCL = (BRC/BRCMED)**THETA(11)
ENDIF


; ------- BSV
BSVCL   = ETA(1)
BSVV    = ETA(2)
BSVBIO     = ETA(3)
BSVKA      = ETA(4)
BSVMTT     = ETA(5)
```

```
; BOV
BOVBIO     = ETA(OCC_BIO)
BOVKA   = ETA(OCC_KA)
BOVMTT     = ETA(OCC_MTT)

;---------Typical values----------------------------------------------
TVCL  = THETA(1) * ALLMCLFFM * BRCCL
TVV   = THETA(2) * ALLMVFFM
TVBIO      = THETA(3)
TVKA  = THETA(4) *PATKAMTT
TVMTT      = THETA(5) /PATKAMTT
TVNN  = THETA(8)

;-----------Define individual parameters----------------------------
CL  = TVCL*EXP(BSVCL) ; CLEARANCE
V   = TVV*EXP(BSVV) ; CENTRAL VOL.
BIO = TVBIO*EXP(BSVBIO + BOVBIO) ; BIOAVAILABILITY
KA  = TVKA*EXP(BSVKA + BOVKA) ; ABS. RATE CONSTANT
MTT = TVMTT*EXP(BSVMTT + BOVMTT) ; LAG TIME
NN    = TVNN
;-------------------------------------------------------------
; re-parameterization
F1 = BIO
KTR = (NN+1)/MTT
K12   =     KTR  ;Rate between transit CMT
K23   =     KTR   ;Rate between transit CMT
K34   =     KTR   ;Rate between transit CMT
```

```
K45   =     KTR   ;Rate between transit CMT
K56   =     KTR   ;Rate between transit CMT
K67   =     KTR   ;Rate between transit CMT
K78   =     KTR   ;Rate between transit CMT
K89   =     KTR   ;Rate between transit CMT
K9T10 =     KTR   ;Rate between transit CMT
K10T11 = KTR   ;Rate between transit CMT
K11T12 = KTR ;Rate between transit CMT
K12T13 = KA
K13T0 =   CL/V
S13   =     V
;-------------------------------------------------------------------
$ERROR
IPRED = A(13)/V

IRES = DV-IPRED

; LLOQ
LLOQ = 0.117

PROP = IPRED*THETA(6)
ADD = 0.2*LLOQ + THETA(7)

; For ADD, in this case we are coding THETA(.) as the additive error
on top of 20% of the LLOQ.
; So the lower bound of THETA(.) can be zero. If it goes to zero, we
can fix it, and the additive error
```

```
; will then be constrained to 20% of LLOQ + the value in THETA(.).
; REMEMBER about this when you report the value of ADD and its uncertainty! NONMEM gives uncertainty on THETA, not ADD
; An alternative approach is to set the lower bound of the THETA for the additive error to 20% of the LLOQ.
; In that case, one does not have to worry about adjusting the precision. On the other hand, this cannot be done if you have different LLOQs within your analysis (e.g. different labs)

; For BLQ==1 (i.e. first BLQ value in a series), we add extra additive error on the concentrations, since the value in DV has been imputed
IF(ICALL.NE.4.AND.RIF_BLQ==1) ADD = ADD + (LLOQ/2)

; For BLQ==2 (i.e. the trailing BLQ values in a series), we don't want these to influence the fit,
; we only want them for simulation-based diagnostics such as the VPC.
; So we define a separate error structure for these points. It has no proportional component
; (PROP = 0, as we would not want these points to affect our estimate of proportional error)
; and a FIXED and HUGE additive component (ADD = 1000000000, large with respect to the readings of concentration),
; so that the values do not affect the fit.
; It's also a good idea to repeat the diagnostic plots without the BLQ=2 points
IF(ICALL.NE.4.AND.RIF_BLQ==2) THEN
     PROP = 0
```

```
      ADD = 100000000
ENDIF

W = SQRT(ADD**2+PROP**2)

IF (W.LE.0.000001) W=0.000001 ; to protect IWRES from overflow

IWRES = IRES/W

Y = IPRED + W*ERR(1)

; To prevent simulation (ICALL==4) of negative values. It set a
positive lower bound for Y, so that VPCs in the log-scale can be
plotted
IF (ICALL==4.AND.Y<=LLOQ) THEN
      Y=LLOQ/2
      RIF_BLQ = 1
ENDIF

; To calculate time after dose.
IF(AMT.GT.0) THEN
      TIMEDOSE = TIME
      AMOUNTDOSE = AMT
ENDIF

TAD = TIME-TIMEDOSE
```

```
VARCL = BSVCL ;+ BOVCL

VARBIO = BSVBIO + BOVBIO

VARAUC = BSVBIO + BOVBIO - BSVCL ;- BOVCL

VARABS = BSVKA + BOVKA - BSVMTT - BOVMTT

VARKA = BSVKA + BOVKA

VARMTT = BSVMTT + BOVMTT


;-----------------------RETRIEVE AMOUNT IN EACH COMPARTMENT

AA1 = A(12)

AA2 = A(13)


$THETA  (0,8.8248,20) ; 1 CL [L/h]

$THETA  (0,56.7748,100) ; 2 V [L]

$THETA  1 FIX ; 3 BIO

$THETA  (0,1.3798,5) ; 4 KA [1/h]

$THETA  (0,0.34167,2) ; 5 MTT [h]

$THETA  (0,0.172284,0.5) ; 6 PROP [%]

$THETA  0 FIX ; 7 ADD [mg/L]

$THETA  11 FIX ; 8 NN

$THETA  (-3,0.668258,3) ; 9 SURVIV_ABSORP

$THETA  (-3,0.380226,3) ; 10 DIED_ABSORP

$THETA  (-10,-0.3525,10) ; 11 BRCCL_POWER


$OMEGA  0.179394  ;   1 BSV CL

$OMEGA  0  FIX  ;    2 BSV V

$OMEGA  0  FIX  ;  3 BSV BIO

$OMEGA  0  FIX  ;   4 BSV KA
```

```
$OMEGA  0  FIX  ;  5 BSV MTT

$OMEGA  BLOCK(1)
 0.0453815  ; 6,7 BOVBIO
$OMEGA  BLOCK(1) SAME

$OMEGA  BLOCK(1)
 1.41447  ;  8,9 BOVKA
$OMEGA  BLOCK(1) SAME

$OMEGA  BLOCK(1)
 0.879587  ; 10,11 BOVMTT
$OMEGA  BLOCK(1) SAME

$SIGMA  1  FIX

$ESTIMATION MSFO=RIF.msf MAXEVAL=9999 PRINT=1 METHOD=1
            INTERACTION NOABORT NSIG=3 NONINFETA=1 ETASTYPE=1 SIGL=9

$COVARIANCE PRINT=E UNCONDITIONAL MATRIX=R PRECOND=1
```

Isoniazid

```
;; 1. Based on:
; Model desc: Isoniazid.Model.KDHTB
; Settings for the memory of NONMEM
$SIZES      PD=-1000 LVR=-150 LTH=-200 MAXFCN=10000000 LNP4=-150000
```

```
$PROBLEM    |ADVAN13_TRANS1_PZA_DATA|

$INPUT      ID DAT2=DROP TIME OCC WHAT=DROP
            EVID_RIF AMT_RIF RIFCONC RIF_BLQ MDV_RIF
            EVID AMT DV INH_BLQ MDV
            EVID_PZA AMT_PZA PZACONC PZA_BLQ MDV_PZA
            AMT_EMB VPC_TIME
            PATIENT HOSPITALIZED DIED AGE SEXF WT HT FFM FAT BRC

; DEFINE ETAS FOR OCCASSION
$ABBREVIATED REPLACE ETA(OCC_BIO)=ETA(,7 to 8 by 1)
$ABBREVIATED REPLACE ETA(OCC_KA)=ETA(,9 to 10 by 1)
$ABBREVIATED REPLACE ETA(OCC_MTT)=ETA(,12 to 13 by 1)

; IGNORE=@ will skip any line starting with any non-numerical
character
$DATA      alldat_final_simulated.csv IGNORE=@

$SUBROUTINE ADVAN5 TRANS1 ;TOL=9 ATOL=9 ; TOL is the precision to
solve differential equations

;Sim_start
$PRIOR      NWPRI NPEXP=1 PLEV=0.9999
;Sim_end
```

```
$MODEL      NCOMPS=10 ; NUMBER OF COMPARTMENTS (ABSORPTION COMPATMENT
(DEFINED AS FIRST ONE) AND CENTRAL COMPARTMENT DEFIEND AS 2ND
COMPARTMENT
            COMP=(TRANSIT1,DEFDOSE) ;1 GUT TRANIST 1 (F1 is associated
with first compartment)
            COMP=(TRANSIT2) ;2 GUT TRANIST 2
            COMP=(TRANSIT3) ;3 GUT TRANIST 3
            COMP=(TRANSIT4) ;4 GUT TRANIST 4
            COMP=(TRANSIT5) ;5 GUT TRANIST 5
            COMP=(TRANSIT6) ;6 GUT TRANIST 6
            COMP=(TRANSIT7) ;7 GUT TRANIST 7
            COMP=(ABS) ;8 GUT ABS
            COMP=("CENTRAL",DEFOBS) ;9 CENTRAL CMT
            COMP=(PERI) ; 10 PERIPHERAL CMT

;Sim_start
$MIX
NSPOP=2
P(1) = THETA(3)
P(2) = 1 - THETA(3)
;Sim_end

$PK
;-------------------------Allometric scaling-----------------------
TVFFM = 43.5
TVWT = 56
TVFAT = 11.3
```

```
ALLMCLWT=(WT/TVWT)**0.75
ALLMVWT=WT/TVWT

ALLMCLFFM=(FFM/TVFFM)**0.75
ALLMVFFM=FFM/TVFFM

ALLMCLFAT=(FAT/TVFAT)**0.75
ALLMVFAT=FAT/TVFAT

;------------------For Mixture Modelling----------------------------
;Sim_start
EST = MIXEST
;EST = POP
;DUMMY_THETA = THETA(3)
IF(MIXNUM.EQ.1) THEN
      TVCL = THETA(4) *ALLMCLFFM
ELSE
      TVCL = THETA(5) *ALLMCLFFM
ENDIF
;IF(POP.EQ.1) THEN
       ;   TVCL=THETA(4)
       ;ELSE
       ;   TVCL=THETA(5)
       ;ENDIF
;Sim_end
```

```
;--------------------Imputing missing values to median--------------
; LACTATE_IMP = LACTATE
; IF (LACTATE.EQ.-99) LACTATE_IMP = 1.6

; TIMETOBREAKFAST_IMP = TIMETOBREAKFAST
; IF (TIMETOBREAKFAST.EQ.-999) TIMETOBREAKFAST_IMP = -4.82

; CRP_IMP = CRP
; IF (CRP.EQ.-99) CRP_IMP = 127

; AST_IMP = AST
; IF (AST.EQ.-99) AST_IMP = 37.5

; ALT_IMP = ALT
; IF (ALT.EQ.-99) ALT_IMP = 24

; TOTALPROTEIN_IMP = TOTALPROTEIN
; IF (TOTALPROTEIN.EQ.-999) TOTALPROTEIN_IMP = 80

; ALBUMIN_IMP = ALBUMIN
; IF (ALBUMIN.EQ.-99) ALBUMIN_IMP = 30

; UREA_IMP = UREA
; IF (UREA.EQ.-99) UREA_IMP = 5

; CREATININE_IMP = CREATININE
; IF (CREATININE.EQ.-99) CREATININE_IMP = 68
```

```
; CD4_IMP = CD4
; IF (CD4.EQ.-99) CD4_IMP = 71.5

;----------------Hospitalized Effect on Variability in CL-----------
; Allometry for liver-------------------------------------------
ALLMCL_WT_HEP = (WT/TVWT)**0.75
ALLMV_WT_HEP = (WT/TVWT)

ALLMCL_FFM_HEP = (WT/TVFFM)**0.75
ALLMV_FFM_HEP = (WT/TVFFM)
;--------------------Typical values (thetas & etas)-----------------
TVVRATIO = EXP(THETA(1))
TVQ = EXP(THETA(2))*ALLMCLFFM
;population parameters
;TVCL         = THETA(1)
TVV          = THETA(6) *ALLMVFFM
TVBIO        = THETA(7)
TVKA         = THETA(8)
TVMTT        = THETA(9)
TVNN         = THETA(10)
TVV3 = (TVV/TVVRATIO)*ALLMVFFM

;BSV
BSVCL        = ETA(1)
BSVV         = ETA(2)
BSVBIO           = ETA(3)
```

```
BSVKA            = ETA(4)
BSVQ       =ETA(5)
BSVV3            =ETA(6)

;BOV
BOVBIO     = ETA(OCC_BIO) ;7-8
BOVKA       = ETA(OCC_KA) ;9-10
BSVMTT     = ETA(11)
BOVMTT  = ETA(OCC_MTT) ;12-13

;-----------Individual parameters-------------------------------
VRATIO = TVVRATIO ;
CL    = TVCL*EXP(BSVCL)                    ; Clearance
V2     = TVV*EXP(BSVV)                      ; CENTRAL VOL.
BIO   = TVBIO*EXP(BSVBIO + BOVBIO)         ; BIOAVAILABILITY
KA    = TVKA*EXP(BSVKA + BOVKA) ; ABS. RATE
Q     = TVQ*EXP(BSVQ)
V3    = TVV3*EXP(BSVV3)
;LAG   = TVLAG*EXP(BSVLAG + BOVLAG) ; LAG TIME
MTT   = TVMTT*EXP(BSVMTT + BOVMTT) ; MEAN TRANSIT TIME
NN    = TVNN

VARCL       = BSVCL ;+ BOVCL
VARBIO      = BSVBIO + BOVBIO
VARAUC      = BSVBIO + BOVBIO - BSVCL ;- BOVCL
VARABS      = BSVKA + BOVKA - BSVMTT - BOVMTT
VARKA       = BSVKA + BOVKA
```

```
VARMTT      = BSVMTT + BOVMTT

;--------------------------HEPATIC CL-----------------------------;
TVQH=THETA(11)*ALLMCL_WT_HEP   ; PLASMA FLOW RATE
TVFU=THETA(12)            ; UNBOUND PLASMA FRACTION OF INH

QH=TVQH
FU=TVFU
CLINT=CL

;--------  Transfer constants for liver model ---------

; define hepatic extraction
EH   = (CLINT*FU)/((CLINT*FU)+QH) ; fraction undergoing first pass
extraction
FH   = 1 - EH ; fraction available after 1st pass to go to systemic
circulation



;-----------------------------------Re-parameterization------------
F1 = BIO
KTR = (NN+1)/MTT
K12   =     KTR  ;Rate between transit CMT
K23   =     KTR   ;Rate between transit CMT
K34   =     KTR   ;Rate between transit CMT
K45   =     KTR   ;Rate between transit CMT
K56   =     KTR   ;Rate between transit CMT
```

```
K67   =     KTR   ;Rate between transit CMT
K78   =     KTR   ;Rate between transit CMT
K89   =     KA   ;Rate between transit CMT

K90 = CL/V2 ;(rate constant of elimination)
K9T10 = Q/V2
K10T9 = Q/V3

;------------Error model-----------------------------------------------
$ERROR
IPRED = A(9)/V2
IRES = DV-IPRED

LLOQ = 0.105

PROP = IPRED*THETA(13)
ADD = 0.2*LLOQ + THETA(14)

; For ADD, in this case we are coding THETA(.) as the additive error
on top of 20% of the LLOQ.
; So the lower bound of THETA(.) can be zero. If it goes to zero, we
can fix it, and the additive error
; will then be constrained to 20% of LLOQ + the value in THETA(.).
; REMEMBER about this when you report the value of ADD and its
uncertainty! NONMEM gives uncertainty on THETA, not ADD
; An alternative approach is to set the lower bound of the THETA for
the additive error to 20% of the LLOQ.
```

```
; In that case, one does not have to worry about adjusting the
precision. On the other hand, this cannot be done if you have different
LLOQs within your analysis (e.g. different labs)

; For BLQ==1 (i.e. first BLQ value in a series), we add extra additive
error on the concentrations, since the value in DV has been imputed
IF(ICALL.NE.4.AND.INH_BLQ==1) ADD = ADD + (LLOQ/2)

; For BLQ==2 (i.e. the trailing BLQ values in a series), we don't want
these to influence the fit,
; we only want them for simulation-based diagnostics such as the VPC.
; So we define a separate error structure for these points. It has no
proportional component
; (PROP = 0, as we would not want these points to affect our estimate
of proportional error)
; and a FIXED and HUGE additive component (ADD = 1000000000, large
with respect to the readings of concentration),
; so that the values do not affect the fit.
; It's also a good idea to repeat the diagnostic plots without the
BLQ=2 points
IF(ICALL.NE.4.AND.INH_BLQ==2) THEN
      PROP = 0
      ADD = 100000000
ENDIF

W = SQRT(ADD**2+PROP**2)
```

```
IF (W.LE.0.000001) W=0.000001 ; to protect IWRES from overflow

IWRES = IRES/W

Y = IPRED + W*ERR(1)

; To prevent simulation (ICALL==4) of negative values. It set a
positive lower bound for Y, so that VPCs in the log-scale can be
plotted
IF (ICALL==4.AND.Y<=LLOQ) THEN
      Y=LLOQ/2
      INH_BLQ = 1
ENDIF

; To calculate time after dose.
IF(AMT.GT.0) THEN
      TIMEDOSE = TIME
      AMOUNTDOSE = AMT
ENDIF

TAD = TIME-TIMEDOSE

;--------------RETRIEVE AMOUNT IN EACH COMPARTMENT------------------
AA1 = A(8)
AA2 = A(9)
AA3 = A(10)
```

```
$THETA  (-10,0.653065,10) ; 1 VRATIO [LOG]
$THETA  (-10,0.35836,10) ; 2 Q [LOG]
;Sim_start
$THETA  (0,0.645125,1) ; 3 PROB_FAST
;$THETA  0 FIX ; 3 PROB_FAST
;Sim_end
$THETA  (0,25.5488,100) ; 4 CL_FAST [L/h]
$THETA  (0,9.76422,40) ; 5 CL_SLOW [L/h]
$THETA  (0,59.0219) ; 6 V [L]
$THETA  1 FIX ; 7 BIO
$THETA  (0,2.42706) ; 8 KA [1/h]
;$THETA  (0,2.20652,50) ; 7 Q
;$THETA  (0,82.0861) ; 8 V3
$THETA  (0,0.441855,3) ; 9 MTT [h]
$THETA  7 FIX ; 10 NN
$THETA  0 FIX ; 11 QH
$THETA  0 FIX ; 12 FU
$THETA  (0,0.138966) ; 13 PROP [%]
$THETA  0 FIX ; 14 ADD [mg/L]
;$THETA  (-5,0.728585,5) ; 15 BXPAR
; PRIORS FOR VRATIO ----------------------------------------------
--;Sim_start
$THETAP  0.703 FIX ; logVRATIO
;Sim_end

$OMEGA  0.0642373  ;   1 BSV CL
$OMEGA  0  FIX  ;    2 BSV V
```

```
$OMEGA  0  FIX  ;  3 BSV BIO
$OMEGA  0  FIX  ;   4 BSV KA
$OMEGA  0  FIX  ;     5 BSVQ
$OMEGA  0  FIX  ;    6 BSVV3

$OMEGA  BLOCK(1)
 0.122052  ; 7,8 BOVBIO
$OMEGA  BLOCK(1) SAME
;----------------------------------------------------------------------
$OMEGA  BLOCK(1)
 1.48417  ; 9,10 BOVKA
$OMEGA  BLOCK(1) SAME

$OMEGA  0  FIX  ;  11 BSVMTT
$OMEGA  BLOCK(1)
 0.994496  ; 12,13 BOVMTT
$OMEGA  BLOCK(1) SAME

; PRIORS DATA FOR THETAS VRATIO
;Sim_start
$THETAPV  BLOCK(1) FIX
 0.1  ;     VRATIO
;Sim_end

$SIGMA  1  FIX

;Sim_start
```

```
$ESTIMATION MSFO=INH.msf MAXEVAL=9999 PRINT=1 METHOD=1
            INTERACTION NOABORT NSIG=3 NONINFETA=1 ETASTYPE=1 SIGL=9

$COVARIANCE PRINT=E UNCONDITIONAL MATRIX=R PRECOND=1

;Sim_end
```

Pyrazinamide

```
;; 1. Based on:
; Model desc: Pyrazinamide.Model.KDHTB
; Settings for the memory of NONMEM
$SIZES      PD=-1000 LVR=-150 LTH=-200 MAXFCN=10000000 LNP4=-150000
$PROBLEM    |ADVAN13_TRANS1_PZA_DATA|
$INPUT      ID DAT2=DROP TIME OCC WHAT=DROP
            EVID_RIF AMT_RIF RIFCONC RIF_BLQ MDV_RIF
                EVID_INH AMT_INH INHCONC INH_BLQ MDV_INH
            EVID AMT DV PZA_BLQ MDV
            AMT_EMB
            VPC_TIME
            PATIENT HOSPITALIZED DIED
                AGE SEXF WT HT FFM FAT BRC

; DEFINE ETAS FOR OCCASSION
$ABBREVIATED REPLACE ETA(OCC_BIO)=ETA(,6 to 7 by 1)
$ABBREVIATED REPLACE ETA(OCC_KA)=ETA(,8 to 9 by 1)
$ABBREVIATED REPLACE ETA(OCC_MTT)=ETA(,10 to 11 by 1)
```

```
; IGNORE=@ will skip any line starting with any non-numerical
character
$DATA      alldat_final_simulated.csv IGNORE=@
$SUBROUTINE ADVAN5 TRANS1 ;TOL=9 ATOL=9 ; TOL is the precision to
solve differential equations

$MODEL      NCOMPS=5 ; NUMBER OF COMPARTMENTS (ABSORPTION COMPATMENT
(DEFINED AS FIRST ONE) AND CENTRAL COMPARTMENT DEFIEND AS 2ND
COMPARTMENT
            COMP=(TRANSIT1,DEFDOSE) ;1 GUT TRANIST 1 (F1 is associated
with first compartment)
            COMP=(TRANSIT2) ;2 GUT TRANIST 2
            COMP=(TRANSIT3) ;3 GUT TRANIST 3
            COMP=(ABS) ;4 GUT ABS
            COMP=("CENTRAL",DEFOBS) ;5 CENTRAL CMT

$PK
;----------------------------Allometric scaling----------;
TVFFM = 43.5
TVWT = 56
TVFAT = 11.3

ALLMCLWT=(WT/TVWT)**0.75
ALLMVWT=WT/TVWT

ALLMCLFFM=(FFM/TVFFM)**0.75
ALLMVFFM=FFM/TVFFM
```

```
ALLMCLFAT=(FAT/TVFAT)**0.75
ALLMVFAT=FAT/TVFAT

;----------------------Imputing missing values to median--------;
LACTATE_IMP = LACTATE
; IF (LACTATE.EQ.-999) LACTATE_IMP = 1.6

; TIMETOBREAKFAST_IMP = TIMETOBREAKFAST
; IF (TIMETOBREAKFAST.EQ.-999) TIMETOBREAKFAST_IMP = -4.82

; CRP_IMP = CRP
; IF (CRP.EQ.-999) CRP_IMP = 127

; AST_IMP = AST
; IF (AST.EQ.-999) AST_IMP = 37.5

; ALT_IMP = ALT
; IF (ALT.EQ.-999) ALT_IMP = 24

; TOTALPROTEIN_IMP = TOTALPROTEIN
; IF (TOTALPROTEIN.EQ.-999) TOTALPROTEIN_IMP = 80

; ALBUMIN_IMP = ALBUMIN
; IF (ALBUMIN.EQ.-999) ALBUMIN_IMP = 30

; UREA_IMP = UREA
```

```
; IF (UREA.EQ.-999) UREA_IMP = 5

; CREATININE_IMP = CREATININE
; IF (CREATININE.EQ.-999) CREATININE_IMP = 68

;-----------Hospitalized Effect on Variability in CL----------------
PATETACL = 1
IF(PATIENT.EQ.1) PATETACL = THETA(9)
IF(PATIENT.EQ.2) PATETACL = THETA(10)

;--------------------Typical values (thetas & etas)-----------------
;population parameters
TVCL        = THETA(1) * ALLMCLFFM
TVV         = THETA(2) * ALLMVFFM
TVBIO       = THETA(3)
TVKA        = THETA(4)
TVMTT       = THETA(5)
TVNN        = THETA(8)

;BSV
BSVCL       = ETA(1) * PATETACL
BSVV        = ETA(2)
BSVBIO     = ETA(3)
BSVKA      = ETA(4)
BSVMTT     = ETA(5)

;BOV
```

```
BOVBIO     = ETA(OCC_BIO)
BOVKA       = ETA(OCC_KA)
BOVMTT     = ETA(OCC_MTT)

;-----------Individual parameters-----------------------------------
CL    = TVCL*EXP(BSVCL)                    ; Clearance
V     = TVV*EXP(BSVV)                      ; CENTRAL VOL.
BIO   = TVBIO*EXP(BSVBIO + BOVBIO)         ; BIOAVAILABILITY
KA    = TVKA*EXP(BSVKA + BOVKA) ; ABS. RATE CONSTANT
MTT   = TVMTT*EXP(BSVMTT + BOVMTT) ; MEAN TRANSIT TIME
NN    = TVNN

VARCL       = BSVCL ;+ BOVCL
VARBIO      = BSVBIO + BOVBIO
VARAUC      = BSVBIO + BOVBIO - BSVCL ;- BOVCL
VARABS = BSVKA + BOVKA - BSVMTT - BOVMTT
VARKA = BSVKA + BOVKA
VARMTT = BSVMTT + BOVMTT

;--------------------Re-parameterization------------
F1 = BIO
KTR = (NN+1)/MTT
K12   =     KTR  ;Rate between transit CMT
K23   =     KTR   ;Rate between transit CMT
K34   =     KTR   ;Rate between transit CMT

K45 = KA
```

```
K50   = CL/V

;--------------------------------Error model------------------
$ERROR
IPRED = A(5)/V
IRES = DV-IPRED

LLOQ = 0.203

PROP = IPRED*THETA(6)
ADD = 0.2*LLOQ + THETA(7)

; For ADD, in this case we are coding THETA(.) as the additive error on top of 20% of the LLOQ.
; So the lower bound of THETA(.) can be zero. If it goes to zero, we can fix it, and the additive error
; will then be constrained to 20% of LLOQ + the value in THETA(.).
; REMEMBER about this when you report the value of ADD and its uncertainty! NONMEM gives uncertainty on THETA, not ADD
; An alternative approach is to set the lower bound of the THETA for the additive error to 20% of the LLOQ.
; In that case, one does not have to worry about adjusting the precision. On the other hand, this cannot be done if you have different LLOQs within your analysis (e.g. different labs)

; For BLQ==1 (i.e. first BLQ value in a series), we add extra additive error on the concentrations, since the value in DV has been imputed
```

```
IF(ICALL.NE.4.AND.PZA_BLQ==1) ADD = ADD + (LLOQ/2)

; For BLQ==2 (i.e. the trailing BLQ values in a series), we don't want
these to influence the fit,
; we only want them for simulation-based diagnostics such as the VPC.
; So we define a separate error structure for these points. It has no
proportional component
; (PROP = 0, as we would not want these points to affect our estimate
of proportional error)
; and a FIXED and HUGE additive component (ADD = 1000000000, large
with respect to the readings of concentration),
; so that the values do not affect the fit.
; It's also a good idea to repeat the diagnostic plots without the
BLQ=2 points
IF(ICALL.NE.4.AND.PZA_BLQ==2) THEN
      PROP = 0
      ADD = 100000000
ENDIF

W = SQRT(ADD**2+PROP**2)

IF (W.LE.0.000001) W=0.000001 ; to protect IWRES from overflow

IWRES = IRES/W

Y = IPRED + W*ERR(1)
```

```
; To prevent simulation (ICALL==4) of negative values. It set a
positive lower bound for Y, so that VPCs in the log-scale can be
plotted
IF (ICALL==4.AND.Y<=LLOQ) THEN
      Y=LLOQ/2
      PZA_BLQ = 1
ENDIF
; To calculate time after dose.
IF(AMT.GT.0) THEN
      TIMEDOSE = TIME
      AMOUNTDOSE = AMT
ENDIF
TAD = TIME-TIMEDOSE

;------------------RETRIEVE AMOUNT IN EACH COMPARTMENT------------
AA1 = A(4)
AA2 = A(5)

$THETA  (0,2.61378,20) ; 1 CL [L/h]
$THETA  (0,35.9666,200) ; 2 V [L]
$THETA  1 FIX ; 3 BIO
$THETA  (0,1.91548,10) ; 4 KA [1/h]
$THETA  (0,0.378744,3) ; 5 MTT [h]
$THETA  (0,0.113882,0.7) ; 6 PROP [%]
$THETA  (0,2.4809,10) ; 7 ADD [mg/L]
$THETA  3 FIX ; 8 NN
$THETA  (0,1.69826) ; 9 SURVIV_PATETACL
```

```
$THETA  (0,3.56122) ; 10 DIED_PATETACL

$OMEGA  0.0395359  ;   1 BSV CL
$OMEGA  0  FIX  ;    2 BSV V
$OMEGA  0  FIX  ;  3 BSV BIO
$OMEGA  0  FIX  ;   4 BSV KA
$OMEGA  0  FIX  ;  5 BSV MTT

$OMEGA  BLOCK(1)
 0.011176  ; 6,7 BOVBIO
$OMEGA  BLOCK(1) SAME

$OMEGA  BLOCK(1)
 0.568935  ;  8,9 BOVKA
$OMEGA  BLOCK(1) SAME

$OMEGA  BLOCK(1)
 1.0298  ; 10,11 BOVMTT
$OMEGA  BLOCK(1) SAME

$SIGMA  1  FIX

$ESTIMATION MSFO=PZA.msf MAXEVAL=9999 PRINT=1 METHOD=1
            INTERACTION NOABORT NSIG=3 NONINFETA=1 ETASTYPE=1 SIGL=9

$COVARIANCE PRINT=E UNCONDITIONAL MATRIX=R PRECOND=1
```

Final NONMEM code for results presented in Chapter 5

```
;; 1. Based on: 051
; Model Desc: final.both.plasma.param
$SIZES      PD=-1000 LVR=-150 LTH=-200 MAXFCN=10000000 LNP4=-150000
            DIMTMP=1000 ; Settings for the memory of NONMEM
$PROBLEM    Include metabolite data include RHO
; If possible, include post-gestational age (PGA) in the dataset. If
not, can calculate it as below.
$INPUT      ID VISITID PVID=DROP DAT2=DROP TIME WHAT=DROP CMTX=DROP
            VPC_TIME OCC EVID MDV DV UMOL BLQ DOSEWITHSAMPLE ADDEDDOSE
            PREDAILY DAYTTT FORM FORM_WHAT=DROP ROUTE ROUTE_WHAT=DROP
            NUMTAB MGINTAB AMT AMT_UMOL MGPERKG AGE SEXF WT HT
            GESAGE_WK FLAG DVID L2 ALB_VCSF ALB_PLASMA ALB_LCSF ALB_LP
            ALB_VP TP_VCSF TP_LCSF
$DATA      alldatnm_27.11.21-updated.csv IGNORE=@ IGNORE(FLAG.EQ.2)

;IGNORE(DVID.GT.2)

;$ABBREVIATED  PROTECT  ;TO  PROTECT  YOUR  CODE  AGAINST  UNDEFINED
OPERATIONS (ALWAYS CHECK YOUR FUNCTIONS)
$ABBREVIATED DECLARE INTEGER NDOSE INTEGER MAX_ACCUM_DOSES

$ABBREVIATED REPLACE ETA(OCC_MTT)=ETA(,3 to 8 by 1)
$ABBREVIATED REPLACE ETA(OCC_KA)=ETA(,9 to 14 by 1)
$ABBREVIATED REPLACE ETA(OCC_LAG)=ETA(,15 to 20 by 1)
$ABBREVIATED REPLACE ETA(OCC_BIO)=ETA(,21 to 26 by 1) ;6 occasions
```

```
$SUBROUTINE ADVAN13 TRANS1 TOL=9 ATOL=9
; ;Sim_start

; $PRIOR      NWPRI NPEXP=1 PLEV=0.9999
; ;Sim_end
$MODEL      NCOMP=6 COMP=(LIV) COMP=(CENTRAL) COMP=(METABOLITE)
            COMP=(LCSF) COMP=(VCSF) COMP=(ECF)
$PK
;Allometric Scaling
TVWT   = 11  ; Median weight in kg
ALLMCL = (WT/TVWT)**0.75
ALLMV  = WT/TVWT

;Maturation of CL
;This uses PGA (post gestational age). If you don't have it, use
AGEM  = AGE*12 ; to convert age to months (if in years)
PMA   = AGEM + 9 ; to add 9 months
PMA50 = (THETA(5)) ; this is the log of age50, so the estiamate is in
the log scale
GAMMA = EXP(THETA(6))
MATCL = 0

IF (PMA>0) MATCL=1/(1+(EXP(-GAMMA*(LOG(PMA)-PMA50))))

;Age Effect on BIO
;BIO increases linearly with Age until AGE_BIO_BR years, plateaus
BIO_BIRTH = EXP(THETA(8))
```

```
AGE_BIO_BR = EXP(THETA(9))

AGE_BIO_SL = (1-BIO_BIRTH) / AGE_BIO_BR
;
AGE_BIO = 1
IF (AGE<AGE_BIO_BR) AGE_BIO = BIO_BIRTH + AGE_BIO_SL * AGE

;Typical Parameters (Parent)
TVV     = EXP(THETA(1)) * ALLMV
CLSS    = EXP(THETA(2))
;CLBS  = EXP(THETA(12))
CLBS    = CLSS/EXP(THETA(3)) ;RATIO SHOULD BE AROUND 2
IND50   = EXP(THETA(4))
TVCL    = (CLBS+(CLSS-CLBS)*(1-EXP(-LOG(2)*DAYTTT/IND50))) * ALLMCL *
MATCL

;Typical Parameters (Saturation)
QH = THETA(22)* (WT/70)**0.75
FU = THETA(23)
VH = THETA(24)* (WT/70)

LOGKM = THETA(7) ; LOG KM - claculated from data set - median of max
conc in the liver
;place holder thetas
DUMMY_10   = THETA(10)
DUMMY_11   = THETA(11)
DUMMY_12   = THETA(12)
```

```
DUMMY_13   = THETA(13)
DUMMY_14   = THETA(14)
DUMMY_15   = THETA(15)
DUMMY_16   = THETA(16)

;TVCL    = EXP(THETA(1)) * ALLMCL * MATCL

TVMTT   = THETA(17)
TVNN    = THETA(18)
TVBIO   = THETA(19)*AGE_BIO

;Typical Parameters (Metabolite)
TVCLM   = THETA(25) * ALLMCL * MATCL
TVVM    = THETA(26) * ALLMV
TVFM    = THETA(27)

;Typical Parameters (Effect)
;PD Parameters
TVKE0_L = THETA(31)
TVKE0_V = THETA(32)
TVKE0_E = THETA(33)
;Accumulation ratios (pseudo-partition coefficients)
TVRL  = THETA(34)
TVRV  = THETA(35)
TVRE  = THETA(36)
```

```
;Between-Subject/Occasion Variability
;Parent
BSVCL   = ETA(1)
BSVBIO     = ETA(2)
BOVMTT  = ETA(OCC_MTT) ;3-8
BOVKA   = ETA(OCC_KA)  ;9-14
BOVLAG  = ETA(OCC_LAG) ;15-20
BOVBIO     = ETA(OCC_BIO) ;21-26

;;Metabolite
fac = THETA(43)
BSVCLM  = ETA(1)* fac
DUMMY  = ETA(27)
;BSVCLM  = ETA(1)* fac
;BSVFM   = ETA(27)
;;Effect
BSVRLV   = ETA(28)
BSVRV   = ETA(29)
BSVRE   = ETA(30)

;Individual Parameters (Parent)----------------------------------
CL    = TVCL * EXP(BSVCL)            ;total clearance
V     = TVV              ;volume of distribution
;KA    = TVKA * EXP(BOVKA)    ;absorption rate constant
;LAG   = TVLAG * EXP(BOVLAG) ;lag time
MTT   = TVMTT * EXP(BOVMTT) ;mean transit time
NN    = TVNN                   ;number of transit compartments
```

```
BIO   = TVBIO * EXP(BSVBIO + BOVBIO) ;bioavailability

;Individual Parameters (Metabolite)----------------------------------
CLM  = TVCLM * EXP(BSVCLM)   ;metabolite clearance
VM   = TVVM    ;metabolite compartment volume
FM   = TVFM                  ;fraction metabolized

;FM_LOGIT = LOG(TVFM / (1-TVFM))
;FM = EXP(FM_LOGIT + BSVFM) / (1 + EXP(FM_LOGIT + BSVFM))

;K12 = FM * (CL/V) ;transfer from central to metabolite compartment
CLINT = CL
VMAX  = CLINT*EXP(LOGKM) ; max enzimatic rate from eq. CLint = Vmax/KM
;VMAX  = CLINT*KM ; max enzimatic rate from eq. CLint = Vmax/KM


;K10 = (CL/V) ;(1-FM)* (CL/V)
;K20 = CLM/VM ;elimination from metabolite compartment


;Individual Parameters (Effect)---------------------------------
;PD Parameters
KE0_L = TVKE0_L
KE0_V = TVKE0_V
KE0_E = TVKE0_E

;Accumulation factors
```

```
RL  = TVRL * EXP(BSVRLV)
RV  = TVRV * EXP(BSVRLV)
RE  = TVRE * EXP(BSVRE)

K24  =  (CL/V)*1E-12  ;negligible  mass  transfer  from  central  to
effect(lumbar) compartment
K25  =  (CL/V)*1E-12  ;negligible  mass  transfer  from  central  to
effect(ventricular) compartment
K26  =  (CL/V)*1E-12  ;negligible  mass  transfer  from  central  to
effect(ECF) compartment

;Initialization of Compartments---------------------------------
A_0(1) = 1E-12   ; Liver
A_0(2) = 1E-12   ; Central
A_0(3) = 1E-12   ; Metabolite
A_0(4) = 1E-12   ;lumbar
A_0(5) = 1E-12   ;ventricular
A_0(6) = 1E-12   ;ECF

;Reparameterization (Transit)----------------------------
;-----Transit Compartments with Dose Accumulation-----------
; IMPORTANT!!! This code will NOT work if ALAG1 (or ALAGx) is defined
in the code above.
; DO NOT USE ALAGx, use the parameter TLAG or re-assign it below
; If you want to use a delay before the transit starts the absorption,
re-assign the variable here.
; NOTE that you MUST uncomment also CALLFL=-2
```

```
;TLAG    = TVTLAG + BVVTLAGTR ;Additive model
; TLAG = Reassign here a variable added above! Do NOT use ALAGx!!!
TLAG = 0
; CALLFL = -2

; Setting CALLFL = -2 makes sure the PK subroutine gets called with
every event record,
; with ADDL and lagged doses, and at modeled event times that are not
explicitily a line in the dataset.
; It is here so that the TLAG and ADDL work
; It does not apply to the ERROR or ADVAN9 or ADVAN15 routines.

; Set SS = 0 if SS is not used in the dataset
SS = 0

; IMPORTANT!!! This sets the maximum number of doses that will be
remembered by NONMEM the super-imposition
; With MAX_ACCUM_DOSES=2, the code "accumulates" the latest 2 dose.
; If you want to increase this, you must also uncomment below the code
for the doses beyond the 2nd
MAX_ACCUM_DOSES = 2

; This is the time after which the transit should be turned off
(absorption completed)
; It is meant to save computational time when accumulating if you are
SURE that there is no absprtion
; at times after dose longer than FORGET.
```

```
; A reasonable value would be several times MTT, i.e. FORGET >
10*MAX(MTT)
FORGET = 1000

F1 = 0 ; I need to set bioavailability in compartment 1 to 0 for this
implementation of the transit compartment absorption

KTR = (NN+1)/MTT ; **The number of actual transit compartments is
NN+1, so this number can never be 0**

IF (NEWIND/=2.OR.EVID>=3) THEN ; For each new individual or RESET or
RESET+DOSE event

     NDOSE = 0 ; Reset the dose number

     DOSETIMESS = 0
     PIZZASS = 0
     KTRVECSS = -1
     NNVECSS = -1
     SWITCHSS = 0

     DOSETIME0 = 0
     PIZZA0 = 0
     KTRVEC0 = -1
     NNVEC0 = -1

     DOSETIME1 = 0
```

```
      PIZZA1 = 0
      KTRVEC1 = -1
      NNVEC1 = -1
ENDIF

; This works for ANY dose, also for ADDL non-event doses (thanks to
CALLFL=-2)

IF(AMT >0 .AND. MOD(NDOSE,MAX_ACCUM_DOSES) == 0) THEN
      DOSETIME0 = TIME + TLAG
      PIZZA0 = LOG(BIO*AMT*KTR + 1E-12) - GAMLN(NN+1)
      KTRVEC0 = KTR
      NNVEC0 = NN
ENDIF

IF(AMT >0 .AND. MOD(NDOSE,MAX_ACCUM_DOSES) == 1) THEN
      DOSETIME1 = TIME + TLAG

      PIZZA1 = LOG(BIO*AMT*KTR + 1E-12) - GAMLN(NN+1)
      KTRVEC1 = KTR
      NNVEC1 = NN
ENDIF

; If the dose is one of the trailing ones in a ADDL series (captured
by DOSREC()/=0)
; DOSREC: an array containing PK SYSTEM information (AMT,TIME,CMT
et.c) describing the next non-event dose time (ADDL or LAG)
```

```
;other wise it contains zeros
; the correct time is that of the extra non-event dose records, stored
in the variable DOSTIM

; I am using SWITCHSSNXT so that, as soon as another record is seen,
the SS switch goes off.
; I am using a switch as opposed to SS per se because the original SS
value carries on with ADDL series,
; that should not be treated as SS
SWITCHSS = 0
; (USING ADDL with SS) In such a series of ADDL doses, SS would remain
the same as the originating dose event record
; but DOSREC(i)>0. Hence, DOSREC(i)==0 makses sure that the SS code
gets executed only the first time
; This takes care of the SS part of the dose, if SS is used
; DOSREC()==0 makes sure this is NOT a trailing ADDL dose.

IF(AMT >0 .AND. SS>0 .AND. DOSREC(AMT)==0) THEN
      SWITCHSS = 1
      DOSETIMESS = TLAG
      PIZZASS = LOG(BIO*AMT*KTR + 1E-12) - GAMLN(NN+1)
      KTRVECSS = KTR
      NNVECSS = NN
ENDIF

; Increase dose counter
IF(AMT >0) NDOSE = NDOSE + 1
```

```
; Define scaling to adjust moles of parent and metabolite (MET/PAR)
SCALE_MOLES = 780.90/822.94
;DES (Transit)-----------------------------------------


$DES
TRANSIT = 0
KTT = 0
TEMPO = T-DOSETIME0
IF (SWITCHSS==0 .AND. TEMPO>0 .AND. TEMPO<FORGET .AND. KTRVEC0>0) THEN
      KTT = KTRVEC0*(TEMPO)
      TRANSIT = TRANSIT + EXP(PIZZA0 + NNVEC0*LOG(KTT) - KTT)
ENDIF

TEMPO = T-DOSETIME1
IF (SWITCHSS==0 .AND. TEMPO>0 .AND. TEMPO<FORGET .AND. KTRVEC1>0) THEN
      KTT = KTRVEC1*(TEMPO)
      TRANSIT = TRANSIT + EXP(PIZZA1 + NNVEC1*LOG(KTT) - KTT)
ENDIF

; It the SWITCHSS is on, this is executed within the routine to find
the SS values.
; DOSETIMESS is centred around 0 (+TLAG) for this calculation. The
values of PIZZA, KTR and NN are those from the latest dose record
(NDOSE)
IF (SWITCHSS >0 .AND. T >DOSETIMESS) THEN ;
      KTT = KTRVECSS*(T-DOSETIMESS)
```

```
      TRANSIT = EXP(PIZZASS + NNVECSS*LOG(KTT) - KTT)
ENDIF

CH = A(1)/VH ; drug conc in liver
; set saturable elimindation to zero for pts with negative
concentrations in liver
; product of a logarith cannot be negative - this would not work
; normal Michalis-Mentel equation gives you a rate =k*A = CL*C
; but we want to get CL, so you divide the rate by concentration -
and get saturable clearance
; equation is placed in $DES because saturable clearance changes over
time
SAT_CL=0
IF (CH>0) SAT_CL=VMAX/(1+EXP(-(LOG(CH)-LOGKM))) / (CH)
;IF (CH>0) SAT_CL = VMAX/(1+EXP(-(LOG(CH)-LOG(KM)))) / (CH)
;transformation based on better Emax model, wider search in log
parametrisation
EH  = (SAT_CL*FU)/((SAT_CL*FU)+QH) ; fraction undergoing first pass
extraction
FH  = 1 - EH ;fraction available after 1st pass to go to systemic
circulation

;Define the rate constants=====

K10 = (1-FM)*(QH*EH/VH) ; non-metabolite conversion (all drug is -->
metabolite FM is 1)
K12 = (QH*FH/VH)    ; rate transfer to parent centra;
```

```
K21 = (QH/V) ; rate transfer from parent central to liver

K13 = FM*(QH*EH/VH)
K30 = CLM/VM

DADT(1) = TRANSIT -K10*A(1) - K12*A(1) + K21*A(2) - K13*A(1)
DADT(2) = K12*A(1) - K21*A(2)
DADT(3) = K13*A(1)*SCALE_MOLES - K30*A(3)

C2 = A(2)/V

DADT(4) =  KE0_L*(RL*C2 - A(4))    ;A(4) IS ACTUALLY CONC IN EFFECT
CMT
DADT(5) =  KE0_L*(RL*C2 - A(5))    ;A(5) IS ACTUALLY CONC IN EFFECT
CMT
DADT(6) =  KE0_E*(RE*C2 - A(6))    ;A(6) IS ACTUALLY CONC IN EFFECT
CMT
;====================================================================
==
; ;-----Calculating the AUC-----------------------------------------
;CP = A(2)/V                ; plasma concentration
; DADT(Z) = CP ; This code for AUC integrates the concentration. It
works for any model, but you have to be careful to trim the right
times
; AUC = Z ; AUC as obtained integrating the concentration in $DES
```

```
; AUC_INF = DOSE * BIO / CL ; this works for any linear model, it is
the theoretical AUC from a "clean" single dose or SS. Use the final
individual parameters for this

$ERROR
CP  = A(2)/V
CM  = A(3)/VM
CEL = A(4)
CEV = A(5)
CEE = A(6)

;PK(Parent)-----------------------------------------------------
IPRED_P = CP
LLOQ_P  = 0.117  ;mg/L
PROP_P  = IPRED_P*THETA(20)
ADD_P   = 0.2*LLOQ_P + THETA(21)

IF(ICALL.NE.4.AND.BLQ==1.AND.DVID==1) THEN
      ADD_P = ADD_P + (LLOQ_P/2)
ENDIF
W_P = SQRT((ADD_P)**2 + (PROP_P)**2)
;;PK(Metabolite)-------------------------------------------------
IPRED_M = CM
LLOQ_M  = 0.0391 ;mg/L
PROP_M  = IPRED_M*THETA(28)
ADD_M   = 0.2*LLOQ_M + THETA(29)
```

```
IF(ICALL.NE.4.AND.BLQ==1.AND.DVID==2) THEN
      ADD_M = ADD_M + (LLOQ_M/2)
ENDIF
;
W_M = SQRT((ADD_M)**2 + (PROP_M)**2)

;PD(Lumbar CSF)-----------------------------------------------
IPRED_L = CEL
LLOQ_L  = 0.005  ;mg/L
PROP_L  = IPRED_L*THETA(37)
ADD_L   = 0.2*LLOQ_L + THETA(38)

IF(ICALL.NE.4.AND.BLQ==1.AND.DVID==3) ADD_L = ADD_L + (LLOQ_L/2)




W_L = SQRT((ADD_L)**2 + (PROP_L)**2)   ; PD(Lumbar)



;PD(Ventricular CSF)------------------------------------------
IPRED_V = CEV
LLOQ_V  = 0.005  ;mg/L
PROP_V  = IPRED_V*THETA(39)
ADD_V   = 0.2*LLOQ_V + THETA(40)
IF(ICALL.NE.4.AND.BLQ==1.AND.DVID==4) ADD_V = ADD_V + (LLOQ_V/2)

W_V = SQRT((ADD_V)**2 + (PROP_V)**2)   ; PK(Ventricular)
```

```
;PD(ECF)-----------------------------------------------------
IPRED_E = CEE
LLOQ_E  = 0.005  ;mg/L
PROP_E  = IPRED_E*THETA(41)
ADD_E   = 0.2*LLOQ_E + THETA(42)
IF(ICALL.NE.4.AND.BLQ==1.AND.DVID==5) ADD_E = ADD_E + (LLOQ_E/2)

W_E = SQRT((ADD_E)**2 + (PROP_E)**2)   ; PK(ECF)
     ; Correlation
     RHO = THETA(30)

      ERROR_P  = W_P * ERR(1)
      ERROR_M  = W_M *(RHO*ERR(1) + SQRT(1-RHO**2)*ERR(2) )
      ERROR_L  = W_L * ERR(3)
      ERROR_V  = W_V * ERR(4)
      ERROR_E  = W_E * ERR(5)

   ;Redefine IPRED & weighting
      IPRED = IPRED_P
      W = W_P
      ERROR_TERM = ERROR_P

      IF (DVID==2) THEN
         IPRED = IPRED_M
         W     = W_M
         ERROR_TERM = ERROR_M
     ENDIF
```

```
      IF (DVID==3) THEN
         IPRED = IPRED_L
         W     = W_L
         ERROR_TERM = ERROR_L
      ENDIF

      IF (DVID==4) THEN
         IPRED = IPRED_V
         W     = W_V
         ERROR_TERM = ERROR_V
      ENDIF

      IF (DVID==5) THEN
         IPRED = IPRED_E
         W     = W_E
         ERROR_TERM = ERROR_E
      ENDIF

; Protective code
      IF (W.LE.0.000001) W=0.000001
;---------------------------------------------------------------
      IRES = DV-IPRED
      IWRES = IRES/W

      Y = IPRED + ERROR_TERM
;---------------------------------------------------------------
```

```
; To prevent simulation (ICALL==4) of negative values, set a positive
lower bound for Y, so that VPCs in the log-scale can be plotted
IF (DVID==1.AND.ICALL==4.AND.Y<=LLOQ_P) Y=LLOQ_P/2
IF (DVID==2.AND.ICALL==4.AND.Y<=LLOQ_M) Y=LLOQ_M/2
IF (DVID==3.AND.ICALL==4.AND.Y<=LLOQ_L) Y=LLOQ_L/2
IF (DVID==4.AND.ICALL==4.AND.Y<=LLOQ_V) Y=LLOQ_V/2
IF (DVID==5.AND.ICALL==4.AND.Y<=LLOQ_E) Y=LLOQ_E/2
;---------------------------------------------------------------
IF(AMT.GT.0) THEN
      TIMEDOSE = TIME
      AMOUNTDOSE = AMT
ENDIF

TAD = TIME-TIMEDOSE

VPC_MODEL = VPC_TIME
IF (VPC_TIME.GT.20) VPC_MODEL = VPC_TIME - 24

;---------RETRIEVE AMOUNT IN EACH COMPARTMENT-----------------
A_LIV = A(1)
A_CENT = A(2)
A_MET = A(3)
A_LCSF = A(4)
A_VCSF = A(5)
A_ECF = A(6)

; Initial estimates
```

```
$THETA  (0,2.90407,4.25) FIX ; 1 V [log] [L]
$THETA  (0,3.54883,3.91) FIX ; 2 CLSS [log] [L/h]
$THETA  (0.1,0.470361,10) FIX ; 3 CLSS/CLBS [log] []
$THETA  (0.001,1.50692,10) FIX ; 4 IND50 [log] [day]
$THETA  (-0.5,2.498,7.5) FIX ; 5 PMA50 [log] [months]
$THETA  (-2,1.19242,5) FIX ; 6 GAMMA [log]
$THETA  (0,2.20482,10) FIX ; 7 KM [log] [mg/L]
$THETA  -0.444026 FIX ; 8 BIO_BIRTH [log]
$THETA  1.03066 FIX ; 9 AGE_BIO_BR [log]
;--------------------
$THETA  0 FIX ; 10 DUMMY []
$THETA  0 FIX ; 11 DUMMY []
$THETA  0 FIX ; 12 DUMMY []
$THETA  0 FIX ; 13 DUMMY []
$THETA  0 FIX ; 14 DUMMY []
$THETA  0 FIX ; 15 DUMMY []
$THETA  0 FIX ; 16 DUMMY []
;--------------------
$THETA  (0,0.251427,5) FIX ; 17 MTT
$THETA  (0,0.269422,10) FIX ; 18 NN
$THETA  1 FIX ; 19 BIO
$THETA  (0,0.337661,0.5) FIX ; 20 PROP []
$THETA  0 FIX ; 21 ADD [mg/L]
$THETA  (0,90,100) FIX ; 22 QH
$THETA  (0,0.2,1) FIX ; 23 FU
$THETA  (0,1,2) FIX ; 24 VH
;--------------------
```

```
$THETA  (0,13.7449,100) FIX ; 25 CLM [L/h]; 9.3
$THETA  (0,7.76036,100) FIX ; 26 VM [L]; 1.36
$THETA  1 FIX ; 27 FM []
$THETA  (0,0.486173,1) FIX ; 28 PROP_M []
$THETA  0 FIX ; 29 ADD_M [mg/L]
$THETA  (0,0.856693,1) FIX ; 30 RHO []
;--------------------
$THETA  (0,0.163008,10) ; 31 KE0_LV
;$THETA  (0,0.217026,10) ; 32 KE0_V
$THETA  1 FIX ; 32 KE0_V
$THETA  (0,0.330311,10) ; 33 KE0_E
$THETA  (0,0.0459849,1) ; 34 RLV
;$THETA  (0,0.0460171,1) ; 35 RV
$THETA  1 FIX ; 35 RV
$THETA  (0,0.00435468,1) ; 36 RE
;$THETA  1 FIX ; 36 RE
;--------------------
$THETA  (0,0.785606,1) ; 37 PROP_L []
$THETA  0 FIX ; 38 ADD_L [mg/L]
$THETA  (0,0.554107,1) ; 39 PROP_V []
$THETA  0 FIX ; 40 ADD_V [mg/L]
$THETA  (0,0.511272,1) ; 41 PROP_E []
$THETA  0 FIX ; 42 ADD_E [mg/L]
$THETA  (0.5,2.9232,10) FIX ; 43 fac

; PRIORS FOR CL & V ----------------------------------------------
; ;Sim_start
```

```
; $THETAP  2.85 FIX ; 1 lnV
; 2.15 FIX ; 2 lnCL
; 0.693 FIX ; 3 ln(CLSS/CLBS)
; 1.50 FIX ; 4 lnIND50
; 2.524127 FIX ; 5 lnPMA50
; 1.169381 FIX ; 6 lnGAMMA
; 2.110213 FIX ; 7 lnKM
; -0.42312 FIX ; 8 lnBIO_BIRTH
; 1.000632 FIX ; 9 lnAGE_BIO_BR
; ;Sim_end

; ;Sim_start
; $THETAPV  BLOCK(9) FIX
; 0.1  ;          V
; 0 0.1  ;         CL
; 0 0 0.01  ;  CLSS/CLBS
; 0 0 0 0.01  ;      IND50
; 0 0 0 0 0.01  ;      PMA50
; 0 0 0 0 0 0.01  ;      GAMMA
; 0 0 0 0 0 0 0.01  ;        KMv
; 0 0 0 0 0 0 0 0.01  ;  BIO_BIRTH
; 0 0 0 0 0 0 0 0 0.01  ; AGE_BIO_BR
; ;Sim_end

$OMEGA  0.214469  FIX  ;    1 BSVCL
$OMEGA  0  FIX  ;   2 BSVBIO
```

```
$OMEGA  BLOCK(1) FIX
 3.1973  ; 3-8 BOVMTT
$OMEGA  BLOCK(1) SAME
$OMEGA  BLOCK(1) SAME
$OMEGA  BLOCK(1) SAME
$OMEGA  BLOCK(1) SAME
$OMEGA  BLOCK(1) SAME

$OMEGA  BLOCK(1) FIX
 0  ; 9-14 BOVKA
$OMEGA  BLOCK(1) SAME
$OMEGA  BLOCK(1) SAME
$OMEGA  BLOCK(1) SAME
$OMEGA  BLOCK(1) SAME
$OMEGA  BLOCK(1) SAME

$OMEGA  BLOCK(1) FIX
 0  ; 15-20 BOVLAG
$OMEGA  BLOCK(1) SAME
$OMEGA  BLOCK(1) SAME
$OMEGA  BLOCK(1) SAME
$OMEGA  BLOCK(1) SAME
$OMEGA  BLOCK(1) SAME

$OMEGA  BLOCK(1) FIX
 0.121823  ; 21-26 BOVBIO
$OMEGA  BLOCK(1) SAME
```

```
$OMEGA  BLOCK(1) SAME
$OMEGA  BLOCK(1) SAME
$OMEGA  BLOCK(1) SAME
$OMEGA  BLOCK(1) SAME

$OMEGA  0  FIX  ; 27 DUMMY BSVCLM
;$OMEGA  0  FIX  ;  27 BSVBIO
;$OMEGA  0  FIX  ;   27 BSVFM

$OMEGA  0.0468458  ;  28 BSVRLV
$OMEGA  0  FIX  ;   29 BSVRV
; $OMEGA  0.0668885  ;   29 BSVRV
$OMEGA  1.30138  ;   30 BSVRE
; $OMEGA  0  FIX  ;   28 BSVRL
; $OMEGA  0  FIX  ;   29 BSVRV
; $OMEGA  0  FIX  ;   30 BSVRE

$SIGMA  1  FIX  ;       ERR1
$SIGMA  1  FIX  ;       ERR2
$SIGMA  1  FIX  ;       ERR3
$SIGMA  1  FIX  ;       ERR4
$SIGMA  1  FIX  ;       ERR5
;Sim_start
$ESTIMATION   MSFO=run064.msf   MAXEVAL=9999   PRINT=1   METHOD=1
INTERACTION
```

```
            NOABORT   NSIG=2   NONINFETA=1   ETASTYPE=1   SIGL=6
;NOPRIOR=1

;$SIMULATION ONLYSIMULATION (2239177789 NORMAL)
;Sim_end

$TABLE       ID OCC TIME TAD Y DV MDV PRED RES WRES IPRED IRES
IWRES
            CWRES CWRESI OBJI VPC_TIME TAD MTT NN BIO CL V BSVCL
            BSVBIO BOVKA BOVLAG BOVMTT BOVBIO PROP_P ADD_P CLM
VM FM
            BSVCLM KE0_L KE0_V KE0_E RL RV RE AGE SEXF WT HT
GESAGE_WK
            MGPERKG  MGINTAB  DAYTTT  DVID  A_LIV  A_CENT  A_MET
A_LCSF
            A_VCSF A_ECF NOPRINT NOAPPEND ONEHEADER FORMAT=,
            FILE=mytab064.csv
```

Final NONMEM code for results presented in Chapter 6

```
;Model Description: RIF Final Model LASER-TBM Study
;Settings for the memory of NONMEM
$SIZES      PD=-1000 LVR=-150 LTH=-200 MAXFCN=10000000 LNP4=-150000
            DIMTMP=1000
$PROBLEM    RIF_MODEL_LASER-TBM
$INPUT      ID ....
$DATA      data_rif_nm_2023-11-26.csv IGNORE=@ IGNORE(DVID.EQ.2)
           IGNORE(DVID.EQ.3) IGNORE(DVID.EQ.4) IGNORE(FLAG_ENZ.GT.0)
            IGNORE(ID.EQ.4019)
$SUBROUTINE ADVAN14 TRANS1 TOL=9 ATOL=9
$ABBREVIATED DERIV2=NO
$MODEL      NCOMPS=7 ; NUMBER OF COMPARTMENTS
            COMP=(ABS) ;1 GUT CMT
            COMP=(CENTRAL) ;2 CENTRAL CMT
            COMP=(LIVER) ;3 LIVER CMT
            COMP=(PERI) ;4 PERI CMT
            COMP=(CSF) ; 5 CSF CMT
            COMP=(AUC_P) ; 6 AUC plasma
            COMP=(AUC_CSF) ; 7 AUC CSF

;Using Priors-----------------------------------------------
;Sim_start
$PRIOR    NWPRI NPEXP=1 PLEV=0.9999
;Sim_end

;initialization-of-theta(S)-from the previous run----------
```

```
$THETA  (0,1.09075,100) ; 1 LOGKM (mg/L) (exp)
$THETA  (0,27.3473,125) ; 2 V (L)
$THETA  (0,0.934124,1) ; 3 BIO_ORAL(.)
$THETA  (0,0.485942,3) ; 4 KA (1/h)
$THETA  (0,0.634202,3) ; 5 MTT (h)
$THETA  (0,0.251954,1) ; 6 PROP (%)
;$THETA  (0,1.63193E-05,10) ; 7 ADD (mg/L)
$THETA  0 FIX ; 7 ADD (mg/L)
$THETA  1 FIX ; 8 VH
$THETA  90 FIX ; 9 QH
$THETA  1 FIX ; 10 BIO_IV()
$THETA  (0,10.9971,1000) ; 11 Q
$THETA  (0,31.5279,1000) ; 12 VP
$THETA  (0,19,100) FIX ; 13 NN (.)
;----------------------------
$THETA  (0,46.1064,1000) ; 14 CL_Day3_High
$THETA  (0,33.1219,1000) ; 15 CL_Day3_Std
$THETA  (0,70.2333,1000) ; 16 CL_Day28_High
$THETA  (0,41.411,1000) ; 17 CL_Day28_Std
;----------------------------
$THETA  (0,3.19641,10) ; 18 EQHR (h) --> KE0
$THETA  (0,0.059288,1) ; 19 PPC
$THETA  (0,0.984216,1) ; 20 PROP_CSF []
$THETA  (0,0.0206258,10) ; 21 ADD_CSF [mg/L]
;----------------------------
;THETA Priors (Reference values from reference model of the THETAs)
;Sim_start
```

```
$THETAP  1.21 FIX ; LOGKM
;Sim_end
;Sim_start
$THETAPV  BLOCK(1) FIX
 0.1  ;      LOGKM
;Sim_end
$OMEGA  BLOCK(1)
 0.0642298  ;    1 BSVCL
$OMEGA  BLOCK(1)
 0.0295196  ;     2 BSVV
$OMEGA  BLOCK(1) FIX
 0  ;   3 BSVBIO
$OMEGA  BLOCK(1)
 0.0329715  ; 4-8 BOVBIO
$OMEGA  BLOCK(1) SAME
$OMEGA  BLOCK(1) SAME
$OMEGA  BLOCK(1) SAME
$OMEGA  BLOCK(1) SAME
$OMEGA  BLOCK(1)
 0.609918  ; 9-13 BOVKA
$OMEGA  BLOCK(1) SAME
$OMEGA  BLOCK(1) SAME
$OMEGA  BLOCK(1) SAME
$OMEGA  BLOCK(1) SAME
$OMEGA  BLOCK(1)
 1.23318  ; 14-18 BOVMTT
$OMEGA  BLOCK(1) SAME
```

```
$OMEGA  BLOCK(1) SAME

$OMEGA  BLOCK(1) SAME

$OMEGA  BLOCK(1) SAME

$OMEGA  BLOCK(1) FIX

 0  ; 19-20 BVVCL

$OMEGA  BLOCK(1) SAME

$OMEGA  BLOCK(1)

 0.0288515  ;  21 BSV D2

$OMEGA  0.00215  FIX  ; 22 Variance HTfemale

$OMEGA  0.00170  FIX  ; 23 Variance HTmale

$OMEGA  BLOCK(1) FIX

 0  ; 24-25 BVVPPC

$OMEGA  BLOCK(1) SAME

$OMEGA  BLOCK(1) FIX

 0  ;  26 BSVPPC

$SIGMA  1  FIX

$SIGMA  1  FIX


$PK

;-------Typical values of covariates

TVWT = 60  ;median wt from the data set

TVFAT = 14

TVFFM = 46

;---------Allometric scaling and covariates

; ALLMCL_FFM = (FFM_IMP/TVFFM)**0.75

; ALLMV_FFM = (FFM_IMP/TVFFM)
```

```
;- Imputation of HT and FFM all individuals -
IMP_HTM = ((0.00133*WT) + 1.51)*EXP(ETA(22)) ;for females
IF (SEXF.EQ.0)   IMP_HTM = ((0.00281*WT) + 1.53)*EXP(ETA(23)) ;for
males
IMP_FFM = (37.99 * (IMP_HTM**2) * WT) / (35.98 * (IMP_HTM**2) + WT);
for females
IF (SEXF.EQ.0)   IMP_FFM = (42.92 * (IMP_HTM**2) * WT) / (30.93 *
(IMP_HTM**2) + WT);for males

IF(FFM.NE.-99)   ALLMCL_FFM = (FFM/TVFFM)**0.75
IF(FFM.EQ.-99)  ALLMCL_FFM = (IMP_FFM/TVFFM)**0.75
IF(FFM.NE.-99)  ALLMV_FFM  = (FFM/TVFFM)
IF(FFM.EQ.-99)  ALLMV_FFM  = (IMP_FFM/TVFFM)

;Hepatic allometry
IF(FFM.NE.-99)   ALLMCL_H_FFM = (FFM/56.1)**0.75
IF(FFM.EQ.-99)  ALLMCL_H_FFM = (IMP_FFM/56.1)**0.75
IF(FFM.NE.-99)  ALLMV_H_FFM  = (FFM/56.1)
IF(FFM.EQ.-99)  ALLMV_H_FFM  = (IMP_FFM/56.1)

;PARAMTERS
TVLOGKM = THETA(1) ; LOGKM
TVV = THETA(2)*ALLMV_FFM
TVBIO_ORAL = THETA(3)
TVKA  = THETA(4)

TVMTT      = THETA(5)
```

```
TVBIO_IV = THETA(10)
TVCL = THETA(14)*ALLMCL_FFM
IF (RIFHIGH.EQ.0.AND.PK_VISIT_2.EQ.3) TVCL = THETA(15)*ALLMCL_FFM
IF (RIFHIGH.EQ.1.AND.PK_VISIT_2.EQ.28) TVCL = THETA(16)*ALLMCL_FFM
IF (RIFHIGH.EQ.0.AND.PK_VISIT_2.EQ.28) TVCL = THETA(17)*ALLMCL_FFM
TVVH    = THETA(8)*ALLMV_H_FFM
TVQH    = THETA(9)*ALLMCL_H_FFM
TVQ     = THETA(11)*ALLMCL_FFM
TVV2    = THETA(12)*ALLMV_FFM
TVNN    = THETA(13)
TVEQHR  = THETA(18)
TVPPC   = THETA(19)

;Defining ETAs
BSVCL = ETA(1)
BSVV = ETA(2)
BSVBIO = ETA(3)

;Defining Between OCC variability;
BOVBIO = 0
BOVKA  = 0
BOVMTT = 0
IF (OCC==1) THEN ;PREDOSE PK_VISIT=3
      BOVBIO = ETA(4)
      BOVKA  = ETA(9)
      BOVMTT = ETA(14)
      ;BOVCL  = ETA(19)
```

```
ENDIF
IF (OCC==2) THEN
      BOVBIO = ETA(5)
      BOVKA  = ETA(10)
      BOVMTT = ETA(15)
      ;BOVCL  = ETA(19)
ENDIF
IF (OCC==3) THEN
      BOVBIO = ETA(6)
      BOVKA  = ETA(11)
      BOVMTT = ETA(16)
      ;BOVCL  = ETA(19)
ENDIF
IF (OCC==4) THEN
      BOVBIO = ETA(7)
      BOVKA  = ETA(12)
      BOVMTT = ETA(17)
      ;BOVCL  = ETA(20)
ENDIF
IF (OCC==5) THEN
      BOVBIO = ETA(8)
      BOVKA  = ETA(13)
      BOVMTT = ETA(18)
      ;BOVCL  = ETA(20)
ENDIF

BVVCL = 0
```

```
IF (PK_VISIT==3) BVVCL=ETA(19)

IF (PK_VISIT==28) BVVCL=ETA(20)

BSVD2 = ETA(21)

BVVPPC = 0

IF (PK_VISIT==3)  BVVPPC=ETA(24)

IF (PK_VISIT==28) BVVPPC=ETA(25)

BSVPPC = ETA(26)

;-----------------------------------------------------------

CL        = (TVCL)*EXP(BSVCL+BVVCL)

V           = (TVV)*EXP(BSVV)

KA          = (TVKA)*EXP(BOVKA)

MTT   = (TVMTT)*EXP(BOVMTT)

NN       = TVNN

D2       = DUR*EXP(BSVD2)

BIO_ORAL = (TVBIO_ORAL)*EXP(BSVBIO+BOVBIO)

BIO_IV   = TVBIO_IV

VH=TVVH

QH=TVQH

LOGKM     = TVLOGKM;*EXP(BSVKM)

VMAX  = CL*EXP(LOGKM) ; max enzymatic rate

Q      =    TVQ

V2     =    TVV2


EQHR = TVEQHR

KE0  = LOG(2)/EQHR

PPC = TVPPC*EXP(BVVPPC+BSVPPC)
```

```
K24 = Q/V
K42 = Q/V2

F2 = 0
IF(RIFIV.EQ.1) F2=BIO_IV
;Transit code
F1=0 ; I need to set bioavailability in compartment 1 to 0 for this
implementation of the transit compartment absorption
KTR = (NN+1)/MTT ; The number of actual transit compartments is NN+1,
so this number can never be 0
IF (NEWIND/=2.OR.EVID>=3.AND.CMT.EQ.1) THEN ; new individual, or reset
event
    ; The values read here will be stored in TDOS and PD in this very
PK call.
      TNXD=TIME ; Time of the dose
      PNXD=AMT ; Amount. If it's zero, the DE is deactivated.

      TIMEDOSE = TIME
      AMOUNTDOSE = AMT
ENDIF

TDOS=TNXD ; This will either save here the temporary values if it's a
new individual...
PD=PNXD ; ...or the values which were read one record ahead during
the execution of the previous record.
```

```
IF(AMT>0.AND.CMT.EQ.1) THEN ; This reads one record ahead and stores
the data to be used when running the following record
; IF(AMT.GT.0.AND.ALAG1.EQ.0) THEN ; Use this INSTEAD if there is
ALAG, as it will also checks if the ALAG is not 0. Note that you
normally do not want to include both ALAG and transit, this is a very
exceptional case
      TNXD=TIME
      PNXD=AMT
ENDIF
PIZZA = LOG(BIO_ORAL*PD*KTR + 1E-12) - GAMLN(NN+1)    ; without
+0.00001, it won't work with ETAs in bioavailability

A_0(1) = 1E-12 ;ABS
A_0(2) = 1E-12 ;CENT
A_0(3) = 1E-12 ;LIV
A_0(4) = 1E-12 ;PERI
A_0(5) = 1E-12 ;CSF
;-------------------------------------------------------------
$DES
;Transit code
TEMPO = T-TDOS ; this is time after dose for the transit, it should
always be >= 0
KTT = 0
TRANSIT = 0
IF(PD.GT.0.AND.TEMPO.GT.0) THEN ; This happens only id PD>0, so only
if a dose has been detected
      KTT = KTR*(TEMPO)
```

```
      TRANSIT = EXP(PIZZA+NN*LOG(KTT)-KTT)
ENDIF
;Saturable CL (Michaelis-Menten)
CH = A(3)/VH ;Conc. in liver
SAT_CL=0
IF (CH>0) SAT_CL = VMAX / (CH + EXP(LOGKM))

EH    =  (SAT_CL)/((SAT_CL)+QH)  ;  fraction  undergoing  first  pass
extraction
FH   = 1 - EH ;fraction available after 1st pass to go to systemic
circulation

K30=(QH*EH/VH)
K32= (QH*FH/VH) ;from liver to plasma
K23=(QH/V)      ;frm plasma to liver

DADT(1) = TRANSIT-KA*A(1) ;gut
DADT(2) = K32*A(3)-K23*A(2) - K24*A(2) + K42*A(4);plasma
DADT(3) = KA*A(1)-K32*A(3)+K23*A(2)-K30*A(3) ;liver
DADT(4) = K24*A(2)-K42*A(4) ; 2nd cmt
CP_DES = A(2)/V
DADT(5) = KE0*(PPC*CP_DES - A(5)) ;CSF
DADT(6) = CP_DES
DADT(7) = A(5)
;-------------------------------------------------------------
$ERROR
; DEFINE LLOQ VALUE
```

```
; LLOQ could be study-specific, e.g if you have data from different
labs in your analysis
LLOQ_P = 0.117 ; DEFINE YOUR OWN LLOQ HERE
; DEFINE censoring threshold (CENS_THR)
; Generally the same as LLOQ, but not if the LLOQ data was released
by the lab.
; If censoring threshold is not explicitly indicated, we can generally
assume it to be the limit of detection (LOD).
; The signal-to-noise ratio is generally assumed to be 10 at the LLOQ,
and 3 at the LOD
; https://en.wikipedia.org/wiki/Detection_limit;
; Keizer RJ, Jansen RS, Rosing H, Thijssen B, Beijnen JH, Schellens
JHM, Huitema ADR.
;  Incorporation  of  concentration  data  below  the  limit  of
quantification in population pharmacokinetic analyses.
; Pharmacol Res Perspect [Internet]. 2015 Mar;3(2):e00131. Available
from: http://doi.wiley.com/10.1002/prp2.131

CENS_THR_P = LLOQ_P
CP = A(2)/V
IPRED_P = CP
PROP_P = IPRED_P*THETA(6)
ADD_P = THETA(7)+(CENS_THR_P*0.2)
; ADD is defined as 20% of LLOQ + THETA(.)

IF (ICALL/=4.AND.CENS==1.AND.DVID==1) THEN
      ADD_P = ADD_P +(CENS_THR_P*0.5)
```

```
ENDIF

W_P = SQRT((ADD_P)**2 + (PROP_P)**2)
ERROR_P  = W_P * ERR(1)
NO_FIT = 0
CENS_THR_VPC_P = CENS_THR_P
IMPUTED_CENS_VPC_P = CENS_THR_P/2
; For CENS==2 (i.e. the trailing CENSORED values in a series that were
imputed to CENS_THR/2), we don't want these to influence the fit,
; we only want them for simulation-based diagnostics such as the VPC.
; So we define a separate error structure for these points. It has no
proportional component
; (PROP = 0, as we would not want these points to affect our estimate
of proportional error)
; and a FIXED and HUGE additive component (ADD = 1000000000, large
with respect to the readings of concentration),
; so that the values do not affect the fit. It's also a good idea to
repeat the diagnostic plots without the CENS=2 points

IF (ICALL/=4.AND.CENS==2.AND.DVID==1) THEN
      PROP_P = 0
      ADD_P = 10000000000
      NO_FIT = 1
ENDIF

;Repeat for CSF observations---------------------------------------
LLOQ_E = 0.005
```

```
CENS_THR_E = LLOQ_E
CE = A(5)

IPRED_E = CE
PROP_E = IPRED_E*THETA(20)
ADD_E = THETA(21)+(CENS_THR_E*0.5)

IF (ICALL/=4.AND.CENS==1.AND.DVID==5) THEN
      ADD_E = ADD_E +(CENS_THR_E*0.5)
ENDIF

W_E = SQRT((ADD_E)**2 + (PROP_E)**2)
ERROR_E  = W_E * ERR(2)
NO_FIT = 0
CENS_THR_VPC_E = CENS_THR_E
IMPUTED_CENS_VPC_E = CENS_THR_E/2

IF (ICALL/=4.AND.CENS==2.AND.DVID==5) THEN
      PROP_E = 0
      ADD_E = 10000000000
      NO_FIT = 1
ENDIF
;----------------------------------------------------------------------
;Redefine IPRED & weighting
IPRED = IPRED_P
W = W_P
ERROR_TERM = ERROR_P
```

```
CENS_THR_VPC = CENS_THR_VPC_P
IMPUTED_CENS_VPC = IMPUTED_CENS_VPC_P

IF (DVID==5) THEN
      IPRED = IPRED_E
      W     = W_E
      ERROR_TERM = ERROR_E
      CENS_THR_VPC = CENS_THR_VPC_E
      IMPUTED_CENS_VPC = IMPUTED_CENS_VPC_E
ENDIF

; Protective code
IF (W.LE.0.000001) W=0.000001
IRES=DV-IPRED
IWRES=IRES/W
Y = IPRED + ERROR_TERM

; To prevent simulation (ICALL==4) of negative values. It set a
positive lower bound for Y, so that VPCs in the log-scale can be
plotted
IF (ICALL==4.AND.Y<=CENS_THR_VPC) Y = IMPUTED_CENS_VPC
; To calculate time after dose.
IF(AMT.GT.0) THEN
      TIMEDOSE = TIME
      AMOUNTDOSE = AMT
ENDIF
TAD = TIME-TIMEDOSE
```

```
;;Retrieve amount in each compartment
A_GUT   = A(1)
A_CENT  = A(2)
A_LIV   = A(3)
A_PERI  = A(4)
A_CSF   = A(5)
AUC_P   = A(6)
AUC_CSF = A(7)

$ESTIMATION METHOD=1 INTER MAXEVAL=9999 PRINT=1 NOABORT NSIG=3 SIGL=6
            NONINFETA=1 ETASTYPE=1
```

Final NONMEM code for results presented in Chapter 7

```
;; 1. Based on:
;Model desc: Final.model
;Settings for the memory of NONMEM
$SIZES      PD=-1000 LVR=-150 LTH=-200 MAXFCN=10000000 LNP4=-150000
            DIMTMP=1000
$PROBLEM    LNZ_MODEL
$INPUT      ID DV AMT …
$DATA      dat.csv IGNORE=@
$ABBREVIATED DECLARE INTEGER NDOSE INTEGER MAX_ACCUM_DOSES
$SUBROUTINE ADVAN13 TRANS1 TOL=9 ATOL=9 ;SSTOL=6 SSATOL=6
$MODEL      NCOMPS=5 ; NUMBER OF COMPARTMENTS
            COMP=(ABS,DEFDOSE) ;1 GUT ABS
            COMP=(CENTRAL) ;2 CENTRAL CMT
            COMP=(CSF) ; 3 CSF CMT
            COMP=(AUC_P) COMP=(AUC_CSF)

;initialization-of-theta(S)-from the previous run
$THETA  (0,7.33136) ; 1 CLMAX (L/H)
$THETA  (0,40.8985,100) ; 2 V (L)
$THETA  (0,1.21424,3) ; 3 KA (1/H)
$THETA  (0,0.211549,3) ; 4 MTT (H)
$THETA  1 FIX ; 5 BIO()
$THETA  (0,5.67065,100) ; 6 NN ()
$THETA  (0.01,0.21648,10) ; 7 PROP (%)
$THETA  (1e-5,0.163042,2) ; 8 ADD (mg/L)
$THETA  (0,26.2736) ; 9 KM
```

```
$THETA  (0,0.197959,10) ; 10 KE0
$THETA  (0,0.364727,1) ; 11 PPC
$THETA  (0,0.3) ; 12 PROP_E []
$THETA  0 FIX ; 13 ADD_E [mg/L]
$THETA  (0,1.18242,10) ; 14 BRK
$THETA  1 FIX ; 15 AMP
$THETA  0 FIX ; 16 INT

$OMEGA  BLOCK(1)
 0.00884734  ; 1 BSVCLMAX
$OMEGA  BLOCK(1) FIX
 0  ;     2 BSVV
$OMEGA  BLOCK(1) FIX
 0  ;    3 BSVKA
$OMEGA  BLOCK(1) FIX
 0  ;   4 BSVMTT
$OMEGA  BLOCK(1) FIX
 0  ;   5 BSVBIO
$OMEGA  BLOCK(1)
 0.772478  ; 6-10 BOVKA
$OMEGA  BLOCK(1) SAME
$OMEGA  BLOCK(1) SAME
$OMEGA  BLOCK(1) SAME
$OMEGA  BLOCK(1) SAME
$OMEGA  BLOCK(1)
 1.19782  ; 11-15 BOVMTT
$OMEGA  BLOCK(1) SAME
```

```
$OMEGA  BLOCK(1) SAME

$OMEGA  BLOCK(1) SAME

$OMEGA  BLOCK(1) SAME

$OMEGA  BLOCK(1) FIX

 0  ; 16-20 BOVBIO

$OMEGA  BLOCK(1) SAME

$OMEGA  BLOCK(1) SAME

$OMEGA  BLOCK(1) SAME

$OMEGA  BLOCK(1) SAME

$OMEGA  0.00215  FIX  ; 21 Variance HTfemale

$OMEGA  0.00170  FIX  ; 22 Variance HTmale

$OMEGA  BLOCK(1)

 0.0411842  ; 23-24 BVVCLMAX

$OMEGA  BLOCK(1) SAME

$OMEGA  BLOCK(1) FIX

 0  ;   25 BSVKM

$OMEGA  BLOCK(1) FIX

 0  ;  26 BSVKE0

$OMEGA  BLOCK(1) FIX

 0  ;  27 BSVPPC

$OMEGA  BLOCK(1) FIX

 0  ; 28-29 BVVPPC

$OMEGA  BLOCK(1) SAME

$SIGMA  1  FIX


$PK

;--------- Handling of missing data ----------
```

```
;- Imputation of HT and FFM all individuals -
                      IMP_HTM = ((0.00133*WTNEW) + 1.51)*EXP(ETA(21))
;for females
IF (SEXF.EQ.0)  IMP_HTM = ((0.00281*WTNEW) + 1.53)*EXP(ETA(22)) ;for
males

                      IMP_FFMNEW = (37.99 * (IMP_HTM**2) * WTNEW) /
(35.98 * (IMP_HTM**2) + WTNEW); for females
IF (SEXF.EQ.0)  IMP_FFMNEW = (42.92 * (IMP_HTM**2) * WTNEW) / (30.93
* (IMP_HTM**2) + WTNEW);for males

;Adding Dose as covriate
IF(AMT.GT.0) DOSE_LZD = AMT

;-------Typical values of covariates
TVWT = 60 ;median wt from the data set
TVFFM = 45
;---------Allometric scaling and covariates
ALLMCL_WT = (WTNEW/TVWT)**0.75
ALLMV_WT = (WTNEW/TVWT)

IF(FFMNEW.NE.-99)     ALLMCL_FFM = (FFMNEW/TVFFM)**0.75
IF(FFMNEW.EQ.-99)   ALLMCL_FFM = (IMP_FFMNEW/TVFFM)**0.75

IF(FFMNEW.NE.-99)     ALLMV_FFM = (FFMNEW/TVFFM)
IF(FFMNEW.EQ.-99)   ALLMV_FFM = (IMP_FFMNEW/TVFFM)
;-------------------------------------------------------------
```

```
; Covariate Testing
COV     = CSF_PROTEIN
COV_MED = 0.995

IF (COV.LT.0) THEN
      COV = COV_MED
ENDIF

BRK = THETA(14) ;lower limit must be 0
AMP = THETA(15)
INT = THETA(16) ;intercept - lower limit must be 0
SLP = (AMP - INT)/(BRK - 0)
SLP_AFTER = 0

IF(COV.LE.BRK)   COV_EFF=(SLP*(COV-BRK))
IF(COV.GT.BRK)   COV_EFF=(SLP_AFTER*(COV-BRK))

;PARAMTERS
TVCLMAX = THETA(1) *ALLMCL_FFM
TVV   = THETA(2)*ALLMV_FFM  ;  Volume  Typical  Value  WITH  ALLOMETRIC
SCALLING
TVKA  = THETA(3)                        ; First Order oral abs Typical
Value
TVMTT       = THETA(4)                        ; Typical-VALUE-FOR-MTT
TVBIO       = THETA(5)                        ; Typical BIO value
TVNN        = THETA(6)                        ;      NUMBER-OF-TRANSIT-
COMPS
```

```
TVKM    = THETA(9)
;EFFECT Parameters
TVKE0 = THETA(10)
TVPPC = THETA(11)*(1+COV_EFF)
;-------------------------------------------------------------
;Defining ETA's
;BETWEEN    SUBJETS    VARIABILITY----------------------------------
BSVCLMAX    = ETA(1)
BSVV       = ETA(2)
BSVKA           = ETA(3)
BSVMTT          = ETA(4)
BSVBIO          = ETA(5)

;Defining Between Visit variability
BVVCLMAX = 0
IF (PK_VISIT == 3) BVVCLMAX = ETA(23) ;eta for visit day3
IF (PK_VISIT == 28)   BVVCLMAX = ETA(24) ;eta for visit day28

;Defining Between OCC VARIABILITY-----------------------------------
BOVCL = 0
BOVKA = 0
BOVMTT = 0
BOVBIO = 0
BOVLAG  = 0

;Defining Between OCC variability;
;OCCASION 1
```

```
IF (OCC==1) THEN
      BOVKA = ETA(6)
      BOVMTT = ETA(11)
      BOVBIO = ETA(16)
      ;BVVCLMAX = ETA(23)   ;eta for visit day3
      BVVPPC = ETA(28);eta for visit day3
ENDIF
;OCCASION 2
IF (OCC==2) THEN
      BOVKA = ETA(7)
      BOVMTT = ETA(12)
      BOVBIO = ETA(17)
      ;BVVCLMAX = ETA(23)   ;eta for visit day3
      BVVPPC = ETA(28);eta for visit day3
ENDIF
;OCCASION 3
IF (OCC==3) THEN
      BOVKA = ETA(8)
      BOVMTT = ETA(13)
      BOVBIO = ETA(18)
      ;BVVCLMAX = ETA(24)   ;eta for visit day28
      BVVPPC = ETA(29);eta for visit day28
ENDIF
;OCCASION 4
IF (OCC==4) THEN
      BOVKA = ETA(9)
      BOVMTT = ETA(14)
```

```
      BOVBIO = ETA(19)
      ;BVVCLMAX = ETA(24) ;eta for visit day28
      BVVPPC = ETA(29);eta for visit day28
ENDIF
;OCCASION 5
IF (OCC==5) THEN
      BOVKA = ETA(10)
      BOVMTT = ETA(15)
      BOVBIO = ETA(20)
      ;BVVCLMAX = ETA(23) ;eta for visit day3 (24h dose)
      BVVPPC = ETA(28);eta for visit day3   (24h dose)
ENDIF

BSVKM            = ETA(25)
BSVKE0       = ETA(26)
BSVPPC       = ETA(27)
;-----------------------------------------------------------------V
      = (TVV)*EXP(BSVV)
KA          = (TVKA)*EXP(BSVKA+BOVKA)
MTT   = (TVMTT)*EXP(BSVMTT+BOVMTT)
BIO   = (TVBIO)*EXP(BSVBIO+BOVBIO)
NN          = TVNN;*EXP(BSVNN)
CLMAX  = TVCLMAX*EXP(BSVCLMAX+BVVCLMAX)
KM     = TVKM*EXP(BSVKM)
VMAX   = CLMAX*KM

;Effect parameters
```

```
KE0 = TVKE0 * EXP(BSVKE0)
PPC = TVPPC * EXP(BSVPPC+BVVPPC)
K23 = (CLMAX/V)*1E-12 ;negligible mass transfer from central to effect
(CSF) compartment
;-------------------------------------------------------------;
Transit code
F1=0 ; needed for this implementation of the transit compartment
absorption
KTR = (NN+1)/MTT ; The number of actual transit compartments is NN+1,
so this number can never be 0
IF (NEWIND/=2.OR.EVID>=3) THEN ; new individual, or reset event
    ; The values read here will be stored in TDOS and PD in this very
PK call.
      TNXD=TIME ; Time of the dose
      PNXD=AMT ; Amount. If it's zero, the DE is deactivated.
      TIMEDOSE = TIME
      AMOUNTDOSE = AMT
ENDIF

TDOS=TNXD ; This will either save here the temporary values if it's a
new individual...
PD=PNXD ; ...or the values which were read one record ahead during
the execution of the previous record.

IF(AMT>0) THEN ; This reads one record ahead and stores the data to
be used when running the following record
```

```
; IF(AMT.GT.0.AND.ALAG1.EQ.0) THEN ; Use this INSTEAD if there is
ALAG, as it will also checks if the ALAG is not 0. Note that you
normally do not want to include both ALAG and transit, this is a very
exceptional case
      TNXD=TIME
      PNXD=AMT
ENDIF

; To speed up the computation, I calculate here all the non-time-
varying quantities used in $DES
PIZZA = LOG(BIO*PD*KTR + 1E-12) - GAMLN(NN+1)  ; without +0.00001, it
won't work with ETAs in bioavailability

A_0(1) = 1E-12 ;ABS
A_0(2) = 1E-12 ;CENT
A_0(3) = 1E-12 ;CSF
A_0(4) = 1E-12
A_0(5) = 1E-12
;-----------------------------------------------------------------$DES
C2 = A(2)/V

TEMPO = T-TDOS ; this is time after dose for the transit, it should
always be >= 0
KTT = 0
TRANSIT = 0
IF(PD.GT.0.AND.TEMPO.GT.0) THEN ; This happens only id PD>0, so only
if a dose has been detected
```

```
      KTT = KTR*(TEMPO)
      TRANSIT = EXP(PIZZA+NN*LOG(KTT)-KTT)
ENDIF
DADT(1) = TRANSIT -KA*A(1)
DADT(2) = KA*A(1) - ((VMAX/(KM+C2))/V)*A(2)
DADT(3) = KE0*(PPC*C2 - A(3)) ;A(3) IS ACTUALLY CONC IN EFFECT CMT
DADT(4) = C2;*TSS1
DADT(5) = A(3);*TSS1

$ERROR
; In the dataset, flag CENSORED values:
      ; CENSORED==0 means that the value given by lab isn't censored
      ; CENSORED==1 means that the DV value was CENSORED and we would
like to use it in the model fit
      ; CENSORED==2  same as above but we don't want it to affect the
model fit but we leave it there for diagnostics

LLOQ_LZD=0.100
LLOQ_P = 0.100
LLOQ_E = 0.100
CENS_THR = LLOQ_LZD

CP = A(2)/V
CE = A(3)

IPRED_P = CP
PROP_P  = IPRED_P*THETA(7)
```

```
ADD_P   = THETA(8) + (0.2*CENS_THR)

IF(ICALL.NE.4.AND.BLQ_LNZ==1.AND.DVID==1) THEN
      ADD_P = ADD_P + (LLOQ_P/2)
ENDIF

W_P = SQRT((ADD_P)**2 + (PROP_P)**2)

IPRED_E = CE
PROP_E  = IPRED_E*THETA(12)
ADD_E   = THETA(13) + (0.2*CENS_THR)

IF(ICALL.NE.4.AND.BLQ_LNZ==1.AND.DVID==2) THEN
      ADD_E = ADD_E + (LLOQ_E/2)
ENDIF

W_E = SQRT((ADD_E)**2 + (PROP_E)**2)

       ERROR_P  = W_P * ERR(1)
       ERROR_E  = W_E * ERR(1)

    ;Redefine IPRED & weighting
       IPRED = IPRED_P
       W = W_P
       ERROR_TERM = ERROR_P

       IF (DVID==2) THEN
```

```
          IPRED = IPRED_E
          W     = W_E
          ERROR_TERM = ERROR_E
      ENDIF
       ; Protective code
       IF (W.LE.0.000001) W=0.000001
      IRES = DV-IPRED
      IWRES = IRES/W

       Y = IPRED + ERROR_TERM
; To prevent simulation (ICALL==4) of negative values, set a positive
lower bound for Y, so that VPCs in the log-scale can be plotted
IF (DVID==1.AND.ICALL==4.AND.Y<=LLOQ_P) Y=LLOQ_P/2
IF (DVID==2.AND.ICALL==4.AND.Y<=LLOQ_E) Y=LLOQ_E/2
;---------------------------------------------------------------
 IF(AMT>0) THEN
      TIMEDOSE = TIME
      AMOUNTDOSE = AMT
ENDIF

TAD2 = TIME-TIMEDOSE
TSOD = TAD2
IF(OCC.EQ.1.OR.OCC.EQ.3) TSOD = 24 - TAD2

 ; RETRIEVE AMOUNT IN EACH COMPARTMENT-------------------------A_GUT
= A(1)
A_CENT  = A(2)
```

```
A_CSF   = A(3)

AUC_P   = A(4)

AUC_CSF = A(5)


VARCLMAX = BSVCLMAX + BVVCLMAX

VARPPC = BSVPPC + BVVPPC

CONC_MOD = A(2)/V

;-------------------------------------------------------------

$ESTIMATION METHOD=1 INTER MAXEVAL=9999 PRINT=1 NOABORT NSIG=3 SIGL=6

            NONINFETA=1 ETASTYPE=1

$TABLE     …
```

References

Aarnoutse, R. E., G. S. Kibiki, K. Reither, H. H. Semvua, F. Haraka, C. M. Mtabho, S. G. Mpagama, et al. 2017. "Pharmacokinetics, Tolerability, and Bacteriological Response of Rifampin Administered at 600, 900, and 1,200 Milligrams Daily in Patients with Pulmonary Tuberculosis." *Antimicrobial Agents and Chemotherapy* 61 (11). https://doi.org/10.1128/AAC.01054-17.

Abdelgawad, Noha, Maxwell Chirehwa, Charlotte Schutz, David Barr, Amy Ward, Saskia Janssen, Rosie Burton, et al. 2024. "Pharmacokinetics of Antitubercular Drugs in Patients Hospitalized with HIV-Associated Tuberculosis: A Population Modeling Analysis." *Wellcome Open Research* 7 (March): 72. https://doi.org/10.12688/WELLCOMEOPENRES.17660.3.

Abdelgawad, Noha, Mvuwo Tshavhungwe, Ursula Rohlwink, Helen McIlleron, Mahmoud T. Abdelwahab, Lubbe Wiesner, Sandra Castel, et al. 2023. "Population Pharmacokinetic Analysis of Rifampicin in Plasma, Cerebrospinal Fluid, and Brain Extracellular Fluid in South African Children with Tuberculous Meningitis." *Antimicrobial Agents and Chemotherapy* 67 (3). https://doi.org/10.1128/AAC.01474-22/FORMAT/EPUB.

Abdelwahab, Mahmoud Tareq, Sean Wasserman, James C. M. Brust, Keertan Dheda, Lubbe Wiesner, Neel R. Gandhi, Robin M. Warren, et al. 2021. "Linezolid Population Pharmacokinetics in South African Adults with Drug-Resistant Tuberculosis." *Antimicrobial Agents and Chemotherapy* 65 (12). https://doi.org/10.1128/AAC.01381-21.

Acocella, G. 1978. "Clinical Pharmacokinetics of Rifampicin." *Clinical Pharmacokinetics* 3 (2): 108–27. https://doi.org/10.2165/00003088-197803020-00002.

Acocella, G., V. Pagani, M. Marchetti, G. C. Baroni, and F. B. Nicolis. 1971. "Kinetic Studies on Rifampicin. I. Serum Concentration Analysis in Subjects Treated with Different Oral Doses over a Period of Two Weeks." *Chemotherapy* 16 (6): 356–70. https://doi.org/10.1159/000220750.

Acocella, Gianni. 1983. "Pharmacokinetics and Metabolism of Rifampin in Humans." *Clinical Infectious Diseases* 5 (Supplement_3): S428–32. https://doi.org/10.1093/clinids/5.Supplement_3.S428.

Adams, Craig H., Cedric J. Werely, Thomas C. Victor, Eileen G. Hoal, Gawie Rossouw, and Paul D. van Helden. 2003. "Allele Frequencies for Glutathione S-Transferase and N-Acetyltransferase 2

Differ in African Population Groups and May Be Associated with Oesophageal Cancer or Tuberculosis Incidence." *Clinical Chemistry and Laboratory Medicine* 41 (4): 600–605. https://doi.org/10.1515/CCLM.2003.090.

Alghamdi, Wael A., Mohammad H. Al-Shaer, Guohua An, Abdullah Alsultan, Maia Kipiani, Ketevan Barbakadze, Lali Mikiashvili, et al. 2020. "Population Pharmacokinetics of Linezolid in Tuberculosis Patients: Dosing Regimen Simulation and Target Attainment Analysis." *Antimicrobial Agents and Chemotherapy* 64 (10). https://doi.org/10.1128/AAC.01174-20.

Alghamdi, Wael A., Mohammad H. Al-Shaer, and Charles A. Peloquin. 2018. "Protein Binding of First-Line Antituberculosis Drugs." *Antimicrobial Agents and Chemotherapy* 62 (7). https://doi.org/10.1128/AAC.00641-18.

Alipanah, Narges, Leah Jarlsberg, Cecily Miller, Nguyen Nhat Linh, Dennis Falzon, Ernesto Jaramillo, and Payam Nahid. 2018. "Adherence Interventions and Outcomes of Tuberculosis Treatment: A Systematic Review and Meta-Analysis of Trials and Observational Studies." https://doi.org/10.1371/journal.pmed.1002595.

Anderson, B. J., and N. H.G. Holford. 2008. "Mechanism-Based Concepts of Size and Maturity in Pharmacokinetics." *Annual Review of Pharmacology and Toxicology* 48: 303–32. https://doi.org/10.1146/annurev.pharmtox.48.113006.094708.

Anderson, Brian J., and Nick H.G. Holford. 2009. "Mechanistic Basis of Using Body Size and Maturation to Predict Clearance in Humans." *Drug Metabolism and Pharmacokinetics* 24 (1): 25–36. https://doi.org/10.2133/dmpk.24.25.

Androulakis, Ioannis P. 2016. "Quantitative Systems Pharmacology: A Framework for Context." *Current Pharmacology Reports 2016 2:3* 2 (3): 152–60. https://doi.org/10.1007/S40495-016-0058-X.

Asaumi, Ryuta, Karsten Menzel, Wooin Lee, Ken ichi Nunoya, Haruo Imawaka, Hiroyuki Kusuhara, and Yuichi Sugiyama. 2019. "Expanded Physiologically-Based Pharmacokinetic Model of Rifampicin for Predicting Interactions With Drugs and an Endogenous Biomarker via Complex Mechanisms Including Organic Anion Transporting Polypeptide 1B Induction." *CPT: Pharmacometrics & Systems Pharmacology* 8 (11): 845–57.

https://doi.org/10.1002/PSP4.12457.

Bartanusz, Viktor, Daniela Jezova, Betty Alajajian, and Murat Digicaylioglu. 2011. "The Blood–Spinal Cord Barrier: Morphology and Clinical Implications." *Annals of Neurology* 70 (2): 194–206. https://doi.org/10.1002/ana.22421.

Battal, B, M Kocaoglu, N Bulakbasi, G Husmen, H Tuba Sanal, and C Tayfun. 2011. "Cerebrospinal Fluid Flow Imaging by Using Phase-Contrast MR Technique." *The British Journal of Radiology* 84: 758–65. https://doi.org/10.1259/bjr/66206791.

Beal, S. L. 2001. "Ways to Fit a PK Model with Some Data below the Quantification Limit." *Journal of Pharmacokinetics and Pharmacodynamics* 28 (5): 481–504. https://doi.org/10.1023/A:1012299115260.

Beal, Stuart L, Alison J Boeckmann, and Lewis B Sheiner. 2017. "NONMEM 7.4.3. User Guide - Part VI PREDPP Guide," no. April.

Becker, C., J. B. Dressman, G. L. Amidon, H. E. Junginger, S. Kopp, K. K. Midha, V. P. Shah, S. Stavchansky, and D. M. Barends. 2008. "Biowaiver Monographs for Immediate Release Solid Oral Dosage Forms: Pyrazinamide." *Journal of Pharmaceutical Sciences* 97 (9): 3709–20. https://doi.org/10.1002/jps.21250.

Becker, C., J.B. Dressman, G.L. Amidon, H.E. Junginger, S. Kopp, K.K. Midha, V.P. Shah, S. Stavchansky, and D.M. Barends. 2007. "Biowaiver Monographs for Immediate Release Solid Oral Dosage Forms: Isoniazid**A Project of the International Pharmaceutical Federation FIP, Groupe BCS, Www.Fip.Org/Bcs." *Journal of Pharmaceutical Sciences* 96 (3): 522–31. https://doi.org/10.1002/jps.20765.

Becker, C., J.B. B. Dressman, H.E. E. Junginger, S. Kopp, K.K. K. Midha, V.P. P. Shah, S. Stavchansky, and D.M. M. Barends. 2009. "Biowaiver Monographs for Immediate Release Solid Oral Dosage Forms: Rifampicin." *Journal of Pharmaceutical Sciences* 98 (7): 2252–67. https://doi.org/10.1002/jps.21624.

Beer, Ronny, Bettina Pfausler, and Erich Schmutzhard. 2009. "Management of Nosocomial External Ventricular Drain-Related Ventriculomeningitis." *Neurocritical Care* 10 (3): 363–67. https://doi.org/10.1007/s12028-008-9155-y.

Bhatt, Kamlesh, and Padmini Salgame. 2007. "Host Innate Immune Response to Mycobacterium Tuberculosis." *Journal of Clinical Immunology* 27 (4): 347–62. https://doi.org/10.1007/s10875-007-9084-0.

Blot, Stijn I., Federico Pea, and Jeffrey Lipman. 2014. "The Effect of Pathophysiology on Pharmacokinetics in the Critically Ill Patient--Concepts Appraised by the Example of Antimicrobial Agents." *Advanced Drug Delivery Reviews* 77 (November): 3–11. https://doi.org/10.1016/j.addr.2014.07.006.

Boeree, Martin J., Andreas H. Diacon, Rodney Dawson, Kim Narunsky, Jeannine Du Bois, Amour Venter, Patrick P.J. Phillips, et al. 2015. "A Dose-Ranging Trial to Optimize the Dose of Rifampin in the Treatment of Tuberculosis." *American Journal of Respiratory and Critical Care Medicine* 191 (9): 1058–65. https://doi.org/10.1164/RCCM.201407-1264OC/SUPPL_FILE/DISCLOSURES.PDF.

Boman, G., and V. A. Ringberger. 1974. "Binding of Rifampicin by Human Plasma Proteins." *European Journal of Clinical Pharmacology* 7 (5): 369–73. https://doi.org/10.1007/BF00558209.

Bonate, Peter L. 2013. *Pharmacokinetic-Pharmacodynamic Modeling and Simulation*. 2nd ed. Vol. 53. https://doi.org/10.1017/CBO9781107415324.004.

Brake, Lindsey H.M. Te, Frans G.M. Russel, Jeroen J.M.W. Van Den Heuvel, Gerjo J. De Knegt, Jurriaan E. De Steenwinkel, David M. Burger, Rob E. Aarnoutse, and Jan B. Koenderink. 2016. "Inhibitory Potential of Tuberculosis Drugs on ATP-Binding Cassette Drug Transporters." *Tuberculosis* 96 (January): 150–57. https://doi.org/10.1016/J.TUBE.2015.08.004.

Brake, Lindsey HM te, Veronique de Jager, Kim Narunsky, Naadira Vanker, Elin M Svensson, Patrick PJ Phillips, Stephen H Gillespie, et al. 2021. "Increased Bactericidal Activity but Dose-Limiting Intolerability at 50 Mg·kg −1 Rifampicin." *Eur Respir J* 58. https://doi.org/10.1183/13993003.00955-2020.

Brenchley, Jason M., David A. Price, Timothy W. Schacker, Tedi E. Asher, Guido Silvestri, Srinivas Rao, Zachary Kazzaz, et al. 2006. "Microbial Translocation Is a Cause of Systemic Immune Activation in Chronic HIV Infection." *Nature Medicine* 12 (12): 1365–71. https://doi.org/10.1038/nm1511.

Brust, James C.M., Neel R. Gandhi, Sean Wasserman, Gary Maartens, Shaheed V. Omar, Nazir A. Ismail, Angela Campbell, et al. 2021. "Effectiveness and Cardiac Safety of Bedaquiline-Based Therapy for Drug-Resistant Tuberculosis: A Prospective Cohort Study." *Clinical Infectious Diseases: An Official Publication of the Infectious Diseases Society of America* 73 (11): 2083. https://doi.org/10.1093/CID/CIAB335.

Burman, W. J., K. Gallicano, and C. Peloquin. 2001. "Comparative Pharmacokinetics and Pharmacodynamics of the Rifamycin Antibacterials." *Clinical Pharmacokinetics* 40 (5): 327–41. https://doi.org/10.2165/00003088-200140050-00002.

Chen, Jiezhong, and Kenneth Raymond. 2006. "Roles of Rifampicin in Drug-Drug Interactions: Underlying Molecular Mechanisms Involving the Nuclear Pregnane X Receptor." *Annals of Clinical Microbiology and Antimicrobials* 5 (1): 3. https://doi.org/10.1186/1476-0711-5-3.

Chen, Ricky Hao, Thi Anh Nguyen, Hannah Yejin Kim, Sophie L. Stocker, and Jan Willem C. Alffenaar. 2025. "Saliva-Based Point-of-Care Assay to Measure the Concentration of Pyrazinamide Using a Mobile UV Spectrophotometer." *Journal of Antimicrobial Chemotherapy* 80 (1): 254–61. https://doi.org/10.1093/JAC/DKAE404.

Chen, Xueyi, Bhavatharini Arun, Oscar J. Nino-Meza, Mona O. Sarhan, Medha Singh, Byeonghoon Jeon, Kishor Mane, et al. 2024. "Dynamic PET Reveals Compartmentalized Brain and Lung Tissue Antibiotic Exposures of Tuberculosis Drugs." *Nature Communications 2024 15:1* 15 (1): 1–11. https://doi.org/10.1038/s41467-024-50989-4.

Chen, Yuping, Stephen S. Ferguson, Masahiko Negishi, and Joyce A. Goldstein. 2004. "Induction of Human CYP2C9 by Rifampicin, Hyperforin, and Phenobarbital Is Mediated by the Pregnane X Receptor." *Journal of Pharmacology and Experimental Therapeutics* 308 (2): 495–501. https://doi.org/10.1124/jpet.103.058818.

Chiang, Silvia S., Faiz Ahmad Khan, Meredith B. Milstein, Arielle W. Tolman, Andrea Benedetti, Jeffrey R. Starke, and Mercedes C. Becerra. 2014. "Treatment Outcomes of Childhood Tuberculous Meningitis: A Systematic Review and Meta-Analysis." *The Lancet. Infectious Diseases* 14 (10): 947–57. https://doi.org/10.1016/S1473-3099(14)70852-7.

Chigutsa, Emmanuel, Jotam G. Pasipanodya, Marianne E. Visser, Paul D. van Helden, Peter J. Smith,

Frederick A. Sirgel, Tawanda Gumbo, and Helen McIlleron. 2015. "Impact of Nonlinear Interactions of Pharmacokinetics and MICs on Sputum Bacillary Kill Rates as a Marker of Sterilizing Effect in Tuberculosis." *Antimicrobial Agents and Chemotherapy* 59 (1): 38–45. https://doi.org/10.1128/AAC.03931-14.

Chirehwa, M T, R Rustomjee, T Mthiyane, P Onyebujoh, P Smith, H McIlleron, and P Denti. 2015. "Model-Based Evaluation of Higher Doses of Rifampin Using a Semimechanistic Model Incorporating Autoinduction and Saturation of Hepatic Extraction.[Erratum Appears in Antimicrob Agents Chemother. 2016 May;60(5):3262; PMID: 27107106]." *Antimicrobial Agents & Chemotherapy* 60 (1): 487–94. https://doi.org/10.1128/AAC.01830-15.Address.

Chirehwa, Maxwell T., Helen McIlleron, Roxana Rustomjee, Thuli Mthiyane, Philip Onyebujoh, Peter Smith, and Paolo Denti. 2017. "Pharmacokinetics of Pyrazinamide and Optimal Dosing Regimens for Drug-Sensitive and -Resistant Tuberculosis." *Antimicrobial Agents and Chemotherapy* 61 (8): 8–13. https://doi.org/10.1128/AAC.00490-17.

Chopra, Neha, Spiro Menounos, Jaesung P. Choi, Philip M. Hansbro, Ashish D. Diwan, and Abhirup Das. 2021. "Blood-Spinal Cord Barrier: Its Role in Spinal Disorders and Emerging Therapeutic Strategies." *NeuroSci 2022, Vol. 3, Pages 1-27* 3 (1): 1–27. https://doi.org/10.3390/NEUROSCI3010001.

Cockcroft, D. W., and M. H. Gault. 1976. "Prediction of Creatinine Clearance from Serum Creatinine." *Nephron* 16 (1): 31–41. https://doi.org/10.1159/000180580.

Conradie, Francesca, Andreas H. Diacon, Nosipho Ngubane, Pauline Howell, Daniel Everitt, Angela M. Crook, Carl M. Mendel, et al. 2020. "Treatment of Highly Drug-Resistant Pulmonary Tuberculosis." *New England Journal of Medicine* 382 (10): 893–902. https://doi.org/10.1056/NEJMOA1901814/SUPPL_FILE/NEJMOA1901814_DATA-SHARING.PDF.

Court, R., M. T. Chirehwa, L. Wiesner, B. Wright, W. Smythe, N. Kramer, and H. McIlleron. 2018. "Quality Assurance of Rifampicin-Containing Fixed-Drug Combinations in South Africa: Dosing Implications." *International Journal of Tuberculosis and Lung Disease* 22 (5): 537–43. https://doi.org/10.5588/IJTLD.17.0697.

Cresswell, Fiona V., Lindsey Te Brake, Rachel Atherton, Rovina Ruslami, Kelly E. Dooley, Rob Aarnoutse, and Reinout Van Crevel. 2019. "Intensified Antibiotic Treatment of Tuberculosis Meningitis." *Expert Review of Clinical Pharmacology* 12 (3): 267–88. https://doi.org/10.1080/17512433.2019.1552831.

Cresswell, Fiona V., David B. Meya, Enock Kagimu, Daniel Grint, Lindsey Te Brake, John Kasibante, Emily Martyn, et al. 2021. "High-Dose Oral and Intravenous Rifampicin for the Treatment of Tuberculous Meningitis in Predominantly Human Immunodeficiency Virus (HIV)-Positive Ugandan Adults: A Phase II Open-Label Randomized Controlled Trial." *Clinical Infectious Diseases* 73 (5): 876–84. https://doi.org/10.1093/cid/ciab162.

Dartois, Véronique. 2014. "The Path of Anti-Tuberculosis Drugs: From Blood to Lesions to Mycobacterial Cells." *Nature Reviews. Microbiology* 12 (3): 159. https://doi.org/10.1038/NRMICRO3200.

Daskapan, Alper, Lusiana R. Idrus, Maarten J. Postma, Bob Wilffert, Jos G. W. Kosterink, Ymkje Stienstra, Daniel J. Touw, et al. 2019. "A Systematic Review on the Effect of HIV Infection on the Pharmacokinetics of First-Line Tuberculosis Drugs." *Clinical Pharmacokinetics* 58 (6): 747–66. https://doi.org/10.1007/s40262-018-0716-8.

Davis, Angharad G., Ursula Karin Rohlwink, Alizé Proust, Anthony A. Figaji, and Robert J. Wilkinson. 2019. "The Pathogenesis of Tuberculous Meningitis." *Journal of Leukocyte Biology* 105 (2): 267–80. https://doi.org/10.1002/JLB.MR0318-102R.

Davis, Angharad G., Sean Wasserman, Mpumi Maxebengula, Cari Stek, Marise Bremer, Remy Daroowala, Saalikha Aziz, et al. 2021. "Study Protocol for a Phase 2A Trial of the Safety and Tolerability of Increased Dose Rifampicin and Adjunctive Linezolid, with or without Aspirin, for HIV-Associated Tuberculous Meningitis [LASER-TBM]." *Wellcome Open Research* 6 (June): 136. https://doi.org/10.12688/wellcomeopenres.16783.1.

Davis, Angharad G, Sean Wasserman, Cari Stek, Mpumi Maxebengula, C Jason Liang, Stephani Stegmann, Sonya Koekemoer, et al. 2023. "A Phase 2A Trial of the Safety and Tolerability of Increased Dose Rifampicin and Adjunctive Linezolid, With or Without Aspirin, for Human Immunodeficiency Virus–Associated Tuberculous Meningitis: The LASER-TBM Trial." *Clinical*

Infectious Diseases 76 (8): 1412–22. https://doi.org/10.1093/cid/ciac932.

Deming, W E. 1943. *Statistical Adjustment of Data. Statistical Adjustment of Data.* Oxford, England: Wiley.

Denti, Paolo, Kidola Jeremiah, Emmanuel Chigutsa, Daniel Faurholt-Jepsen, George PrayGod, Nyagosya Range, Sandra Castel, et al. 2015. "Pharmacokinetics of Isoniazid, Pyrazinamide, and Ethambutol in Newly Diagnosed Pulmonary TB Patients in Tanzania." *PLoS ONE* 10 (10): 1–19. https://doi.org/10.1371/journal.pone.0141002.

Denti, Paolo, Roeland E Wasmann, Annelies van Rie, Jana Winckler, Adrie Bekker, Helena Rabie, Anneke C Hesseling, et al. 2021. "Optimizing Dosing and Fixed-Dose Combinations of Rifampicin, Isoniazid, and Pyrazinamide in Pediatric Patients With Tuberculosis: A Prospective Population Pharmacokinetic Study." *Clinical Infectious Diseases*, October. https://doi.org/10.1093/CID/CIAB908.

Dheda, Keertan, Tawanda Gumbo, Gary Maartens, Kelly E Dooley, Ruth McNerney, Megan Murray, Jennifer Furin, et al. 2017. "The Epidemiology, Pathogenesis, Transmission, Diagnosis, and Management of Multidrug-Resistant, Extensively Drug-Resistant, and Incurable Tuberculosis." *The Lancet Respiratory Medicine* 5 (4): 291–360. https://doi.org/10.1016/S2213-2600(17)30079-6.

Diczfalusy, Ulf, Hanna Nylén, Pontus Elander, and Leif Bertilsson. 2011. "4β-Hydroxycholesterol, an Endogenous Marker of CYP3A4/5 Activity in Humans." *British Journal of Clinical Pharmacology* 71 (2): 183. https://doi.org/10.1111/J.1365-2125.2010.03773.X.

Dodd, Peter J., Muhammad Osman, Fiona V. Cresswell, Anna M Stadelman, Nguyen Huu Lan, Nguyen Thuy Thuong Thuong, Morris Muzyamba, Lisa Glaser, Sicelo S Dlamini, and James A. Seddon. 2021. "The Global Burden of Tuberculous Meningitis in Adults: A Modelling Study." Edited by María Elvira Balcells. *PLOS Global Public Health* 1 (12): e0000069. https://doi.org/10.1371/journal.pgph.0000069.

Dodd, Peter J., Courtney M. Yuen, Charalambos Sismanidis, James A. Seddon, and Helen E. Jenkins. 2017. "The Global Burden of Tuberculosis Mortality in Children: A Mathematical Modelling Study." *The Lancet Global Health* 5 (9): e898–906. https://doi.org/10.1016/S2214-

109X(17)30289-9.

Donald, P. R. 2010. "Cerebrospinal Fluid Concentrations of Antituberculosis Agents in Adults and Children." *Tuberculosis* 90 (5): 279–92. https://doi.org/10.1016/j.tube.2010.07.002.

Donald, P. R., J. S. Maritz, and A. H. Diacon. 2011. "The Pharmacokinetics and Pharmacodynamics of Rifampicin in Adults and Children in Relation to the Dosage Recommended for Children." *Tuberculosis (Edinburgh, Scotland)* 91 (3): 196–207. https://doi.org/10.1016/j.tube.2011.02.004.

Dosne, Anne-Gaëlle, Martin Bergstrand, and Mats O. Karlsson. 2017. "An Automated Sampling Importance Resampling Procedure for Estimating Parameter Uncertainty." *Journal of Pharmacokinetics and Pharmacodynamics* 44 (6): 509–20. https://doi.org/10.1007/s10928-017-9542-0.

Dosne, Anne Gaëlle, Martin Bergstrand, Kajsa Harling, and Mats O. Karlsson. 2016. "Improving the Estimation of Parameter Uncertainty Distributions in Nonlinear Mixed Effects Models Using Sampling Importance Resampling." *Journal of Pharmacokinetics and Pharmacodynamics* 43 (6): 583–96. https://doi.org/10.1007/s10928-016-9487-8.

Dousa, Khalid M., Sebastian G. Kurz, Charles M. Bark, Robert A. Bonomo, and Jennifer J. Furin. 2020. "Drug-Resistant Tuberculosis: A Glance at Progress and Global Challenges." *Infectious Disease Clinics of North America* 34 (4): 863–86. https://doi.org/10.1016/J.IDC.2020.06.001.

Dryden, Matthew S. 2011. "Linezolid Pharmacokinetics and Pharmacodynamics in Clinical Treatment." *Journal of Antimicrobial Chemotherapy* 66 (Supplement 4): iv7–15. https://doi.org/10.1093/jac/dkr072.

Egelund, E. F., A. Alsultan, and C. A. Peloquin. 2015. "Optimizing the Clinical Pharmacology of Tuberculosis Medications." *Clinical Pharmacology & Therapeutics* 98 (4): 387–93. https://doi.org/10.1002/CPT.180.

Egle, Hannes, Rainer Trittler, Klaus Kümmerer, and Sebastian W. Lemmen. 2005. "Linezolid and Rifampin: Drug Interaction Contrary to Expectations?" *Clinical Pharmacology & Therapeutics* 77 (5): 451–53. https://doi.org/10.1016/J.CLPT.2005.01.020.

Ellard, Gordon A., and Patricia T. Gammon. 1976. "Pharmacokinetics of Isoniazid Metabolism in

Man." *Journal of Pharmacokinetics and Biopharmaceutics* 4 (2): 83–113. https://doi.org/10.1007/BF01086149.

Erwin, Emily R., Angela P. Addison, Sarah Finney John, Omonike Arike Olaleye, and Rosemarie C. Rosell. 2019. "Pharmacokinetics of Isoniazid: The Good, the Bad, and the Alternatives." *Tuberculosis* 116 (November 2018): S66–70. https://doi.org/10.1016/j.tube.2019.04.012.

Ette, Ene I., and Paul J. Williams. 2007. *Pharmacometrics The Science of Quantitative Pharmacology*.

Farmer, Kevin C. 1999. "Methods for Measuring and Monitoring Medication Regimen Adherence in Clinical Trials and Clinical Practice." *Clinical Therapeutics* 21 (6): 1074–90. https://doi.org/10.1016/S0149-2918(99)80026-5.

Fermeli, Dionysia D., Theodoros D. Marantos, Alexandros Leonidas D. Liarakos, George D. Panayiotakopoulos, Vasileios K. Dedes, and Georgios I. Panoutsopoulos. 2020. "Linezolid: A Promising Agent for the Treatment of Multiple and Extensively Drug-Resistant Tuberculosis." *Folia Medica* 62 (3): 444–52. https://doi.org/10.3897/folmed.62.e48742.

Figaji, a a, a G Fieggen, and J C Peter. 2003. "Endoscopic Third Ventriculostomy in Tuberculous Meningitis." *Child's Nervous System* 19 (4): 217–25. https://doi.org/10.1007/s00381-003-0730-4.

Figaji, Anthony A., and A. Graham Fieggen. 2010. "The Neurosurgical and Acute Care Management of Tuberculous Meningitis: Evidence and Current Practice." *Tuberculosis* 90 (6): 393–400. https://doi.org/10.1016/j.tube.2010.09.005.

Finch, Christopher K., Cary R. Chrisman, Anne M. Baciewicz, and Timothy H. Self. 2002. "Rifampin and Rifabutin Drug Interactions: An Update." *Archives of Internal Medicine* 162 (9): 985–92. https://doi.org/10.1001/ARCHINTE.162.9.985.

Fontes, Fabio L., Steven A. Rooker, Jamie K. Lynn-Barbe, Michael A. Lyons, Debbie C. Crans, and Dean C. Crick. 2024. "Pyrazinoic Acid, the Active Form of the Anti-Tuberculosis Drug Pyrazinamide, and Aromatic Carboxylic Acid Analogs Are Protonophores." *Frontiers in Molecular Biosciences* 11 (February): 1350699. https://doi.org/10.3389/FMOLB.2024.1350699/BIBTEX.

Fox, W, G A Ellard, and D A Mitchison. 1999. "Studies on the Treatment of Tuberculosis Undertaken

by the British Medical Research Council Tuberculosis Units, 1946-1986, with Relevant Subsequent Publications." *The International Journal of Tuberculosis and Lung Disease : The Official Journal of the International Union against Tuberculosis and Lung Disease* 3 (10 Suppl 2): S231-79. http://www.ncbi.nlm.nih.gov/pubmed/10529902.

Gafar, Fajri, Roeland E. Wasmann, Helen M. McIlleron, Rob E. Aarnoutse, H. Simon Schaaf, Ben J. Marais, Dipti Agarwal, et al. 2023. "Global Estimates and Determinants of Antituberculosis Drug Pharmacokinetics in Children and Adolescents: A Systematic Review and Individual Patient Data Meta-Analysis." *European Respiratory Journal* 61 (3). https://doi.org/10.1183/13993003.01596-2022.

Gandelman, Kuan, Tong Zhu, Odette A. Fahmi, Paul Glue, Kenny Lian, R. Scott Obach, and Bharat Damle. 2011. "Unexpected Effect of Rifampin on the Pharmacokinetics of Linezolid: In Silico and In Vitro Approaches to Explain Its Mechanism." *The Journal of Clinical Pharmacology* 51 (2): 229–36. https://doi.org/10.1177/0091270010366445.

Garcia-Prats, Anthony J., H. Simon Schaaf, Heather R. Draper, Maria Garcia-Cremades, Jana Winckler, Lubbe Wiesner, Anneke C. Hesseling, and Rada M. Savic. 2019. "Pharmacokinetics, Optimal Dosing, and Safety of Linezolid in Children with Multidrug-Resistant Tuberculosis: Combined Data from Two Prospective Observational Studies." Edited by Claudia M. Denkinger. *PLoS Medicine* 16 (4): e1002789. https://doi.org/10.1371/journal.pmed.1002789.

Garcia-Prats, Anthony J, Elin M Svensson, Jana Winckler, Heather R Draper, Lee Fairlie, Louvina E van der Laan, Masebole Masenya, et al. 2021. "Pharmacokinetics and Safety of High-Dose Rifampicin in Children with TB: The Opti-Rif Trial." *Journal of Antimicrobial Chemotherapy* 76 (12): 3237–46. https://doi.org/10.1093/jac/dkab336.

Gausi, Kamunkhwala, Elisa H. Ignatius, Xin Sun, Soyeon Kim, Laura Moran, Lubbe Wiesner, Florian von Groote-Bidlingmaier, et al. 2021. "A Semi-Mechanistic Model of the Bactericidal Activity of High-Dose Isoniazid against Multi-Drug-Resistant Tuberculosis." *American Journal of Respiratory and Critical Care Medicine*.

Gebhart, Benjamin C., Brian C. Barker, and Boaz A. Markewitz. 2007. "Decreased Serum Linezolid Levels in a Critically Ill Patient Receiving Concomitant Linezolid and Rifampin."

Pharmacotherapy 27 (3): 476–79. https://doi.org/10.1592/PHCO.27.3.476.

Gumbo, Tawanda, Arnold Louie, Mark R. Deziel, Weiguo Liu, Linda M. Parsons, Max Salfinger, and George L. Drusano. 2007. "Concentration-Dependent Mycobacterium Tuberculosis Killing and Prevention of Resistance by Rifampin." *Antimicrobial Agents and Chemotherapy* 51 (11): 3781–88.

Gupta, Amita, Girish Nadkarni, Wei Teng Yang, Aditya Chandrasekhar, Nikhil Gupte, Gregory P. Bisson, Mina Hosseinipour, and Naveen Gummadi. 2011. "Early Mortality in Adults Initiating Antiretroviral Therapy (ART) in Low- and Middle-Income Countries (LMIC): A Systematic Review and Meta-Analysis." *PLOS ONE* 6 (12): e28691. https://doi.org/10.1371/JOURNAL.PONE.0028691.

Hallare, Jericho, and Valerie Gerriets. 2023. "Half Life - StatPearls - NCBI Bookshelf." 2023. https://www.ncbi.nlm.nih.gov/books/NBK554498/.

Hashemian, Seyed Mohammad Reza, Tayebeh Farhadi, and Mojdeh Ganjparvar. 2018. "Linezolid: A Review of Its Properties, Function, and Use in Critical Care." *Drug Design, Development and Therapy* 12 (June): 1759–67. https://doi.org/10.2147/DDDT.S164515.

Hashimoto, Satsuki, Kyoko Honda, Kohei Fujita, Yuka Miyachi, Kazuya Isoda, Ko Misaka, Yukio Suga, et al. 2018. "Effect of Coadministration of Rifampicin on the Pharmacokinetics of Linezolid: Clinical and Animal Studies." *Journal of Pharmaceutical Health Care and Sciences* 4 (1): 1–9. https://doi.org/10.1186/s40780-018-0123-1.

Hedaya, Mohsen A. 2012. *Basic Pharmacokinetics*. Routledge. https://doi.org/10.1201/b11681.

Hill, Martha N., Nancy Houston Miller, and Sabina DeGeest. 2011. "Adherence and Persistence with Taking Medication to Control High Blood Pressure." *Journal of the American Society of Hypertension* 5 (1): 56–63. https://doi.org/10.1016/j.jash.2011.01.001.

Hoefnagel, D., R. Dammers, M. P. Ter Laak-Poort, and C. J.J. Avezaat. 2008. "Risk Factors for Infections Related to External Ventricular Drainage." *Acta Neurochirurgica* 150 (3): 209–14. https://doi.org/10.1007/s00701-007-1458-9.

Hole, Kristine, Birgit M. Wollmann, Camilla Nguyen, Tore Haslemo, and Espen Molden. 2018. "Comparison of CYP3A4-Inducing Capacity of Enzyme-Inducing Antiepileptic Drugs Using 4b-

Hydroxycholesterol as Biomarker." *Therapeutic Drug Monitoring* 40 (4): 463–68. https://doi.org/10.1097/FTD.0000000000000518.

Holford, Nick H.G., and Brian J. Anderson. 2017. "Allometric Size: The Scientific Theory and Extension to Normal Fat Mass." *European Journal of Pharmaceutical Sciences* 109 (May): S59–64. https://doi.org/10.1016/j.ejps.2017.05.056.

Hong, Eunjin, Lisa M. Almond, Peter S. Chung, Adupa P. Rao, and Paul M. Beringer. 2022. "Physiologically-Based Pharmacokinetic-Led Guidance for Patients With Cystic Fibrosis Taking Elexacaftor-Tezacaftor-Ivacaftor With Nirmatrelvir-Ritonavir for the Treatment of COVID-19." *Clinical Pharmacology & Therapeutics* 111 (6): 1324–33. https://doi.org/10.1002/CPT.2585.

Hosseinipour, Mina C., Gregory P. Bisson, Sachiko Miyahara, Xin Sun, Agnes Moses, Cynthia Riviere, Fredrick K. Kirui, et al. 2016. "Empirical Tuberculosis Therapy versus Isoniazid in Adult Outpatients with Advanced HIV Initiating Antiretroviral Therapy (REMEMBER): A Multicountry Open-Label Randomised Controlled Trial." *The Lancet* 387 (10024): 1198–1209. https://doi.org/10.1016/S0140-6736(16)00546-8.

Imperial, Marjorie Z., Jerry R. Nedelman, Francesca Conradie, and R. M. Savic. 2022. "Proposed Linezolid Dosing Strategies to Minimize Adverse Events for Treatment of Extensively Drug-Resistant Tuberculosis." *Clinical Infectious Diseases* 74 (10): 1736–47. https://doi.org/10.1093/cid/ciab699.

Ingen, Jakko Van, Rob E. Aarnoutse, Peter R. Donald, Andreas H. Diacon, Rodney Dawson, Georgette Plemper Van Balen, Stephen H. Gillespie, and Martin J. Boeree. 2011. "Why Do We Use 600 Mg of Rifampicin in Tuberculosis Treatment?" *Clinical Infectious Diseases* 52 (9): e194–99. https://doi.org/10.1093/CID/CIR184.

Jaipuriar, Ravi Shekhar, Ravindra Kumar Garg, Imran Rizvi, Hardeep Singh Malhotra, Neeraj Kumar, Amita Jain, Rajesh Verma, Praveen Kumar Sharma, Shweta Pandey, and Ravi Uniyal. 2019. "Early Mortality among Immunocompetent Patients of Tuberculous Meningitis: A Prospective Study." *The American Journal of Tropical Medicine and Hygiene* 101 (2): 357–61. https://doi.org/10.4269/ajtmh.19-0098.

Jamis-Dow, C. A., A. G. Katki, J. M. Collins, and R. W. Klecker. 1997. "Rifampin and Rifabutin and

Their Metabolism by Human Liver Esterases." *Xenobiotica* 27 (10): 1015–24. https://doi.org/10.1080/004982597239994.

Janmahasatian, Sarayut, Stephen B Duffull, Susan Ash, Leigh C Ward, Nuala M Byrne, and Bruce Green. 2005. "Quantification of Lean Bodyweight." *Clin Pharmacokinet* 44: 1051–65.

Jeremiah, Kidola, Paolo Denti, Emmanuel Chigutsa, Daniel Faurholt-Jepsen, George PrayGod, Nyagosya Range, Sandra Castel, et al. 2014. "Nutritional Supplementation Increases Rifampin Exposure among Tuberculosis Patients Coinfected with HIV." *Antimicrobial Agents and Chemotherapy* 58 (6): 3468–74. https://doi.org/10.1128/AAC.02307-13.

Johansson, Åsa M., and Mats O. Karlsson. 2013. "Multiple Imputation of Missing Covariates in NONMEM and Evaluation of the Method's Sensitivity to η-Shrinkage." *AAPS Journal* 15 (4): 1035–42. https://doi.org/10.1208/s12248-013-9508-0.

Joint United Nations Programme on HIV/AIDS (UNAIDS). 2024. "Fact Sheet 2024 - Latest Global and Regional HIV Statistics on the Status of the AIDS Epidemic." https://www.unaids.org/en.

Jonsson, E. Niclas, and Joakim Nyberg. 2022. "A Quantitative Approach to the Choice of Number of Samples for Percentile Estimation in Bootstrap and Visual Predictive Check Analyses." *CPT: Pharmacometrics & Systems Pharmacology* 11 (6): 673. https://doi.org/10.1002/PSP4.12790.

Kamp, Jasper, Mathieu S. Bolhuis, Simon Tiberi, Onno W. Akkerman, Rosella Centis, Wiel C. de Lange, Jos G. Kosterink, Tjip S. van der Werf, Giovanni B. Migliori, and Jan Willem C. Alffenaar. 2017. "Simple Strategy to Assess Linezolid Exposure in Patients with Multi-Drug-Resistant and Extensively-Drug-Resistant Tuberculosis." *International Journal of Antimicrobial Agents* 49 (6): 688–94. https://doi.org/10.1016/j.ijantimicag.2017.01.017.

Kaojarern, Sming, Kingfah Supmonchai, Prida Phuapradit, Chintana Mokkhavesa, and sarinee Krittiyanunt. 1991. "Effect of Steroids on Cerebrospinal Fluid Penetration of Antituberculous Drugs in Tuberculous Meningitis." *Clinical Pharmacology and Therapeutics* 49 (1): 6–12. https://doi.org/10.1038/CLPT.1991.2.

Keizer, R. J., M. O. Karlsson, and A. Hooker. 2013. "Modeling and Simulation Workbench for NONMEM: Tutorial on Pirana, PsN, and Xpose." *CPT: Pharmacometrics and Systems Pharmacology* 2 (6): 1–9. https://doi.org/10.1038/psp.2013.24.

Kempker, Russell R, Alison G C Smith, Teona Avaliani, Mariam Gujabidze, Tinatin Bakuradze, Shorena Sabanadze, Zaza Avaliani, et al. 2022. "Cycloserine and Linezolid for Tuberculosis Meningitis: Pharmacokinetic Evidence of Potential Usefulness." *Clinical Infectious Diseases* 75 (4): 682–89. https://doi.org/10.1093/cid/ciab992.

Kengo, Allan, Ruth Nabisere, Kamunkhwala Gausi, Joseph Musaazi, Allan Buzibye, Denis Omali, Rob Aarnoutse, et al. 2023. "Dolutegravir Pharmacokinetics in Ugandan Patients with TB and HIV Receiving Standard- versus High-Dose Rifampicin." *Antimicrobial Agents and Chemotherapy* 67 (11). https://doi.org/10.1128/AAC.00430-23/SUPPL_FILE/AAC.00430-23-S0001.DOCX.

Kenneth L. Schaecher FACP, CPC, M D. 2013. "The Importance of Treatment Adherence in HIV." *Supplements and Featured Publications*, Addressing Adherence Challenges Associated With Antiretroviral Therapy: Focus on Noninfectious Diarr, 19 (12 Suppl). https://www.ajmc.com/view/a472_sep13_schaecher_s231.

Kenny, M. T., and B. Strates. 1981. "Metabolism and Pharmacokinetics of the Antibiotic Rifampin." *Drug Metabolism Reviews* 12 (1): 159–218. https://doi.org/10.3109/03602538109011084.

Kho, Chun Min, Siti Kartini Enche Ab Rahim, Zainal Arifin Ahmad, and Norazharuddin Shah Abdullah. 2017. "A Review on Microdialysis Calibration Methods: The Theory and Current Related Efforts." *Molecular Neurobiology* 54 (5): 3506–27. https://doi.org/10.1007/s12035-016-9929-8.

Kim, Andrew Hyoung Jin, Bora Kim, Su jin Rhee, Yujin Lee, Joong Shin Park, Seung Mi Lee, Sun Min Kim, et al. 2018. "Assessment of Induced CYP3A Activity in Pregnant Women Using 4β-Hydroxycholesterol: Cholesterol Ratio as an Appropriate Metabolic Marker." *Drug Metabolism and Pharmacokinetics* 33 (3): 173–78. https://doi.org/10.1016/J.DMPK.2018.04.004.

Koletsi, Despina, and Nikolaos Pandis. 2017. "Conditional Logistic Regression." https://doi.org/10.1016/j.ajodo.2017.04.009.

Kyeyune, Rachel, Saskia Den Boon, Adithya Cattamanchi, J. Lucian Davis, William Worodria, Samuel D. Yoo, and Laurence Huang. 2010. "Causes of Early Mortality in HIV-Infected TB Suspects in an East African Referral Hospital." *Journal of Acquired Immune Deficiency Syndromes* 55 (4): 446–50. https://doi.org/10.1097/QAI.0b013e3181eb611a.

Lacroix, C., T. Phan Hoang, J. Nouveau, C. Guyonnaud, G. Laine, H. Duwoos, and O. Lafont. 1989.

"Pharmacokinetics of Pyrazinamide and Its Metabolites in Healthy Subjects." *European Journal of Clinical Pharmacology* 36 (4): 395–400. https://doi.org/10.1007/BF00558302.

Lal, Satinder, S. N. Singhal, D. M. Burley, and G. Crossley. 1972. "Effect of Rifampicin and Isoniazid on Liver Function." *British Medical Journal* 1 (5793): 148–50. https://doi.org/10.1136/bmj.1.5793.148.

Lange, E.C.M. de. 1997. "Methodological Considerations of Intracerebral Microdialysis in Pharmacokinetic Studies on Drug Transport across the Blood–Brain Barrier." *Brain Research Reviews* 25 (1): 27–49. https://doi.org/10.1016/S0165-0173(97)00014-3.

Lange, Elizabeth C.M. De. 2013. "Utility of CSF in Translational Neuroscience." *Journal of Pharmacokinetics and Pharmacodynamics* 40 (3): 315–26. https://doi.org/10.1007/S10928-013-9301-9/FIGURES/7.

Lanni, Faye, Rosleine Antilus Sainte, Mark Hansen, Paul Parigi, Firat Kaya, Katherine LoMauro, Bernard Siow, et al. 2023. "A Preclinical Model of TB Meningitis to Determine Drug Penetration and Activity at the Sites of Disease." Edited by Jared A. Silverman. *Antimicrobial Agents and Chemotherapy* 67 (12). https://doi.org/10.1128/aac.00671-23.

Leach, Karen L., Steven J. Brickner, Mark C. Noe, and Paul F. Miller. 2011. "Linezolid, the First Oxazolidinone Antibacterial Agent." *Annals of the New York Academy of Sciences* 1222 (1): 49–54. https://doi.org/10.1111/j.1749-6632.2011.05962.x.

Li, Huimin, Jie Lu, Jinrong Liu, Yuhong Zhao, Xin Ni, and Shunying Zhao. 2016. "Linezolid Is Associated with Improved Early Outcomes of Childhood Tuberculous Meningitis." *The Pediatric Infectious Disease Journal* 35 (6): 607–10. https://doi.org/10.1097/INF.0000000000001114.

Lindbom, Lars, Jakob Ribbing, and E.Niclas Jonsson. 2004. "Perl-Speaks-NONMEM (PsN)—a Perl Module for NONMEM Related Programming." *Computer Methods and Programs in Biomedicine* 75 (2): 85–94. https://doi.org/10.1016/j.cmpb.2003.11.003.

Linnet, K. 1998. "Performance of Deming Regression Analysis in Case of Misspecified Analytical Error Ratio in Method Comparison Studies." *Clinical Chemistry* 44 (5): 1024–31. http://www.ncbi.nlm.nih.gov/pubmed/9590376.

Litjens, Carlijn H.C., Rob E. Aarnoutse, and Lindsey H.M. te Brake. 2020. "Preclinical Models to Optimize Treatment of Tuberculous Meningitis – A Systematic Review." *Tuberculosis* 122 (May): 101924. https://doi.org/10.1016/J.TUBE.2020.101924.

Litjens, Carlijn H C, Rob E Aarnoutse, Eleonora W J van Ewijk-Beneken Kolmer, Elin M Svensson, Angela Colbers, David M Burger, Martin J Boeree, et al. 2019. "Protein Binding of Rifampicin Is Not Saturated When Using High-Dose Rifampicin." *Journal of Antimicrobial Chemotherapy* 74 (4): 986–90. https://doi.org/10.1093/jac/dky527.

Loktionov, Alexandre, William Moore, Steven P. Spencer, Hester Vorster, Theo Nell, Ian K. O'Neill, Sheila A. Bingham, and John H. Cummings. 2002. "Differences in N-Acetylation Genotypes between Caucasians and Black South Africans: Implications for Cancer Prevention." *Cancer Detection and Prevention* 26 (1): 15–22. https://doi.org/10.1016/S0361-090X(02)00010-7.

Loos, U., E. Musch, J. C. Jensen, G. Mikus, H. K. Schwabe, and M. Eichelbaum. 1985. "Pharmacokinetics of Oral and Intravenous Rifampicin during Chronic Administration." *Klinische Wochenschrift* 63 (23): 1205–11. https://doi.org/10.1007/BF01733779.

Loxton, Nicholas W., Ursula K. Rohlwink, Mvuwo Tshavhungwe, Lindizwe Dlamini, Muki Shey, Nico Enslin, and Anthony Figaji. 2021. "A Pilot Study of Inflammatory Mediators in Brain Extracellular Fluid in Paediatric TBM." *PLOS ONE* 16 (3): e0246997. https://doi.org/10.1371/JOURNAL.PONE.0246997.

Maartens, Gary, and Constance A. Benson. 2015. "Linezolid for Treating Tuberculosis: A Delicate Balancing Act." *EBioMedicine* 2 (11): 1568. https://doi.org/10.1016/J.EBIOM.2015.10.014.

Mah, A., H. Kharrat, R. Ahmed, Z. Gao, E. Der, E. Hansen, R. Long, D. Kunimoto, and R. Cooper. 2015. "Serum Drug Concentrations of INH and RMP Predict 2-Month Sputum Culture Results in Tuberculosis Patients." *International Journal of Tuberculosis and Lung Disease* 19 (2): 210–15. https://doi.org/10.5588/ijtld.14.0405.

Manyelo, Charles M., Regan S. Solomons, Gerhard Walzl, and Novel N. Chegou. 2021. "Tuberculous Meningitis: Pathogenesis, Immune Responses, Diagnostic Challenges, and the Potential of Biomarker-Based Approaches." Edited by Colleen Suzanne Kraft. *Journal of Clinical Microbiology* 59 (3): 1–16. https://doi.org/10.1128/JCM.01771-20.

Mariappan, T. T., and Saranjit Singh. 2003. "Regional Gastrointestinal Permeability of Rifampicin and Isoniazid (Alone and Their Combination) in the Rat." *International Journal of Tuberculosis and Lung Disease* 7 (8): 797–803.

Mariappan, T.T., Saranjit Singh, Rajesh Pandey, and G.K. Khuller. 2005. "Determination of Absolute Bioavailability of Rifampicin by Varying the Mode of Intravenous Administration and the Time of Sampling." *Clinical Research and Regulatory Affairs* 22 (3–4): 119–28. https://doi.org/10.1080/10601330500371524.

Martino, Maurizio de, Lorenzo Lodi, Luisa Galli, and Elena Chiappini. 2019. "Immune Response to Mycobacterium Tuberculosis: A Narrative Review." *Frontiers in Pediatrics* 7 (August): 464617. https://doi.org/10.3389/FPED.2019.00350/BIBTEX.

McGee, Bryan, Reynaldo Dietze, David Jamil Hadad, Lucilia Pereira Dutra Molino, Ethel Leonor Noia Maciel, W. Henry Boom, Moises Palaci, John L. Johnson, and Charles A. Peloquin. 2009. "Population Pharmacokinetics of Linezolid in Adults with Pulmonary Tuberculosis." *Antimicrobial Agents and Chemotherapy* 53 (9): 3981–84. https://doi.org/10.1128/AAC.01378-08.

McIlleron, H, P Wash, A Burger, P Folb, and P Smith. 2002. "Widespread Distribution of a Single Drug Rifampicin Formulation of Inferior Bioavailability in South Africa." *International Journal of Tuberculosis and Lung Disease* 6 (4): 356–61. http://www.ncbi.nlm.nih.gov/pubmed/11936746.

McIlleron, Helen, and Saye H. Khoo. 2011. "Interactions between Antituberculosis and Antiretroviral Agents." *Antituberculosis Chemotherapy* 10: 191–202. https://doi.org/10.1159/000324217.

McIlleron, Helen, Roxana Rustomje, Mahnaz Vahedi, Thuli Mthiyane, Paolo Denti, Catherine Connolly, Wasima Rid, Alexander Pym, Peter J. Smith, and Philip C. Onyebujoh. 2012. "Reduced Antituberculosis Drug Concentrations in HIV-Infected Patients Who Are Men or Have Low Weight: Implications for International Dosing Guidelines." *Antimicrobial Agents and Chemotherapy* 56 (6): 3232–38. https://doi.org/10.1128/AAC.05526-11.

McIlleron, Helen, Peter Wash, André Burger, Jennifer Norman, Peter I. Folb, and Pete Smith. 2006. "Determinants of Rifampin, Isoniazid, Pyrazinamide, and Ethambutol Pharmacokinetics in a

Cohort of Tuberculosis Patients." *Antimicrobial Agents and Chemotherapy* 50 (4): 1170–77. https://doi.org/10.1128/AAC.50.4.1170-1177.2006.

McLeay, Sarah C., Glynn A. Morrish, Carl M.J. Kirkpatrick, and Bruce Green. 2012. "The Relationship between Drug Clearance and Body Size." *Clinical Pharmacokinetics* 51 (5): 319–30. https://doi.org/10.2165/11598930-000000000-00000.

Meagher, Alison K., Alan Forrest, Craig R. Rayner, Mary C. Birmingham, and Jerome J. Schentag. 2003. "Population Pharmacokinetics of Linezolid in Patients Treated in a Compassionate-Use Program." *Antimicrobial Agents and Chemotherapy* 47 (2): 548–53. https://doi.org/10.1128/AAC.47.2.548-553.2003.

Millard, James, Henry Pertinez, Laura Bonnett, Eva Maria Hodel, Véronique Dartois, John L Johnson, Maxine Caws, et al. 2018. "Linezolid Pharmacokinetics in MDR-TB: A Systematic Review, Meta-Analysis and Monte Carlo Simulation." *Journal of Antimicrobial Chemotherapy*, no. April: 1–8. https://doi.org/10.1093/jac/dky096.

Mindermann, Thomas, Werner Zimmerli, and Otmar Gratzl. 1998. "Rifampin Concentrations in Various Compartments of the Human Brain: A Novel Method for Determining Drug Levels in the Cerebral Extracellular Space." *Antimicrobial Agents and Chemotherapy* 42 (10): 2626–29. https://doi.org/10.1128/AAC.42.10.2626.

Mitchison, D A, and J B Selkon. 1956. "The Bactericidal Activities of Antituberculous Drugs." *American Review of Tuberculosis* 74 (2 Part 2): 109–16; discussion, 116–23. https://doi.org/10.1164/artpd.1956.74.2-2.109.

Mockeliunas, Laurynas, Lina Keutzer, Marieke G G Sturkenboom, Mathieu S Bolhuis, Lotte M G Hulskotte, Onno W Akkerman, and Ulrika S H Simonsson. 2022. "Model-Informed Precision Dosing of Linezolid in Patients with Drug-Resistant Tuberculosis." *Pharmaceutics* 14 (4): 753. https://doi.org/10.3390/pharmaceutics14040753.

Monedero-Recuero, Ignacio, Medea Gegia, Douglas Fraser Wares, Sarabjit S Chadha, and Fuad Mirzayev. 2021. "Situational Analysis of 10 Countries with a High Burden of Drug-Resistant Tuberculosis 2 Years Post-UNHLM Declaration: Progress and Setbacks in a Changing Landscape." https://doi.org/10.1016/j.ijid.2021.06.022.

Morgan, Denis J., and Kelly M. Bray. 1994. "Lean Body Mass as a Predictor of Drug Dosage." *Clinical Pharmacokinetics* 26 (4): 292–307. https://doi.org/10.2165/00003088-199426040-00005.

Mould, D. R., and R. N. Upton. 2012. "Basic Concepts in Population Modeling, Simulation, and Model-Based Drug Development." *CPT: Pharmacometrics and Systems Pharmacology* 1 (1). https://doi.org/10.1038/psp.2012.4.

Mould, DR, and RN Upton. 2013. "Basic Concepts in Population Modeling, Simulation, and Model-Based Drug Development—Part 2: Introduction to Pharmacokinetic Modeling Methods." *CPT: Pharmacometrics & Systems Pharmacology* 2 (4): 1–14. https://doi.org/10.1038/psp.2013.14.

Mthiyane, Thuli, James Millard, John Adamson, Yusentha Balakrishna, Cathy Connolly, Andrew Owen, Roxana Rustomjee, Keertan Dheda, Helen McIlleron, and Alexander S. Pym. 2020. "N -Acetyltransferase 2 Genotypes among Zulu-Speaking South Africans and Isoniazid and N -Acetyl-Isoniazid Pharmacokinetics during Antituberculosis Treatment." *Antimicrobial Agents and Chemotherapy* 64 (4). https://doi.org/10.1128/AAC.02376-19.

Muda, Mohd Rahimi, Sabariah Noor Harun, Syed Azhar Syed Sulaiman, Siti Maisharah Sheikh Ghadzi, Mohd Rahimi Muda, Sabariah Noor Harun, Syed Azhar Syed Sulaiman, Siti Maisharah Sheikh Ghadzi, Mara Selangor, and Malaysia Correspondence Siti Maisharah Sheikh Ghadzi. 2022. "Population Pharmacokinetics Analyses of Rifampicin in Adult and Children Populations: A Systematic Review." *British Journal of Clinical Pharmacology* 88 (7): 3132–52. https://doi.org/10.1111/bcp.15298.

Muliaditan, Morris, and Oscar Della Pasqua. n.d. "How Long Will Treatment Guidelines for TB Continue to Overlook Variability in Drug Exposure?" https://doi.org/10.1093/jac/dkz319.

Munro, Salla A, Simon A Lewin, Helen J Smith, Mark E Engel, Atle Fretheim, and Jimmy Volmink. 2007. "Patient Adherence to Tuberculosis Treatment: A Systematic Review of Qualitative Research" 4: 1230. https://doi.org/10.1371/journal.pmed. 0040238.

Myrianthefs, Pavlos, Sophia L. Markantonis, Konstantinos Vlachos, Maria Anagnostaki, Eleni Boutzouka, Dimitris Panidis, and Georgios Baltopoulos. 2006. "Serum and Cerebrospinal Fluid Concentrations of Linezolid in Neurosurgical Patients." *Antimicrobial Agents and Chemotherapy* 50 (12): 3971–76. https://doi.org/10.1128/AAC.00051-06.

Nau, Roland, Fritz Sörgel, and Helmut Eiffert. 2010. "Penetration of Drugs through the Blood-Cerebrospinal Fluid/Blood-Brain Barrier for Treatment of Central Nervous System Infections." *Clinical Microbiology Reviews* 23 (4): 858–83. https://doi.org/10.1128/CMR.00007-10.

Nau, Roland, Fritz Sörgel, and Hilmar W. Prange. 1994. "Lipophilicity at PH 7.4 and Molecular Size Govern the Entry of the Free Serum Fraction of Drugs into the Cerebrospinal Fluid in Humans with Uninflamed Meninges." *Journal of the Neurological Sciences* 122 (1): 61–65. https://doi.org/10.1016/0022-510X(94)90052-3.

Nicholls, David G., and Stuart J. Ferguson. 2013. "Ion Transport Across Energy-Conserving Membranes." *Bioenergetics*, 13–25. https://doi.org/10.1016/B978-0-12-388425-1.00002-6.

Nyang'wa, Bern-Thomas, Catherine Berry, Emil Kazounis, Ilaria Motta, Nargiza Parpieva, Zinaida Tigay, Varvara Solodovnikova, et al. 2022. "A 24-Week, All-Oral Regimen for Rifampin-Resistant Tuberculosis." *New England Journal of Medicine* 387 (25): 2331–43. https://doi.org/10.1056/NEJMoa2117166.

Okazaki, Fumiyasu, Yasuhiro Tsuji, Yoshihiro Seto, Chika Ogami, Yoshihiro Yamamoto, and Hideto To. 2019. "Effects of a Rifampicin Pre-Treatment on Linezolid Pharmacokinetics." *PLoS ONE* 14 (9): 1–8. https://doi.org/10.1371/journal.pone.0214037.

Owen, Joel S, and Jill Fiedler-kelly. 2014. *Introduction to Population Pharmacokinetic/Pharmacodynamic Analysis with Nonlinear Mixed Effects Models*.

Paladino, Joseph A. 2002. "Linezolid: An Oxazolidinone Antimicrobial Agent." *American Journal of Health-System Pharmacy* 59 (24): 2413–25. https://doi.org/10.1093/ajhp/59.24.2413.

Palenzuela, Lluis, Noah M. Hahn, Robert P. Nelson, Janet N. Arno, Carol Schobert, Robert Bethel, Lisa A. Ostrowski, et al. 2005. "Does Linezolid Cause Lactic Acidosis by Inhibiting Mitochondrial Protein Synthesis?" *Clinical Infectious Diseases : An Official Publication of the Infectious Diseases Society of America* 40 (12): e113–16. https://doi.org/10.1086/430441/3/40-12-E113-TBL001.GIF.

Panjasawatwong, Navarat, Thanaporn Wattanakul, Richard M. Hoglund, Nguyen Duc Bang, Thomas Pouplin, Wichit Nosoongnoen, Vi Nguyen Ngo, Jeremy N. Day, and Joel Tarning. 2020. "Population Pharmacokinetic Properties of Antituberculosis Drugs in Vietnamese Children with

Tuberculous Meningitis." *Antimicrobial Agents and Chemotherapy* 65 (1). https://doi.org/10.1128/AAC.00487-20.

Paolo, Antonello Di, Giovanni Gori, Carlo Tascini, Romano Danesi, and Mario Del Tacca. 2013. "Clinical Pharmacokinetics of Antibacterials in Cerebrospinal Fluid." *Clinical Pharmacokinetics* 52 (7): 511–42. https://doi.org/10.1007/S40262-013-0062-9.

Pardridge, William M. 2012. "Drug Transport across the Blood–Brain Barrier." *Journal of Cerebral Blood Flow & Metabolism* 32 (11): 1959. https://doi.org/10.1038/JCBFM.2012.126.

Parkin, Donald P., Santie Vandenplas, Frederik J.H. Botha, Michel L. Vandenplas, Heiner I. Seifart, Paul D. Van Helden, Barend J. Van Der Walt, Peter R. Donald, and Pieter P. Van Jaarsveld. 1997. "Trimodality of Isoniazid Elimination: Phenotype and Genotype in Patients with Tuberculosis." *American Journal of Respiratory and Critical Care Medicine* 155 (5): 1717–22. https://doi.org/10.1164/ajrccm.155.5.9154882.

Parsons, R. L. 1977. "Drug Absorption in Gastrointestinal Disease With Particular Reference to Malabsorption Syndromes." *Clinical Pharmacokinetics* 2 (1): 45–60. https://doi.org/10.2165/00003088-197702010-00004.

Peh, Kai Qi Elizabeth, Yu Heng Kwan, Hendra Goh, Hasna Ramchandani, Jie Kie Phang, Zhui Ying Lim, Dionne Hui Fang Loh, et al. 2021. "An Adaptable Framework for Factors Contributing to Medication Adherence: Results from a Systematic Review of 102 Conceptual Frameworks." *Journal of General Internal Medicine* 36 (9): 2784–95. https://doi.org/10.1007/s11606-021-06648-1.

Peloquin, Charles A., Amy E. Bulpitt, George S. Jaresko, Roger W. Jelliffe, Gordon T. James, and David E. Nix. 1998. "Pharmacokinetics of Pyrazinamide under Fasting Conditions, with Food, and with Antacids." *Pharmacotherapy: The Journal of Human Pharmacology and Drug Therapy* 18 (6): 1205–11. https://doi.org/10.1002/j.1875-9114.1998.tb03138.x.

Peloquin, Charles A., George S. Jaresko, Chan Loi Yong, Anther C.F. Keung, Amy E. Bulpitt, and Roger W. Jelliffe. 1997. "Population Pharmacokinetic Modeling of Isoniazid, Rifampin, and Pyrazinamide." *Antimicrobial Agents and Chemotherapy* 41 (12): 2670–79. https://doi.org/10.1128/AAC.41.12.2670.

Peloquin, Charles A., Rocsanna Namdar, Michael D. Singleton, and David E. Nix. 1999. "Pharmacokinetics of Rifampin Under Fasting Conditions, With Food, and With Antacids." *Chest* 115 (1): 12–18. https://doi.org/10.1378/chest.115.1.12.

Pintado, Vicente, Rosario Pazos, Manuel Enrique Jiménez-Mejías, Azucena Rodríguez-Guardado, Beatriz Díaz-Pollán, Carmen Cabellos, Juan Manuel García-Lechuz, et al. 2020. "Linezolid for Therapy of Staphylococcus Aureus Meningitis: A Cohort Study of 26 Patients." *Infectious Diseases (London, England)* 52 (11): 808–15. https://doi.org/10.1080/23744235.2020.1789212.

Plock, N., C. Buerger, C. Joukhadar, S. Kljucar, and Charlotte Kloft. 2007. "Does Linezolid Inhibit Its Own Metabolism? - Population Pharmacokinetics as a Tool to Explain the Observed Nonlinearity in Both Healthy Volunteers and Septic Patients." *Drug Metabolism and Disposition* 35 (10): 1816–23. https://doi.org/10.1124/dmd.106.013755.

Polasa, K, KJ Murthy, and K Krishnaswamy. 1984. "Rifampicin Kinetics in Undernutrition." *British Journal of Clinical Pharmacology* 17 (4): 481–84. https://doi.org/10.1111/j.1365-2125.1984.tb02377.x.

Rastogi, Nalin, Valérie Labrousse, and Khye Seng Goh. 1996. "In Vitro Activities of Fourteen Antimicrobial Agents Against Drug Susceptible and Resistant Clinical Isolates of Mycobacterium Tuberculosis and Comparative Intracellular Activities Against the Virulent H37Rv Strain in Human Macrophages." *Current Microbiology* 33 (3): 167–75. https://doi.org/10.1007/s002849900095.

Reiber, H. 2001. "Dynamics of Brain-Derived Proteins in Cerebrospinal Fluid." *Clinica Chimica Acta* 310 (2): 173–86. https://doi.org/10.1016/S0009-8981(01)00573-3.

Reiber, Hansotto. 2003. "Proteins in Cerebrospinal Fluid and Blood: Barriers, CSF Flow Rate and Source-Related Dynamics." *Restorative Neurology and Neuroscience* 21 (3–4): 79–96.

Roberts, Derek J., and Richard I. Hall. 2013. "Drug Absorption, Distribution, Metabolism and Excretion Considerations in Critically Ill Adults." *Expert Opinion on Drug Metabolism & Toxicology* 9 (9): 1067–84. https://doi.org/10.1517/17425255.2013.799137.

Rockwood, Neesha, Graeme Meintjes, Maxwell Chirehwa, Lubbe Wiesner, Helen Mcilleron, and

Robert J Wilkinson. 2016. "HIV-1 Coinfection Does Not Reduce Exposure to Rifampin, Isoniazid, and Pyrazinamide in South African Tuberculosis Outpatients" 60 (10): 6050–59. https://doi.org/10.1128/AAC.00480-16.Address.

Rohlwink, Ursula K., Anthony Figaji, Katalin A. Wilkinson, Stuart Horswell, Abdul K. Sesay, Armin Deffur, Nico Enslin, et al. 2019. "Tuberculous Meningitis in Children Is Characterized by Compartmentalized Immune Responses and Neural Excitotoxicity." *Nature Communications* 10 (1): 3767. https://doi.org/10.1038/s41467-019-11783-9.

Rohlwink, Ursula K., Tracy Kilborn, Nicky Wieselthaler, Ebrahim Banderker, Eugene Zwane, and Anthony A. Figaji. 2016. "Imaging Features of the Brain, Cerebral Vessels and Spine in Pediatric Tuberculous Meningitis With Associated Hydrocephalus." *The Pediatric Infectious Disease Journal* 35 (10): e301–10. https://doi.org/10.1097/INF.0000000000001236.

Rohlwink, Ursula K., Katya Mauff, Katalin A. Wilkinson, Nico Enslin, Emmanuel Wegoye, Robert J. Wilkinson, and Anthony A. Figaji. 2017. "Biomarkers of Cerebral Injury and Inflammation in Pediatric Tuberculous Meningitis." *Clinical Infectious Diseases : An Official Publication of the Infectious Diseases Society of America* 65 (8): 1298–1307. https://doi.org/10.1093/CID/CIX540.

Ruiz-Bedoya, Camilo A., Filipa Mota, Elizabeth W. Tucker, Farina J. Mahmud, Maria I. Reyes-Mantilla, Clara Erice, Melissa Bahr, et al. 2022. "High-Dose Rifampin Improves Bactericidal Activity without Increased Intracerebral Inflammation in Animal Models of Tuberculous Meningitis." *Journal of Clinical Investigation* 132 (6). https://doi.org/10.1172/JCI155851.

Rupprecht, T. A., and H.-W. Pfister. 2005. "Clinical Experience with Linezolid for the Treatment of Central Nervous System Infections." *European Journal of Neurology* 12 (7): 536–42. https://doi.org/10.1111/j.1468-1331.2005.01001.x.

Saleh, Mohammed A.A., Chi Fong Loo, Jeroen Elassaiss-Schaap, and Elizabeth C.M. De Lange. 2021. "Lumbar Cerebrospinal Fluid-to-Brain Extracellular Fluid Surrogacy Is Context-Specific: Insights from LeiCNS-PK3.0 Simulations." *Journal of Pharmacokinetics and Pharmacodynamics* 48 (5): 725–41. https://doi.org/10.1007/S10928-021-09768-7/FIGURES/4.

Sarkar, Susmita, Advaita Ganguly, and Hoon H Sunwoo. 2017. "Current Overview of Anti-Tuberculosis Drugs: Metabolism and Toxicities." https://doi.org/10.4172/2161-1068.1000209.

Savic, RM, R. Ruslami, JE Hibma, A. Hesseling, G. Ramachandran, AR Ganiem, S. Swaminathan, et al. 2015. "Pediatric Tuberculous Meningitis: Model-Based Approach to Determining Optimal Doses of the Anti-Tuberculosis Drugs Rifampin and Levofloxacin for Children." *Clinical Pharmacology & Therapeutics* 98 (6): 622–29. https://doi.org/10.1002/cpt.202.

Schaberg, T, K Rebhan, and H Lode. 1996. "Risk Factors for Side-Effects of Isoniazid, Rifampin and Pyrazinamide in Patients Hospitalized for Pulmonary Tuberculosis." *European Respiratory Journal* 9 (10): 2026–30. https://doi.org/10.1183/09031936.96.09102026.

Schoonjans, Frank, Dirk De Bacquer, and Pirmin Schmid. 2011. "Estimation of Population Percentiles." *Epidemiology (Cambridge, Mass.)* 22 (5): 750. https://doi.org/10.1097/EDE.0B013E318225C1DE.

Schutz, Charlotte, Maxwell Chirehwa, David Barr, Amy Ward, Saskia Janssen, Rosie Burton, Robert J. Wilkinson, et al. 2020. "Early Antituberculosis Drug Exposure in Hospitalized Patients with Human Immunodeficiency Virus-Associated Tuberculosis." *British Journal of Clinical Pharmacology* 86 (5): 966–78. https://doi.org/10.1111/bcp.14207.

Sekaggya-Wiltshire, Christine, Amrei Von Braun, Mohammed Lamorde, Bruno Ledergerber, Allan Buzibye, Lars Henning, Joseph Musaazi, et al. 2018. "Delayed Sputum Culture Conversion in Tuberculosis–Human Immunodeficiency Virus–Coinfected Patients With Low Isoniazid and Rifampicin Concentrations." *Clinical Infectious Diseases* 67 (5): 708–16. https://doi.org/10.1093/cid/ciy179.

Sheiner, Lewis B, Donald R Stanski, Samuel Vozeh, Ronald D Miller, Jay San Ham, and Cauf Francisco. 1979. "Simultaneous Modeling of Pharmacokinetics and Pharmacodynamics: Application to d-Tubocurarine."

Siegler, D. I., D. M. Burley, M. Bryant, K. M. Citron, and Susan M. Standen. 1974. "EFFECT OF MEALS ON RIFAMPICIN ABSORPTION." *The Lancet* 304 (7874): 197–98. https://doi.org/10.1016/S0140-6736(74)91487-1.

Sirgel, Frik A., P. Bernard Fourie, Peter R. Donald, Nesri Padayatchi, Roxana Rustomjee, Jonathan Levin, Giorgio Roscigno, Jennifer Norman, Helen McIlleron, and Denis A. Mitchison. 2005. "The Early Bactericidal Activities of Rifampin and Rifapentine in Pulmonary Tuberculosis." *American*

Journal of Respiratory and Critical Care Medicine 172 (1): 128–35. https://doi.org/10.1164/rccm.200411-1557OC.

Smith, P. J., J van Dyk, and A. Fredericks. 1999. "Determination of Rifampicin, Isoniazid and Pyrazinamide by High Performance Liquid Chromatography after Their Simultaneous Extraction from Plasma." *The International Journal of Tuberculosis and Lung Disease : The Official Journal of the International Union against Tuberculosis and Lung Disease* 3 (11 Suppl 3): S325-8; discussion S351-2. https://europepmc.org/article/med/10593712.

Smythe, Wynand, Akash Khandelwal, Corinne Merle, Roxana Rustomjee, Martin Gninafon, Mame Bocar Lo, Oumou Bah Sow, et al. 2012. "A Semimechanistic Pharmacokinetic-Enzyme Turnover Model for Rifampin Autoinduction in Adult Tuberculosis Patients." *Antimicrobial Agents and Chemotherapy* 56 (4): 2091–98. https://doi.org/10.1128/AAC.05792-11.

Snyder, Ben D, Thomas M Polasek, and Matthew P Doogue. 2012. "Drug Interactions: Principles and Practice." *Aust Prescr* 35: 85–88. www.australianprescriber.com.

Stalker, Dennis J., and Gail L. Jungbluth. 2003. "Clinical Pharmacokinetics of Linezolid, a Novel Oxazolidinone Antibacterial." *Clinical Pharmacokinetics* 42 (13): 1129–40. https://doi.org/10.2165/00003088-200342130-00004/FIGURES/TAB5.

Stott, K. E., H. Pertinez, M. G.G. Sturkenboom, M. J. Boeree, R. Aarnoutse, G. Ramachandran, A. Requena-Méndez, et al. 2018. "Pharmacokinetics of Rifampicin in Adult TB Patients and Healthy Volunteers: A Systematic Review and Meta-Analysis." *Journal of Antimicrobial Chemotherapy* 73 (9): 2305–13. https://doi.org/10.1093/jac/dky152.

Sturgill-Koszycki, Sheila, Paul H. Schlesinger, Prasanta Chakraborty, Pryce L. Haddix, Helen L. Collins, Agnes K. Fok, Richard D. Allen, Stephen L. Gluck, John Heuser, and David G. Russell. 1994. "Lack of Acidification in Mycobacterium Phagosomes Produced by Exclusion of the Vesicular Proton-ATPase." *Science* 263 (5147): 678–81. https://doi.org/10.1126/SCIENCE.8303277.

Subbarao, Sathyavani, Katalin A. Wilkinson, Clare L. Van Halsema, Suhasini Subba Rao, Tom Boyles, Netanya S. Utay, Robert J. Wilkinson, and Graeme Meintjes. 2015. "Raised Venous Lactate and Markers of Intestinal Translocation Are Associated with Mortality among In-Patients with HIV-Associated TB in Rural South Africa." *Journal of Acquired Immune Deficiency Syndromes* 70 (4):

406–13. https://doi.org/10.1097/QAI.0000000000000763.

Sun, Feng, Qiaoling Ruan, Jiali Wang, Shu Chen, Jialin Jin, Lingyun Shao, Ying Zhang, and Wenhong Zhang. 2014. "Linezolid Manifests a Rapid and Dramatic Therapeutic Effect for Patients with Life-Threatening Tuberculous Meningitis." *Antimicrobial Agents and Chemotherapy* 58 (10): 6297–6301. https://journals.asm.org/doi/10.1128/AAC.02784-14.

Sundell, Jesper, Emile Bienvenu, David Janzén, Sofia Birgersson, Angela Äbelö, and Michael Ashton. 2020. "Model-Based Assessment of Variability in Isoniazid Pharmacokinetics and Metabolism in Patients Co-Infected With Tuberculosis and HIV: Implications for a Novel Dosing Strategy." *Clinical Pharmacology and Therapeutics* 108 (1): 73–80. https://doi.org/10.1002/cpt.1806.

Svensson, Elin M., Sofiati DIan, Lindsey Te Brake, Ahmad Rizal Ganiem, Vycke Yunivita, Arjan Van Laarhoven, Reinout Van Crevel, Rovina Ruslami, and Rob E. Aarnoutse. 2020. "Model-Based Meta-Analysis of Rifampicin Exposure and Mortality in Indonesian Tuberculous Meningitis Trials." *Clinical Infectious Diseases* 71 (8): 1817–23. https://doi.org/10.1093/cid/ciz1071.

Svensson, Robin J., Rob E. Aarnoutse, Andreas H. Diacon, Rodney Dawson, Stephen H. Gillespie, Martin J. Boeree, and Ulrika S.H. Simonsson. 2018. "A Population Pharmacokinetic Model Incorporating Saturable Pharmacokinetics and Autoinduction for High Rifampicin Doses." *Clinical Pharmacology and Therapeutics* 103 (4): 674–83. https://doi.org/10.1002/cpt.778.

Tan, Tina Q., and Ram Yogev. 2008. "Clinical Pharmacology of Linezolid: An Oxazolidinone Antimicrobial Agent." *Expert Review of Clinical Pharmacology* 1 (4): 479–89. https://doi.org/10.1586/17512433.1.4.479.

Thakur, Kiran, Mitashee Das, Kelly E. Dooley, and Amita Gupta. 2018. "The Global Neurological Burden of Tuberculosis." *Seminars in Neurology* 38 (2): 226–37. https://doi.org/10.1055/S-0038-1651500/ID/JR180017-21/BIB.

Tietjen, Anna K., Niklas Kroemer, Dario Cattaneo, Sara Baldelli, and Sebastian G. Wicha. 2021. "Population Pharmacokinetics and Target Attainment Analysis of Linezolid in Multidrug-resistant Tuberculosis Patients." *British Journal of Clinical Pharmacology*, no. February: 1–10. https://doi.org/10.1111/bcp.15102.

Timmins, Graham S., and Vojo Deretic. 2006. "Mechanisms of Action of Isoniazid." *Molecular*

Microbiology 62 (5): 1220–27. https://doi.org/10.1111/j.1365-2958.2006.05467.x.

Toorn, Ronald van, H. Simon Schaaf, Jacoba A. Laubscher, Sabine L. van Elsland, Peter R. Donald, and Johan F. Schoeman. 2014. "Short Intensified Treatment in Children with Drug-Susceptible Tuberculous Meningitis." *The Pediatric Infectious Disease Journal* 33 (3): 248–52. https://doi.org/10.1097/INF.0000000000000065.

Török, M. E. 2015. "Tuberculous Meningitis: Advances in Diagnosis and Treatment." *British Medical Bulletin* 113 (1): 117–31. https://doi.org/10.1093/BMB/LDV003.

Tucker, Elizabeth W., Beatriz Guglieri-Lopez, Alvaro A. Ordonez, Brittaney Ritchie, Mariah H. Klunk, Richa Sharma, Yong S. Chang, et al. 2018. "Noninvasive 11C-Rifampin Positron Emission Tomography Reveals Drug Biodistribution in Tuberculous Meningitis." *Science Translational Medicine* 10 (470): 1–12. https://doi.org/10.1126/scitranslmed.aau0965.

Tupin, Audrey, Maxime Gualtieri, Françoise Roquet-Banères, Zakia Morichaud, Konstantin Brodolin, and Jean Paul Leonetti. 2010. "Resistance to Rifampicin: At the Crossroads between Ecological, Genomic and Medical Concerns." *International Journal of Antimicrobial Agents* 35 (6): 519–23. https://doi.org/10.1016/J.IJANTIMICAG.2009.12.017.

Ungerstedt, Urban, and Elham Rostami. 2004. "Microdialysis in Neurointensive Care." *Current Pharmaceutical Design* 10 (18): 2145–52. https://doi.org/10.2174/1381612043384105.

Upton, R. N., and D. R. Mould. 2014. "Basic Concepts in Population Modeling, Simulation, and Model-Based Drug Development: Part 3-Introduction to Pharmacodynamic Modeling Methods." *CPT: Pharmacometrics and Systems Pharmacology* 3 (1): 1–16. https://doi.org/10.1038/psp.2013.71.

Viaggi, Bruno, Antonello Di Paolo, Romano Danesi, Marialuisa Polillo, Laura Ciofi, Mario Del Tacca, and Paolo Malacarne. 2011. "Linezolid in the Central Nervous System: Comparison between Cerebrospinal Fluid and Plasma Pharmacokinetics." *Http://Dx.Doi.Org/10.3109/00365548.2011.582140* 43 (9): 721–27. https://doi.org/10.3109/00365548.2011.582140.

Vilchèze, Catherine, and William R. Jacobs. 2019. "The Isoniazid Paradigm of Killing, Resistance, and Persistence in Mycobacterium Tuberculosis." *Journal of Molecular Biology* 431 (18): 3450–61.

https://doi.org/10.1016/J.JMB.2019.02.016.

Villani, P., M. B. Regazzi, F. Marubbi, P. Viale, L. Pagani, F. Cristini, B. Cadeo, G. Carosi, and R. Bergomi. 2002. "Cerebrospinal Fluid Linezolid Concentrations in Postneurosurgical Central Nervous System Infections." *Antimicrobial Agents and Chemotherapy* 46 (3): 936–37. https://doi.org/10.1128/AAC.46.3.936-937.2002.

Volmink, Jimmy, and Paul Garner. 2008. "Directly Observed Therapy for Treating Tuberculosis." *Chinese Journal of Evidence-Based Medicine* 8 (7): 513–14. https://doi.org/10.1002/14651858.CD003343.PUB2/MEDIA/CDSR/CD003343/REL0002/CD003343/IMAGE_N/NCD003343-CMP-006-01.PNG.

Wagner, Christian, Yuzhuo Pan, Vicky Hsu, Vikram Sinha, and Ping Zhao. 2016. "Predicting the Effect of CYP3A Inducers on the Pharmacokinetics of Substrate Drugs Using Physiologically Based Pharmacokinetic (PBPK) Modeling: An Analysis of PBPK Submissions to the US FDA." *Clinical Pharmacokinetics* 55 (4): 475–83. https://doi.org/10.1007/S40262-015-0330-Y/METRICS.

Wang, P-Y., S-Y. Xie, Q. Hao, C. Zhang, and B-F. Jiang. 2012. "NAT2 Polymorphisms and Susceptibility to Anti-Tuberculosis Drug-Induced Liver Injury: A Meta-Analysis." *The International Journal of Tuberculosis and Lung Disease : The Official Journal of the International Union against Tuberculosis and Lung Disease* 16 (5): 589–95. https://doi.org/10.5588/ijtld.11.0377.

Wang, Zhiwei. 2012. "Optimized 1:N Case- -Control M Match Usi Ng SAS®."

Wasmann, Roeland E., Elin M. Svensson, A. Sarah Walker, Michelle N. Clements, and Paolo Denti. 2021. "Constructing a Representative In-Silico Population for Paediatric Simulations: Application to HIV-Positive African Children." *British Journal of Clinical Pharmacology* 87 (7): 2847–54. https://doi.org/10.1111/BCP.14694.

Wasserman, Sean, Rosleine Antilus-Sainte, Noha Abdelgawad, Narineh M. Odjourian, Melissa Cristaldo, Maureen Dougher, Firat Kaya, Matthew Zimmerman, Paolo Denti, and Martin Gengenbacher. 2024. "Rifabutin Central Nervous System Concentrations in a Rabbit Model of Tuberculous Meningitis." *Antimicrobial Agents and Chemotherapy* 68 (8). https://doi.org/10.1128/AAC.00783-24/FORMAT/EPUB.

Wasserman, Sean, James C.M. Brust, Mahmoud T. Abdelwahab, Francesca Little, Paolo Denti, Lubbe Wiesner, Neel R. Gandhi, Graeme Meintjes, and Gary Maartens. 2022. "Linezolid Toxicity in Patients with Drug-Resistant Tuberculosis: A Prospective Cohort Study." *The Journal of Antimicrobial Chemotherapy* 77 (4): 1146–54. https://doi.org/10.1093/JAC/DKAC019.

Wasserman, Sean, Angharad Davis, Cari Stek, Maxwell Chirehwa, Stephani Botha, Remy Daroowala, Marise Bremer, et al. 2021. "Plasma Pharmacokinetics of High-Dose Oral versus Intravenous Rifampicin in Patients with Tuberculous Meningitis: A Randomized Controlled Trial." *Antimicrobial Agents and Chemotherapy* 65 (8): e0014021. https://doi.org/10.1128/AAC.00140-21.

Wasserman, Sean, Angharad Davis, Robert J. Wilkinson, and Graeme Meintjes. 2019. "Key Considerations in the Pharmacotherapy of Tuberculous Meningitis." *Expert Opinion on Pharmacotherapy* 20 (15): 1791–95. https://doi.org/10.1080/14656566.2019.1638912.

Wasserman, Sean, Graeme Meintjes, and Gary Maartens. 2016. *Linezolid in the Treatment of Drug-Resistant Tuberculosis: The Challenge of Its Narrow Therapeutic Index*. Vol. 14. https://doi.org/10.1080/14787210.2016.1225498.

Wehrli, Walter. 1983. "Rifampin: Mechanisms of Action and Resistance." *Reviews of Infectious Diseases* 5 (Supplement_3): S407–11. https://doi.org/10.1093/CLINIDS/5.SUPPLEMENT_3.S407.

Wilkins, Justin J., Grant Langdon, Helen McIlleron, Goonaseelan (Colin) Pillai, Peter J. Smith, and Ulrika S. H. Simonsson. 2006. "Variability in the Population Pharmacokinetics of Pyrazinamide in South African Tuberculosis Patients." *European Journal of Clinical Pharmacology* 62 (9): 727–35. https://doi.org/10.1007/s00228-006-0141-z.

Wilkins, Justin J., Radojka M. Savic, Mats O. Karlsson, Grant Langdon, Helen McIlleron, Goonaseelan Pillai, Peter J. Smith, and Ulrika S.H. Simonsson. 2008. "Population Pharmacokinetics of Rifampin in Pulmonary Tuberculosis Patients, Including a Semimechanistic Model to Describe Variable Absorption." *Antimicrobial Agents and Chemotherapy* 52 (6): 2138–48. https://doi.org/10.1128/AAC.00461-07.

Wilkins, Justin J, Grant Langdon, Helen McIlleron, Goonaseelan Colin Pillai, Peter J Smith, and Ulrika

Sh H Simonsson. 2011. "Variability in the Population Pharmacokinetics of Isoniazid in South African Tuberculosis Patients." *British Journal of Clinical Pharmacology* 72 (1): 51–62. https://doi.org/10.1111/j.1365-2125.2011.03940.x.

Wilkinson, Robert J., Ursula Rohlwink, Usha Kant Misra, Reinout van Crevel, Nguyen Thi Hoang Mai, Kelly E. Dooley, Maxine Caws, et al. 2017. "Tuberculous Meningitis." *Nature Reviews Neurology* 13 (10): 581–98. https://doi.org/10.1038/nrneurol.2017.120.

Williamson, Beth, Kelly E. Dooley, Yuan Zhang, David J. Back, and Andrew Owen. 2013. "Induction of Influx and Efflux Transporters and Cytochrome P450 3A4 in Primary Human Hepatocytes by Rifampin, Rifabutin, and Rifapentine." *Antimicrobial Agents and Chemotherapy* 57 (12): 6366–69. https://doi.org/10.1128/AAC.01124-13.

Wolzak, Nena Katrina, Melissa Louise Cooke, Heidi Orth, and Ronald Van Toorn. 2012. "The Changing Profile of Pediatric Meningitis at a Referral Centre in Cape Town, South Africa." *Journal of Tropical Pediatrics* 58 (6): 491–95. https://doi.org/10.1093/TROPEJ/FMS031.

World Health Organization. 2021a. *Technical Report on Critical Concentrations for Drug Susceptibility Testing of Isoniazid and the Rifamycins (Rifampicin, Rifabutin and Rifapentine)*. https://www.who.int/publications/i/item/technical-report-on-critical-concentrations-for-drugsusceptibility-testing-of-isoniazid-and-therifamycins-(rifampicin-rifabutin-and-rifapentine).

———. 2024a. "WHO Operational Handbook on Tuberculosis." *Module 1: Prevention - Tuberculosis Preventive Treatment, Second Edition*. https://apps.who.int/iris/bitstream/handle/10665/340256/9789240022614-eng.pdf.

World Health Organization, (WHO). 2014. "Guidance for National Tuberculosis Programmes on the Management of Tuberculosis in Children." www.who.int.

———. 2021b. "WHO Consolidated Guidelines on Tuberculosis. Module 1: Prevention. Tuberculosis Preventive Treatment." *Tuberculosis, Lung Diseases, HIV Infection*. https://doi.org/10.30978/tb2021-2-86.

———. 2022a. *WHO Consolidated Guidelines on Tuberculosis. WHO Press*.

———. 2022b. *WHO Consolidated Guidelines on Tuberculosis Module 5: Management of Tuberculosis*

in Children and Adolescents. *WHO*.

———. 2022c. *WHO Operational Handbook on Tuberculosis: Module 4: Treatment: Drug-Susceptible Tuberculosis Treatment*. World Health Organization.

———. 2022d. *WHO Operational Handbook on Tuberculosis: Module 5: Management of Tuberculosis in Children and Adolescents*. World Health Organization.

World Health Organization (WHO). 2022. "WHO Operational Handbook on Tuberculosis Module 5: Management of Tuberculosis in Children and Adolescents." In *WHO Operational Handbook on Tuberculosis. Module 5: Management of Tuberculosis in Children and Adolescents. Geneva: World Health Organization; 2022. Licence: CC BY-NC-SA 3.0 IGO.*, 56. https://apps.who.int/iris/bitstream/handle/10665/340256/9789240022614-eng.pdf.

World Health Organization, (WHO). 2023a. *Global Tuberculosis Report 2023*. Geneva PP - Geneva: World Health Organization. https://iris.who.int/handle/10665/373828.

World Health Organization (WHO). 2023. "Global Tuberculosis Report 2023." *January*.

World Health Organization, (WHO). 2023b. "Tuberculosis in the WHO African Region: 2023 Progress Update." World Health Organization. Regional Office for Africa.

———. 2024b. *WHO Consolidated Guidelines on Tuberculosis: Module 1: Prevention: Tuberculosis Preventive Treatment*. 2nd ed. Geneva PP - Geneva: World Health Organization. https://iris.who.int/handle/10665/331170.

Yamamoto, Yumi, Meindert Danhof, and Elizabeth C.M. de Lange. 2017. "Microdialysis: The Key to Physiologically Based Model Prediction of Human CNS Target Site Concentrations." *AAPS Journal* 19 (4): 891–909. https://doi.org/10.1208/s12248-017-0050-3.

Zent, C., and P. Smith. 1995. "Study of the Effect of Concomitant Food on the Bioavailability of Rifampicin, Isoniazid and Pyrazinamide." *Tubercle and Lung Disease : The Official Journal of the International Union against Tuberculosis and Lung Disease* 76 (2): 109–13. https://doi.org/10.1016/0962-8479(95)90551-0.

Zhang, Chao, Paolo Denti, Jan Stefan Van Der Walt, Yuan Ren, Peter Smith, Mats O. Karlsson, and Helen McIlleron. 2012. "Population Pharmacokinetic Model for Adherence Evaluation Using Lamivudine Concentration Monitoring." *Therapeutic Drug Monitoring* 34 (4): 481–84.

https://doi.org/10.1097/FTD.0b013e31825c6067.

Zhang, Xin, Matthew E. Falagas, Konstantinos Z. Vardakas, Rui Wang, Rong Qin, Jin Wang, and Youning Liu. 2015. "Systematic Review and Meta-Analysis of the Efficacy and Safety of Therapy with Linezolid Containing Regimens in the Treatment of Multidrug-Resistant and Extensively Drug-Resistant Tuberculosis." *Journal of Thoracic Disease* 7 (4): 603–15. https://doi.org/10.3978/J.ISSN.2072-1439.2015.03.10.

Zhang, Ying. 2005. "The Magic Bullets and Tuberculosis Drug Targets." *Annual Review of Pharmacology and Toxicology* 45 (1): 529–64. https://doi.org/10.1146/annurev.pharmtox.45.120403.100120.

Zhang, Ying, Wanliang Shi, Wenhong Zhang, and Denis Mitchison. 2014. "Mechanisms of Pyrazinamide Action and Resistance." Edited by Graham F. Hatfull and William R. Jacobs Jr. *Microbiology Spectrum* 2 (4): 479–91. https://doi.org/10.1128/microbiolspec.MGM2-0023-2013.

Zvada, Simbarashe P., Paolo Denti, Peter R. Donald, H. Simon Schaaf, Stephanie Thee, James A. Seddon, Heiner I. Seifart, Peter J. Smith, Helen M. McIlleron, and Ulrika S.H. Simonsson. 2014. "Population Pharmacokinetics of Rifampicin, Pyrazinamide and Isoniazid in Children with Tuberculosis: In Silico Evaluation of Currently Recommended Doses." *Journal of Antimicrobial Chemotherapy* 69 (5): 1339–49. https://doi.org/10.1093/jac/dkt524.